Prepared for:

Rijkswaterstaat / RIKZ

Source term investigation
SWAN

A162

July 1999

Alkyon
Hydraulic Consultancy & Research

Client **Rijkswaterstaat/RIKZ**

Title **Source term investigation SWAN**

Abstract

In this study the source terms of the third generation wave prediction model SWAN have been investigated. The purpose of this study is to examine possible sources for observed discrepancies in the prediction of the significant wave height and the mean wave period in the Westerschelde estuary and other areas as well. The following aspects of the modelling of wind waves have been addressed: the horizontal variation of the wind profile after a land-sea transition and the subsequent wave modelling, existing and alternative source functions for wind input, whitecapping dissipation and non-linear quadruplet wave-wave interactions, an analysis of the behaviour of the spectrum and source terms at high frequencies, a sensitivity analysis of SWAN, a verification of SWAN against field data and a calibration of SWAN against known growth curves.

References Project DIJKBEKL, RIKZ nr. RKZ-436, Onderzoek golfmodel SWAN in Westerschelde

Rev.	Originator		Date	Remarks	Checked by		Approved by	
0	G.v.Vledder		2/11/1998	draft			GvVledder	
1	G.v.Vledder		19/11/1998	pre-final	D.P. Hurdle		G.v.Vledder	
2	G.v.Vledder		7/7/1999	revised final	D.P.Hurdle		G.v.Vledder	

Document Control		Contents		Status
Report number:	A162R1r2	text pages:	83	☐ preliminary
Keywords:	SWAN, source term, wave modelling, wave spectrum, wind modelling	tables:	15	☐ draft
		figures:	87	☒ final
Project number:	A162	appendices:	1	
File location:	P:\a162\report\A162R1R2.DOC			

Alkyon
Hydraulic Consultancy & Research

postal address
PO Box 248
8300 AE, Emmeloord
The Netherlands

visiting address
De Deel 21, Emmeloord
tel : +31 527 62 09 09
fax: +31 527 61 00 20

e-mail
info@alkyon.nl
internet
http://www.alkyon.nl

Executive's summary

In this study the source terms of the third generation wave prediction model SWAN have been investigated. The purpose of this study is to examine possible sources for observed discrepancies in the prediction of the significant wave height and the mean wave period in the Westerschelde estuary and other areas as well. The following aspects of the modelling of wind waves have been addressed: the horizontal variation of the wind profile after a land-sea transition and the subsequent wave modelling, existing and alternative source functions for wind input, whitecapping dissipation and non-linear quadruplet wave-wave interactions, an analysis of the behaviour of the spectrum and source terms at high frequencies, a sensitivity analysis of SWAN, a verification of SWAN against field data and a calibration of SWAN against known growth curves.

Contents

List of symbols

List of tables

List of figures

Contents

List of symbols

a	Charnock constant
a	offset of linear regression analysis
a_i	coefficient in wind model of Burgers and Makin
b	slope of linear regression analysis
b_i	coefficient in wind model of Burgers and Makin
c	phase velocity (m/s)
C_d	surface drag coefficient (-)
C_{ds}	scaling coefficient of whitecapping dissipation
c_g	group velocity (m/s)
C_{nl}	scaling coefficient of nonlinear quadruplet interaction source term
c_{pm}	conversion factor between peak and mean wave period
C_{ql}	scaling coefficient of whitecapping in quasi-linear wind model of Janssen (1991)
c_{sm}	conversion factor between significant and mean wave period
C_0	drag coefficient (-), in model of Stewart (1974)
d	depth (m)
d_1	first order index of agreement
d_2	second order index of agreement
E_{tot}	total wave variance (m^2)
$E(f)$	energy density spectrum (m^2/Hz)
F	Fetch (m)
f	frequency (Hz)
F	fetch (m)
$\tilde{F}$	dimensionless fetch (normalised with U_{10})
F_*	dimensionless fetch (normalised with u_*)
f_p	peak frequency (Hz)
f_{PM}	Pierson-Moskowitz frequency (Hz)
g	gravitational acceleration (m/s^2)
G	coupling coefficient of nonlinear quadruplet interactions
H	filter function for linear wave growth source term
H	wave height (s)
$\tilde{H}$	dimensionless wave height (normalised with U_{10})
H_*	dimensionless wave height (normalised with u_*)
H_s	significant wave height (m)
$\tilde{H}_s$	dimensionless significant wave height (normalised with U_{10})
$\vec{i}$	spectral base, e.g. (f,θ)
k	wave number (1/m)
$\bar{k}$	mean wave number (1/m)

$\hat{k}$	special mean wave number (1/m)
k_m	mean wave number (1/m)
k_p	peak wave number (1/m)
L	wave length (m)
m_i	i-th frequency moment of energy density spectrum $E(f)$
N	number of data points
n_i	action density at wave number k_i
$P(\ )$	atmospheric turbulent pressure spectrum
r	coefficient of linear correlation
R	depth scaling coefficient of Discrete Interaction Approximation
s	mean wave steepness
s_{PM}	mean wave steepness of a Pierson-Moskowitz spectrum
S_{wc}	source term for dissipation by whitecapping (m²/Hz/s)
S_{in}	source term for wind input (m²/Hz/s)
S_{nl}	source term for nonlinear quadruplet interactions (m²/Hz/s)
S_{tot}	total source term (m²/Hz/s)
t	time (s)
T	temperature (°)
T	wave period (s)
$\widetilde{T}$	dimensionless wave period (normalised with U_{10})
T_*	dimensionless wave period (normalised with u_*)
T_{air}	air temperature (°)
T_{land}	land temperature (°)
T_m	mean wave period (s)
$\widetilde{T}_m$	dimensionless mean wave period (normalised with U_{10})
$T_{m-1,0}$	mean wave period (s), based on spectral moments, m_{-1} and m_0
T_{m01}	mean wave period (s), based on spectral moments, m_0 and m_1
T_{m02}	mean wave period (s), based on spectral moments, m_0 and m_2
T_{pm}	mean peak period (s)
T_p	peak period (s)
$\widetilde{T}_p$	dimensionless peak period (normalised with U_{10})
T_{pb}	block peak period (s)
T_{pbeq}	equivalent block peak period (s), for double peaked spectra
T_{pd}	dominant wave period (s)
T_s	significant wave period (s)
$\widetilde{T}_s$	dimensionless significant wave period (normalised with U_{10})
u_λ	wind speed at height equal to wave length λ (m/s)
U_u	upwind wind velocity (m/s), as used in wind model of Taylor and Lee (1984)
U_{10}	wind speed at 10 m height (m/s)
$\overline{U}_{10}$	average wind speed (m/s)

u_*	friction velocity (m/s)
x	fetch (m)
$\bar{x}$	mean of observed data values
x_i	observed data value with sequence number i
$\bar{y}$	mean of predicted data values
y_i	predicted data value with sequence number i
$\hat{y}_i$	best-fit value corresponding to x_i and y_i
z	height (m)
z_e	effective roughness lengths (m)
z_0	roughness length (m)
z_{ou}	upwind roughness length (m)

α	Phillips' constant for linear wave growth
$\tilde{\alpha}$	mean squared wave steepness
α_{BJ}	coefficient in depth-induced wave breaking (in Battjes-Janssen model)
$\tilde{\alpha}_{PM}$	mean squared wave steepness of Pierson-Moskowitz spectrum
β	Miles' constant for exponential wave growth
γ	peak enhancement factor in JONSWAP spectrum
γ_{BJ}	coefficient in depth-induced wave breaking (in Battjes-Janssen model)
δ	delta function
δ	fraction in dissipation source function of Janssen (1991)
δ_i	thickness of internal boundary layer (m)
δS_{nl}	incremental change in action density in Discrete Interaction Approximation
ΔR	incremental change in wind speed
ΔT	temperature difference (°)
$\tilde{\varepsilon}$	dimensionless total wave energy (normalised with U_{10})
ε_*	dimensionless total wave energy (normalised with u_*)
κ	von Karman constant
κ	spectral narrowness
λ	wave length (m)
λ	shape parameter of wave number configuration in Discrete Interaction Approximation
$\tilde{\nu}$	dimensionless peak frequency (normalised with U_{10})
ν_*	dimensionless peak frequency (normalised with u_*)
π	circular constant
θ	direction
θ_w	wind direction
ρ_a	density of air (kg/m^3)
ρ_w	density of water (kg/m^3)
σ	radian frequency (= $2\pi f$)
σ_a, σ_b	left and right widths of peak enhancement in JONSWAP spectrum

τ	total surface stress (m^2/s^2)
τ	swell decay time (s)
τ_w	wave induced stress (m^2/s^2)
Γ	Coefficient in JONSWAP bottom friction formulation (m^2s^{-3})
ω	radian frequency (rad)
$\hat{\omega}$	mean radian frequency (rad)
ω_m	mean radian frequency (rad)
ω_p	radian peak frequency
Ψ_d	coefficient in dissipation model of Hasselmann (1974)

Acronyms

ABL	Atmospheric Boundary Layer
BIAS	difference between mean of computed and observed data values
DIA	Discrete Interaction Approximation
EBL	Ekman Boundary Layer
HISWA	HIndcasting Shallow water Waves
IBL	Internal Boundary Layer
JONSWAP	JOint North Sea Wave Project
PBL	Planetary Boundary Layer
RMSE	Root Mean Square Error
$RMSE_s$	Root Mean Square Error, Systematic part
$RMSE_u$	Root Mean Square Error, Unsystematic part
SBL	Surface Boundary Layer
SI	Scatter Index
SWAN	Simulating WAves Nearshore
WAM	Wave Model

List of tables

List of figures

The Figures 4.8 and 4.14 have been included in the text, they are marked below with the symbol *).

1 Introduction

1.1 Background

In the Netherlands, numerical prediction models are used to determine the design wave conditions for dikes and other structures. Until a few years ago the HISWA wave model (Holthuijsen et al., 1989) has been used for this purpose. Recently, the SWAN wave model has been developed by Delft University of Technology (Holthuijsen et al., 1993). This model can be considered as the successor to the HISWA model, because it is based on a more advanced description of the physics and because it is a fully discrete spectral wave model.

Recently wave model computations have been carried out by RIKZ with the SWAN wave model in the Westerschelde, an estuary located in the south of the Netherlands. The results of these computations were compared with results from the HISWA wave model. The results were quite remarkable, with SWAN giving higher wave heights along the dikes than the HISWA model (see RIKZ, 1997). Due to these large differences and the fact that the design conditions should be conservative, results of the SWAN wave model are now used for the determination of the design conditions. In addition, results of SWAN wave model computations were compared to a number of wave measurements under storm conditions.

Based on the wave model computations with the SWAN in the Westerschelde, the following conclusions were drawn:

- The differences between SWAN and HISWA occur both for severe storm conditions and for normal storm conditions,
- in the case that SWAN is applied with the Nelson formulation for energy dissipation too much dissipation takes places on horizontal banks,
- in the outer delta and in the mouth of the Westerschelde (near Vlissingen) turning off the Nelson formulation for energy dissipation improves the results of the prediction by SWAN,
- inside the Westerschelde estuary the effects of using the Nelson formulation are small,
- in the inner area of the Westerschelde, where local wave growth is dominant, it is found that HISWA under predicts the wave heights whereas SWAN over predicts the wave heights and under predicts the mean and peak wave periods, and, .
- at very short fetches (up to ± 1 à 5 km) the wave model results are unreliable due to uncertainties in the wind field that is used for wave model computations.

In addition, it is has been found by Gautier (1997) that currents may affect the wave conditions considerably. Moreover, it is known from various studies (e.g. de Jong, 1997) that the last few computational points close to land are unreliable.

1.2 Objective

The objective of the study is to investigate the possible causes for the observed differences in the SWAN model results. If possible, these causes should be remedied such that SWAN gives better predictions of the wave conditions that are typical for the Westerschelde.

1.3 Scope of work

To realise the above objective the following main tasks have been be carried out:
1. Investigation of the wind field after a land-sea transition,
2. investigation of existing (i.e. those implemented in the SWAN model) and alternative source terms,
3. verification of SWAN against wave measurements in the Westerschelde and other available wave data sets,
4. calibration of SWAN against parameterised growth curves from literature.

The outline of the study will be detailed in Chapter 2.

1.4 Acknowledgements

This study has been performed in co-operation with many people from different institutes. The author of this study thanks the following people for their support and fruitful discussions:
Dr. L.H. Holthuijsen and Dr. N. Booij of Delft University of Technology, Delft, The Netherlands,
Dr. C. Mastenbroek of ARGOSS, Vollenhove, The Netherlands, for his help in the wind modelling.
ir. J.H. Andorka Gal, drs. A. Radder and ir. J.G. de Ronde of the National Institute for Coastal and Marine Management, The Hague, The Netherlands (RIKZ;).
Dr. V. Kudryavtsev of the Ukrainian Institute for Marine Sciences in Sebastopol, Ukraine and Dr. V. Makin from the Royal Dutch Meteorological Institute in de Bilt, The Netherlands, for their help with the wind modelling after a land-sea transition.
ir. D. Beyer of RIZA, Lelystad, The Netherlands, for his help in providing and describing the IJsselmeer wave and wind data
The ARCADIA program was obtained from Digital Hydraulics BV, Dordrecht, The Netherlands.
Figure 3.4 was kindly provided by Dr. R. Kaiser of the Forschungsstelle Norderney, Germany.
The wave data for Lake George have been provided by Dr. I.R. Young of the Australian Defence Force Academy, Canberra, Australia.
Information about the SWAN modelling for Lake George was provided by Dr. R.C. Ris of WL | delft hydraulics, Delft, the Netherlands.

Part of the descriptions of the source terms for wind input, whitecapping dissipation and nonlinear quadruplet wave-wave interactions was reprinted with permission from WL | delft hydraulics from report H1861 (delft hydraulics, 1992).

The present work has been carried out ALKYON by Dr. G.Ph. van Vledder with the help of D.P. Hurdle (M.Sc.), Mrs. R. de Boer and Mrs. N. Durand.

Preface to this edition

The present report is a revision of the issue of November 1998. In this edition of the report special attention has been paid to the verification of SWAN against field measurements.

2 Study approach

2.1 Introduction

This study aims to improve the performance of SWAN in the Westerschelde. However, some of the physical effects which play an important role in the Westerschelde can also play an important role in other very different situations. Consideration of these situations, in particular locations where measured data is available, can give improved modelling results for the Westerschelde. Therefore a wider range of situations has been considered. This includes an investigation of alternative source functions (i.e. source functions that are not yet included in the SWAN model). Further, it is known that land-sea effects and atmospheric (in)stability affect the structure of the wind field at the downwind side of a land-sea transition.

Based on the above consideration the following tasks have been defined:
1. Analysis of the wind field after a land-sea transition,
2. analysis of physical processes in the Westerschelde by a source term analysis,
3. verification of SWAN against high quality field measurements,
4. calibration of SWAN against growth curves from literature.

Each of these tasks will be further outlined below.

2.2 Wind modelling after a land-sea transition

It is well known that the wind profile after a land-sea transition varies with fetch. A first study to this effect has been performed by Taylor and Lee (1984) who developed simple guidelines to compute the spatial variation of the wind speed after a land-sea transition. In the present study, attention will also be paid to the role of atmospheric stability on the variation of wind speed with fetch. To that end the effect of land-sea temperature differences on the wind profile have been investigated.

2.3 Physical processes

From various studies it is known that SWAN is capable of reproducing growth curves for more or less academic situations, e.g. Lake George, or a rectangular basin. When the SWAN is applied in the Westerschelde, however, the results deviate from the expectations and generally accepted growth curves. Preliminary computations indicate that SWAN under predicts the wave period (e.g. peak period, mean wave period). These deviations may result from the following effects, some of which may also occur simultaneously:
- wave decay in opposing winds,
- swell-wind sea interactions in the Westerschelde estuary,
- numerical effects of wave propagation and refraction due to the complicated and irregular bottom topography, and
- wave current effects.

To investigate the above effects, the following subjects will be addressed:

- the effect of including alternative source functions for wave growth by wind and whitecapping dissipation,
- the effect of swell on the evolution of the wave field, and
- the effect of non-linear quadruplet interactions on the growth of young waves.

The effect of currents on the development of the wave field will not be part of this study.

Alternative source functions

The growth of wind waves is the result of a balance between energy input by wind, dissipation by whitecapping and a transfer of wave energy between spectral components by non-linear wave-wave interactions. In the present version of SWAN (30.75) the main source functions for wind input, whitecapping dissipation and nonlinear wave-wave interactions are similar to those included in the finite depth version of the WAM model (WAMDI, 1988). The wind input and whitecapping dissipation are according to (Komen et al., 1984), where as the nonlinear interactions are modelled by means of the Discrete Interaction Approximation (Hasselmann et al., 1985). There is no reason to stick with these source functions and therefore a number of alternative source functions are considered. For deep water conditions three types of source functions are important: wave growth by wind input (Stewart, 1974; Burgers and Makin, 1993 and Janssen 1991), dissipation by whitecapping (e.g. Tolman and Chalikov, 1996) and non-linear quadruplet interactions (Tracy and Resio, 1982, and Lin and Perrie, 1998). For each type of source function differences exist between their results when applied to a particular wave spectrum. Also, it is very important that the spectral source term balance in a wave spectrum is modelled properly. Therefore, a number of these source functions has been compared.

The effect of swell on the evolution of a wave field

On the basis of various studies based on field measurements and theoretical studies it is has been concluded that swell has a damping influence on the growth of wind waves (Young and Sobey, 1985; Donelan, 1987; Masson, 1993). These damping effects may be due to various types of interaction between swell waves and wind generated waves.

One of these interactions are the nonlinear wave-wave interactions between sets of four waves, the so-named quadruplets. These interactions can be studied numerically by using wave models that include a method for computing these interactions. An efficient method is to use a 1-dimensional model that includes a source term for these interactions, but also for source terms for wave growth by wind input and dissipation by whitecapping. In present day operational third-generation wave models, like SWAN and WAM these interactions are approximated with the Discrete Interaction Approximation (DIA). The DIA has been developed by Hasselmann et al. (1985??). This method has many shortcomings and is not suited to study the interaction between swell and young growing waves in detail. Therefore, an exact method has been used to compute the non-linear four-wave interactions.

In literature a number of techniques have been described with which these interactions can be computed for a given energy density spectrum (Tracy and Resio, 1982; Resio and Perrie, 1991; and Rasmussen, 1995). In the present study the model of Resio and Perrie has been used. The results of these exact computations have been compared with the results of the DIA to identify the shortcomings of this method.

The effect of non-linear quadruplet interactions on the growth of very young waves.

The initial growth of waves takes place at very high frequencies. In present day third generation wave models, the prediction of wave growth is affected by numerical techniques. For instance the use of a parametric tail has a large influence. As noted by Banner and Young (1994), the use of a constrained tail affects the growth of the waves considerably. Also, the fact that the start of the parametric tail is fixed in the SWAN model may cause problems. In this respect the SWAN model deviates from the WAM model where a breathing parametric tail is used. Another problem may be related to the performance of the DIA at high frequencies.

2.4 Verification of the SWAN wave model against field data

To get insight in the nature of the prediction error of SWAN when applied to field data, a verification of SWAN has been performed against three sets of measured wave data, viz. Lake George, the IJsselmeer and the Westerschelde.

Presently, the SWAN model is not capable of reproducing growth in the Westerschelde. In particular the peak period is consistently underestimated. A number of methods can be followed to obtain formulations to improve the SWAN model.

For the present study three datasets with field measurement have been used for the verification of SWAN against field measurements. These data have been obtained in Lake George, the IJsselmeer and in the Westerschelde.

2.5 Calibration of SWAN

The calibration of SWAN against measurements is only possible for high quality wave measurements. The available measurements in Westerschelde are not suited for this purpose because important influences play a role which can not be quantified, such as wave-current interaction, swell-sea interaction, inhomogeneous upper boundary conditions, and uncertainties in the wind field. Therefore, SWAN has been calibrated against known growth curves from literature. Proper growth curves are those of Wilson (1965), and of Kahma and Calkoen (1992). The calibration of SWAN has been performed with the ARCADIA package of Digital Hydraulics.

2.6 Outline of the report

The outline of this report is as follows. In Chapter 3 the wind modelling at short fetches is addressed. In this chapter attention will be given to the effects of land-sea boundaries on the horizontal variation of the wind speed at 10 m height, but also on the effects on atmospheric stability on the variation of the wind speed. Thereafter, the effect of a spatially varying wind profile on the fetch-limited growth are investigated and discussed.

In Chapter 4 various existing and alternative source functions are described and there properties discussed. In this study only 'deep' water source terms for wind input, dissipation by whitecapping and nonlinear quadruplet wave-wave interactions are investigated.

The effect of swell on the growth of wind waves is studied in Chapter 5. This chapter consists of 2 parts. First, a literature survey is carried out to the effects of long (swell) waves on the generation of short (wind) waves. Secondly, the numerical effect of the occurrence of a swell peak in a wind wave system on the amount of dissipation is investigated.

Chapter 6 addresses the source term balance at high frequencies (i.e. at frequencies above the peak frequency). Here, special attention is given to the role of the nonlinear quadruplet wave-wave interactions.

In Chapter 7 the results of a sensitivity analysis with the SWAN model are described. Attention is given to the effect of various numerical settings on the wave evolution for a fetch of 25 km and a wind speed of 20 m/s.

The verification of SWAN against three sets of field data is described in Chapter 8. Attention is be given to the performance of SWAN in terms of a number of integral wave parameters, but also to the spectral shape.

In Chapter 9 the methodology and computational results of the calibration of SWAN against known growth curves from literature are described. To that end an experimental version of the SWAN has been used to facilitate the setting of additional parameters in the formulation for whitecapping dissipation and nonlinear quadruplet wave-wave interactions.

Conclusions are formulated in Chapter 10 and recommendations for further studies on the SWAN (and other third generation models) are given in Chapter 11.

3 Wind modelling at short fetches

3.1 Introduction

Presently, most wave model computations for the coastal waters in the Netherlands area are carried out with homogenous wind fields. Various studies, however, indicate that the wind field is spatially inhomogeneous after a land-sea transition. At this transition, the effects of differences in surface roughness and temperature affect the development of the wind field. One of the first studies in which this was realised is the one by Taylor and Lee (1984). They developed a model to describe the evolution of the surface boundary layer for a neutral atmosphere. From their model it follows that the evolution length of this boundary layer depends on wind speed. It is therefore not possible to define a non-dimensional (horizontal) wind profile.

In various studies detailed computations have been performed with three-dimensional atmospheric models. One of such studies was performed by the Deutsche WetterAmt (Kaiser, 1997) for the German Wadden island Norderney.

From other computations it follows that the effect of variations in surface roughness on the wind speed are larger for lower wind speeds than for higher wind speeds. The variation of wind speed should therefore be accounted for in wave modelling.

In Section 3.3 an overview is given of some results of the Taylor and Lee model and the computations performed for the island of Norderney. To study the effects of islands on the wave growth behind an island or land mass, a model was developed by Kudryavtsev (1995). This model, together with some results is presented in Section 3.4. With this model a number of situations have been simulated to obtain (horizontal) wind profiles at the leeward side of an island or land mass. Subsequently, these profiles have been used as input for the SWAN wave model. The results of these computations are presented in Section 3.5.

3.2 Variation of wind speed after a land-sea transition

It is now well known that the wind speed after a land-sea transition is not constant, but varies if one moves further offshore (cf. Young and Verhagen, 1996). This effect has consequences for the scaling of wave growth to non-dimensional parameters. At the shore line a discontinuity exists in the surface roughness from a rough to an aerodynamically smooth roughness. As a result of this discontinuity an internal boundary layer develops within the terrestrial boundary layer. The development of such an internal boundary layer has been investigated by Taylor and Lee (1984) and Smith and MacPherson (1987), and in the context of fetch limited wave growth by Dobson et al., (1989) and Kahma and Calkoen (1992).

Taylor and Lee (1984) have developed a model for the variation of the wind speed at 10 m height. In their model they assume that the thickness of the internal boundary layer δ_i can be represented by:

$$\delta_i = 0.75 z_0 \left(\frac{x}{z_0} \right)^{0.8} \tag{3.1}$$

where x is the fetch length and z0 the roughness length. Using this assumption, it follows that the fractional change in wind speed, $\Delta R = (U(x)-U_u)/U_u$ can be described by:

$$\Delta R = \begin{cases} 0 & \text{for } z \geq \delta_i \\ \dfrac{\ln(z/z_0)\ln(\delta_i/z_{0u})}{\ln(z/z_{0u})\ln(\delta_i/z_0)} - 1 & \text{for } z < \delta_i \end{cases} \tag{3.2}$$

Here, the subscript i refers to quantities at the 'upwind' boundary. In order to apply this model, one needs to know the upwind surface roughness z_{0u} and the roughness along the fetch x, z_0. As is common use, the surface roughness is estimated from the Charnock relationship (Charnock, 1955):

$$z_0 = a u_*^2 / g \tag{3.3}$$

with the Charnock constant a=0.0185 (Wu, 1982). The friction velocity u_* can be estimated from the drag coefficient C_d at 10 m height as given by Wu (1982):

$$u_*^2 = C_{10} U_{10}^2 \tag{3.4}$$

$$C_{10} = \begin{cases} 1.2875 \times 10^{-3} & \text{for} \quad U_{10} < 7.5\, m/s \\ (0.8 + 0.065\, U_{10}) \times 10^{-3} & \text{for} \quad U_{10} \geq 7.5\, m/s \end{cases} \tag{3.5}$$

Young and Verhagen (1996) calibrated this model against recorded wind profiles along Lake George to find optimal values of the upwind surface roughness z_{0u}. They found typical values of z_{0u} in the range 0.1 m to 0.5. The high value corresponds to a light eucalyptus forest whereas the lower value corresponds to grassland with an occasional tree.

A typical variation of the wind speed according to the model of Taylor and Lee is given in Figure 3.1 for the case of an upwind velocity U_u of 10 m/s and an upwind land roughness of 0.1 m. Comparisons between the predictions of the model of Taylor and Lee (1984) and observations have been published by Dobson et al. (1989) and Young and Verhagen (1996). Figure 3.2 is taken from Dobson et al. (1989) and shows the comparison of the Taylor and Lee (1984) guidelines prediction for the fetch variation of offshore winds with the Smith and MacPherson (1987) measured aircraft winds at 50 m- elevation. Figure 3.3 is taken from Young and Verhagen (1996) and it shows three examples of a comparison between the model of Taylor and Lee (1994) and observations in Lake George.

The model of Taylor and Lee (1984) is based on simple assumptions concerning the development of the internal boundary layer after the transition in surface roughness. A totally different approach is based on the use of three-dimensional atmospheric models. Such models are in use at different meteorological institutes and have been used to study the spatial variation of wind speed in detail. An example of such a computational exercise by the 'Deutsche WetterAmt' is shown in Figure 3.4. This figure shows the two-

dimensional variation of the surface wind speed U_{10} over the German Wadden island. The result of one of those computations clearly shows the effect of the difference in surface roughness on the wind speed at 10 m height. Just behind the island the wind speed is smaller compared to the wind speed at the upwind side of the island. As the boundary layer develops the wind speed increases again to the upwind value. A striking feature of these computational results is that the contour lines of constant wind speed more or less reflect the contour of the upwind land-sea transition. This may be an indication that the effect of cross-wind mixing is small and that the development of wind field may be treated as quasi one-dimensional.

The observed variations in wind speed have only been used in wave growth studies by Dobson et al. (1989) and Young and Verhagen (1996). For the analysis of wave growth along the profile they suggest to use a representative wind speed $\overline{U_{10}}$ for the scaling of wave parameters computed as the average along the fetch length investigated:

$$\overline{U_{10}} = \frac{1}{x}\int_0^x U_{10}(x)dx \qquad (3.6)$$

In practice the variation of the wind profile is not always available along the fetch and simple rules must be used to compute appropriate scaled parameters.

3.3 The wind model

Section 3.3 of the report has been contributed by ARGOSS.

3.3.1 Basic description

The model developed by Kudryavtsev and Makin (1996) describes the effects of changing surface conditions on the structure of the downwind planetary boundary layer. This change can be triggered by a change in surface roughness, or by a variation in the surface temperature experienced by the air flow.

Homogeneous surface conditions

When the atmospheric boundary layer is in equilibrium, which means the surface conditions are homogeneous over some distance, the atmospheric is divided into three layers. In the upper layer, the free atmosphere, the air flow is basically geostrophic, and independent of the underlying surface conditions. At moderate to high latitudes the flow patters in this part of the atmosphere are governed by a balance between the Coriolis force and atmospheric pressure gradients.

The layer below the free atmosphere that is affected by the presence of a surface is called the Atmospheric Boundary Layer (ABL). Though the Coriolis force still plays a role in the upper part of this layer, the flow in the ABL can be thought of as being dragged along by the geostrophic flow in the free atmosphere. Hence the vertical structure of the flow in the ABL is largely dependent on the vertical transport of horizontal momentum of the geostrophic flow. The dominant mechanism by which this vertical transport takes place is turbulence.

The intensity of the mixing caused by turbulence is often expressed in terms of an eddy viscosity. Close to the surface, in the so-called Surface Boundary Layer (SBL), the size of the turbulent eddies is limited by the presence of the surface. This causes the eddy viscosity to increase linearly with height, which, in a neutral boundary layer, gives rise to a logarithmic wind profile. In the remaining part of the ABL, the Ekman Boundary Layer (EBL), the eddy viscosity is largely independent of height. Though not as dominant as in the free atmosphere, the Coriolis force does affect the flow in the EBL: the Coriolis force acting on the flow in the EBL is able to rotate the wind vector. This explains why the wind direction close to the surface is usually not the same as the direction of the geostrophic flow overhead.

In the model of Kudryavtsev and Makin, the considerations above lead to a description of the ABL divided into two layers: the SBL and the EBL. For both of these layers appropriate terms in the balance equations for horizontal momentum and mass conservation (continuity) are retained. At the top of the SBL the solutions for the velocity profile are matched. Hence for a given geostrophic wind, stratification and surface roughness, this model is able to calculate the vertical wind profile. In the present context, where we are interested in the effects of steps in the surface conditions on the ABL, this description is called the background situation, i.e. the situation that is reached after an infinite fetch.

Stratification

Apart from the height, the level of turbulence is also affected by the aerodynamic roughness of the surface, and by the stratification of the air flow. The roughness effect is straightforward: a rougher surface represents a greater drag to the air flow, and hence slows down the flow more effectively. The vertical structure of the boundary layer can also be affected by the temperature profile, in which case the air column is said to be stratified.

Due to gravity the air pressure decreases with height. When a parcel of air is moved upwards without exchanging heat with its environment, it will expand and cool down. To account for this effect the concept of potential temperature is introduced. The potential temperature of a dry parcel of air is the temperature it would have when it would be expanded or compressed to a standard atmospheric pressure. The stratification of the atmosphere is said to be neutral when the potential temperature is constant with height. When the potential temperature decreases with height, the air is unstable. In that case air parcels close to the surface are positively buoyant. This means that if they move upwards and expand, they are warmer and hence lighter than their new environment. In the opposite case, when the potential temperature increases with height, the stratification is stable.

The stratification of the atmosphere affects the turbulent structure. In a stable ABL the eddies are inhibited from mixing the fluid effectively, as the vertical mixing process in that case involves lifting heavier air upwards, and replace it with less densely packed air. Hence in a stable atmosphere the flow close to the surface is less effectively coupled with the air flow overhead. This explains why the wind over land seems to weaken at the end of a clear afternoon: when the land and the air immediately above it start to cool down, the air flow becomes stably stratified. This inhibits the turbulence from dragging it along with the geostrophic flow, and hence the wind speed close to the surface decreases. Note that interaction between the stratification and the turbulent mixing is two-way: not only

does the stratification affect the turbulence, but the turbulence also affects the vertical profile of the potential temperature.

The model of Kudryavtsev and Makin (1996) takes into account the stratification of the boundary layer by keeping track of the (potential) temperature profile. This potential temperature profile depends on the temperature of both the surface and the free atmosphere, on the temperature profile upwind and on the vertical turbulent mixing. The effects of vertical gradients in the potential temperature on the turbulence are modelled using empirical similarity functions.

Roughness or temperature jumps

When the surface conditions experienced by the ABL *do* change, for instance at a land-sea boundary, the situation becomes slightly more complicated. It is obvious that the effects of a change in surface roughness or temperature is not affecting the whole ABL instantaneously. The changes in wind speed and turbulence intensity resulting from the change in surface conditions has to be communicated upwards by the turbulence. Hence a new layer comes into existence: the internal boundary layer (IBL). In the IBL the flow is aware of the change in surface conditions, above this layer the old situation persists. The height of the IBL increases with fetch, and the rate at which this happens is a function of the turbulent intensity.

In the model of Kudryavtsev and Makin (1996), the ABL downwind of a change in the surface conditions is divided in three vertical layers. Directly following the change in surface roughness or temperature the IBL divides the SBL into two. As the depth of the IBL is growing with fetch, at some distance it will exceed that of the SBL. From that point on it divides the EBL into two separate layers. The evolution of the depth of the IBL with fetch is governed by a separate equation.

From the above it is clear that if a second change in surface conditions were to occur, this would result in a four layer structure. This situation may be relevant, for instance, to describe the effects of the presence of an island of finite width on the air flow. A first IBL starts to develop when the ABL adjusts to the conditions over the land. After the air flow has crossed the island, a second IBL will start to develop inside the first. Below the effect of the finite width of an island is illustrated with a few examples.

A popular model to estimate the effects of roughness jumps is that of Taylor and Lee (1984). This model differs on two major points from the one used in this study. First of all, the ABL is not divided into two layers. Effectively the whole boundary layer is assumed to consist only of a SBL. The second difference is that Taylor and Lee ignore the effects of stratification. This makes that their model can not handle stratified flows, or jumps in surface temperature.

Aerodynamical roughness of the land and water surface

In general the surface roughness of the land is not homogeneous. Grass land, for instance, is much smoother than a city. However, no detailed surface roughness maps of the area if interest are available for the present study. Therefore we will assume an average aerodynamical roughness of 10 cm. Note that this value is identical to the value used by Young and Verhagen (1996) for the case of a grassy upwind land mass.

The roughness of the water is calculated using the Charnock relation, which assumes that the aerodynamical drag over the water is sustained by gravity waves which are essentially in equilibrium with the local wind (i.e. fully developed). For all but very short fetches this is a good assumption, which is consistent with measurements (e.g. Yelland and Taylor, 1996). For very short fetches, when the wave field is underdeveloped, the Charnock relation probably overestimates the surface roughness. In order not to complicate our model this effect is ignored.

Some workers have hypothesised that the aerodynamical roughness of a developing sea might actually be larger than that of a fully developed sea (e.g. Janssen, 1991). As the air-sea interface is an exceedingly complex system to model, theoretical considerations on this topic do not carry much weight. In any case, the analysis of comprehensive data sets of turbulence measurements over the open ocean (e.g. Yelland and Taylor, 1996) do not show this phenomenon.

Validation

Kudryavtsev and Makin (1996) compare their model with several field experiments. The NIBWAK experiment (Bergstrom et al, 1986) shows that the wind speed drops after it crosses the coastline blowing inland. In the Öresund experiment (Gryning, 1985) it was shown that, flowing from land over the sea, the wind speed can actually drop despite the fact that the water is much smoother than the land. This anomaly can occur when a stable boundary layer develops when warm air flows over cold water.

In the Agulhas Current experiment (Jury, 1994) it was found that water temperature gradients can cause near surface wind jets. This jet over the axis of the warmest water is thought to be caused by secondary circulations set up by enhanced pressure gradients and baroclinic effects. The winds in the core of this jet at 400 to 600 m above the surface exceed the geostrophic wind speed by 50 %. This phenomenon could be reproduced with the numerical model (see Kudryavtsev and Makin, 1996, for further details).

3.3.2 Case studies Westerschelde estuary

The model of Kudryavtsev and Makin is one-dimensional in the horizontal plane, as it essentially follows the development of the ABL along a line parallel to the wind direction. In order to be able to assess the boundary layer effects on the wave growth, a quasi two-dimensional model has been developed for the Westerschelde estuary. This model calculates the wind speed on each point on the Westerschelde in two stages: first the one-dimensional model is run for the appropriate parameters, assuming the geometry of the problem is wind blowing over land of infinite width before it reaches the water (i.e. land-sea). The influence of the fact that the islands involved actually have a finite width of a dozen kilometres or so is assessed in a separate set of calculations below.

The figures below show the distribution of the wind speed, wind stress and wind direction over the Westerschelde for three cases. In all cases the wind speed over land is set at 35 m/s. The cases differ in the surface temperatures that are imposed: in the first case ('spring') the land and the approaching air mass are assumed to be 10 degrees warmer than the water, in the second case ('summer') they are assumed to be the same, and in the third case ('autumn') the water is assumed to be 10 degrees warmer. The

results of the quasi-two dimensional computations is shown in the Figures 3.5 through 3.7 for respectively the warm, cold and neutral island.

In absence of temperature differences ('summer') the changes in the ABL are purely caused by the difference in surface roughness between land and sea. Over the water the wind speed increases from its land value of 35 m/s to over 40 m/s after a fetch of some 20 km. In the spring, with cold water below relatively warm air, a stabely stratified flow develops over the water. For a given geostrophic flow this gives a reduction of the wind speed in the SBL. Hence the increase in wind speed with fetch seen in the 'summer' example is counterbalanced by this stratification effect.

Not surprisingly the opposite is the case in the last example ('autumn'). With warm water below cold air, an unstable ABL will develop with fetch. This increases the effect of the wind speed acceleration by a factor of two compared to the neutral 'summer' case. Note that the rotation of the wind vector can be neglected in all cases.

3.3.3 Development of the ABL behind an island

In the above calculations it is assumed that the ABL approaching the land-sea boundary is fully adjusted to the conditions over land. In the case of Northerly winds over the Westerschelde estuary this assumption does not hold, as the land to the North of the estuary (Walcheren, North and South Beveland) has a width of some 20 to 30 km. In the following examples we will estimate the effects of this finite width on the ABL over the water. This means the geometry of the problem now has two roughness and temperature jumps: the first when the approach flow hits the land, the second when it flows out over the water again. We will examine three cases: a warm island in a cold sea, a cold island in a warm sea and a case where the temperatures are homogeneous.

Case A. Warm island in the cold sea. ($T_{water} = 10^{\circ}$, $T_{land} = 20^{\circ}$ and $T_{air} = 20^{\circ}$)

The stratification of the undisturbed marine Planetary Boundary Layer (PBL) is stable. This means that the vertical gradient of potential temperature above the sea is positive.

As the air flows over the warm island, an unstable internal boundary layer (IBL) develops in the lower part of PBL. During an initial stage the wind speed decreases (due to the larger roughness of the land), but in the course of IBL development the wind speed increases as the role of unstable stratification becomes dominant.

If the width of the island is in the range of fetches where the acceleration of wind speed takes place, then the air flow just behind the island is also accelerated. The spatial scale of enhanced winds (in comparison with the open sea, blue dash-dot line) is defined by the distance at which the new IBL (developing behind the island) attains the IBL height developed over the island. Further (as soon as the new IBL reaches the undisturbed atmosphere) the influence of the island on the wind fields disappears. In Figure 3.8 the island with width 100 km relates to the case when the increase in wind speed is the most pronounced (full red line). The dashed red line shows the wind behind the island with a width of 25 km.

After the island of an infinite width (green line) the marine boundary layer does not relax to its initial state. Far from the upwind coast the stratification of the PBL fully

adjusted to the land is stable, though its air temperature is higher than over the sea. The result is that the IBL developing behind the infinite island is stabely stratified, but stronger than air flow before the island. This explains why the wind speed behind the infinite island is weakened in comparison with one in the open sea.

Case B: Cold island in the warm sea. ($T_{water} = 20°$, $T_{land} = 10°$ and $T_{air} = 10°$)

The stratification of the PBL over the open sea is now unstable. Its vertical structure is typical for a well mixed boundary layer with approximately constant wind speed and temperature with height. Over the island an approximately neutrally stratified IBL develops. Due to the relatively large roughness the 10 m wind speed is decreases from 45 m/s upstream to 35 m/s over land. The results are shown in Figure 3.9. The new IBL which rapidly develops behind the island is unstabely stratified. The 10 m wind speed increases until the IBL height reaches the IBL depth developed above the island. Since this always occurs, the influence of island on wind speed disappears at some distance which is defined by island width.

Case C: Island, sea and free atmosphere are of the same temperature.
($T_{water} = 20°$, $T_{land} = 20°$ and $T_{air} = 20°$)

In this case the peculiarities in wind field behind the island are completely caused by the differences between sea and land roughnesses. The spatial distribution of the wind speed is related with the restoring of PBL vertical structure towards the one which is typical for the sea surface. As it follows from Fig. 3.10 for the island of finite width it is always possible (dashed red line corresponds to island of 25 km width; full red line to 100 km wide island). In the case of infinite island the wind speed (full green line in Fig.3.10) can not return to that values that were in PBL before the island. The reason for this is that the IBL developing behind the island never reaches the PBL depth fully adjusted to the land roughness.

Summary

To assess the influence of changing surface conditions on the development of the atmospheric boundary layer over the Westerschelde estuary a model developed by Kudryavtsev and Makin has been applied. In this model the effects of both changes in surface temperature and in surface roughness are incorporated. For realistic assumptions concerning the expected changes roughness and temperature, it is found that the order of magnitude of both effects are the same.

The effects of both phenomena can be summarised as follows. As the water surface is generally smoother than land, the wind speed in the lower part of the boundary layer tends to increase with fetch over the water. If the water is colder than the air, giving rise to a stabely stratified boundary layer over the water, this effect is counterbalanced. At a very short fetch the wind speed increases, but as the boundary layer becomes more stabely stratified, it decreases again. If, on the other hand, the water is warmer than the air, the increase of wind speed with fetch is enhanced.

3.4 Wind profiles behind an island

The results presented in Section 3.3 show the effect of differences in surface roughness, atmospheric stability and island widths on the spatial variation of the wind field. These results were extended with systematic computations with a one-dimensional model which is able to include an arbitrary island width. To that end a slightly adapted version of the model of Kudryavtsev and Makin has been applied to a number of cases. These cases differ with respect to the wind speed at sea in front of the island, the temperature difference, the roughness of the island and the width of the island. An overview of the various cases is shown in Table 3.1.

Case	U10 (m/s)	$\Delta T=T_{land}-T_{wat}$ (°)	Roughness z_0 (m)	Island width (km)
W20TP5	20	+5	0.1	25
W20TM5	20	-5	0.1	25
W20TN0	20	0	0.1	25
W25TP5	25	+5	0.1	25
W25TM5	25	-5	0.1	25
W25TN0	25	0	0.1	25
W30TP5	30	+5	0.1	25
W30TM5	30	-5	0.1	25
W30TN0	30	0	0.1	25
R25TP5	25	+5	0.05	25
R25TM5	25	-5	0.05	25
R25TN0	25	0	0.05	25
T25TP5	25	+5	0.1	10
T25TM5	25	-5	0.1	10
T25TN0	25	0	0.1	10
F25TP5	25	+5	0.1	50
F25TM5	25	-5	0.1	50
F25TN0	25	0	0.1	50

Table 3.1: Summary of island cases used for the computation of the wind speed behind an island.

The effect of various temperature differences between the sea and land temperature on the variation of the wind speed and temperature is shown in the Figures 3.11 through 3.13 for wind speeds of 20, 25 and 30 m/s. Figure 3.11 shows the results for a warm island with a temperature difference of +5 °C. As can be seen in this figure the wind speeds drops to a value of about 85% as the wind feels the rough land surface. After a few kilometres the wind starts increasing to an equilibrium value. This equilibrium value is not reached since at the end of the island the surface roughness decreases significantly and the wind speed increases very fast to a higher value than the wind speed before the island. This overshoot is visible for all wind speeds. In relative quantities this overshoot is the highest for the lowest wind speed.

Figure 3.12 show the results for a cold island with a temperature difference of -5°. In this case the wind speeds drop to somewhat lower values than the warm island, but they do not increase above the island. After the island the wind speeds increase rapidly with an

overshoot of only a few percent. Similar to the warm island, the overshoot is the highest for the lowest wind speed. Figure 3.13 shows the results for the neutral island where no temperature differences exist. As can be seen the wind speeds drops rapidly to an equilibrium value. Also, after the island the wind speed increases rather rapidly to its original value.

An other way to look at the variation of wind speed and temperature over the island is given in Figure 3.14 in which the results are shown for a wind speed of 25 m/s but for varying temperature differences. As can be seen in this figure, the decrease in wind speed above the island is the largest for the cold island. On the other hand, the overshoot in wind speed is the highest for the warm island.

One of the great uncertainties in the modelling of the sea-land-sea effects on the variation of the wind profile is the choice of land surface roughness. To illustrate the effect of a surface roughness on the development of the wind computations have been made for a surface roughness of 0.05 m and 0.1 m. A comparison of the results is shown in Figure 3.15 for the case of a warm island. As expected the decrease in the wind speeds is lower for the smoother land roughness than for the default roughness of 0.1 m. At the end of the island there is the more pronounced overshoot for the wind speed behind the island. This is due to the fact that the wind has not dropped so much over the island compared to the case with a roughness of 0.1 m. The effect on the temperature profile is only a few percent. For a cold island the results are shown in Figure 3.16. These results are comparable with the results for the warm island. In contrast to the warm island, the differences in the variation of the air temperature are more visible. The results for a neutral island are shown in Figure 3.17. Here, the results show a similar behaviour over the island as the previous two cases. Behind the island, however, the results are almost equal to one another.

The effect of the island width on the development of the wind speed over and behind the island is shown in the Figures 3.18 through 3.20 for a warm, cold and neutral island respectively. Computations have been made for island widths of 10, 25 and 50 km. As shown in Figure 3.18 the effect of a narrow island (10 km) is much smaller than for the wider islands (25 km and 50 km). Only for the wider islands an overshoot in wind speed is visible. It can also be seen that over the island the curves overlap (at least within the accuracy of the numerical model used to calculate these wind profiles). The results in Figure 3.19 show the results for the cold island. It can be seen that there are hardly any differences in the shape of the variation of wind speed over and behind the island. The only important difference is the fact that for the smaller island the wind speed increases more rapidly than for the wider island. For the neutral island the results are shown in Figure 3.20. For island widths of 10 and 25 km the results are very similar. For the island of 50 km width the wind speed needs more fetch to catch up with the original wind speed at sea.

3.5 The effect of a varying wind field on wave growth

The results of the computations shown in Section 3.4 have been used as input in SWAN wave model computations to assess the effect of a varying wind field on the growth of waves at short fetches. To that end model was set-up based on a one-dimensional modelling of the wave growth over a fetch of 25 km. Computations were carried with a frequency range of 0.03 - 1.0 Hz, 36 directions over the full circle and default numerical

settings. In all computations the spatial step was 50 m. The wind speed along the fetch was given at intervals of 100 m.

Results of the computations are all given in comparison with a constant wind speed of 25 m/s. Not all results of the wave model computations are shown here. Only the most relevant are presented here.

Figure 3.21 shows the results for a warm island with a width of 25 km. The figure shows the variation of the significant wave height and mean wave period T_{m01} for the varying wind speed and a constant wind speed. Also shown are the differences between the two cases. It can be seen at a fetch of 1 km the significant wave heights is somewhat smaller for the varying wind than for the constant wind. For a fetch of 25 km, however, the opposite occurs at which point the significant wave height is about 3 % higher. The effect on the mean wave period is negligible.

The results for the cold island are shown in Figure 3.22. Here it can be seen that the significant wave height is about 4% lower for the varying wind than for the constant wind. The mean wave period is about 3% lower for the varying wind than for the constant wind. For the neutral island the results for the significant wave height are shown in Figure 3.23 and they are comparable with the cold island whereas for the mean period the results are almost similar.

The effect of a different land roughness on the wave evolution behind the island is shown in Figure 3.24 for a roughness of 0.05 m and one of 0.1 m. The effect on the significant wave height is rather small, up to 2 %. For the mean wave period the effect is negligible.

The effect of the island width on the wave evolution behind the island is shown in Figure 3.25 for a wind speed of 25 m/s and a warm island. The results show that the significant wave height is somewhat higher for the wider island than for the smaller island. This is in line with the results shown in Figure 3.18 where the highest overshoot in wind speed occurs for an island width of 50 km. Results for a cold island are shown in Figure 3.26 where the highest wave height occur for the most narrow island. This is consistent with the results shown in Figure 3.19.

Finally, a sensitivity run was performed for two constant wind speeds, one of 23 m/s and one of 25 m/s. The reason to perform these computation is that in many cases a constant wind speed is used and that this wind speed is usually taken from a measuring station located some distance offshore. As shown in many previous plots, the wind speed just behind the island is up to 30% smaller than the 'open sea' wind speed, and it is likely that one might take such a low wind speed to be used for the whole fetch. A better approach might be to take the average wind speed behind the island as indicated by Dobson et al. (1989) and Young and Verhagen (1996). The results of the wave model computations is shown in Figure 3.27. They show that the differences in significant wave height and mean wave period are higher than the differences between a constant and a varying wind field.

3.6 Discussion of results

In this Chapter results are shown of the wind and wave modelling at short fetches for various types of atmospheric stability, wind speeds, land surface roughness and island width. The atmospheric stability is included on the basis of the temperature difference between land and water. Five differences have been included in the analysis, -10°,-5°, 0°, +5° and +10°. This range is wide enough to cover most of the differences occurring in nature. This was confirmed by an analysis of observed temperature difference which have occurred recently during winter storms in the Westerschelde. Only when a polar low reaches the Netherlands a higher difference in temperatures may occur. For design conditions, however, it is expected that the temperature difference is at most 5°. The island widths used in this study cover the range of effective widths occurring in the south west of the Netherlands.

The results of the wind model show different results for the various cases with respect to the atmospheric stability. The most surprising result is the overshoot in wind speed for the cases of a warm island. Unfortunately, no validation data are available to verify this behaviour. For the cold and neutral island the results are more in line with the widely used model of Taylor and Lee (1984). Because of this lack of data it is recommended that future measurement campaigns include a number of measuring stations along the fetch which are able to measure both wind speed and air temperature.

The effects on the resulting growth curves for the wave evolution behind the island are not large, they remain in the order of 5%. These differences are smaller than the error for taking a 'wrong' wind speed differing only 2 m/s. This is a surprising results and it implies that a significant improvement in wave modelling can not be achieved by a detailed modelling of the wind field over and behind an island, because larger errors are made by choosing an incorrect wind speed.

The results of the one-dimensional computations show that at present it is not worthwhile to set-up a quasi two-dimensional model for computing the horizontal variation of the wind speed over and behind island because of the large uncertainties in surface roughness over the island but also because it has only a small effect on the wave evolution at short fetches.

The effect of atmospheric stability has also been addressed by Voorrips et al. (1995) who studied the related effect of atmospheric stratification on the growth of wind waves. In their study they used the WAM model (WAMDI, 1988) in fetch-limited situations. For a given wind speed at 10 m height, they found that the significant wave height was increased by about 10% in unstable situations compared to neutral situations. These findings are in line with the results of Kahma and Calkoen (1992).

4 Source functions for wind wave models

4.1 Introduction

The source functions that are presently implemented in the SWAN wave model are mainly taken from the WAM model (WAMDI, 1988), and where necessary adapted for shallow water. This holds for the source functions for wind input, dissipation by whitecapping, non-linear quadruplet interactions and bottom friction. The SWAN model includes two source function that have specially been formulated for water of finite depth. These are the source term for depth-limited wave breaking (based on the formulation of Battjes-Janssen, 1978) and the source term for triad wave-wave interactions (Eldeberky and Battjes, 1995).

In this Chapter a number of existing (i.e. already implemented in SWAN) and alternative source functions for wave growth by wind, whitecapping dissipation and non-linear quadruplet interactions are described. Part of this description have also appeared in the SWAN user manual (Delft University of Technology, 1998), Van Vledder (1990), Van Vledder et al. (1994) and in DELFT HYDRAULICS (1994a,b). Source functions for finite-depths are not included in this summary, although some remarks are made about the depth scaling in the application of the Discrete Interaction Approximation for finite depth.

Since this study is about the source terms for the SWAN model, all equations are (re)written to the convention used in the SWAN manual. This implies that spectra are given in term of the intrinsic radian frequency σ and direction θ.

4.2 Wind input

4.2.1 Introduction

The first systematic studies of the generation of waves by the action of the wind date back to the beginning of the twenties century. After some unsuccessful theories describing the growth of wind waves (e.g. Jeffreys, 1925), considerable knowledge was made by Phillips (1957) and Miles (1957) in two complementary papers describing the principles of the flux of momentum and energy from the atmosphere to the wave field.

In the growth of wind waves two phases can be distinguished. In the first phase the waves have no effect on the wind profile, whilst they do affect the wind profile in the second phase. The first phase was studied by Phillips (1957), who found that the energy of a wave component increases linearly with time. The second phase was analysed by Miles (1957) who found that the rate of input of energy of a wave component is proportional to the energy density of that wave component, such that the energy density growth rate is much larger than the linear growth rate of the waves.

In wave modelling two wind input source functions can be distinguished, a linear growth term and an exponential growth term. These two term refer to the above mentioned work of Phillips and Miles respectively. The growth of the energy density of a wave component is usually expressed as:

$$\frac{\partial E}{\partial t} = \alpha + \beta E \tag{4.1}$$

where α is the linear growth term and βE the exponential one. In most spectral wave prediction models only the exponential term is used. In a numerical wave model the source term for wind input is given by:

$$S_{in}(\sigma,\theta) = \alpha + \beta E(\sigma,\theta) \tag{4.2}$$

in which α describes linear growth and βE exponential growth. It should be noted that the SWAN model is driven by the wind speed at 10 m elevation U_{10} whereas the computations use the friction velocity u_*. For the WAM Cycle 3 formulation in SWAN the transformation from U_{10} to u_* is computed with the equations given by Wu (1982), see the Equations (3.4) and (3.5).

In the following a number of source terms for wind input will be described. First, a description is given of a source term for linear wave growth. Thereafter a number of formulations are given for exponential growth.

4.2.2 Linear growth term

Cavaleri and Malanotte Rizzoli (1981) have proposed an expression for the linear growth of wind waves. They refer to an expression of α given by Phillips (1957) as:

$$\alpha(\vec{k}) = \frac{\pi}{\rho_w^2 g^2}\sigma^2 P(\vec{k},\sigma) \tag{4.3}$$

where ρ_w is the density of water, g the acceleration due to gravity, $\vec{k}$ the wave number vector, and where $P(k,\sigma)$ the atmospheric turbulent pressure spectrum. Cavaleri and Malanotte Rizzoli (1981) suggest an approximate expressions for $P(k,\sigma)$ given by Phillips (1960, pp. 123-125, Eq. 4.6.4) which is based on measurements of Willmarth and Woolridge (1962) in a wind tunnel. The resulting expressions for $P(k,\sigma)$ and $\alpha(k)$ are:

$$P(\vec{k},\sigma) = \frac{80\rho_a}{\pi k^2 \sigma} C_d^2 U^4 \tag{4.4}$$

and

$$\alpha(\vec{k}) = 80\frac{\rho_a^2}{\rho_w^2}\frac{\sigma}{g^2 k^2} C_d^2 U^4 \tag{4.5}$$

in which $C_d = 0.0012$ is the drag coefficient and U the wind speed component in the direction of the wave component. Expression (4.5) can be written in terms of the rate change of energy density on a (k,θ) or (f,θ) grid:

$$\alpha(k,\theta) = \alpha(\vec{k})k = \frac{\rho_a^2}{\rho_w^2}\frac{80}{g^2 k}C_d^2 U^4 \tag{4.6}$$

and

$$\alpha(f,\theta) = \alpha(\vec{k})\frac{2\pi k}{c_g} = (4\pi)80\frac{\rho_a^2}{\rho_w^2}g^{-2}u_*^4 \tag{4.7}$$

With $c_g = \sigma/(2k)$, $\rho_a/\rho_w = 1.3\times10^{-3}$ and $u_*^2 = C_d U^2$, Eq. (4.5) can be written as:

$$S_{lin}(\sigma,\theta) \approx 1.70\times10^{-3} g^{-2} u_*^4/(2\pi) \tag{4.8}$$

with u_* the friction velocity. Expression (4.8) has been modified by Tolman (1992) to eliminate growth for frequencies lower than σ_{PM} (i.e. the equilibrium radian peak frequency for a fully developed sea state according to Pierson and Moskowitz, 1964):

$$\alpha = \frac{1.5\times10^{-3}}{g^2 2\pi}\left[u_* \max(0,\cos(\theta-\theta_w)\right]^4 \times H \tag{4.9}$$

with H a filter function given by:

$$H = \exp(-(\sigma/\sigma^*_{PM})^{-4}) \quad \text{with} \quad \sigma^*_{PM} = \frac{0.13g}{28u_*}2\pi \tag{4.10}$$

In which $f_{PM} = 1/(2\pi)g/(28u_*)$.

The filter for low frequencies is added to this formulation to ensure that the range of the discrete frequency grid to low frequencies does not influence mean wave parameters at initial growth and hence initial growth itself. This is because initial growth takes place at high frequencies. The linear source term is relevant only for truly initial growth, because it is several orders of magnitude smaller than the exponential growth rate.

4.2.3 Exponential growth terms

The Snyder et al. model

An expression for the exponential growth term is given by Snyder et al. (1981). It has been re-scaled with the friction velocity u_* by Komen et al. (1984):

$$S_{in}(\vec{i}) = \max\left\{0,\ \frac{1}{4}\frac{\rho_a}{\rho_w}\left[\frac{28u_*}{\sigma/k}\cos(\theta-\theta_w)-1\right]\right\}\sigma E(\vec{i}) \tag{4.11}$$

in which ρ_a and ρ_w are the densities of air and water respectively, u_* is the friction velocity, σ is the intrinsic radian frequency, k is the wave number, θ and θ_w are the direction of the wave component and wind respectively, and $E(\vec{i})$ is energy density. The friction velocity u_* is computed from the wind speed at 10 m height U_{10} using Eqs. (3.4) and (3.5).

Boundary-layer model of Burgers and Makin

Burgers and Makin (1993) have developed a model which parameterizes the growth of wind waves by the action of the wind. The model is formulated in terms of the Miles β parameter, defined as:

$$\beta = \frac{1}{\sigma E}\frac{\partial E}{\partial t} \tag{4.12}$$

with σ the intrinsic frequency and E the energy density of a wave component. The computation of the parameter β is based on the ratio u_λ / c, with u_λ the wind velocity on height λ and c the phase velocity, and on the equivalent drag coefficient c_0.

The parameter β is computed according to:

$$\begin{aligned}
10^4\beta &= -a_1(u_\lambda/c)^2 - a_2 && \text{for} \quad u_\lambda/c < a_3 \\
10^4\beta &= -a_4(u_\lambda/c) && \text{for} \quad a_3 < u_\lambda/c < 0 \\
10^4\beta &= b_1(u_\lambda/c)^2 - b_2(u_\lambda/c) && \text{for} \quad 0 < u_\lambda/c < b_3 \\
10^4\beta &= b_4(u_\lambda/c) - b_5 && \text{for} \quad b_3 < u_\lambda/c < b_6 \\
10^4\beta &= b_7(u_\lambda/c - 1)^2 + b_8 && \text{for} \quad b_6 < u_\lambda/c
\end{aligned} \tag{4.13}$$

with

$$\begin{aligned}
a_1 &= 0.25 + 395c_0 \\
a_2 &= 0.35 + 150c_0 \\
a_3 &= -1.0 \\
a_4 &= a_1a_3 + a_2/a_3
\end{aligned} \tag{4.14}$$

and

$$
\begin{aligned}
b_1 &= 0.30 + 300c_0 \\
b_2 &= b_1 b_3 \\
b_3 &= 1.075 + 75c_0 \\
b_4 &= \left(b_7 (b_6 - 1)^2 + b_8\right) / (b_6 - b_3) \\
b_5 &= b_3 b_4 \\
b_6 &= 1.2 + 300c_0 \\
b_7 &= 0.35 + 240c_0 \\
b_8 &= -0.06 + 470c_0
\end{aligned}
\qquad (4.15)
$$

The directional dependence of the wind input function is parameterised as follows:

$$\beta = \beta(u_\lambda \cos(\theta)/c, 0°) \quad \text{for } |\theta| \le 60° \text{ and } |\theta| > 90° \qquad (4.16)$$

and

$$\beta = \frac{90° - |\theta|}{90° - 60°}\beta(u_\lambda \cos 60°/c, 0°) + \frac{|\theta| - 60°}{90° - 60°}\beta(u_\lambda / c, 90°) \text{ for } 60° < |\theta| \le 90° \qquad (4.17)$$

with

$$10^4 \beta(u_\lambda / c, 90°) = -(0.2 + 200c_0)(u_\lambda / c) \qquad (4.18)$$

Note that there is a discontinuity for angles close to 90°. Eq. (4.18) predicts a finite value whereas Eq. (4.16) predicts a β value equal to zero. This property of this parameterisation is known with the authors and needs more attention. They note, however, that the effect is small.

The ratio u_λ / c is computed by assuming a logarithmic wind profile:

$$u(z) = \frac{u_*}{\kappa} \ln\left(\frac{z}{z_0}\right) \qquad (4.19)$$

where the local roughness length z_0 follows from Charnock's relation using Eq. (3.3) but with a=0.0144. Based on the definition of the drag coefficient $c_0 = u_*^2 / u_z^2$ we find:

$$\frac{u_\lambda}{c} = \frac{1}{\sqrt{c_0}} \frac{u_*}{c}. \qquad (4.20)$$

Substitution of Eq. (4.20) into Eq. (4.19) yields:

$$\frac{u_\lambda}{u_*} = \frac{1}{\sqrt{c_0}} = -\frac{1}{\kappa} \ln\left(\frac{a u_*^2}{g\lambda}\right). \qquad (4.21)$$

Another assumption is that the height of the boundary layer is equal to the wave length L of the wave with phase velocity c. With

$$\lambda = L = \frac{2\pi}{k}. \tag{4.22}$$

For deep water Eq. (4.22) cab rewritten as $\lambda = 2\pi c^2/g$ and Eq. (4.21) can be written as

$$\frac{1}{\sqrt{c_0}} = -\frac{1}{k}\ln\left[\frac{a}{2\pi}\left(\frac{u_*}{c}\right)^2\right]. \tag{4.23}$$

The friction velocity u_* is computed from the wind speed at 10 m U_{10} height using the Eqs. (3.3) and (3.4) given by Wu (1982).

Janssen formulation

In the theory of Janssen (1991), the Miles "constant" β is estimated from the non-dimensional critical height λ:

$$\begin{aligned} \beta &= \frac{1.2}{\kappa^2}\lambda \ln^4 \lambda \qquad \text{for} \quad \lambda \le 1 \\ \lambda &= \frac{gz_e}{c^2}e^r \\ r &= \frac{\kappa c}{|u_* \cos(\theta - \theta_w)|} \end{aligned} \tag{4.24}$$

where κ is the Von Karman constant, equal to 0.41 and z_e is the effective surface roughness. If the non-dimensional critical height λ>1, the Miles constant β is set equal to 0. Janssen (1991) assumes that the wind profile is given by:

$$U(z) = \frac{u_*}{\kappa}\ln\left[\frac{z + z_0 - z_e}{z_e}\right] \tag{4.25}$$

in which $U(z)$ is the wind speed at height z (10 m in the SWAN model) above the mean water level, z_0 is the roughness length. The effective roughness length z_e depends on the roughness length z_0 and the sea state through the wave induced stress τ_w and the total surface stress τ:

$$z_e = \frac{z_0}{\sqrt{1 - \tau_w/\tau}} \qquad \text{and} \qquad z_0 = \hat{a}\frac{u_*^2}{g}. \tag{4.26}$$

The second of these two equations is a Charnock-like relation in which $\hat{a}$ is a constant equal to 0.01. The wave stress vector τ_w is given by:

$$\vec{\tau}_w = \rho_w \int_0^{2\pi} \int_0^{\infty} \sigma\beta E(\sigma,\theta) \frac{\vec{k}}{k} d\sigma d\theta \qquad (4.27)$$

The value of U_* can be determined for a given wind speed U_{10} and a given wave spectrum $E(\sigma,\theta)$ from the above set of equations. In the SWAN model the iterative procedure of Mastenbroek et al. (1993) is used.

Stewart formulation

Stewart (1974) combined general theoretical arguments with some basic experimental knowledge on turbulence over rough surfaces, and proposed the following expression to β:

$$\beta = 1.2 \frac{\rho_a}{\rho_w} \sqrt{C_0} \left| \frac{u_\lambda}{c} \right| \left(\frac{u_\lambda}{c} - 1 \right) \qquad (4.28)$$

in which C_0 is a drag coefficient. It is noted here that Stewart did not address directional aspects in his proposed formulation for wind input. For application in a wave model, the factor β is multiplied with the cosine of the angular difference.

Tolman and Chalikov

Tolman and Chalikov (1996) have derived an expression for the wind input source function. This source function is very similar to the one presented by Burgers and Makin (1993). Because of this strong similarity it is not reproduced here.

4.2.4 Comparison of source functions

For a number of target spectra a comparison has been made of the various wind input source functions. In Figure 4.1 a comparison is made of the wind input source function as given by Komen et al. (1984), Janssen (1989,1991), Burgers and Makin (1993) and Stewart (1974). The target spectrum is a JONSWAP spectrum with a peak frequency of 0.5 Hz and a peak enhancement factor of 3.3. The wind speed is 20 m/s. As can be seen in this figure the shape of wind input source functions is very similar, whereas the main difference is in the magnitude of the various formulations. The highest input is for the Burgers and Makin term.

For a JONSWAP spectrum with a lower peak frequency of 0.2 Hz, the shapes are not similar. Especially in the high frequency range differences occur. It is noted that for this spectrum the Burgers and Makin formulation is very similar to the expression given by Stewart, see Figure 4.2.

For a fully grown Pierson Moskowitz spectrum, the results are given in Figure 4.3. As can be seen in this figure, the Janssen term gives (relatively) a lot of wave growth on the forward face of the spectrum in the region where the swell waves are travelling faster (based on the phase speed) than the wind. The formulation of both Burgers and Makin (1993) and Stewart (1974) have a negative wind input for these swell waves.

Finally, the wind input source functions have been computed for the case of an opposing wind of 20 m/s for a fully grown Pierson-Moskowitz spectrum with a peak period of 20 s. The results of the comparison are shown in Figure 4.4. As can be seen in this figure, the Komen source is equal to zero, as expected. Strangely enough the Janssen formulation gives a positive wind input for the lowest frequencies. (This may be due to an incorrect equation or evaluation of the equations). The Burgers and Makin source term has a relatively large negative wind input, implying that momentum is transferred from the waves to the atmosphere. The Stewart source term gives a small negative wind input for the lowest frequencies and a small positive wind input for the other parts of the spectrum. It is noted, however, that the directional dependence of the wind input in the Stewart formulation is not based on any findings of Stewart. It is therefore doubtful if they are correctly implemented in the model use for this study.

4.3 Dissipation by whitecapping

The quantitative description of the dissipation of wave energy by wave breaking is very difficult, because it is a non-linear process with very short time scales. The precise form of the dissipation source function is not (yet) known. A first theoretical study of whitecapping and its effect on the energy spectrum was given by Hasselmann (1974). He assumed that dissipation of wave energy is related to the wave number spectrum in a quasi-linear manner:

$$S_{ds}\left(\vec{k}\right) = -\Psi_d \omega^2 E\left(\vec{k}\right) \tag{4.29}$$

in which Ψ_d is a constant for a given spectrum. It depends on integral spectral parameter, such as the average wave steepness.

Expression (4.29) was studied numerically by Komen et al. (1984) in an investigation of the structure of the energy balance equation of a fully developed wave spectrum. For deep water they proposed the following expression:

$$S_{ds}(\vec{i}) = -C_{ds}\omega_m \left(\frac{\omega}{\omega_m}\right)^2 \left(\frac{\tilde{\alpha}}{\tilde{\alpha}_{PM}}\right)^2 E(\vec{i}) \tag{4.30}$$

in which $\vec{i}$ represents the spectral space, and with $C_{ds} = 3.33 \times 10^{-5}$ a tuneable proportionality coefficient and in which ω_m is the mean radian frequency defined by:

$$\omega_m = 2\pi \frac{\int f\, E\left(\vec{i}\right) d\vec{i}}{E_{tot}} \tag{4.31}$$

with E_{tot} the total wave energy:

$$E_{tot} = \int E(\vec{i})\, d\vec{i} \tag{4.32}$$

The term $\tilde{\alpha}$ is a measure for the integral squared wave steepness, defined as:

$$\tilde{\alpha} = E_{tot}\omega_m^4 / g^2 \tag{4.33}$$

and $\tilde{\alpha}_{PM} = 4.57 \times 10^{-3}$ is the integral squared wave steepness for a Pierson-Moskowitz spectrum.

Expression (4.30) is used in the EXACT-NL model. For use in the WAM model (WAMDI, 1988) expression (4.30) has been slightly modified for reasons of numerical stability and re-scaling:

$$S_{ds}(\vec{i}) = -C\hat{\omega}\left(\frac{\omega}{\hat{\omega}}\right)^2\left(\frac{\hat{\alpha}}{\hat{\alpha}_{PM}}\right)^2 E(\vec{i}) \tag{4.34}$$

in which:

$$\left.\begin{aligned} C &= 2.36 \times 10^{-5} \\ \hat{\alpha}_{PM} &= 0.66\,\tilde{\alpha}_{PM} = 3.02 \times 10^{-3} \\ \hat{\alpha} &= E_{tot}\hat{\omega}^4 / g^2 \\ \hat{\omega} &= \left[\int \frac{1}{\omega} E(\vec{i})\, d\vec{i} \,/\, E_{tot}\right]^{-1} \end{aligned}\right\} \tag{4.35}$$

The factor 0.66 in Eq. (4.35) arise because of the fact that another definition is used for the mean radian frequency. This value is equal to the ratio of $\hat{\omega} / \omega_m \approx 0.9$ for a mean JONSWAP spectrum to the fourth power. Thus $\alpha_{PM} \approx (\omega / \omega m)\ \alpha_{PM}$.

For application in intermediate-water depths, the expression of Komen et al. (1984) was re-formulated by the WAMDI group (1988). Their modified equation reads:

$$S_{ds}(\vec{i}) = -C\hat{\omega}\frac{k}{\hat{k}}\left(\frac{\hat{\alpha}}{\hat{\alpha}_{PM}}\right)^2 E(\vec{i}) \tag{4.36}$$

in which

$$\left.\begin{aligned} \hat{\alpha} &= E_{tot}\hat{k}^2 \\ \hat{k} &= \left[\int \frac{1}{\sqrt{k}} E(\vec{i})\, d\vec{i} \,/\, E_{tot}\right]^{-2} \end{aligned}\right\} \tag{4.37}$$

For deep water, expression (4.36) transforms to expression (4.34). Note that $\hat{k}$ is computed similarly as $\hat{\omega}$.

Recently, Janssen (1991) proposed a source term which should be used in combination with his quasi-linear source term for wind input.

$$S_{ds}(\vec{i}) = -C_{ql}\hat{\omega}\,\hat{k}^4 E_{tot}^2 \left((1-\delta)\frac{k}{\hat{k}} + \delta\left(\frac{k}{\hat{k}}\right)^2 \right) E(\vec{i}) \qquad (4.38)$$

with $\delta = 0.5$ and $C_{ql} = 4.5$.

Tolman and Chalikov (1996) have also derived a source function for the dissipation by whitecapping in a wind wave spectrum. In their model, a large number of parameters have been fitted to data generated in extensive numerical experiments. Due to this large number of fitted parameters, this model seems to generally applicable. A strong point, however, of their method is the fact that they make a distinction between low and high frequency dissipation. This is a step in the good direction to make the dissipation less sensitive to the occurrence of swell in a wind wave system.

It is found that the magnitude of the whitecapping dissipation depends strongly on the mean wave frequency, which in turn is quite sensitive to the occurrence of a swell system. To illustrate this sensitivity, three sets of computations have been made. In each computation a double peaked wave spectrum is used: a wind sea peak at 5 s and a significant wave height of 1 m, and a swell peak at 15 s, with a varying significant wave height of 0.1 m, 0.2 m and 0.5 m respectively.

In Figure 4.5 the whitecapping dissipation is computed for a wind sea spectrum, a swell spectrum with Hs=0.1 m and a combined wind sea/swell wave system. It can be seen that the whitecapping of wind sea part reduces slightly in the case that a low swell is present. In the case of a moderate height swell system (Hs=0.2) the effect is more pronounced, see Figure 4.6. Finally, for a swell system of equal height with the wind-sea part, i.e. with Hs=1 m, the effect on the whitecapping dissipation of the wind sea part of the spectrum is dramatic, see Figure 4.7, the whitecapping for the wind-sea part of the spectrum almost vanishes. This implies that the net source function will increase and that wave growth will be enhanced in the case of a combined sea/swell system.

This strong dependence is not as can be expected on the basis of physical arguments. On the contrary, as will be shown in Chapter 5, the presence of swell will weaken the growth of wind waves. This effect is probably a numerical artefact, and should be replaced by a better and more stable method, such that the presence of swell does not affect the mean wave frequency of the wind sea part of the spectrum.

4.4 Non-linear quadruplet wave-wave interactions

4.4.1 Theoretical background

To first order, ocean waves can be regarded as the superposition of free and independent spectral components. At higher order, however, there is an interaction between spectral components resulting in a transfer of energy, as shown by Phillips (1960). These interactions were described in detail in a series of papers by Hasselmann (1962, 1963a, b). He found that a set of four waves, called a tetrad or quadruplet, could exchange energy when the following resonance conditions are satisfied:

$$\vec{k}_1 + \vec{k}_2 = \vec{k}_3 + \vec{k}_4 \tag{4.39}$$

$$\omega_1 + \omega_2 = \omega_3 + \omega_4 \tag{4.40}$$

in which ω_i is the radian frequency and k_j the wave number (j=1,...4). For deep water the frequency and the wave number are related via the dispersion relations $\omega^2 = gk$. The four interacting wave numbers that are involved in such an interaction are called quadruplets.

Hasselmann (1963a) described the nonlinear interactions in terms of their action density, n, defined as the ratio of the energy density divided by the radian frequency. The rate of change in action density at a certain wave number k_1 due to all quadruplet interactions involving this wave number is given by:

$$\begin{aligned}\frac{\partial n_1}{\partial t} = {} & \iiint G\left(\vec{k}_1,\vec{k}_2,\vec{k}_3,\vec{k}_4\right)\times\delta(\omega_1+\omega_2-\omega_3-\omega_4)\times\delta(\vec{k}_1+\vec{k}_2-\vec{k}_3+\vec{k}_4) \\ & \times\left[n_1n_3(n_4-n_2)+n_2n_4(n_3-n_1)\right]d\vec{k}_1d\vec{k}_2d\vec{k}_3\end{aligned} \tag{4.41}$$

where $n_i = n(\vec{k}_i)$ is the action density at wave number $\vec{k}_i$ and G is a complicated coupling coefficient. The delta functions in Eq. (4.41) ensure that contributions to the integral only occur for quadruplets that satisfy the resonance conditions. The integral expression (4.41) is also known as the Boltzmann integral for wind waves, in analogy to similar expression used in theoretical physics to describe the rate of change of particle density distributions in a system of interacting particles. The nonlinear energy transfer conserves both the total energy, wave action and momentum of the wave field. The effect of the nonlinear interactions is to redistribute the energy within a spectrum. The main effect of the nonlinear interaction is that its stabilises the spectral shape and causes a downward shift of the peak frequency (Young and Van Vledder, 1993).

4.4.2 Exact computation of nonlinear quadruplet interactions

The numerical evaluation of the Boltzmann integral is quite difficult for a number of reasons. First, the computation time required to solve the Boltzmann integral is very large due to the six-fold integral, and because of the complexity of the coupling coefficient. Numerous techniques have been proposed for the solution of the Boltzmann

integral. An overview of various techniques has been given by Young and Van Vledder (1993). In this report only a few methods are described.

Hasselmann and Hasselmann (1981) developed a symmetric integration technique using the principle of detailed balance. Further, savings were made by using various symmetries in the interaction coefficient. Additional savings were made by pre-filtering the integration domain. Hasselmann and Hasselmann (1981) show that only 5-10% of the interacting wave number quadruplets contribute 95% of the nonlinear transfer. The result is a decrease in computation time by a factor of up to 100. The symmetric integration technique has been included in the one-dimensional model EXACT-NL (Hasselmann and Hasselmann, 1985a).

The EXACT-NL model has been used in various investigations of physical processes. Komen et al. (1984) used this model to investigate the existence of a fully developed wind sea, and were able to derive a coefficient for the whitecapping dissipation formulation.

Another method to solve the Boltzmann integral was proposed by Webb (1978) involving a transformation of the six-fold Boltzmann integral into a series of line integrals around 'egg-shaped' loci. These loci result from the removal of the delta functions. Although this operation simplifies the mathematical formulation of the problem, the number of possible loci along which line integrals need to be performed is enormous. Hence, the technique is still computationally expensive and not suitable for application in operational wave prediction models.

For deep water, the Webb method can speeded up considerably since then loci are geometrically similar. In addition, the line integrals for different loci could be related to each other using a simple scaling relation. To take maximum advantage of the form of the deep water dispersion relation and the similarity scaling of the loci, a computational wave number grid of the form $k_i = ak_{i-1}$ is required. This scaling technique was developed by Tracy and Resio (1982) and Resio and Perrie (1991). The resulting method was also used by Young and Van Vledder (1993) in their study to the role of nonlinear wave-wave interaction in wind wave evolution.

Although the solution of technique of Webb, Tracy and Resio does not take advantage of the symmetries, inherent in the Boltzmann integral, it is comparable in computational effort to the EXACT-NL model.

Still, the exact methods are not practical for application in operational wave prediction models like WAM and SWAN. To that end various approximations have been developed, varying from narrow peak approximations to the Discrete Interaction Approximation (DIA) (Hasselmann et al., 1985). The main feature of the DIA is the fact that this method uses the same number of degrees of freedom as the discretized spectrum. The development of the DIA triggered the development of the first third generation wave prediction model WAM (WAMDI, 1988). The DIA is also used in the SWAN wave model (Holthuijsen et al., 1993).

4.4.3 The Discrete Interaction Approximation

In recent years an approximation to the EXACT-NL method has been developed which is known as the Discrete Interaction Approximation (DIA) . This approximation is based on the principal feature of the nonlinear transfer that this transfer is already fairly well reproduced by interactions between only a few closely neighbouring wave numbers (Hasselmann et al., 1985). In this approximation the nonlinear transfer is computed by considering the interactions between only one type of wave number quadruplet and its mirror-image of an intermediate-range interaction configuration.

In each of these quadruplets $\left(\vec{k}_1, \vec{k}_2, \vec{k}_3, \vec{k}_4\right)$ two wave numbers are equal $\vec{k}_1 = \vec{k}_2 \equiv \vec{k}$. The other two wave numbers $\vec{k}_3$ and $\vec{k}_4$ are of different magnitude and lie at an angle (denoted by θ_3 and θ_4 respectively) to the wave number $\vec{k}$, as required by the resonance conditions (2.1). The second configuration is obtained from the first by reflecting the wave numbers $\vec{k}_3$ and $\vec{k}_4$ around the $\vec{k}$ -axis.

Satisfactory agreement with the computations with the EXACT model was obtained by Hasselmann et al. (1985) with the configuration in which the frequencies of the interacting wave numbers are related by:

$$f_1 = f_2 = f \tag{4.42}$$

$$f_3 = f^+ = (1+\lambda)f \tag{4.43}$$

$$f_4 = f^- = (1-\lambda)f \tag{4.44}$$

with $\lambda = 0.25$. The agreement was not only good for the growth curves of the dimensionless total energy E^* and mean wave frequency f_m^*, but also with respect to the phenomenon of overshoot during wave growth.

From the resonance conditions (4.39) and (4.40) the angles θ_3 and θ_4 between the wave number vectors $\vec{k}^+ = \vec{k}_3$ and $\vec{k}^- = \vec{k}_4$ and the central wave number $\vec{k}$ are computed as 11.5° and -33.6° respectively. This wave number configuration is shown in Figure 4.8.

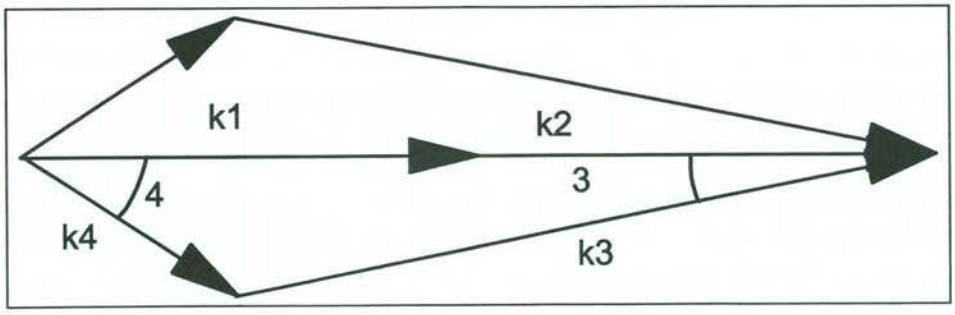

Figure 4.8: Basic wave number configuration of Discrete Interaction Approximation

The rates of change of energy density in a spectrum $E(f,\theta)$ due to the interactions within one wave number quadruplet are given by:

$$\begin{pmatrix} \delta S_{nl} \\ \delta S^{+}{}_{nl} \\ \delta S^{-}{}_{nl} \end{pmatrix} = \begin{pmatrix} 2 \\ -1 \\ -1 \end{pmatrix} C g^{-4} f^{11} \left[E^2 \left(\frac{E^+}{(1+\lambda)^4} + \frac{E^-}{(1-\lambda)^4} \right) - \frac{2EE^+E^-}{(1-\lambda^2)^4} \right] \qquad (4.45)$$

in which g is the gravitational acceleration, C a proportionality constant equal to 600. δS is the rate of change of energy density due to the nonlinear interactions, f is frequency, E, E^+ and E^- are the energy densities at the interacting wave numbers.

To compute the nonlinear transfer for a discretized energy density spectrum equation (4.45) has to be applied for both wave number quadruplets, with the central wave number k looping over all spectral bins of the spectrum.

To compare the DIA with exact computations the method of Tracy and Resio (1982) has been used. Figure 4.9 shows the comparison for a JONSWAP spectrum with fp=0.4 and a peak enhancement factor of 3.3 (this is the same spectrum as originally presented by Hasselmann et al., 1985). As can be seen the DIA is able to reproduce the position of the first positive peak although its magnitude is too high. The most striking errors occur in the position and magnitude of the low frequency peak. They are exaggerated considerably. Especially in the high frequency range the interactions are much too high. The DIA is based on local interactions around the wave number considered. This implies that the DIA will show better results for narrow spectra. This is indeed the case, as shown in Figure 4.10 where a comparison has been made for a JONSWAP spectrum with a peak enhancement factor of 7. As can be seen, the first positive and first negative lobe now predicted rather well. However, in the region behind the peak, a kind of oscillation occurs relatively high peaks in the nonlinear transfer occur. For a very wide spectrum, say a Pierson Moskowitz spectrum, the DIA does a very bad job. This is shown in Figure 4.11.

The present comparison between the DIA and exact solutions was made for a few target spectra. This is not always a fair comparison because the nonlinear interactions are quite sensitive to the spectral shape. In a wave model run, e.g. in a fetch computation, the spectral shape is generally not equal to a theoretical JONSWAP spectrum and many types of spectra shapes occur for which the DIA may do a better job.

The interactions in the DIA are scaled with the frequency to the power 11 and the power 3 in the energy densities. This implies that the interactions are much weaker for lower frequencies. This is shown in Figure 4.12, in which a comparison is made of the nonlinear interactions for a JONSWAP spectrum with a peak period of 15 s. Apart from the fact that again the agreement with exact computations is not good, it can be seen that the magnitude of the transfer is much smaller than for spectra with lower peak periods.

The Discrete Interaction Approximation has a few scaling parameters. The DIA uses one wave number configurations of a certain shape, determined by the parameter λ. In the standard version of the DIA the value $\lambda = 0.25$ is used. The only reason that this value is used, is that tests were made with various values of λ, ranging from 0.2, 0.25 and 0.3. The results of computation with different wave number configurations are shown in

Figure 4.13. Apart from a scale factor, it can be seen that the shape of the transfer can be affected by choosing an other value of the coefficient λ. It is noted that no attempt has been made to choose an optimal value for the scaling coefficient. Further, directional aspects have not been studied here.

The DIA is quite sensitive to changes in the spectral shape in the high frequency range, this is a direct effect of the dependence to the power 11 to frequency. As can be seen in the previous figures the DIA shows rather large peak in the high frequency range. These peaks will affect the total source in the high frequency range, thereby affecting the integration process of the source function. To get rid of these peaks all kind of numerical tricks have been formulated to avoid instabilities of which a spectral delimiter is one.

Despite its shortcomings the DIA has been rather successful. Models like WAM were able to reproduce the basic growth curves for large scale ocean applications. This success is the more striking since only one basic wave number quadruplet is used to estimate the non-linear interactions. Models like the EXACT-NL model (Hasselmann and Hasselmann, 1985a) for instance use thousands of wave number configurations to compute the non-linear interactions to any desired degree of accuracy.

The results shown in the previous figures indicate that the DIA is not a good approximation as is generally believed. Large errors occur when a systematic comparison is made with exact computations for theoretical target spectra. Still, the DIA works quite well in the WAM and SWAN model. This is due to the fact that the main effects of the nonlinear interactions is reproduced in the DIA, viz. a transfer of wave energy to the forward face of the spectrum, and a stabilisation of the spectral shape. Moreover, the limitations of the DIA for higher frequencies are partly overruled by the effects of dissipation and wind input.

4.4.4 Depth scaling of discrete interaction approximation

Following the WAM group (WAMDI, 1988) a simple depth-scaling is applied to compute the nonlinear interactions in shallow water. Herterich and Hasselmann (1980) investigated the scaling behaviour of the nonlinear interactions of narrow peaked spectra in shallow water. They was found that the nonlinear transfer for an energy density spectrum $E(f,\theta)$ at a given water depth could be computed from the nonlinear energy transfer for deep water, multiplied by a factor R, constant for all spectral bins. The result that this factor was confirmed by numerical computations with the EXACT-NL model by Hasselmann and Hasselmann (1981). In practice the following method is applied:

For a given energy spectrum $E(f,\theta)$ on a water depth d, the source term for the quadruplet interactions $S(f,\theta)$ is computed as:

$$S_{nl,d}(f,\theta) = S_{nl,\infty}(f,\theta) \times R(\bar{k}d) \qquad (4.46)$$

with $R(\bar{k}d)$ a function which depends on the product of the mean wave number $\bar{k}$ and the local water depth d. The function R is based on a parameterisation of results of Herterich and Hasselmann (1980):

$$R(\bar{k}d) = 1 + \frac{5.5}{\bar{k}d}\left(1 - \frac{5}{6}\bar{k}d\right)\exp\left(-\frac{5}{4}\bar{k}d\right) \tag{4.47}$$

The function R is plotted in Fig. 4.14. To avoid too large values for the nonlinear interactions, the product term $\bar{k}d$ has a lower limit of 0.5, resulting in a maximum value of R=4.43.

The mean wave number $\bar{k}$ is computed as:

$$\bar{k} = \int kE(f,\theta)dfd\theta / E_{tot} \tag{4.48}$$

To enhance stability another definition of the mean wave number is used (cf. Eq. 4.37):

$$\hat{k} = \left[\int\int \frac{1}{\sqrt{k}} E(f,\theta)dfd\theta / E_{tot}\right]^{-2} \tag{4.49}$$

Due to this definition, a somewhat different value of the mean wave number is obtained which differs from the standard definition. In third-generation wave models it is therefore implemented as (WAMDI, 1988; Tolman, 1991):

$$\bar{k}d = \tfrac{3}{4}\hat{k}d \tag{4.50}$$

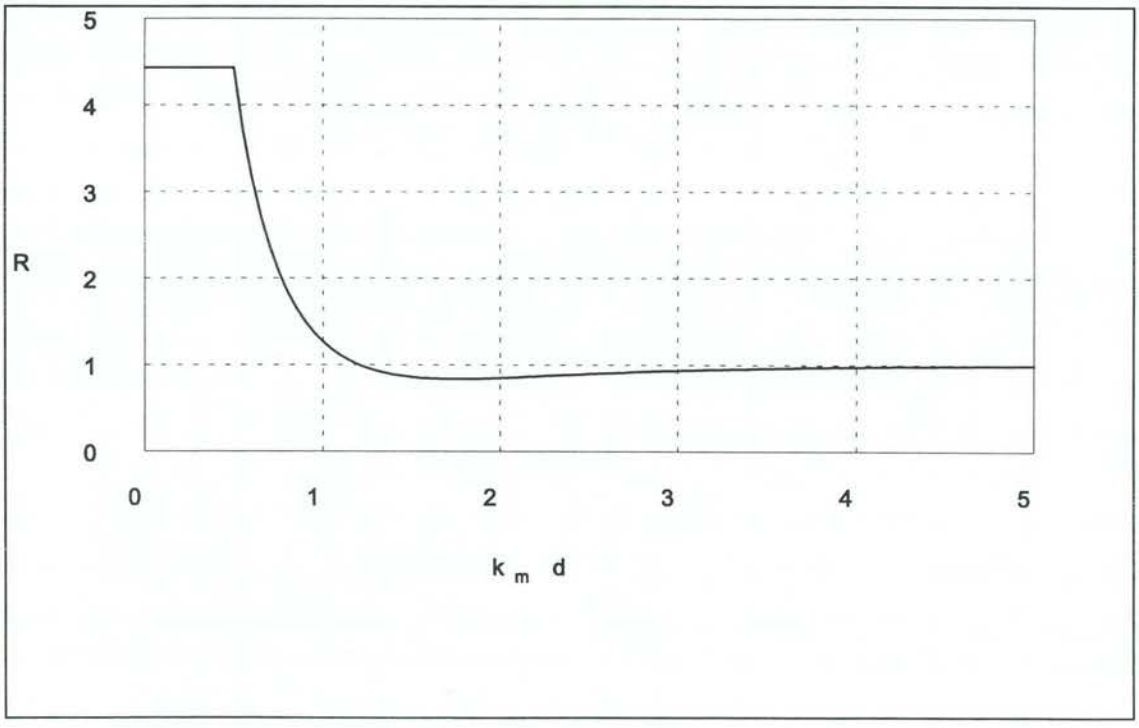

Figure 4.14. Depth scaling factor of Discrete Interaction Approximation as a function of the dimensionless water depth $k_m d$.

It is claimed in the WAM paper (WAMDI, 1988) that for $k_p d > 1.0$ this scaling method reproduces almost the same results as the exact finite depth computations. (In the WAM paper (WAMDI, 1988) the variable $k_p d$ is written as kd, meanwhile suggesting a dependence on wave number, however, inspection of the computer code shows that the scaling function used the constant factor $\bar{k}d$., i.e. it uses a constant factor for all spectral components. It is probably better to compute the non-linear transfer with the discrete interaction approximation directly for a finite water depth.

5 The effect of swell on wave growth

5.1 Introduction

Swell can be considered as waves that are no longer under the influence of the local wind. Such waves have been generated elsewhere and have propagated over long distances. Frequency dispersion causes the spectrum of these waves to be much narrower than the local wind sea. In most numerical wave prediction models it is assumed that there is no interaction between the swell and wind waves. This is assumption is not valid since many observations show that there is some kind of interaction, although the magnitude of this interaction and the nature of its effects are still under investigation.

The interaction between swell and wind waves is a complex process whereby many effects take place simultaneously. Along the Dutch coast, situations where similar interactions take place are frequent. Especially in the Westerschelde estuary and the tidal inlets connecting the Waddensea with the North Sea. Various studies show that waves coming from the North Sea decay on the shallow areas at the entrance of a tidal inlet and that a local wind sea develops causing the spectra to be bi-modal resembling the combination of swell and wind waves, except that the low frequency part of the spectrum is generally broader than a typical ocean swell. From this point on, the low frequency peak of the spectrum will be considered as swell. Further into the estuary or tidal inlet, presence of a swell system is not noticeable anymore. During this transition from a swell system to a local wind sea a number of interactions take place. The three most important processes are:

Firstly, non-linear quadruplet wave-wave interactions exchange energy between different wave components. These interactions have been studied numerically by various authors (e.g. Young et al., 1985; Masson, 1993). These studies indicate that swell and sea waves affect each other only if the sea and swell peaks are close to one another in spectral space.

Secondly, the swell waves may distort the wind profile just above the sea-surface (e.g. Donelan, 1987), thereby affecting the energy flow from the wind field to the waves, and the growth rate of the waves.

Thirdly, the swell waves affect the propagation and dissipation of the shorter waves which ride on the longer swell waves. On the basis of various studies it known that the presence of swell may have a dampening effect on the growth of wind waves (e.g. Hatori et al., 1981 and Donelan, 1987). A dramatic example of this effect was shown in Donelan (1987). In this paper a laboratory experiment is described which indicates that the presence of low frequency swell reduces the growth of the wind waves considerably.

Each of the above phenomena will be discussed below. In Section 5.2 attention is given to the modelling of the non-linear wave-wave interactions in a wave spectrum and the results of some computations are presented. The interaction between swell waves and the wind profile is discussed in Section 5.3. The long wave - short wave interactions are discussed in Section 5.4.

Apart from the physical effects there is also a surprising modelling effect of the presence of a swell system on the growth of wind waves. As shown in Section 4.3 the amount of dissipation by whitecapping is quite sensitive to the presence of a swell peak in the wave spectrum. This sensitivity will be illustrated in Section 5.5 by means of an example from a recent project in which the wave growth in a partially sheltered area was investigated.

5.2 Non-linear interactions

The swell-sea interaction has been studied numerically using wave prediction models by various authors. To that end computations were made with numerical methods which compute the full Boltzmann integral to a given accuracy. The first systematic study to this effect was performed by Young et al. (1985) in which the interaction between a number of double peaked spectra was investigated. A more detailed study was performed by Masson (1993) . The results of both paper will be discussed below.

Young et al., (1985) describe the results of a series of computations with the EXACT-NL model (Hasselmann and Hasselmann, 1981, 1985b) for double peaked spectra. In this study the first spectrum was the standard JONSWAP spectrum:

$$E(f) = \alpha g^2 (2\pi)^{-4} f^{-5} \exp\left\{-\frac{5}{4}\left(\frac{f}{f_p}\right)^4\right\} \gamma^{\exp\left[-\frac{(f-f_p)^2}{2\sigma^2 f_p^2}\right]} \qquad (5.1)$$

with the following parameters: α =0.01, f_p =0.3 Hz, γ =3.3, σ_a =0.07 and with σ_b =0.09.

The second spectrum consisted also of a JONSWAP spectrum, but with different mean direction and peak frequency. A total of 21 combinations was investigated in which the angle between the two spectra varied from 0° to 180° with steps of 30°, and with the following peak frequencies 0.3 Hz, 0.4 Hz and 0.5 Hz. Although the lowest peak frequency of 0.3 Hz can not be regarded as the peak frequency belonging to an ocean swell, the computations give insight into the interaction between the two spectra.

Young et al. (1985) computed the nonlinear interactions in two ways. Firstly, they computed the nonlinear interactions for the combined spectrum, and secondly they computed the nonlinear interaction for each spectrum separately and added the results together. In the cases that the results of both methods are equal one can conclude that the two spectra do not interact. By comparing the difference they infer the amount of coupling between the two spectra. When both peak frequencies are equal, the coupling is the strongest for a directional difference of 0°, and the coupling is virtually negligible when the directional difference is equal to or larger than 90°. The remaining cases represent spectra separated both in frequency and direction. For spectra with equal directions they found that the coupling decreases when the peaks become more separated. For peak frequencies with a difference of 0.1 Hz, they found that the negative lobe of the high frequency nonlinear transfer is significantly enhanced, implying a flow of wave energy from high to low frequencies, thus reducing the possible growth of wave

energy at high frequencies. This finding is in line with the general behaviour of the nonlinear wave-wave transfer in the sense that they favour a uni-modal spectrum.

A similar study was carried out by Masuda (1980), who briefly investigated the interaction of two wave systems by computing the nonlinear interaction term for two spectra with different peak frequencies and by computing the interaction term by a simple superposition. His work, however, is insufficient to fully understand the coupling between the two systems and to draw firm conclusions.

Masson (1993) studied the interaction between a swell and a wind sea system with neighbouring frequency ranges and estimated response times of the interaction. First, Masson studied the interaction between two wave systems in terms of a swell decay time τ obtained by assuming a stationary situation and a narrow swell for which all energy resides in a single frequency. Then, using an equation derived by Hasselmann (1963), it was possible to derive the response time for different values of the ratio between the two peak frequencies and the difference in peak wave direction. The results indicate that the nonlinear coupling causes the swell to decay. In the frequency range just below the peak frequency of the local wind sea, however, the swell grows at the expense of the waves of the local wind sea. The largest coupling was found when the peak frequency of the swell system was about 80% of the peak frequency of the spectrum of the local wind sea. When the swell peak frequency is lower than 60% of the wind sea peak frequency the coupling can be neglected. Masson (1993) also found a dependence of the angle between the two wave systems, with a maximum increase of swell energy for a direction of about 40° and then rapidly decreasing for larger directional differences. These results imply that a coupling between a swell system and a local wind sea is negligible for most cases unless the two peaks are so close in frequency space that the bi-modal structure of the spectrum can hardly be identified. However, Fig. 6 of Masson (1993) may lead to a different conclusion.

5.3 Effect of swell on wave growth by wind

In literature different types of observations cases are described; swell waves propagating in the direction of the wind, with a phase speed exceeding the wind speed; swell waves travelling in a direction opposite to the wind direction, and the case where the angular difference is about 90°.

The idea that swell waves may return momentum to the atmosphere and to produce a 'wave-driven wind' appears to have first been proposed by Harris (1966). This was later confirmed by field observations from Davidson and Frank (1973) and Donelan (1987). Donelan and Dobson (1997) model the interaction between swell and wind in terms of the surface roughness length z_0 or the drag coefficient C_d.

The presence of a swell in a wind sea affects the drag in two ways. First, there is a direct effect. When the swell and wind direction are equal, the presence of a swell decreases the drag thus decreasing the growth rate of the wind waves. When swell encounters an opposing wind, the drag is increased and (negative in term of direction) momentum is transferred to the swell, thereby decreasing its amplitude. There is also an indirect effect via the interaction between the swell and wind sea waves, which also may change the aerodynamic roughness of the sea surface. Donelan and Dobson (1997) do not provide information about what happens to the wind sea.

The above mentioned direct effects have been observed by Donelan (1987) in Lake Ontario. In this case a situation occurred when the wind was blowing for a long time in the same direction as the axis of the Lake, thereby producing relatively large waves at the western side of the Lake, where also the wave observations were performed. At some time the wind direction changed 180° and a situation occurred in which the swell was confronted with opposing winds. The time variation of the wind speed and direction, significant wave height are shown in Figure 5.1 (which is taken from Donelan and Dobson, 1997). It can clearly be seen that the drag decreases when the wind decreases and that the drag increases when the wind has turned about 180°.

It should be noted that the above mentioned effects are only noticeable in situations with light winds and when the difference in phase speed and wind speed are large. In such situations the contribution of the wind sea to the drag is small.

Observations of swell in opposing wind are rare and some researchers performed laboratory experiments to study this interaction in more detail. Experiments of swell in opposing winds have been reported by Young and Sobey (1985) who found insignificant effects, Mitsuyasu (1966) while Mizuno (1976) found a significant attenuation of swell. The results of these experiments show that swell tends to grow in following winds at the expense of the wind sea, and that they attenuate in opposing winds. They also found that the growth rate of the swell in following winds is comparable to the attenuation rate in opposing winds. In opposing winds, the large increase in momentum transfer seems to come from the effect of the swell on the drag since the wind sea is 'flattened' by the swell. The increased momentum transfer to the swell results in its attenuation because its direction is opposed to the direction of swell propagation.

The interaction between swell and wind was also studied by Mitsuyasu and Kusaba (1993) who describe a series of laboratory experiments in which the growth and attenuation rate of swell waves in following and opposing winds was studied. Based on the experiments they found that the growth rate of swell in a following wind is about the same as the attenuation rate for swell in an opposing wind. They present their results in term a the dimensionless growth rate β/f as a function of the ratio of the friction velocity and phase speed u_*/c. The growth rate is given as:

$$\frac{\beta}{f} = 0.34\left(\frac{u_*}{c}\right)^2 \tag{5.2}$$

and the attenuation rate is given by:

$$\frac{\beta}{f} = 0.52\left(\frac{u_*}{c}\right)^{2.37}. \tag{5.3}$$

The mechanism of wind sea attenuation by an existing swell is poorly understood. It probably depends on the steepness of the swell and the relative difference in propagation direction.

5.4 Long-wave short-wave interaction

5.4.1 Modulation of short waves by long waves

Donelan (1987) presents the results of an experiment where paddle generated waves affect the growth of the wind sea dramatically. This phenomenon is illustrated in Figure 5.2 (which is taken from Donelan, 1987). In this wave flume experiment three situations are described. First, only paddle generated 'swell' waves with a very narrow spectral shape and a total variance of 5.47 cm^2. Second, only wind generated waves with a much broader spectrum and a total variance of 16.8 cm^2. Third, paddle waves in combination with a wind generated sea. In the latter case, the swell has grown considerably at the expense of the wind sea. Surprisingly, the total variance of 15.0 cm^2 is much lower than the sum of the variances when paddle waves and the wind were generated separately. In this experiment the wind speed was 11 m/s at a height of 26 cm. The phase speed of the paddle waves was 2.2 m/s.

A disadvantage of this experiment is its small scale and it is not known whether this effect can be scaled to ocean scale waves. Various theories exist in literature describing this effect, although some authors claim the contrary.

A partial explanation of this phenomenon is given by Donelan (1987). The growth of the swell waves comes from the increased stress transferring momentum from the wind to the swell waves. This increase in stress by the swell waves is much larger than the decrease in roughness by the reduced wind sea. Donelan (1987) does not explain the decrease of the wind sea when a swell is present. In 1998, at the WISE meeting in Leuven, Belgium, Donelan (1998) suggested that the decrease of the wind sea may be due to a damping mechanism of the shorter waves riding on the longer swell waves. This mechanism modulates the shorter waves by enhanced wave breaking on the slopes of the swell waves.

In the open ocean, the conditions are much different than those in the experiment. First, the swell waves travel faster than the wind, where in this experiment they travel much slower. Secondly, in the open ocean the relative difference in speeds is generally much smaller, so that the contribution to the stress is also much smaller.

5.4.2 Surface drift

In section 5.3.2 the interaction between swell and wind sea waves was studied in terms of the nonlinear quadruplet interactions exchanging wave energy between different wave components. These interactions, however, cannot explain all observed interactions between swell waves and wind sea waves. In many studies it has been reported that swell waves suppress coexisting wind waves, both for the situation that the swell waves travel with the wind or against the wind. An explanation of this phenomenon has been given by Phillips and Banner (1974) who proposed a mechanism for this interaction in terms of the surface drift. At the crest of a long wave, the wind-drift current in the water is augmented by the orbital velocity of the long waves. This reduces the maximum amplitude that the wind waves can attain before it is suppressed through wave breaking.

Morland (1997) studied in detail the wind profile of short waves riding on a longer swell. In this study the effects of low amplitude swell were investigated. This reduces its

applicability for steep swell. Based on a linear stability analysis Morland (1997) states that a swell in an opposing wind produces different effects. For low swell slopes the wind waves are not much affected. For higher swell slopes, however, the growth rate of the wind waves is enhanced by the swell because the swell waves cause the spectral peak of the wind waves to shift to longer wave lengths, decreasing the dissipation of these waves by whitecapping.

According to observations Mitsuyasu and Yoshida (1989, 1991), however, swell propagating against the wind amplifies the wind waves when the steepness of the swell increases. This discrepancy is not yet resolved, but it may be that another mechanism may play a role.

5.4.3 Diffusion in wave number space

An interesting mechanism for the suppression of the short (wind sea) waves by a train of long (swell) waves has been described by Balk (1996). Balk considers the effect of nonlinear quadruplet interactions within a gravity wave spectrum and concentrates on the effect of diffusion in the wave number -plane, so that wave action is transported to the region of higher wave numbers, where it dissipates more effectively by whitecapping dissipation. This is rather interesting, since the long waves supply energy to the short waves, but this energy gain makes them dissipate faster. This finding, however, is contrary to the results found by Young et al., (1985) who found that the nonlinear interactions 'pump' energy from high to low frequencies.

5.5 The effect of swell on the dissipation by whitecapping

Apart from physical effects of swell on the evolution of growing wind waves, there is also a (surprising) modelling effect of swell affecting wave growth. In present day third generation wave prediction models like SWAN, the dissipation by whitecapping is scaled with the average wave steepness $\hat{\alpha}$ which is proportional to the fourth moment of an average mean frequency $\hat{\omega}$. Numerical experiments have shown that this measure is rather sensitive to the presence of swell. Even a small amount of swell causes a decrease in the value for $\hat{\alpha}$ thus causing a decreased dissipation by whitecapping and an increased wave growth.

Such behaviour has been observed by ALKYON (1998) in a SWAN application with the purpose of computing wave growth in sheltered areas. In this study the wave growth was computed with the SWAN model in a sheltered area that was partially enclosed by dams. At the entrance of this area a wave boundary condition was imposed. From SWAN computations it was found that the wave growth in this area was enhanced considerably for the situation that a wave boundary condition was imposed, compared to the situation that no wave boundary condition was imposed. This enhancement was greater than expected and led to an investigation of the physical processes (i.e. the source terms in SWAN) that were responsible for this phenomenon.

For this investigation the area was schematised as a one-dimensional situation with a length of 2500 m. Four computations were performed. In both computations the wind speed was 20 m/s. The first two computations where made with no wave boundary conditions and the waves started from a zero conditions. In the first computation all physical processes were activated, whereas in the second computation whitecapping was

turned off. In the last two computations a wave boundary conditions of Hs =1 m and a Tp = 6 s was imposed. Like in the first two computations, whitecapping was activated in the third computation and deactivated in the fourth computation. A summary of the incident wave conditions and model settings is shown in Table 5.1.

	Wave boundary conditions	whitecapping
1	off	on
2	off	off
3	Hs = 1 m, Tp = 6 s	on
4	Hs = 1 m, Tp = 6 s	off

Table 5.1: Summary of wave model settings for the investigation of the role of whitecapping in wave growth in a sheltered area.

The growth of the significant wave height for each the four cases is shown in Figure 5.3. The growth curves for the cases that a wave boundary condition is imposed have been computed on the basis of the extra wave growth with respect to the initial condition. To that end the initial wave energy at x=0 m has been subtracted from the growth curves for the cases 3 and 4.

It is noted that for case 2, the wave height at the start of the fetch is not equal to zero. This is due to the numerical method applied in the SWAN model to solve the energy balance equation. It was also found that the wave height at x=0 m, depends on the number of iterations, with the wave height at x=0 increasing with the number of iterations. For case 2, 14 iterations were performed, whereas for the other cases only 4 iterations were needed.

From Figure 5.3 it can be seen that for the cases 1 and 2, the omission of whitecapping dissipation enhances the growth of the significant wave height considerably (as expected). From this figure it also can be seen that for the cases 3 and 4 the effect of whitecapping on the growth of the significant wave height is small. At a fetch of 1500 m, the significant wave height as computed for case 2 is more or less equal to the significant wave height for the cases 3 and 4.

To obtain insight into the source term balance the spatial evolution of the wave spectrum and source functions for wind input, whitecapping dissipation and nonlinear quadruplet interactions are shown in the Figure 5.4 through 5.7 for each of the four cases.

For the cases 1 and 2 the wind sea peak develops as in a normal wave growth situation. For a fetch of 2500 m the peak frequency of the spectrum is about 0.34 Hz. The spectral development is very similar for case 2, although the source term whitecapping dissipation was deactivated.

For the situations with a wave boundary condition (cases 3 and 4) it can be seen in the Figures 5.6 and 5.7 that the wind sea peak develops in the frequency range 0.2 - 0.3 Hz. Comparison of the Figures 5.6 and 5.7 also shows that the growth of the wind sea peak is strongly reduced for the case that whitecapping is activated (as expected). The figures also provide insight into the role of the nonlinear wave-wave interactions.

At first sight, comparison of the results for the development of the wave height (see Fig. 5.3), suggests that the increased wave growth in the presence of an initial swell can be accounted for by the fact that this presence more or less completely suppresses the whitecapping. However, examination of the source terms (Figures 5.4 to 5.7) show that the difference is only partly caused by suppression of the whitecapping and that enhanced wave growth due to wind around the peak frequency of the 'swell' also plays a role. While the first of these effects is almost certainly unrealistic, it is not known whether the second effect is realistic. The observation from field measurements that swell suppresses the growth in height of the wind sea was made in situations where the swell period was greater than 10 seconds. The conclusion may not be valid both for the situation considered here and in the Westerschelde where the incoming waves have a lower wave period order of magnitude 8 s for a wind speed of 25 m/s)

5.6 Discussion of results

In this Chapter various aspects of swell-sea interaction have been discussed. It has been shown that nonlinear quadruplet interactions are able to exchange energy between the swell and the wind sea parts of the spectrum if the locations of the peaks of the two wave systems are not separated too much in wave number space.

Further, the paddle experiment of Donelan (1987) clearly shows that the presence of a swell system reduces the growth rate of the wind sea by an enhanced dissipation mechanism induced by a modulation of the short wind waves riding on the longer swell waves. This trend is in line with various theoretical studies.

Analysis of the source term for whitecapping dissipation has shown that the presence of swell reduces the amount of whitecapping dissipation due to the way in which the proportionality coefficient C_{ds} is computed. This was illustrated by a SWAN application in which the effect of including a wave boundary condition causes an enhanced growth of the wind sea part.

It is interesting to note that from the physical point of view, swell reduces the growth of the wind sea, but that from a numerical point of view swell causes a reduction of the whitecapping dissipation causing an enhance growth of the wind sea.

Based on the above finding it is recommended that the source term for whitecapping dissipation should be replaces by a new one, which is not sensitive to the occurrence of a swell peak and which enhances the dissipation of the wind sea part when a swell is present. The modulation mechanism proposed by Donelan (1998) might be a good candidate. Another method might be the one proposed by Tolman and Chalikov (1996). This method, however, needs further study before it can be applied in the SWAN model.

6 Nonlinear interactions at high frequencies

6.1 Introduction

As shown in Chapter 4, the nonlinear interactions, when computed with the Discrete Interaction Approximation, are quite sensitive to frequency, but also the DIA does a bad job in comparison with exact methods of computing these nonlinear interactions. This implies that the source balance in the high frequency part of the spectrum is likely to be influenced by the behaviour of the DIA.

In wave models the total source function is important and not only one individual source term, how bad it might be, such as the DIA. It is also expected that the errors in the DIA are overwhelmed by a strong wind input source term for higher wind speeds.

Another problem encountered in the analysis of the SWAN model is the position of the cut-off frequency on the evolution of the wave field. Results of SWAN computations with different settings of the cut-off frequency are presented in the next chapter. In this chapter, some aspects of the source term balance are presented.

Related to the cut-off frequency is the effect of the location of the parametric spectral tail. For SWAN the default frequency range is from 0.03 - 1.0 Hz. Unlike other third generation wave model, the start of the parametric spectral tail is fixed, and not breathing like in e.g. the WAM or WAVEWATCH models. Recently, Ris and Bos (WL | delft hydraulics,1998) have studied the effect of a breathing tail on the evolution of the wave field. Some cases studied by them have also been analysed in this Chapter.

6.2 Source term balance in the high frequency range

The source term balance in the high frequency range has been studied for a number of young wind sea spectra, all with a significant wave height of 0.5 m, and peak frequencies of 2, 3 and 4 s. The wind speed in these cases was 20 m/s. For all cases the nonlinear interactions were computed with the DIA and with the exact method of Tracy and Resio. The wind input was computed with the Komen et al. (1984) source term, and the whitecapping dissipation with the standard WAM method.

The results for a spectrum with a peak period of 2 s are shown in Figure 6.1. As can be seen there is large difference with the exact transfer. The DIA has a much stronger signature than the exact solution. This results in a strong effect on the total source term, resulting in a faster growth in the initial stage compared to the 'exact' total source function.

For a peak period of 3 s the results are shown in Figure 6.2. From this figure it follows that there is still a strong difference between the computed nonlinear transfers, but also that the effect of the nonlinear interactions, as computed with the DIA, is much weaker than for the previous case.

For a peak period of 4 s the results are shown in Figure 6.3. As the peak period increases the relative magnitude of the nonlinear interactions diminishes considerably, and the

effect of the nonlinear interactions are hardly visible. This is also due to the fact that the wind input source function is dominant over the other source functions. This was checked by computing the source term balance also for a lower wind speed of 10 m/s for the case of a JONSWAP spectrum with a peak period of 3 s. The results thereof are shown in Figure 6.4. As expected, the relative magnitude of the nonlinear interactions increases, and some effects of the errors in the DIA become visible in the total source function.

6.3 The effect of the cut-off frequency on the nonlinear interactions

The SWAN model differs with other wave prediction models, like the WAM and WAVEWATCH model, in the treatment of the parametric high frequency tail. Unlike the other models, the SWAN does not use a breathing tail. To see if there is any effect on the location on this tail for the source balance for young developing sea, a number of computations have been made with different starting points of this tail. The resulting source term balance is shown in Figure 6.5 for a cut-off frequency of 0.8 Hz and in Figure 6.6 for a cut-off frequency of 0.6 Hz.

The results show that for a lower cut-off frequency the nonlinear transfers increase in magnitude. This is due to the fact that the energy densities in the frequencies above the cut-off frequency are different for the case of a fully prognostic spectrum and a partly parameterised tail. Since the nonlinear interactions are scaled with the energy densities to the third power, it is not surprising that the observed differences occur.

Recently Ris and Bos (WL | delft hydraulics, 1998) implemented a breathing spectral tail in an experimental version of the SWAN model, to study its effect on the evolution of the wave spectrum. They studied a number of cases of which three have been analysed in this study. It is noted here this study has another objective than the study of Ris and Bos (WL | delft hydraulics, 1998). For the present study, three cases were studied with different positions for the start of the parametric tail, all relative to the spectral peak. The following cut-off factors were used in this study , f_c = 2.5 fp, f_c = 1.5 fp and f_c = 1.0 fp. In all cases a JONSWAP spectrum with a peak period of 5 s was used, with a peak enhancement factor of 3.3.

In these computations also the effect of the power of the spectral tail was investigated. There is an ongoing debate in the wave modelling community about the power of the spectral tail. The WAM model uses a power -5, whereas a power of -4 is adopted in the SWAN model. To study these effects the cases provided by Ris were also studied with respect to the effect of applying a spectral tail of the power -4 and -5.

The results of the computation for a power of -5 and -4 are shown in the Figures 6.7 and 6.8 respectively. The situations with a cut-off factor of 2.5 more or less refer to the present situation, in which the tail starts at 1 Hz. From Figure 6.8 it follows that there is hardly any effect on the spectral shape. For a cut-off factor of 1.5 the effect on the spectral shape becomes visible. For a cut-off factor of 1.0 the effect is quite large, the high frequency part of the spectrum is reduced considerably, and the spectral shape deviates from the parametric JONSWAP shape. These effects are visible both for the case of a -4 and a -5 power law for the parametric tail. It is noted here that the actual effect of choosing a low value is to make the spectrum more narrow.

A striking effect is that for lower cut-off frequencies the agreement between the DIA and the exact results show a better agreement. This is due to a number of factors. Since the DIA is a local approximation, the results of the DIA improve as the spectrum becomes more narrow. This improvement concerns two aspects of the nonlinear transfer: firstly, the magnitude of the first negative lobe decreases to an acceptable level, and secondly, the first zero-crossing of the nonlinear transfer become more aligned with the one computed by the exact transfer. It is noted here that this zero-crossing should more or less coincide with the position of the spectral peak.

Another striking feature is the difference between the results for an f^{-4} and an f^{-5} spectrum. For the f^{-4} spectral tail the DIA results show large oscillation in the high frequency range. This can clearly be seen in the upper right panel of Figure 6.8. This can be explained from the fact that the nonlinear interactions scale with the eleventh power of the frequency and the third power of the energy density. For an f^{-4} spectral tail, this implies a dependence of f^{-1} (11 - 3x4= -1), compared to an f^{-4} (11 - 3 x5=-4) dependence for an f^{-5} spectral tail. Small irregularities in the spectral tail are enhanced by the nonlinear interactions and they are the source of instabilities in spectral shape.

The effect of letting the spectral tail begin at the peak frequency has the effect that the nonlinear interactions are more peaked, resulting in more peaked spectra. This overcomes one of the weaknesses of third generation wave models, they all produce too wide spectra compared to wave models which include exact methods of computing the nonlinear interactions (cf. Young and Van Vledder, 1993). Since the spectral shape above the peak frequency is forced to a certain power law, deviations to the actual shape occur. These deviations affect the total source term balance and might affect the growth of the total wave energy.

Finally, it is noted here that a method of applying a spectral tail starting at the peak may yield problems in the case of double peaked spectra, especially in the case where the lower frequency peak is the highest.

7 Sensitivity analysis of SWAN

7.1 Introduction

The purpose of this Chapter is to perform a sensitivity analysis of the SWAN model to various parameter settings. The sensitivity analysis comprises the testing and comparison of computational results for different frequency ranges, step sizes, wind speeds and number of iterations.

In the calibration an attempt is made to modify the setting of some physical processes to obtain a better fit between the SWAN results and growth curves from literature.

In this Chapter comparison is made with growth curves from literature. An overview of some deep water growth curves is given in Appendix A.

7.2 Convergence criteria of SWAN

In the SWAN wave model the action balance equation is solved iteratively to obtain a fully implicit solution. The solution technique uses a four-sweep technique, in which each sweep takes care of the evolution of the wave spectrum in a directional sector of 90° by a forward marching technique. This iteration process is carried out to allow boundary conditions to be matched between the four quadrants. The iteration process ends when the changes in significant wave height and mean wave period are small enough in a specified number of grid points. Three criteria are used to quantify the changes between two iterations:

1. **drel**, the relative difference in significant wave height Hs and mean wave period Tm01,
2. **dHabs**, the absolute difference in significant wave height Hs,
3. **dTabs**, the absolute difference in the mean wave period Tm01.

The number of grid points in which the above three criteria should be met is indicated with the parameter **Npnts**. Further, a maximum number of iterations is specified by the parameter **Nmax** to avoid endless iterations.

By default the following iteration criteria are used:
drel = 3%
dHabs = 0.03 m
dTabs = 0.3 s
Npnts = 97 %
Nmax = 6

For the computations in this chapter and for the verification computations presented in Chapter 8, the maximum number of iterations was set to 15.

7.3 Sensitivity analysis of SWAN

The sensitivity analysis of the SWAN model has been performed with an experimental version of the SWAN model using the 1-d model option. The experimental version has version number 34.00. As a first test of this version of SWAN a comparison was made with wave model data obtained from Delft University of Technology. These data comprise the results of 2-dimensional wave model computations to check the performance of SWAN against known growth curves from literature. It was found that the experimental SWAN version in 1-d mode, produced the same results as the results of the 2-dimensional wave model computations, while using the same frequency and directional discretisation.

In the following only results of the experimental SWAN in 1-d mode will be presented and referred to as SWAN model results. Each SWAN computation is characterised with certain settings for the computational domain (length and space step), the frequency range, wind speed and convergence criteria. An overview of the cases that have been analysed is given in Table 7.1.

convergence criteria

The SWAN model has been used to compute fetch limited growth curve for a wind speed of 20 m/s. In the computations the computational domain was divided into decades , i.e. in intervals which differ by a factor of 10 in length. First a decade of 100 m was used, the wave model results at the end of this domain were used as input data for the next decade. In total 5 decades were used. In addition, for each domain different settings were used for the frequency range, number of frequencies and convergence criteria. The SWAN runs used for these computations have the codes XDEEP0, XDEEP1, XDEEP2, XDEEP3 and XDEEP4. The results of the computations are shown in Figure 7.1. This figure (in slightly different format) has also been published in Ris (1997). From these figures it can be concluded that the SWAN model performs well. The curves computed with SWAN are more or less aligned with the growth curves of Wilson (1965) and Kahma and Calkoen (1992).

Case	xlen	dx	flow	fhigh	mfreq	u10	drel	dhabs	dtabs	npnts	itermax
xdeep0	100	1	0.167	3.0	30	20	0.001	0.001	0.001	100	50
xdeep1	1000	10	0.125	2.0	29	20	0.001	0.001	0.001	100	50
xdeep2	10200	50	0.111	1.0	30	20	0.01	0.005	0.005	100	50
xdeep3	150000	150	0.066	1.0	28	20	0.01	0.005	0.005	100	50
xdeep4	750000	500	0.0446	1.0	32	20	0.03	0.03	0.3	97	35
adeep0	100	1	0.167	3.0	30	20	0.03	0.03	0.3	97	15
adeep1	1000	10	0.125	2.0	29	20	0.03	0.03	0.3	97	15
adeep2	10200	50	0.111	1.0	30	20	0.03	0.03	0.3	97	15
adeep3	150000	150	0.066	1.0	28	20	0.03	0.03	0.3	97	15
adeep4	750000	500	0.0446	1.0	32	20	0.03	0.03	0.3	97	35
f25d20	25000	20	0.03	1.0	30	20	0.03	0.03	0.3	97	15
f25d50	25000	50	0.03	1.0	30	20	0.03	0.03	0.3	97	15
f25d100	25000	100	0.03	1.0	30	20	0.03	0.03	0.3	97	15
f25h06	25000	50	0.03	0.6	30	20	0.03	0.03	0.3	97	15
f25h08	25000	50	0.03	0.8	30	20	0.03	0.03	0.3	97	15
f25h10	25000	50	0.03	1.0	30	20	0.03	0.03	0.3	97	15
f25h12	25000	50	0.03	1.2	30	20	0.03	0.03	0.3	97	15
f25w10	25000	50	0.03	1.0	30	10	0.03	0.03	0.3	97	15
f25w20	25000	50	0.03	1.0	30	20	0.03	0.03	0.3	97	15
f25w30	25000	50	0.03	1.0	30	30	0.03	0.03	0.3	97	15
x25d20	25000	20	0.03	1.0	30	20	0.001	0.005	0.005	100	50
x25d50	25000	50	0.03	1.0	30	20	0.001	0.005	0.005	100	50
x25d10	25000	100	0.03	1.0	30	20	0.001	0.005	0.005	100	50
iter05	25000	50	0.03	1.0	30	20	0.001	0.001	0.001	100	5
iter10	25000	50	0.03	1.0	30	20	0.001	0.001	0.001	100	10
iter20	25000	50	0.03	1.0	30	20	0.001	0.001	0.001	100	20
iter40	25000	50	0.03	1.0	30	20	0.001	0.001	0.001	100	40
iter60	25000	50	0.03	1.0	30	20	0.001	0.001	0.001	100	60

Table 7.1: Overview of numerical settings for the SWAN computations that have been used in the sensitivity analysis.

The previous computations were performed using strict convergence criteria. For practical purposes these criteria are not useful because then many iterations are necessary. Therefore, a test has been performed to compute the fetch limited wave growth using the default operational settings specifying the convergence criteria and maximum number of iterations. The SWAN runs used for these computations have the codes ADEEP0,AXDEEP1, ADEEP2, ADEEP3 and ADEEP4. The results of these computations are shown in Figure 7.2. Comparison of this figure with Figure 7.1 shows are number of differences. Especially for a non-dimensional fetch in the range 10-100, the non-dimensional wave height increases.

The previous SWAN results were given in non-dimensional form. For a better understanding of what happens at short fetches, the previous results are also presented in dimension holding form. For the strict and the operational convergence criteria the results are shown in the Figures 7.3 and 7.4 respectively. Based on these figures the following conclusions can be drawn. For the strict convergence criterion the peak period is predicted rather well, whereas the significant wave height is over predicted by about 40 cm at the end of the fetch. For the operational convergence criterion, the peak period

is slightly over predicted, but the significant wave height is now over predicted by about 50 cm.

grid spacing

The previous results are based on different frequency ranges and step size per computational domain. For practical purpose of wave modelling over short fetches it is more likely that a fixed step size for the whole domain of 25 km is used. To assess the consequences of using a fixed step size, an additional computation was made. This computation has the code F25D50. The results of this computation are shown in Figures 7.5 for the significant wave height and the peak period. In Figure 7.6 also the results for the mean wave period are shown. It is now found that both the peak period and the significant wave height are over predicted. The significant wave height is now over predicted by about 80 cm.

In the previous computation a step size of 50 m has been used. In recent computations for the Westerschelde estuary also step sizes of 20 m and 100 m have been used. To check if another spacing affect the computational results, 2 computations have been made, F25D20 with a step of 20 m, and F25D100 with a step of 100 m. The results of these computations are shown in Figure 7.7. As can be seen the step size has almost no effect on the computational results. Only at the start of fetch, some differences are visible.

cut-off frequency

Another point of interest is the cut-off frequency. SWAN uses a standard cut-off frequency of 1.0 Hz. To assess the effect other choosing another cut-off frequency, computations were made with cut-off frequencies of 0.6 Hz (case F25H06), 0.8 Hz (F25H08), 1.0 Hz (F25H10) and 1.2 Hz (F25H12). The results of these computations are shown in Figure 7.8. As can be seen in this figure, the cut-off frequency has little effect on the present results, with slightly lower significant wave height for a cut-off frequency of 0.6 Hz. This is probably due to the fact that some energy is removed from the tail by adding a parametric spectral tail.

scaling with wind speed

An essential element in the comparison of SWAN results with growth curves is the assumption that the results can be made non-dimensional with wind speed U10 and that the resulting non-dimensional growth curves are equal. This assumption has been tested by using results of SWAN computation with three wind speeds, 10 m/s (code F25W10), 20 m/s (F25W20) and 30 m/s (F25W30). The results of the computations were made non-dimensional with the wind speed U10 and they are shown in Figure 7.9. For comparison, the parametric growth curves of Kahma and Calkoen (1992) are included in this figure. The results have also been normalised with the friction velocity u*. These results are shown in Figure 7.10.

From this figure it can be concluded that the SWAN model does not scale with wind speed U10. The scaling with u* is better, but still not very good, at least for the operational convergence criterion that has been used in the present computations.

The fact that SWAN does not scale with wind speed U10 is not surprising in view of the fact that a similar model, viz. the WAM model shows the same behaviour. This behaviour is probably due to the fact that the WAM and SWAN model use the DIA for computing the nonlinear interactions and not the exact method.

number of iterations

In view of recent experience with the SWAN model it was found that the number of iterations can affect the computational results. To assess the effect of the number of iterations on the results five computations were made in which the number of iterations was set to a fixed value. This was achieved in SWAN by specifying a very strict convergence criterion and setting the maximum number of iterations to 5, 10, 20, 40 and 60. The results for four of these computations is shown in Figure 7.11. A summary of the significant wave height and mean period at a fetch of 25 km is shown in Table 7.2.

Number of iterations	Hs (m)	Tp (s)	Tm01 (s)
5	2.80	5.77	4.75
10	2.87	5.77	4.76
20	2.62	5.77	4.43
40	2.57	5.77	4.32
60	2.54	5.77	4.29

Table 7.2: Significant wave height, peak period and mean wave period as a function of the number of iterations for a fetch of 25 km, and a wind speed of 20 m/s.

From Figure 7.11 and Table 7.2 it can be concluded that the number of iterations affects the final results of a SWAN computation. In addition it is noted that the convergence behaviour of the significant wave height shows an overshoot near 10 iterations. This is an undesirable situation, especially since it is not known which one is the best solution.

8 Verification of SWAN against field measurements

8.1 Introduction

In this Chapter the SWAN model is verified against field measurements. To that end observed wave data obtained in three areas have been used: Lake George, the IJsselmeer and the Westerschelde estuary. Each of these data sets will be shortly described.

Of these areas Lake George is considered to be the most ideal for wave measurements because it is a relatively small closed basin where no currents exist and where detailed wave and wind measurements are available. The IJsselmeer is an artificial lake situated in the middle of the Netherlands. It is a fully enclosed basin where weak currents are present during periods of high winds and where slight variations in water level may occur. Wave and wind observations are only available at one location. Finally, the Westerschelde estuary is quite difficult from a modelling point of view. It is an area characterised by strong variations in depth, and the area is subject to tides causing time and space varying water levels and currents. On the other hand wave data have been obtained at about 10 locations in the outer area of the estuary.

The structure of this Chapter is as follows. In Section 8.2 the SWAN model settings are described. Followed by a description in Section 8.3 of the method to evaluate the model performance of SWAN. In the Section 8.4 through 8.6 the results of the verification for Lake George, the IJsselmeer and the Westerschelde will be presented.

8.2 Wave model settings

For the verification of SWAN the experimental version 45.00 has been used. In all SWAN computations the same (standard) settings were used. The standard convergence criteria as described in Section 7.2, were used. Further the standard physical processes for wave breaking, triads and bottom friction were activated. The wave breaking is modelled according to Battjes-Janssen (1978) with α_{BJ}=1 and γ_{BJ}=0.73. The bottom friction was modelled according to JONSWAP with Γ=0.067 m^2s^{-3}.

Computational results are given in the form of integral wave parameters. For all three data sets frequency spectra were available. Unfortunately directional information was not available that could have been used for verification purposes, or for the Westerschelde, as a wave boundary condition. Based on the observed and computed frequency spectra the following integral wave parameters have been computed:

- Hs: the significant wave height (m).
- T_p: Peak wave period (s).
- T_{pm}: the mean peak period. Tpm is equal to the block peak period Tpb or, in the case of a double peaked wave spectrum, equal to the maximum of the block peak period Tpb and the equivalent peak block peak period Tpbeq. For a uni-modal spectrum the block peak period is defined as the mean period $T_{m-1,0}$ for a region around the spectral peak. The integration limits of this region are based on the frequencies where the spectral density crosses the level of 40% of the energy density at the spectral peak. For a uni-modal spectrum the block peak period Tpb is computed as:

$$T_{pb} = \int_{f_1}^{f_2} \frac{1}{f} E(f)df \,/\, \int_{f_1}^{f_2} E(f)df \qquad (8.1)$$

in which f_1 and f_2 are the integration limits. It is noted that the definition of T_{pb} is similar to the definition of the dominant wave period T_{pd} (IAHR, 1989), in which T_{pd} is computed as the mean wave period T_{m01} for a region around the spectral peak based on a level of 80% of the peak value.

For double peaked spectra the block peak period is computed for each peak separately and then combined into a single value, computed as a weighted average of the individual block periods (see Seijffert, 1993; and Van der Meer, 1997):

$$T_{pbeq} = \sqrt[4]{T_{pb1}^4 \left(\frac{E_1}{E_{tot}}\right) + T_{pb2}^4 \left(\frac{E_2}{E_{tot}}\right)} \qquad (8.2)$$

in which E_i is the total energy per peak and E_{tot} the total energy of the wave spectrum.

Further information about the computation of Tpm can be found in Roskam (1997) and ALKYON (1999).

- T_{m-10}: mean wave period based on the frequency moments m-1 and m0.
- T_{m02}: mean wave period based on the frequency moments m0 and m2.
- κ: spectral narrowness parameter, as defined by Battjes and Van Vledder (1984), κ is close to 1 for a very narrow spectrum.

The parameter T_{m-10} and T_{m02} were chosen to have period measures that put either more weight on the lower frequencies (T_{m-10}) or on the higher frequencies (T_{m02}).

8.3 Evaluation of model performance

The evaluation of the SWAN model performance will be shown graphically in the form of frequency spectra and scatter diagrams. Numerically, the model performance will be expressed in terms of the following statistical parameters, in which x_i and y_i refer to the observed and predicted values respectively:

- BIAS, defined as the difference between the mean of the computations and the mean of the observed data values:

$$BIAS = \frac{1}{N}\sum_{i=1}^{n}(y_i - x_i) \qquad (8.3)$$

- the root mean square error RMSE:

$$RMSE = \left\{\frac{1}{N}\sum_{i=1}^{n}(x_i - y_i)^2\right\}^{1/2} \qquad (8.4)$$

The RMSE can be divided in two parts, a systematic and a non-systematic part. This can be achieved by using the results of a linear regression analysis, yielding a best-fit line $y = a + bx$. Then, for each observed data point x_i a corresponding best-fit point $\hat{y}_i$ can be computed. The systematic part of the RMSE gives the mean squared deviation of the linear regression line to the perfect line. The un-systematic part of the RMSE is a measure for the mean square error with respect to the linear regression line. The use of both the $RMSE_s$ and $RMSE_u$ gives insight into the nature of the prediction error.

- the systematic part of the root mean square error $RMSE_s$:

$$RMSE_s = \left| \frac{1}{N} \sum_{i=1}^{n} (\hat{y}_i - x_i)^2 \right|^{1/2} \tag{8.5}$$

- the unsystematic part of the root mean square error $RMSE_u$:

$$RMSE_u = \left| \frac{1}{N} \sum_{i=1}^{n} (y_i - \hat{y}_i)^2 \right|^{1/2} \tag{8.6}$$

The two parts of the RMSE satisfy the following relation:

$$RMSE_s^2 + RMSE_u^2 = RMSE^2$$

- the standard deviation STDEV, defined as:

$$STDEV = \sqrt{\frac{1}{N-1} \sum_{i=1}^{n} (y_i - x_i - BIAS)^2} \tag{8.7}$$

- the scatter index SI defined as the ratio of the RMSE and the absolute value of the mean $\bar{x}$ of the observations:

$$SI = \frac{RMSE}{|\bar{x}|} \tag{8.8}$$

- the coefficient of linear correlation r, defined as:

$$r = \frac{\sum_{i=1}^{n} (x_i - \bar{x})(y_i - \bar{y})}{\left\{ \sum_{i=1}^{n} (x_i - \bar{x})^2 \right\}^{1/2} \left\{ \sum_{i=1}^{n} (y_i - \bar{y})^2 \right\}^{1/2}} \tag{8.9}$$

- the first order index of agreement d_1 as proposed by Willmoth (1981), defined as:

$$d_1 = 1 - \frac{\sum_{i=1}^{n} |y_i - x_i|}{\sum_{i=1}^{n} \left[|y_i - \bar{x}| + |x_i - \bar{x}| \right]} \tag{8.10}$$

- the second order index of agreement d_2 as proposed by Willmoth et al. (1985), defined as:

$$d_2 = 1 - \frac{\sum_{i=1}^{n} |y_i - x_i|^2}{\sum_{i=1}^{n} \left[|y_i - \bar{x}| + |x_i - \bar{x}| \right]^2} \tag{8.11}$$

An extensive description of the use of graphics and statistical parameters in the evaluation of model performance can be found in DELFT HYDRAULICS (1992).

8.4 Lake George

Lake George is a shallow lake located in the south-east of Australia in which extensive wave observations have been carried out by the University of New South Wales (Young and Verhagen, 1996; Young, 1997). The lake is approximately 20 km long and 10 km wide. It has a relatively uniform bathymetry with an approximate water depth of 2 m. In Lake George an array of 8 wave measurement instruments has been applied. The geometry of Lake George and the locations of the wave measuring instruments are shown in Figure 8.1.

Since the lake has a mildly sloping bottom the northern coast line varies considerably due to seasonal variations in water level and wind effects. Consequently, the distance from the coast line to station 1 varies considerably. To remove this uncertainty for the wave modelling, a straight line is drawn across station 1, perpendicular to the orientation of the wave array, i.e. it was taken equal along a line through station 1 and parallel to the northern shore. This procedure differs a little from the procedure followed by Ris (1997) who took this line perpendicular to the wind direction for each case. The observed frequency spectrum was used as the upwind boundary condition along this line. Since no directional information is available, the directional distribution was schematised with a $\cos^2(\theta)$-distribution.

For all SWAN computations the same grid settings were used. The directional resolution was 10 ° and 30 frequencies were geometrically spaced between 0.125 Hz and 1.1 Hz. The spatial grid resolution was 250 m in both x- y direction and equal to the resolution of the available bottom topography.

It is noted that a constant wind field was used in the present computations for Lake George. A correction as proposed by Taylor and Lee (1984), always assumes a neutral stability of the atmosphere. As shown in Chapter 3, the wind profile depends on the land-water temperature difference and it is possible that the wind profile shows an overshoot in wind speed. Since no information about temperature differences was available, a constant wind speed was used.

The Lake George data set is quite large, therefore a selection has been made to cover a representative range of wind conditions. Since the measurement array is located more or less north to south, only northerly wind conditions have been selected. For the present study 9 conditions have been selected of which the first three have also been analysed by Ris (1997). The dates, times, water level and wind conditions are specified in Table 8.1.

Case	Date	Time	Water level (m/s)	Wind speed (m/s)	Wind direction (°N)
1	19/02/1992	22:00	0.10	6.3	344
2	3/10/1992	17:00	0.30	10.8	342
3	21/11/1992	16:00	0.28	15.2	341
4	12/05/1992	12:00	0.19	9.1	344
5	1/06/1992	22:00	0.28	7.0	342
6	31/10/1992	2:00	0.27	8.3	343
7	9/11/1992	9:00	0.29	4.0	346
8	3/10/1993	15:00	0.28	7.3	342
9	3/10/1993	16:00	0.19	8.8	346

Table 8.1: Summary of cases for verification of SWAN in Lake George

The spectral development as a function of fetch is shown in Figure 8.2 for case 4. In Figure 8.3 a comparison is made of the significant wave height Hs and peak frequency fp as observed and computed for all measurement locations. It is noted that for this case (but also for some of the cases not shown here), the computed wave height at the last two measurement stations 7 and 8 deviates much more from the observed wave height compared to the other stations. It is speculated that some unknown process is responsible for this behaviour. Finally, the performance of SWAN for all 9 cases at all 8 measurement stations is shown in the form of a scatter diagram for the parameters H_s, Tp, Tpm ,κ, T_{m-10} and T_{m02}. The results are shown in the Figures 8.4 through 8.6.

A summary of the statistical properties of the model performance of SWAN in Lake George is given in Table 8.2. In this table the results of station 1 are excluded, because they have been used as the initial condition.

Par	bias	rmse	rmses	rmseu	stdev	r	si	d1	d2
Hs	0.0140	0.0405	0.0273	0.0299	0.0380	0.9484	13.8981	0.8048	0.9612
Tp	-0.0741	0.1730	0.1141	0.1300	0.1560	0.9070	7.8256	0.7364	0.9329
kappa	-0.0368	0.0590	0.0517	0.0285	0.0459	0.3623	11.0211	0.3891	0.5334
Tpm	-0.1119	0.1764	0.1528	0.0882	0.1357	0.9410	8.4489	0.7033	0.9175
Tm-10	-0.1000	0.1668	0.1454	0.0817	0.1329	0.9304	8.6873	0.6818	0.9052
Tm02	0.0589	0.1160	0.0964	0.0645	0.0997	0.9267	7.2303	0.7503	0.9184

Table 8.2 Statistics of model performance of SWAN application in Lake George for the measurement stations 2 through 8.

In view of the remarks about the validity of the results at the stations 7 and 8 the statistical performance indicators have also been computed the stations 2 through 6. The results thereof are shown in Table 8.3.

Par	bias	rmse	rmses	rmseu	stdev	r	si	d1	d2
Hs	0.0100	0.0297	0.0196	0.0223	0.0280	0.9684	10.4207	0.8413	0.9760
Tp	-0.0673	0.1504	0.0860	0.1234	0.1341	0.9083	7.0397	0.7509	0.9386
kappa	-0.0336	0.0561	0.0527	0.0190	0.0446	0.2361	10.2640	0.3519	0.4591
Tpm	-0.1062	0.1554	0.1323	0.0814	0.1122	0.9427	7.6843	0.7157	0.9226
Tm-10	-0.1000	0.1593	0.1386	0.0785	0.1230	0.9243	8.5247	0.6777	0.8980
Tm02	0.0518	0.1024	0.0842	0.0582	0.0880	0.9330	6.5015	0.7689	0.9262

Table 8.3 Statistics of model performance of SWAN application in Lake George for the measurement stations 2 through 6.

The results of the SWAN application in Lake George is quite good. This follows from the scatter diagrams but also from the statistics of model performance shown in the Tables 8.2 and 8.3. The most interesting phenomenon is the behaviour of the period measures Tpm, T_{m-10} and T_{m02}. The scatter diagrams clearly show that the best fit lines (not shown here) are tilted. It is found that T_{m-10} is under predicted for the higher values of T_{m-10}, whereas T_{m02} is under predicted for the lower values of T_{m02}. This behaviour is an indication that the prediction of the forward face of the spectrum is over predicted for relatively lower periods and that the tail of the spectrum is over predicted for relatively high periods. The behaviour of the mean peak period Tpm shows that this period measure is under predicted for the relatively high periods. For relatively short fetches (< 5 km) the prediction of the period measure Tpm is very good.

Comparison of the scatter diagrams with the peak period Tp and the mean peak period Tpm, shows that Tpm has less scatter than the peak period Tp. This is a direct effect of the reduced sensitivity on the statistical variability of spectral estimates, see Young (1995).

The measure of the spectral width parameter κ shows the least agreement in comparison with the other parameters. This can be seen from the scatter diagram and the values of the correlation coefficient and the indices of agreement.

It is noted here that the scatter index SI has almost the same value for κ as for the significant wave height Hs. This is an indication that SI is not generally applicable as a parameter to evaluate model performance.

8.5 IJsselmeer

The IJsselmeer is a large shallow lake located in the central part of the Netherlands. The size is approximately 50 km by 25 km. The average bottom depth is about 5 m, at some locations deeper trenches exist which are the remains of tidal gullies before this lake was created by the closure of the Afsluitdijk. Disadvantages are that fact that the area is quite large resulting in (unknown) inhomogeneities in the wind field. Further, wave data are

only available at one location. At this location only the local wind speed is known such that the spatial distribution of the wind field is unknown.

In the period 1994-1995 wave and wind observations have been carried by the Dutch Ministry of Public Work and Transport, RIZA at location FL2, with Paris co-ordinates x=167861 m, y=530005 m. This location, Rotterdamse Hoek, is located in the south-western part of the lake. An overview of the bottom topography of the IJsselmeer and the measurement location is given in Figure 8.7.

At location FL2, wave observations have been carried out with a step resistance measuring device, with a sampling frequency of 4 Hz. These data were processed in segments of 20 minutes to obtain frequency spectra in the range 0.01 Hz-1.00 Hz at intervals of 0.01 Hz. Every 20 minutes such an analysis has been made.

At the same location the wind speed and direction were measured at a height of 10 m. Information on wind speed and wind direction are available every 10 minutes. To reduce the statistical variability of the wind speed characteristics a moving average has been computed on the basis of the 10 minute wind speeds during the last hour.

For the verification of the SWAN wave model 16 periods have been selected on the basis of stationarity in wind, water level and wave conditions and the availability of observed data. To decrease the statistical variability in wind and water level conditions, the average conditions during these periods have been taken as boundary conditions for the wave model computations. Characteristics of these periods and boundary conditions are summarised in Table 8.4. In this table the parameter N denotes the number of conditions that have been used in the averaging in each period.

Case	Period	N	Water level (m)	Wind speed (m/s)	Wind direction (N°)
1	4-5/12/94 20-01	6	-0.39	11.5	224.2
2	21/1/95 16-18	3	-0.36	13.6	174.4
3	26/1/95 16-18	3	0.08	15.0	24.0
4	16/2/95 02-04	3	0.08	11.3	236.0
5	28/2/95 12-13	2	0.11	11.3	234.5
6	03/3/95 15-16	2	0.24	19.7	236.0
7	16/1/95 08-12	5	-0.22	9.2	189.4
8	16/1/95 21-01	5	-0.23	11.4	193.0
9	21/1/95 08-12	5	-0.28	9.5	210.4
10	23/1/95 12-18	9	-0.10	15.3	250.9
11	25/1/95 00-03	4	-0.09	8.9	231.0
12	27/1/95 10-12	3	0.11	8.6	283.3
13	16/2/95 12-16	5	0.16	14.0	251.8
14	17/2/95 12-16	5	0.23	13.8	263.8
15	01/3/95 12-16	5	0.08	15.0	214.4
16	05/3/95 07-12	6	0.00	13.8	184.0

Table 8.4: Summary of conditions used for the verification of SWAN in the IJsselmeer

In the SWAN modelling the following IJsselmeer specific settings were used. Since the bottom topography was available at a grid of 250 m, the spatial grid was chosen to have

a grid resolution of 250 m. A total of 30 frequencies were used, geometrically distributed in the range 0.03 Hz - 1.0 Hz. The directional resolution was 10°.

To compare the results of the SWAN model with the observations, the observed hourly spectra have been averaged to compute a representative wave spectrum for the periods considered.

An example of such an averaging is shown in the upper panel of Figure 8.8 for period 1. In the lower panel the averaged spectrum is compared with the predicted spectrum. The analysis of the wave model performance is based on the computation of integral wave parameters from the averaged measured spectra and from the computed spectrum.

The results are shown as a scatter diagram of observed parameter values against computed parameter values. For Hs and Tp the results are shown in Figure 8.9. For κ and Tpm in Figure 8.10 and for the period measure Tm-10 and Tm02 they are shown in Figure 8.11. The results of the statistical analysis are shown in Table 8.5.

Par	bias	rmse	rmses	rmseu	stdev	r	si	d1	d2
Hs	0.0156	0.0882	0.0663	0.0581	0.0867	0.9544	11.6537	0.7872	0.9603
Tp	-0.1094	0.2570	0.1794	0.1840	0.2308	0.8914	7.0499	0.7238	0.9177
kappa	-0.0363	0.0498	0.0417	0.0272	0.0328	0.5772	9.2975	0.4119	0.6227
Tpm	-0.1563	0.2389	0.2087	0.1161	0.1761	0.9490	6.7761	0.7472	0.9223
Tm-10	-0.1800	0.2457	0.2311	0.0833	0.1606	0.9674	7.7502	0.7059	0.9068
Tm02	-0.1537	0.2073	0.1883	0.0868	0.1333	0.9478	7.5109	0.6854	0.8987

Table 8.5: Statistics of model performance of SWAN application in the IJsselmeer

The performance of SWAN in the IJsselmeer is rather good. The significant wave height is slightly overestimated for wave heights up to 1 m, whereas for higher wave heights a slight under prediction occurs. The peak period is slightly under predicted. The spectral width by means of the narrowness parameter κ is quite good. The scatter comparable with the one for the Lake George verification. The mean peak period is sligthly under estimated. Both the mean wave period T_{m-10} and T_{m02} are under estimated. It can also be seen that the best fit line on the basis of a linear regression analysis is tilted in a similar manner as for the Lake George verification.

8.6 Westerschelde

The Westerschelde estuary is located in the south west of the Netherlands. An overview of the Westerschelde estuary and outer delta is shown in Figure 8.12. In this area wave measurements are available at a number of stations. These stations also shown in Figure 8.12. A summary of the names and locations of these stations is given in Table 8.6.

Station name	x-coordinate	y-coordinate
SCHB	11244.	419519.
BG2Z	32824.	421369.
DELO	6071.	392601.
SCHW	-7797.	380645.
SCHO	9915.	381366.
WIEL	17667.	383867.
WOV3	34534.	384687.
WOV6	36456.	383405.
WOV5	36967.	381292.
WOV4	40102.	379736.
WOV2	44181.	377914.
WOV1	44375.	374417.

Table 8.6: Summary of stations and locations in the Westerschelde area. Locations are given in the Paris co-ordinate system

The Westerschelde area is characterised by many shallow areas, an irregular coastline, currents and waves from the North Sea. From a modelling point the Westerschelde is a difficult area because the wave conditions are influenced by time-and space varying currents, water levels and wind fields. The difficulties are related to the fact that the stationary version of SWAN is used in the verification and because no detailed information is available about the spatial and temporal variation of the water levels, currents and wind fields. Another problem is that the wave boundary conditions are only available at a few stations in the form of frequency spectra and that directional wave information is only available at the EURO platform which is located more than 40 km from the entrance to the Westerschelde estuary.

For the verification of SWAN in the Westerschelde 15 storms have been selected on the criterion of minimal current effects, because it was not possible (at least in this study) to perform current computations to provide current and water level fields. Based on an analysis of the behaviour of current and water levels in the Westerschelde it was found that the optimum moments for a verification are 1 hour after high water and 1.5 hour after low water. At these moments the water level variation can be considered a flat surface over a relatively large area near Vlissingen. Using this assumption, a constant water level can be specified in the SWAN model input file. Since most of the measurement locations are situated in the western part of the Westerschelde tidal curves observed near Vlissingen have been used for this analysis. The wind speed and wind direction to be used in the computations were taken at the station Hoofdplaat.

A summary of the conditions is given in Table 8.6.

Storm number	Date	Time	Water level (m)	Wind speed (m/s)	Wind direction (°N)
1	19/12/1991	12:00	1.62	13.3	239
2	19/12/1991	19:00	-0.9	10.6	226
3	20/12/1991	1:00	2.72	13.2	284
4	20/12/1991	7:00	0.29	12.5	273
5	20/12/1991	13:00	2.81	12.4	275
6	20/12/1991	19:30	-0.01	15.1	290
7	23/12/1991	15:30	2.55	14.6	229
8	23/12/1991	22:00	-0.56	11.5	303
9	13/3/1992	15:30	-0.09	15.8	282
10	13/3/1992	21:00	1.67	12.1	286
11	14/3/1992	4:00	-0.29	14.9	295
12	14/3/1992	9:30	1.67	12.2	300
13	13/4/1992	11:00	1.68	12.5	248
14	9/5/1992	19:30	1.67	13.4	236
15	25/1/1990	20:00	0.25	22.0	250

Table 8.6: List of conditions used for the verification of SWAN against measurements in the Westerschelde estuary.

For the storms 4, 8, and 12 no observed spectra were available for the computation of spectral parameters, but only integral wave parameters for the significant wave height Hs, peak period Tp and mean wave period Tm02. These values were used in the evaluation of the SWAN model performance. For storm 15 spectral information was only available for the stations BG2Z, DELO and SCHO. For station BG2Z spectral information was not available at hour 20:00, but at the previous and the next hour. These two spectra looked very similar and therefore they were averaged to obtain a representative spectrum for 20:00 hours.

The standard SWAN settings were used for the verification of SWAN in the Westerschelde. The water level was modelled as a flat surface. The wind speed was constant over the whole area, no spatial variation was included. The wave boundary condition was specified as a constant wave spectrum along the boundary of the outer N1 grid in terms of a JONSWAP spectrum with a certain significant Hs and peak period Tp. Because no directional wave information was available the mean wave direction was set equal to the wind direction. In addition, the directional spreading was modelled using a cos2 distribution.

The results of the SWAN computations are presented in the form of a comparison observed and computed frequency spectra. For storm 7 the results are presented for all stations in Figure 8.13. The results for all storms are also shown as a scatter diagram of observed parameter values against computed parameter values. For Hs and Tp the results are shown in Figure 8.14. For κ and Tpm in Figure 8.15 and for the period measure Tm-10 and Tm02 they are shown in Figure 8.16. The results of the statistical analysis are shown in the Tables 8.7.for all stations and in Table 8.8. for the station within the Westerschelde estuary.

The statistics of the SWAN model performance in the Westerschelde are given in Table 8.7 for all stations.

Par	bias	rmse	rmses	rmseu	stdev	r	si	d1	d2
Hs	0.2268	0.4132	0.2277	0.3449	0.3450	0.9497	25.6093	0.8322	0.9628
Tp	0.5952	1.3195	0.6377	1.1552	1.1767	0.8143	24.7858	0.6901	0.8752
kappa	-0.0226	0.1347	0.1047	0.0849	0.1328	0.3916	33.5711	0.4672	0.6040
Tpm	0.4327	0.9445	0.4362	0.8377	0.8387	0.8775	18.4134	0.7278	0.9122
Tm-10	0.2812	0.6339	0.2832	0.5671	0.5675	0.9252	13.7401	0.7900	0.9494
Tm02	-0.0360	0.5020	0.0876	0.4943	0.5007	0.9070	12.6474	0.8053	0.9510

Table 8.7: Statistics of model performance of SWAN application in the Westerschelde estuary (all stations).

Par	bias	rmse	rmses	rmseu	stdev	r	si	d1	d2
Hs	0.1846	0.2853	0.1937	0.2094	0.2166	0.9018	32.8091	0.6876	0.9178
Tp	0.3455	1.2243	0.6779	1.0195	1.1740	0.6578	29.2096	0.5519	0.7882
kappa	-0.0227	0.1630	0.1472	0.0699	0.1614	-0.0017	46.1930	0.2476	0.3374
Tpm	0.1246	0.8697	0.3787	0.7829	0.8605	0.7092	20.7583	0.6216	0.8385
Tm-10	0.1415	0.5732	0.2073	0.5344	0.5552	0.8120	15.5670	0.6577	0.8937
Tm02	-0.0928	0.4806	0.2491	0.4110	0.4715	0.7435	15.1009	0.6296	0.8539

Table 8.8: Statistics of model performance of SWAN application in the Westerschelde estuary for inner points (stations WOV1 through WOV6).

Inspection of the spectral shapes (see Figure 8.13) as observed and predicted by SWAN shows that the observed spectra show a large amount of scatter, but that the general shape is fairly well reproduced.

Inspection of the scatter diagrams (Figures 8.14 through 8.16) shows that the significant wave height is over estimated, especially for the higher wave heights. No firm conclusions can be drawn about the peak period Tp because of the large amount of scatter. This scatter is slightly reduced when the scatter diagram for the mean peak period Tpm is inspected. It is found that the mean peak period is in general slightly over estimated. The scatter in the spectral narrowness is quite large. This is an indication that the spectral shape is not properly predicted by the SWAN model. This is probably a direct effect of the uncertainties associated with the specification of the wave boundary conditions and the complexity of the area. The mean wave period Tm-10 is fairly well reproduced with a tendency for an over prediction. The mean wave period Tm02, however, is slightly under estimated. This is an indication that the amount of wave energy in the spectral tail is underestimated.

8.7 Discussion of results

In this chapter the SWAN model has been verified against measured data from three sources. Based on the results for Lake George it can be concluded that the SWAN model performs very well for this area for which good wave and wind information are available.

The performance for the IJsselmeer is not so good as for Lake George, but still it can be concluded that SWAN performs well. Part of the prediction errors are probably due to uncertainties related to the spatial variation and stationarity of the wind field. It is also possible that land-sea effect affects the wind field.

For the Westerschelde the performance is still quite acceptable, although the scatter in the results larger than for lake George and the IJsselmeer. Here, a number of effect influence the prediction error. First, there is an uncertainty about the proper wave boundary conditions, the water level, the currents and the wind field. In the verification for the Westerschelde, SWAN has been applied in stationary mode, whereas the geophysical conditions in the Westerschelde area can not be regarded as stationary and homogeneous. It is therefore recommended that future SWAN computations for the Westerschelde estuary are performed with improved descriptions of the water level and current fields. It is recommended that that more realistic wind fields are used.

The results for Lake George and the IJsselmeer show a typical trend in the predication of the mean wave periods Tpm, Tm-10 and Tm02. The best-fit line obtained with linear regression analysis is tilted. The higher the observed wave period, the higher the under prediction. This behaviour is a clear indication that the spectral shape is not properly predicted.

9 Calibration of SWAN

9.1 Introduction

The purpose of the calibration is to obtain a (new) set of coefficients for the SWAN model with which the SWAN model is able to reproduce growth curves from literature on the basis of operational settings of the SWAN model. The present version of SWAN has been calibrated against the growth curve of Wilson (1965) using strict convergence criteria and using different decades to have optimal representation of the fetch. In this was a good match was obtained. A disadvantage of this numerical settings causes the SWAN model to perform many iterations. For operational conditions, SWAN is applied with its recommended settings and then SWAN is not able to reproduce the growth curves from literature. Especially the significant wave height is overestimated. To overcome this shortcoming, the SWAN model will be calibrated against known growth curves. It is noted that an overview of known growth curves is included in Appendix A.

For the calibration of SWAN against known growth curves the following approach has been applied:

- from a number of known growth curves (e.g. Kahma & Calkoen, Wilson, Bretschneider) the growth curve of Kahma and Calkoen (1992) was chosen for the initial analysis as the reference. There is, however, no reason NOT to choose any of the other curves. From Figure 7.2 it can be seen that the curves from Wilson (1965) and Kahma and Calkoen (1993) are very similar.
- The tuning has been performed for short fetches up to 25 km. It was the wish of the Client to have a set of input coefficients that works for short fetches. If possible the settings should also work for longer fetches. In the initial phase of the study, the calibration has been set up for a fetch of 25 km.
- One of the deficiencies of the SWAN model is that it over predicts the significant wave height for situations with a constant wind speed. The prediction of the mean wave period, however, is rather good. The calibration has been done on the coefficients of the physical processes. Numerical settings have been left out of the calibration, although they may be important.
- The most simple method of reducing the wave height is to use a lower wind speed. This, however, also reduces the mean wave period. It is therefore necessary to choose settings of source functions that are able to influence either the growth of the mean wave period or of the significant wave height.
- The processes that are able to influence both the wave height and period are the whitecapping dissipation and the nonlinear quadruplet interactions. Therefore a special version of SWAN has been made in which it is possible to set additional parameters of these source terms.

In the present study the ARCADIA program (Digital Hydraulics, 1995a,b) has been applied to calibrate an experimental version of the SWAN wave model against the growth curve of Kahma and Calkoen, 1992).

9.2 Model version of SWAN

The modifications to the SWAN wave model have been made in the source terms for whitecapping and the nonlinear quadruplet interactions. These changes have been implemented in a special version of the SWAN model (30.34). Two types of modifications were made:

- the formulation of the whitecapping source function (Eq. 4.38) was rewritten and extended as follows:

$$S_{ds}(\sigma,\theta) = -\hat{C}_{ds}\hat{\omega}\left(\frac{k}{\hat{k}}\right)^{n}\left((1-\delta)+\delta\left(\frac{k}{\hat{k}}\right)\right)\left(\frac{s}{s_{PM}}\right)^{m} \times E(\sigma,\theta) \qquad (9.1)$$

  in which the variables Cds, n, and m are tuneable coefficients.
- the coefficient λ specifying the shape of the basic wave number quadruplet and the magnitude of these interactions C_{nl4} were made variable.

The following variables were defined as tuneable variables that can be used in the sensitivity analysis and the calibration, the names in brackets are the names of the variables as they appear in the input files for the ARCADIA program.:

C_{ds}	the proportionality factor for whitecapping [CDS2]
n	the power of the wave number ratio [POWK]
m	the power of the wave steepness ratio [POWST]
δ	the fraction of accounting for the wave number ratio, [DELTA]
λ	the wave number configuration parameter for the Discrete Interaction Approximation [LAMBDA]
C_{nl4}	The proportionality factor for nonlinear quadruplet interactions. [CNL4]
s	Integral wave steepness
s_{PM}	Integral wave steepness for a Pierson-Moskowitz spectrum

9.3 Sensitivity analysis

The interest of this project was to find out what are the parameters to be twiddled in SWAN, for the results the model gives to match known growth curves. In that context, the first idea was to try out a large number of parameters to do with dissipation by whitecapping, to do with non-linear interactions, or with the general shape of the spectra and its cut-off frequencies.

But then it was deemed safer for the sensitivity analysis to be restricted to a 'small' number of parameters (those that are expected to have the most direct influence on the wave period). The only parameters considered in this study are CDS2, POWST and POWK (accounting for dissipation by whitecapping), and LAMBDA and CNL4 (for the non-linear interactions). The parameter δ was not used in the actual calibration. Because in the calibration the Komen et al. (1984) wind input term was used, the factor δ was set to zero.

Both sensitivity and calibration runs were performed on the basis of the default settings in SWAN. That is CDS2=0.236e-4, POWST=2, POWK=1 and LAMBDA=0.25, CNL4=3×10^{-7}.

An essential part of the calibration of SWAN is a sensitivity analysis of the effect of variations in input variables on the resulting values for the significant wave height and mean wave period. The normalised effect of these variations is an essential part of the calibration in which these deviations are used to guess the optimal parameter setting. It is also important that these deviations should be linear, otherwise unexpected nonlinear effects affect the calibration. In that context, sensitivity analyses were carried out, intended to test the linearity of the phenomena in the region of interested. This was done by means of a set of three analyses where the constraint on all five parameters were doubled and halved. It revealed strong non-linearity's upon CDS2 and POWST. It was then deemed that the penalty function for those parameters should be quite hard not to get unrealistic results out of the calibration.

Following discussions with Delft University of Technology, it was found that the following uncertainties in all five parameters were realistic and appropriate. That is 10% for CDS2, 5% for POWST, 15% for POWK, 5% for LAMBDA and 3% for CNL4. Those factors account for the confidence on the original values for CDS2, POWST, POWK, LAMBDA and CNL4.

9.4 Configuration of calibration

In the SWAN schematisation, the grid resolution is 50 m in the x-direction (1D model option) while the spectral directional resolution is 10 ° over 30 frequencies. The conditions are deep water (1000 m water depth), over relatively short fetches, 25 km for all cases. The wind speed used in the calibration was 20 m/s.

9.5 Results of calibration

In the calibration of SWAN a percentage must be specified, which directly influences the penalty function of deviations in that parameter. The lower this percentage, the higher the penalty. In this way the results of any calibration with ARCADIA can be influenced, including which parameter is allowed to vary more than an other. Many different settings have been used. In this report only 4 of these settings are summarised in Table 9.1.

Case	CDS2	POWST	POWK	LAMBDA	CNL4
1	5	5	5	5	5
2	10	5	15	3	4
3	0.5	0.5	0.5	5	5
4	5	5	5	0.5	0.5

Table 9.1: Percentage of allowed variations in the calibration of SWAN.

For each case a set of SWAN computations has been made using the ARCADIA shell. For each case 5 sets of computations have been performed to assess the sensitivity (within the given constraints) on the computational results. This formed the basis of a prediction of the optimal settings. Subsequently these optimal settings were used as input in a verification run, to see if the new settings result in a growth curve closer to the specified 'measured' data (In this case the growth curve of Kahma and Calkoen, 1992).

The result of the calibration runs are summarised on Table 9.2, which includes the optimal parameter setting per case.

Case	CDS2	POWST	POWK	LAMBDA	CNL4
0	**0.2360×10^{-4}**	**2**	**1**	**0.25**	**0.3×10^{-8}**
1	0.6481×10^{-4}	2.318	0.117	0.2596	0.438×10^{-8}
2	0.4531×10^{-4}	2.685	0.111	0.2728	0.364×10^{-8}
3	0.4033×10^{-4}	2.497	0.450	0.2517	0.3×10^{-8}
4	0.5551×10^{-4}	2.272	0.134	0.2757	0.3×10^{-8}

Table 9.2: Summary of optimal parameter settings obtained from the calibration of SWAN. The standard settings are summarised in the upper row for case 0.

The results of the calibration are summarised in the Figures 9.1 through 9.4. From these Figures it is concluded that other parameter settings could be found for SWAN, which affect the growth curve of the significant wave height AND the mean wave period in different ways. It is also found that the results for case 2, did not result in a proper parameter setting. It is also noted that the resulting parameter settings resulted in a somewhat wiggling behaviour along the fetch.

The spectral development of the resulting spectra seems OK, they result in peaked spectra and the overshoot, which is characteristic for growing waves, is present in all results. This seems to be a robust feature of the SWAN model.

The best calibration values are the one obtained for case 3, because they are the closest to the present settings and because they give a good agreement between the parameterised growth curve and the computational results.

It is noted that a small adaptation of the growth curve of the significant wave height was made to better comply with the calibration process. Growth curves from literature predict H_s=0 and T_{m01}=0 for a fetch length equal to 0. Some problems were encountered when considering those values as starting point in the comparison of the Kahma and Calkoen curves with those of SWAN, at calibration stage. This has been dealt with by forcing the initial values (for F = 0) to H_s=0.0100m and T_{m01}=1.000s.

9.6 Concluding remarks

There is no facility as such in ARCADIA to constrain the parameters to a given range of values (we cannot specify a maximum value). Only by means of a penalty function can one constrain the allowed variation for each parameter. But when the phenomena are suspected to be non-linear and the calibration is run iteratively, nothing really can prevent the optimal parameters from getting unrealistic.

The ARCADIA model has been used to calibrate the SWAN model against a known growth curve from literature. The results of the calibrations is that the discrepancy between observed and estimated significant wave height and wave period has nearly vanished. The resulting spectra that came out the calibration runs looked like normal JONSWAP spectra and they showed the typical overshoot for young growing waves.

The ARCADIA model has been shown to be an efficient tool for calibrating the SWAN model against observed wave data. Although the calibration did not always produce a good fit for all parameters considered, it provides a good starting point for further calibration studies with the SWAN wave model.

It has been possible to calibrate the SWAN model in such a way that either the growth curve of the significant wave height or of the mean wave period is adapted. This was realised by modifying the source term for whitecapping dissipation in such a way that the frequency distribution of the dissipation was modified. In addition, the SWAN model was extended with an option to specify the parameter value of the quadruplet wave number configuration parameter λ. These changes affect to shape of the total source function, which in turn affects the shape of the spectrum.

The present calibration was carried out for a fetch of 25 km and a wind speed of 20 m/s. It is recommended to test these settings for other fetch lengths and wind speeds, but also for applications to field data.

10 Conclusions

In this study the wave model SWAN has been investigated with respect to its ability to give good predictions at short fetches. To that end the following aspects have been studied:

- the effect of islands and the land-sea boundary on the wind profile and its effect on the wave evolution,
- source functions for wind input, dissipation by whitecapping and nonlinear quadruplet wave-wave interactions,
- the effect of swell on the growth of wind waves,
- the modelling of nonlinear interactions on the source term balance in the spectral tail,
- a sensitivity analysis of SWAN with respect to various numerical and physical settings,
- a verification of SWAN against field data,
- a calibration of SWAN against growth curves from literature.

For each of these aspects the following conclusions can be formulated.

wind and wave modelling after a land-sea transition

- The effect of atmospheric instability, which has been included via the temperature difference between water and land, affects the wind profile both on the island and downwind.
- For a warm island, there is an overshoot in the wind speed, compared to the wind speed in front of the island. This overshoot does not occur for a cold or a neutral island.
- The roughness of the island has a small effect on the wind profile behind the island.
- The width of the island does not have much influence on the wind profile behind the island
- The effect of a spatially varying wind profile, has only a small effect on the growth of the waves behind the island in comparison with computations with a constant wind speed. The difference obtained by using a spatially varying wind field are in the order of 5%.
- Errors up to 10% in wave height and mean wave period are made, when a wrong constant wind speed is used. Such a wrong wind speed can be obtained by measuring just behind an island, thus getting a wind speed which deviates by 10% from a spatially averaged wind speed (for the case investigated in this study)

Source functions

- For the wind input source function, a number of alternative source functions have been formulated in literature. Of these source functions, the one proposed by Burgers and Makin predicts a negative wind input for opposing winds. This feature may be important in wave modelling. It may help as an extra damping mechanism in the SWAN sweep algorithm to get rid of undesirable oscillations.
- The present formulation of the dissipation by whitecapping is very sensitive to the occurrence of a swell system. This causes a lower dissipation rate than can be expected on the basis of a wind sea system alone. This effect is caused by the way in which the mean wave period is computed. This mean wave period, in turn, is used to scale the total dissipation rate.

- The nonlinear quadruplet interactions are modelled with the Discrete Interaction Approximation. This approximation is quite a bad approximation when comparisons have been made with exact methods for specific target spectra. Better approximations are needed, because they affect the source term balance.

The effect of swell on wave growth

- Based on a literature survey it is found that in reality the occurrence of swell, tends to dampen the wave growth of shorter waves. The effect is not large and some authors claim contradictory results. These findings are based on considerations related to the physics of the swell-sea interaction.
- In third generation models like SWAN or WAM, however, the presence of a swell system enhances wave growth, because the dissipation by whitecapping is strongly reduced. This finding is related to the modelling techniques and not to the physics.

The effect on nonlinear interaction for high frequencies

- It is found that the DIA affects the source term balance at high frequencies, resulting in a jumpy behaviour. This is because the nonlinear interactions are scaled with frequency to the power 11. These oscillations are also responsible of introducing wiggles in the total source term, thereby affecting the integration of the wave evolution equation. It is likely, that this behaviour is one of the reasons for having a limiter to keep the integration stable.
- The DIA shows more oscillations for a spectrum with a spectral tail of the power -4 than for a tail with a power of -5.

Sensitive analysis of SWAN (1D-case: deep water)

- The SWAN model over predicts the significant wave height at short fetches
- For the cases investigated, the SWAN wave model is sensitive to the convergence criteria, and an overshoot is noted in the convergence behaviour of the significant wave height.
- The SWAN model is not sensitive to grid spacing of 20 m, 50 m or 100 m for a fetch of 25 km, and a constant wind speed of 20 m/s.
- The SWAN model is not sensitive to the cut-off frequency
- The SWAN model does not scale with wind speed (at least when U10 is used)
- The SWAN model scales with the friction velocity u. ,when the operational convergence criterion is used.
- The SWAN model is sensitive to the number of iterations

Verification of SWAN against field data

- The SWAN model performs very well in Lake George, for the IJsselmeer the performance is good. For the Westerschelde the performance is acceptable.
- The results of the SWAN verification for Lake George clearly indicate that the best fit line of the predicted values for the mean wave periods measures is tilted. The higher the observed wave period, the lower the predicted wave period measure.

Calibration of SWAN

- The SWAN model has been extended with extra input variables which enable more control over the dissipation by whitecapping and nonlinear interactions.
- New parameter settings have been found which produces a good agreement with the growth curve of Kahma and Calkoen for a fetch of 25 km and a wind speed of 20 m/s.

11 Recommendations

In this study a number of shortcomings of the SWAN wave model have been identified. Most of these shortcomings are inherent in third-generation wave prediction models, of which SWAN is one. Some of these shortcomings, however, may be related to the numerical methods applied in the SWAN model, viz. the sweep mechanism. To improve the SWAN model the following recommendations have been formulated:

Physics

- The effect of 'negative' wind input on the evolution should be quantified to assess its importance on wave evolution.
- The directional characteristics of wind input at large angles should be investigated.
- The sensitivity of whitecapping dissipation to the occurrence of a swell in a wind-sea wave system should be changed. This may be achieved by an other definition of the average wave steepness in the present formulation for whitecapping or by dividing the spectrum into a number of separate wave systems and computing the whitecapping dissipation per system, or by introducing a frequency dependent wave steepness.
- The Discrete Interaction Approximation should be replaced by a better approximation. Such a new approximation should retain the basic characteristics of the nonlinear interactions at both low and high frequencies and it should be fast enough to incorporate in operational wave prediction models like the SWAN model.
- Attention should be paid to the power of the spectral tail. Application of an f^{-4} tail might be better on physical ground. From a modelling point of view, however, the use of an f^{-4} tail enhances numerical instabilities.

Numerics

- The optimum number of iterations should be determined for operational applications of the SWAN model.
- The sensitivity of the SWAN model to the number of iterations should be investigated.
- The effect of delimiters on the solution of a SWAN computation should investigated and its effect should be minimised
- A comparison should be made between a one-dimensional SWAN computation and solely forward moving integration technique to assess the effect of the SWAN sweep mechanism on the solution.

Verification of SWAN

- To further analyse the Lake George data for more situations and to compare the results with the finite depth growth curves of Young (1997).
- Additional measurement locations should be performed in the IJsselmeer, in addition better desciprions of the wind field should be constructed, probably on the basis of additional observations around the IJsselmeer.

- For the verification of SWAN in the Westerschelde better descriptions of the water level and current fields should be made, but also more attention should be paid to the specification of the wave boundary condition.
- the scaling of SWAN with wind speed U10 and friction velocity u* should be investigated when the strict convergence criterion is used.

Calibration of SWAN

- The present calibration was carried out for a fetch of 25 km and a wind speed of 20 m/s. It is recommended to test these settings are checked for other fetch lengths and wind speeds, but also for applications to field data.

Wind model

- Measurements should be performed to verify the model of Kudryavtsev and Makin. Such measurements should included data on wind speed and temperatures.
- The model of Kudryavtsev and Makin should be extended with two-dimensional effects.

References

ALKYON, 1998: Golfrandvoorwaarden voor dijkontwerp in door dammen afgeschermde gebieden. D.P. Hurdle, ALKYON Report A314, Vol. A, Golfberekeningen - methodiek en productie (in Dutch), Wave boundary conditions in sheltered areas behind dams, Vol. 1, wave model computations - methodology and production.

ALKYON, 1999: Operational peak period and test. ALKYON Report A411, G.Ph. van Vledder.

Balk, A.M., 1996: The suppression of short waves by a train of long waves. J. Fluid. Mech., Vol. 315, 139-150.

Banner, M.L., and I.R. Young, 1994: Modelling spectral dissipation in the evolution of wind waves. Part I: Assessment of existing model performance. Journal of Physical Oceanography, Vol. 24, 1550-1571.

Battjes, J.A., and J.P.F.M. Janssen, 1978: Energy loss and set-up due to breaking of random waves. Proc. 16th Int. Conf. on Coastal Engineering, ASCE, 569-587.

Battjes, J.A., and G.Ph. van Vledder, 1984: Verification of Kimura's theory for wave group statistics. Proc. 19th Conf. On Coastal Engineering, 642-648.

Bergstrom et al., 1986: A study of wind speed modification and internal boundary layer heights in a coastal region, *Boundary-Layer Meteorol.*, Vol. 42, 313-335.

Bretschneider, C.L.,1973: in Shore Protection Manual, CERC, US Army Corps of Engineers. Tech. Rep. No. 4.

Burgers, G., and V.K. Makin, 1993: Boundary-layer model results for wind-sea growth. J. Phys. Oceanogr., Vol. 23, 372-385.

Cavaleri, L., and P. Malanotte Rizzoli, 1981: Wind Wave Prediction in Shallow Water: Theory and Applications, Journal of Geophys. Res., Vol. 86, No. C11, 10,961-10,973.

Charnock, H., 1955: Wind stress on a water surface. Quarterly Journal Royal Meteo. Soc. Vol. 81, 639-640.

Davidson, K.L., and A.K. Frank, 1973: Wave-related fluctuations in the airflow above natural waves. J. Phys. Oceanogr., Vol. 3, 102-119.

DELFT HYDRAULICS, 1992: Evaluation of model performance. Rep. H1224, G.Ph. van Vledder.

DELFT HYDRAULICS, 1994a: PHIDIAS - a program for the computation of wind-wave energy. DEFDOC- conceptual model, Vol. 2, Part 1 of 1, G.Ph. van Vledder, Report H1861.

DELFT HYDRAULICS, 1994b: Verification of PHIDIAS. DELFT HYDRAULICS Rep. H1914, G.Ph. van Vledder.

Delft University of Technology, 1998: USER MANUAL, SWAN Cycle 2 version 30.75, R.C. Ris, N. Booij, L.H. Holthuijsen, R. Padilla-Hernandez,, and IJ.G. Haagsma.

Digital Hydraulics, 1995a: ARCADIA Primer, Introduction for first users of ARCADIA, N. Booij.

Digital Hydraulics, 1995b: The ARCADIA system, User manual. N. Booij.

Dobson, F., W. Perrie and B. Toulany, 1989: On the deep-water fetch laws for wind-generated surface gravity waves. Atmos.-Oceans, Vol. 27, 210-236.

Donelan, M.A., 1987, The effect of swell on the growth of wind waves. John Hopkins APL Technical Digest, Vol. 8, No. 1, 18-23

Donelan, M.A., and F.W. Dobson, 1997: The influence of swell on the drag. Manuscript to be published.

Donelan, M.A., 1998: Presentation at WISE meeting, Leuven, Belgium.

Eldeberky, Y., and J.A. Battjes, 1995: Parameterisation of triad interactions in wave energy models. Coastal Dynamics '95, Int. Conf. On Coastal Res. In Terms of Large Scale Experiments, Gdansk, Poland.

Gautier, C., 1997: SWAN golfberekeningen in de Waddenzee. Rapport RIKZ

Gryning, S.-E., 1985: The Oeresund experiment - a Nordic mesoscale dispersion experiment over a land-water-land area, *Bull. Americ. Meteorol. Soc.*, Vol. 66, 1403-1407.

Harris, D.L., 1966: The wave-driven wind. J. Atmos. Sci., Vol. 23, 688-693. (quoted in Donelan and Dobson, 1997).

Hasselmann, K., 1962: On the non-linear energy transfer in a gravity-wave spectrum, Part 1: general theory. J. Fluid Mech., Vol. 12, 481-500.

Hasselmann, K., 1963a: On the non-linear energy transfer in a gravity-wave spectrum. Part 2. Conservation theorems; wave-particle analogy; irreversibility. J. Fluid Mech., Vol. 15, 273-281.

Hasselmann, K., 1963b: On the non-linear energy transfer in a gravity-wave spectrum. Part 3. Evaluation of the energy flux and swell-sea interaction for a Neumann spectrum. J. Fluid Mech., Vol. 15, 385-398.

Hasselmann, K., 1974: On the spectral dissipation of ocean waves due to white capping. Bound.-Layer Meteorology., Vol. 6, 107-127.

Hasselmann, K., T.P. Barnett, E. Bouws, H. Carlson, D.E. Cartwright, K. Enke, J.A. Ewing, H. Gianapp, D.E. Hasselmann, P. Kruseman, A. Meerburg, P. Müller, D.J. Olbers, K. Richter, W. Sell, and H. Walden, 1973: Measurements of wind-wave growth and swell decay during the Joint North Sea Wave Project (JONSWAP). Deutsches Hydrographisches Zeitschrift, Reihe A (8°), Nr. 12.

Hasselmann, S., and K. Hasselmann, 1981: A symmetrical method of computing the nonlinear transfer in a gravity wave spectrum. Hamburger Geophysikalische Einzelschriften, Reihe A: Wissenschaftliche Abhandlungen, Heft 52.

Hasselmann, S., and K. Hasselmann, 1985a: Computations and parameterizations of the nonlinear energy transfer in a gravity wave spectrum. Part 1: A new method for efficient computations of the exact nonlinear transfer integral. J. Phys. Oceanogr., Vol. 15, 1369-1377.

Hasselmann, S., and K. Hasselmann, 1985b: The wave model EXACT-NL. In '*Ocean Wave Modeling*', the SWAMP group, Plenum Press, New York and London.

Hasselmann, S., K. Hasselmann, J. H. Allender and T.P. Barnett, 1985: Computations and parameterizations of the nonlinear energy transfer in a gravity wave spectrum. part 2: Parameterizations of the nonlinear energy transfer for application in wave models. J. Phys. Oceanogr., Vol. 15, 1378-1391.

Hatori, M., M. Tokuda and Y. Toba: 1981: Experimental study on strong interaction between regular waves and wind waves-I. J. Oceanogr. Soc. Japan, Vol. 37, 111-119.

Herterich, K., and K. Hasselmann, 1980: A similarity relation for the nonlinear energy transfer in a gravity-wave spectrum. J. Fluid Mech., Vol. 97, Part 1, 215-224.

Holthuijsen, L.H., 1980: Methoden voor golfvoorspelling (part 1 and 2) Technische Adviescommissie voor de Waterkeringen

Holthuijsen, L.H., N. Booij, and T.H.C. Herbers, 1989: A prediction model for stationary, short-crested waves in shallow water with ambient currents. Coastal Engineering, Vol. 13, 23-54.

Holthuijsen, L.H., N. Booij and R.C. Ris, 1993: A spectral wave model for the coastal zone. Proc. WAVES '93 conference, New Orleans.

IAHR, 1989: IAHR Working group on wave generation and analysis. Journal of Waterway, Port, Coastal and Ocean Engineering, Vol. 115, No., 6, (paper 24075).

Janssen, P.A.E.M., G.J. Komen, and W.J.P. de Voogt, 1987: Friction velocity scaling in wind-wave generation. Bound.-Layer Meteorology, Vol. 38, 29-35.

Janssen, P.A.E.M., 1989: Wave induced stress and the drag of air flow over sea waves. J. Phys. Oceanogr., Vol. 19, 745-754.

Janssen, P.A.E.M., 1991: Quasi-linear theory of wind-wave generation applied to wave forecasting. J. Phys. Oceanogr., Vol. 21, 1631-1642.

Jeffreys, H., 1925: On the formation of waves by wind. Proc. Roy. Soc. **A**107., 189-206.

Jong, J. de, 1997: Toepassing SWAN bij Petten. Afstudeerverslag Technische Universiteit Delft. (in Dutch), Application of SWAN at Petten.

Jury, 1994: A thermal front within the marine atmospheric boundary layer over the Agulhas Current south of Africa: composite aircraft observation. *J. Geophys. Res.*, Vol. 99, 3297-3304.

Kahma, K.K., and C.J. Calkoen, 1992: Reconciling discrepancies in the observed growth rates of wind waves. J. Phys. Oceanogr., Vol. 22, 1389-1405.

Kaiser, R., 1997: personal communication.

Kitaigorodskii, S.A., 1962: Application of the theory of similarity to the analysis of wind-generated water waves as a stochastic process, Bull. Acad. Sci. USSR Geophys. Ser. No. 1, 73p.

Komen, G.J., S. Hasselmann, and K. Hasselmann, 1984: On the existence of a fully developed wind-sea spectrum. Journal of Phys. Oceanogr., Vol. 14, 1271-1285.

Kudryavtsev, V.N., 1995: A model of atmospheric boundary layer transformation above sea surface temperature front. Moskoy Hydrofizicheskii Zurnal, Vol. 2, 1-30 (In Russian).

Kudryavtsev, V.N., and V.K. Makin, 1996: Transformation of wind in the coastal zone. KNMI. Scientific report WR 96-04.

Lin, R., and W. Perrie, 1998: Nonlinear interactions in a coastal wave model. The reduced Interaction Approximation. In 'Nonlinear Ocean Waves', Advances in Fluid Mechanics, Vol. 17, 61-87.

Masuda, A., 1980: Nonlinear energy transfer between wind waves. J. Phys. Oceanogr., Vol. 10, 2082-2093.

Masson, D., 1993: On the non-linear coupling between swell and wind waves. J. Phys. Oceanogr., Vol. 23, 1249-1258.

Mastenbroek, C., G. Burgers, and P.A.E.M. Janssen, 1993: The dynamical coupling of a wave model in a storm surge model through the atmospheric boundary layer. J. Phys. Oceanogr., Vol. 23, 1856-1866.

Miles, J.W., 1957: On the generation of surface waves by shear flows. J. Fluid Mech., Vol.3, 185-204.

Mitsuyasu, H., 1966: Interaction between water waves and wind. Rep. Res. Inst. Appl. Mech., Kyushu University, Vol. 14, 67-88.

Mitsuyasu, H., and Y. Yoshida, 1989: Air-sea interactions under the existence of swell propagating against the wind, Bulletin of the Res. Inst. Appl. Mech.,, Kyushu Univ. (in Japanese), Vol. 68, 47-71. (quoted in Mitsuyasu and Kusaba, 1993).

Mitsuyasu, H., and Y. Yoshida, 1991: The effect of swell on the growth of wind waves, in 'Oceanography of Marginal Sea. Ed. K. Takano, Elsevier, pp. 381-391.

Mitsuyasu, H., and T. Kusaba, 1993: The effect of swell on certain air-sea interaction phenomena. Proc. of the symposium on the air-sea interface, radio and acoustic sensing, Turbulence and wave dynamics, Marseilles, France, 24-30 June 1993. 49-53.

Mizuno, S., 1976: Pressure measurements above mechanically generated water waves (I), Rep. Inst. Appl. Mech. Kyushu Univ., Vol. 23, 113-129.

Morland, L.C., 1997: The growth of wind waves at the crests and troughs of a low amplitude swell. Phys. Fluids, Vol. 9, 6, June 1997, 1657-1664.

Phillips, O.M., 1957: On the generation of surface waves by turbulent wind, Journal of Fluid Mech., Vol. 2, 417.

Phillips, O.M., 1960: On the dynamic of unsteady gravity waves of finite amplitude. Part 1, J. Fluid Mech., Vol. 9, 193-217.

Phillips, O.M., and M.L. Banner, 1974: Wave breaking in the presence of wind drift and swell. J. Fluid. mech., Vol. 66, 625-640.

Pierson , W.J. and L. Moskowitz, 1964: A proposed spectrum form for fully developed wind sea based on similarity theory of Kitaigorodskii, J. Geophys. Res., Vol. 69, 5181-5190.

Rasmussen, J. H., 1995: Non-linear wave-wave interactions. Thesis Institute of Hydrodynamics and Hydraulic Engineering & Technical University of Denmark.

Resio, D.T., and W. Perrie, 1991: A numerical study of nonlinear energy fluxes due to wave-wave interactions - Part 1, J. Fluid Mechanics.

RIKZ, 1997: RIKZ/OS 97.112x. Anonymous.

Ris, R.C., 1997: Spectral modelling of wind waves in coastal areas. Ph.D. Thesis Delft University of Technology.

Roskam, A.P., 1996: Randvoorwaarden voor golfperioden langs de Nederlandse kust (In Dutch); Boundary conditions for wave periods along the Dutch coast, Report RIKZ-96.019.

Seijffert, J.J.W., 1991: Golfoploop bij twee-toppig spectrum (in Dutch); Wave-run-up for double peaked wave spectra. RWS-DWW Note.

Smith, P.C., and J.I. MacPherson, 1987: Cross-shore variations of near-surface wind velocity and atmospheric turbulence at the land-sea boundary during CASP. Atmos.-Ocean, Vol. 25, 279-303.

Snyder, R.L., F.W. Dobson, J.A. Elliot, and R.B. Long, 1981: Array measurements of atmospheric pressure fluctuations above surface gravity waves. J. Fluid Mech., Vol., 102, 1-59.

Sverdrup, H.U., and W.H. Munk, 1947: Wind, sea and swell: Theory of relations for forecasting. US Navy Hydrographic Office, H.O. Pub. No. 601.

Stewart, R.W., 1974: The air-sea momentum exchange. Boundary Layer Meteorology. Vol. 6, 151-167.

Taylor, P.A. and R.J. Lee, 1984: Simple guidelines for estimating wind speed variations due to small scale topographic features. Climat. Bull. Vol. 18, 3-32.

Tracy, B., and D.T. Resio, 1982: Theory and calculation of the nonlinear energy transfer between sea waves in deep water. WIS report 11.

Tolman, H.L., 1991: A third-generation model for wind waves on slowly varying, unsteady, and inhomogeneous depths and currents. J. Phys. Oceanogr., Vol. 21, 782-797.

Tolman, H.L., 1992: Effects of Numerics on the Physics in a Third-Generation Wind-Wave Model, Journal of Physical Oceanography, Vol. 22, 1095-1111.

Tolman, H.L., and D. Chalikov, 1996: Source terms in a third-generation wind wave model. Journal of Phys. Oceanography, Vol. 26, 1497-2518.

Van der Meer, J.W., 1997: Golfoploop en golfoverslag bij dijken (in Dutch): Wave run-up and wave overtopping at dikes, delft hydraulics, Report H2458/H3051-June 1997, Delft.

Van Vledder, G. Ph., 1990: The directional response of wind generated waves. Ph.D. thesis, Delft University of Technology.

Van Vledder, G.Ph., J.G. de Ronde, and M.J.F. Stive, 1994: Performance of a full spectral wave model in shallow water. Proc. 24th ICCE. Kobe, Japan.

Voorrips, A.C., V.K. Makin, and G.J. Komen, 1995: The influence of atmospheric stratification on the growth of water waves. Boundary-Layer Meteorology, Vol. 72, 287-303.

WAMDI group: S. Hasselmann, K. Hasselmann, E. Bauer, PA.E.M. Janssen, G.J. Komen, L. Bertotti, P. Lionello, A. Guillaume, V.J. Cardone, J.A. Greenwood, M. Reistad, L. Zambresky and J.A. Ewing, 1988: The WAM model - a third generation ocean wave prediction model. J. Phys. Oceanogr., Vol. 18, 1775-1810.

Webb, D.J., 1978: Nonlinear transfer between sea waves. Deep-Sea Res., Vol. 25, 279-298.

Willmarth, W.W., and C.E. Woolridge, 1962: Measurements of the fluctuating pressure at the wall beneath a thick turbulent boundary layer, J. Fluid Mech., Vol. 14, 187.

Willmoth, C.J., 1981: On the validation of models. J. Phys. Geography., Vol. 2, 184-194.

Willmoth, C.J., S.G. Ackleson, R.E. Davis, J.J. Feddema, K.M. Klink, D.R. Legates, J.O'Donnel, and C.M. Rowe, 1985: Statistics for the evaluation and comparison of models. J. Geophys. Res., Vol. 90, No. C5, 8995-9005.

Wilson, B.W., 1955: Graphical approach to the forecasting of waves in moving fetches. Beach Erosion Board. Corps of Engineers, Dept. of the Army, Tech. Memo No. 73.

Wilson, B.W.,1965: Numerical prediction of ocean waves in the North Atlantic for December 1959, Deutsche. Hydrogr. Z., Vol. 18, No. 3, 114-130.

WL | delft hydraulics, 1998: Effects of a self scaling cut-off frequency on wave growth in SWAN, Internal report H339, WL | delft hydraulics, the Netherlands, R.C. Ris and K.J. Bos.

Wu, J., 1982: Wind-stress coefficients over sea surface from breeze to hurricane, J. Geophys. Res., Vol. 87, C12, 9704-9706.

Young, I.R., 1995: The determination of confidence limits associated with estimates of the spectral peak frequency., Ocean Engineering, Vol. 22, No. 7, 669-686.

Young, I.R., 1997: The growth rate of finite depth wind-generated waves, Coastal Engineering, Vol. 32, 181-195..

Young, I.R., S. Hasselmann and K. Hasselmann, 1985: Calculation of the nonlinear wave-wave interactions in cross seas. Hamburger Geophysikalische Einzelschriften. Reihe A: Wissenschaftliche Abhandlungen. Heft 74.

Young, I.R., and R.J. Sobey, 1985: Measurements of the wind-wave energy in an opposing wind, J. Fluid. Mech., Vol. 151, 427-442.

Young, I.R., and G.Ph. van Vledder, 1993: A review of the central role of nonlinear interactions in wind-wave evolution. Philos. Trans. Royal Soc. London, Vol. 342, 505-524.

Young, I.R., and L.A. Verhagen, 1996: The growth of fetch limited waves in water of finite depth. Part 1. Total energy and peak frequency. Coastal Engineering, Vol. 29, 47-78.

fig3-1.m

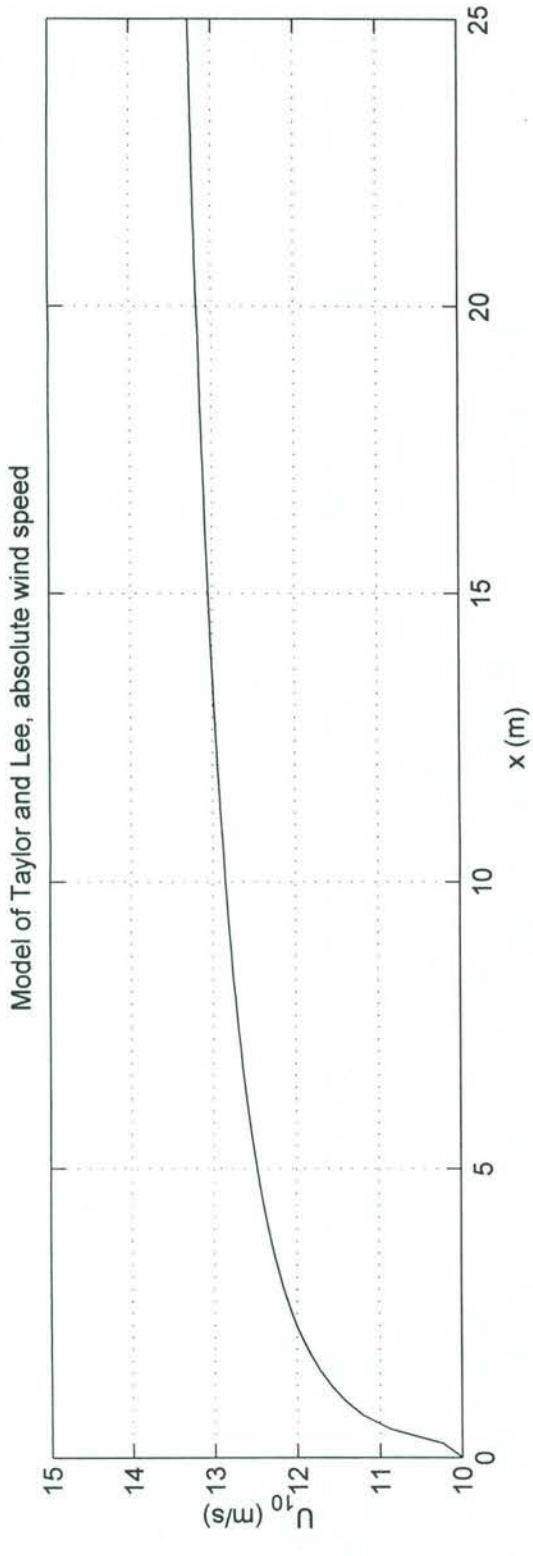

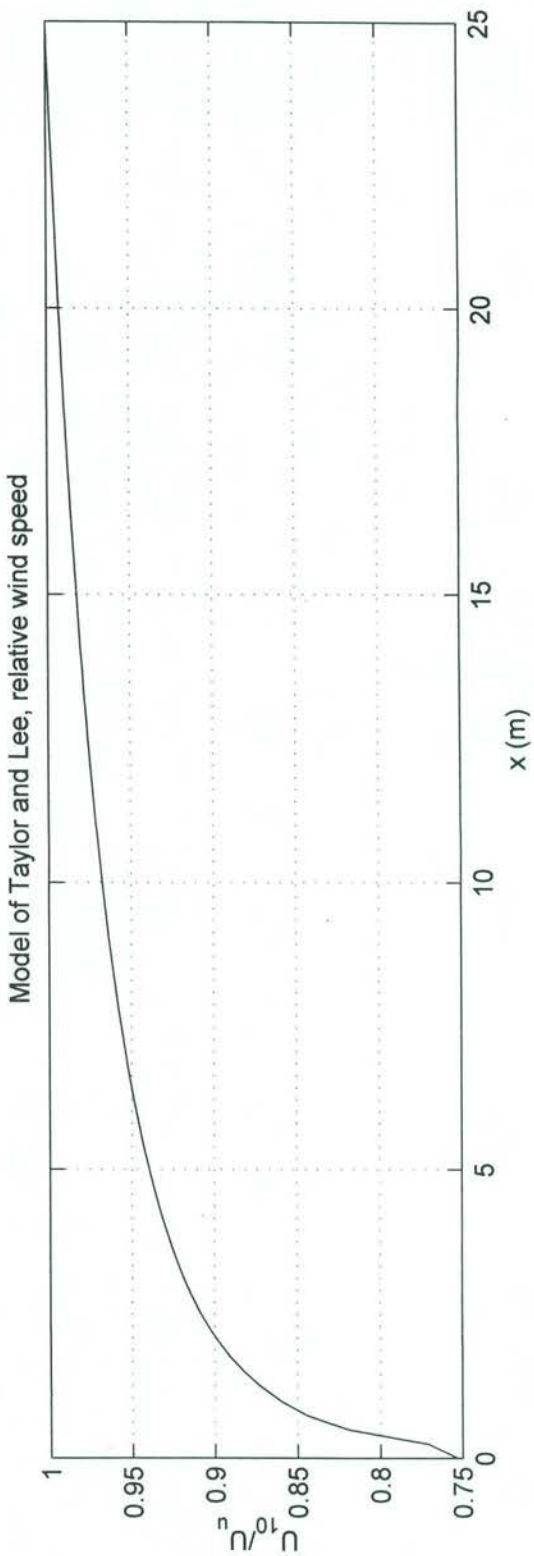

Variation of wind speed at 10 m height according to the model of Taylor and Lee (1984) for an upwind wind speed of 10 m/s and an upwind surface roughness of 0.1 m

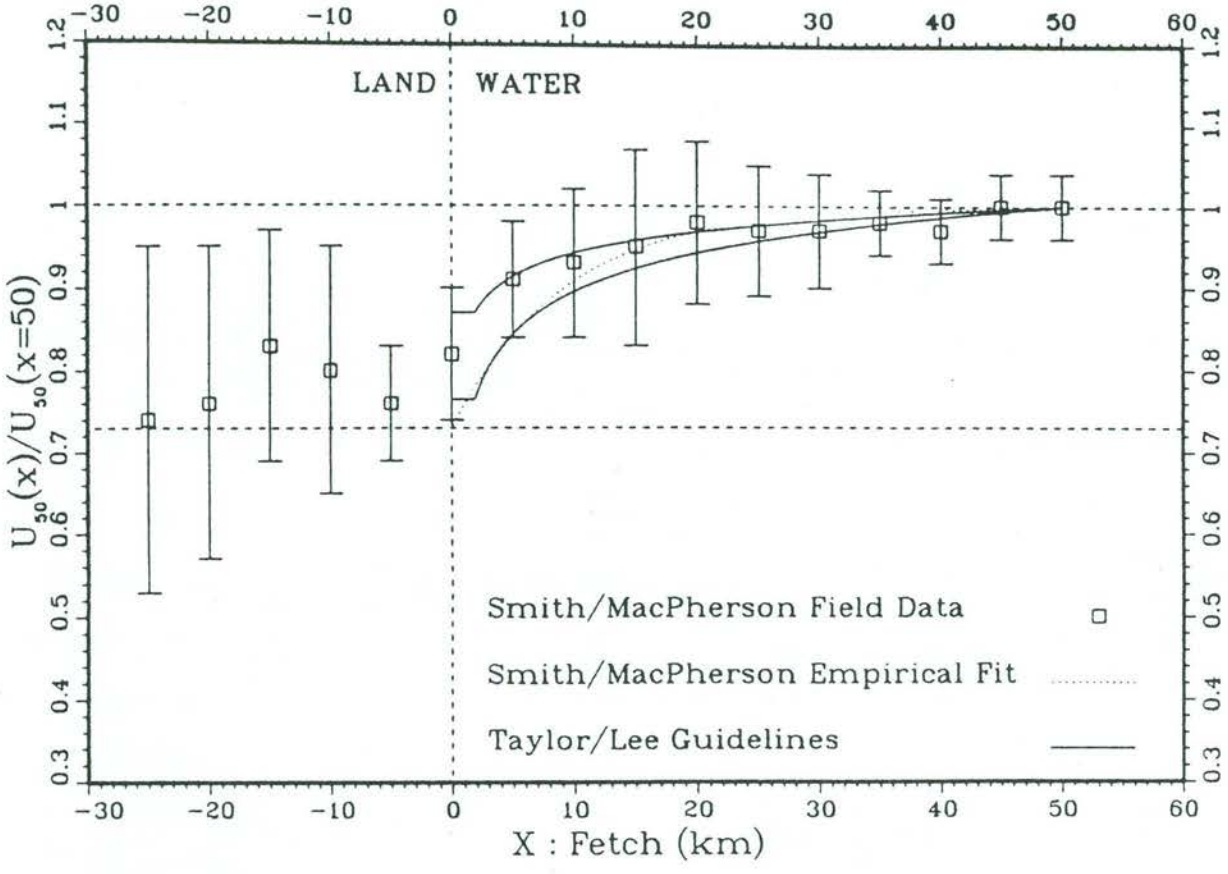

Fig. 3 Comparison of the Taylor and Lee (1984) "guidelines" prediction for the fetch variation of offshore winds with the Smith and MacPherson (1987) measured aircraft winds at 50-m elevation. Squares with error bars are the measured ratios and standard deviations of 50-m winds at a 50-km fetch to those at fetch x. Smith/MacPherson exponential fit (···); Taylor-Lee guidelines calculation for upwind roughness length = 0.07 m (top) and 1 m (bottom) (—).

Comparison of observed offshore wind speeds from Dobson et al. (1989) and predictions of the model of Taylor and Lee (1984)			
Source term investigation SWAN	A162	Alkyon	Fig 3.2

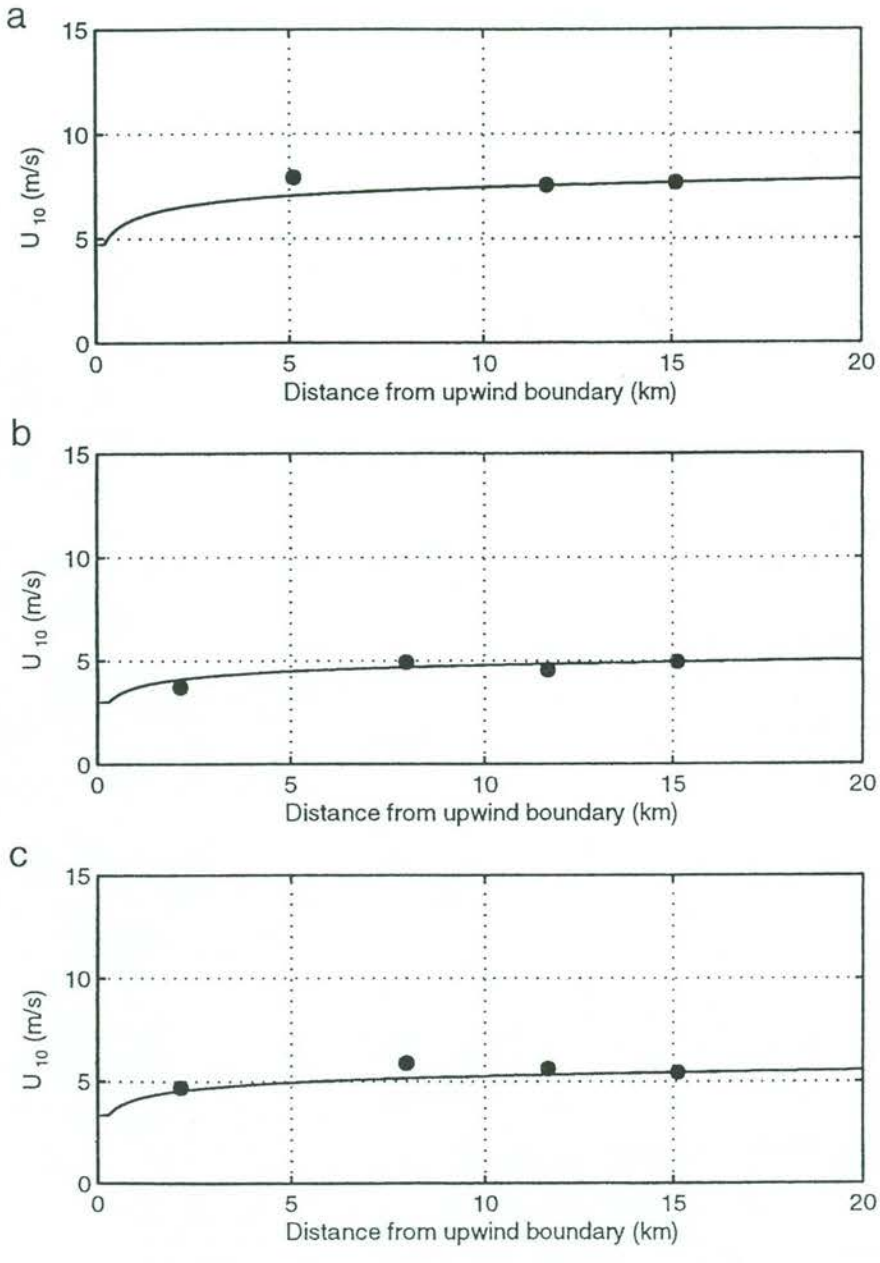

Comparison of observed wind speeds in Lake George from Young and Verhagen (1996) and fitted predictions of the model of Taylor and Lee (1984)

fig3-4.m

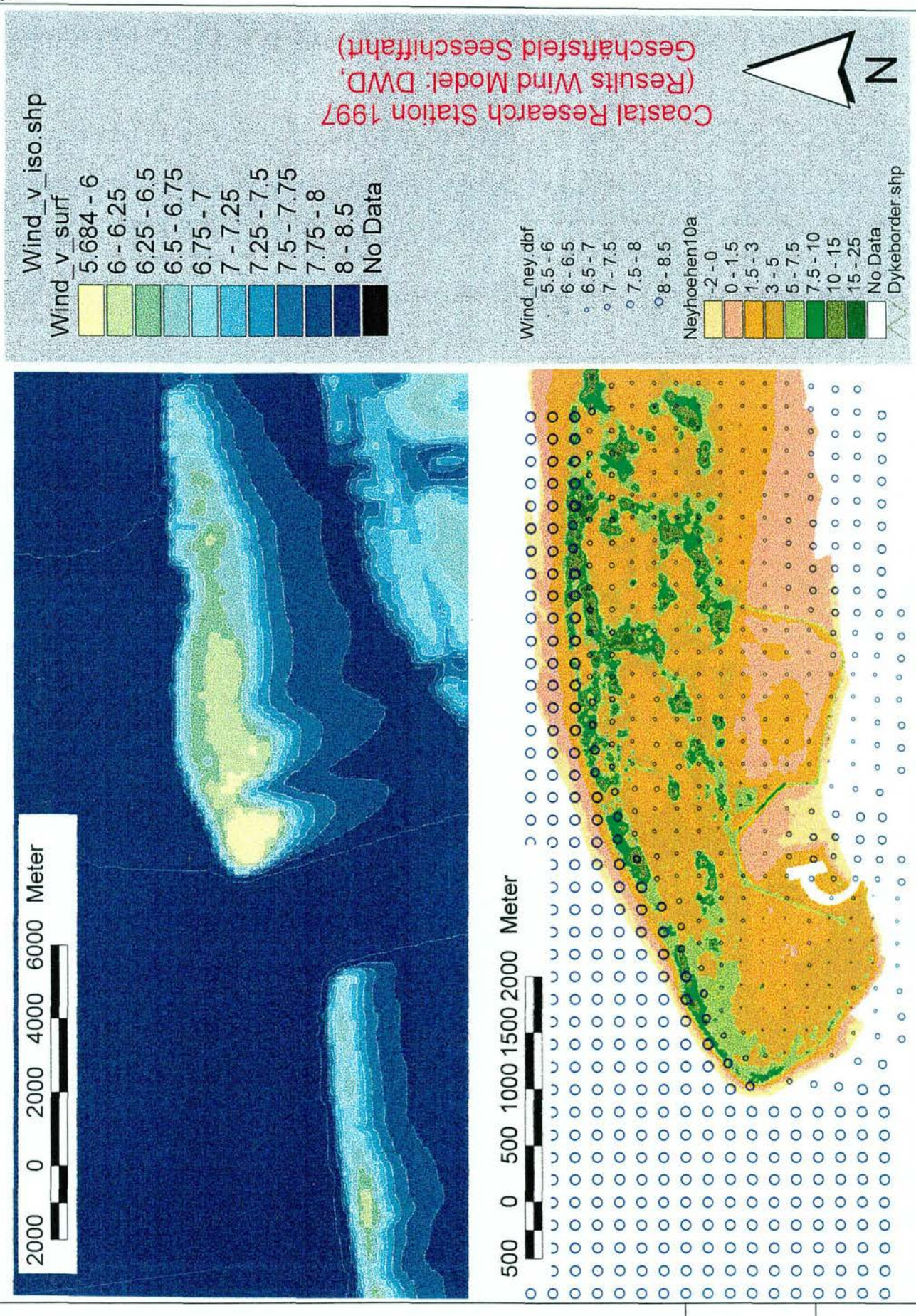

Two-dimensional variation of the wind speed around the island of Norderney computed with a three-dimensional atmospheric model

Source term investigation SWAN	A162	Alkyon	Fig 3.4

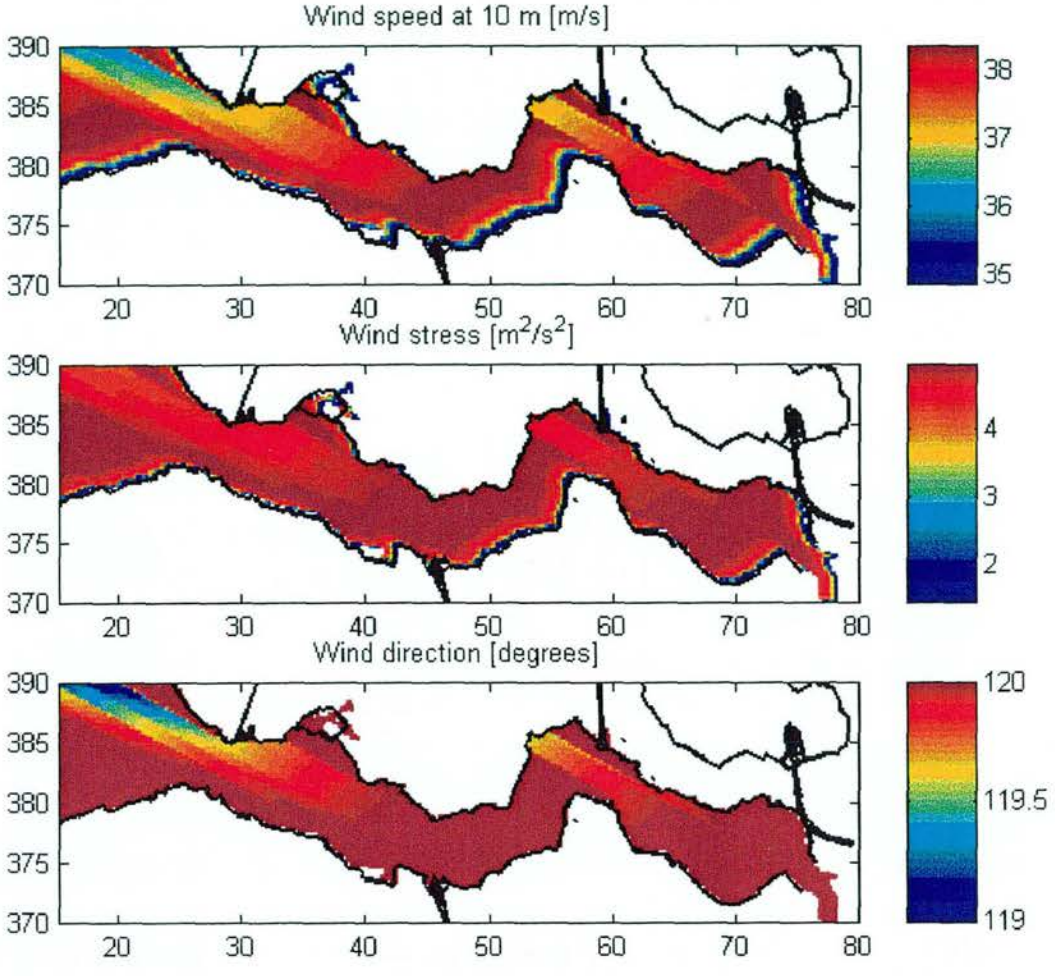

long-fetch-catastrophe-spring

Wind speed at 10 m above land 35 m/s from 120°
Temperature land: 20° C
Potential temperature air above land: 20° C
Temperature water 10° C
Roughness land: 10 cm, roughness water: 0.018 u_x^2/g

Spatial variation of surface wind speed, wind stress and wind direction in the Westerschelde for a land temperature of 20° and a water temperature of 10°.			
Source term investigation SWAN	A162	Alkyon	Fig 3.5

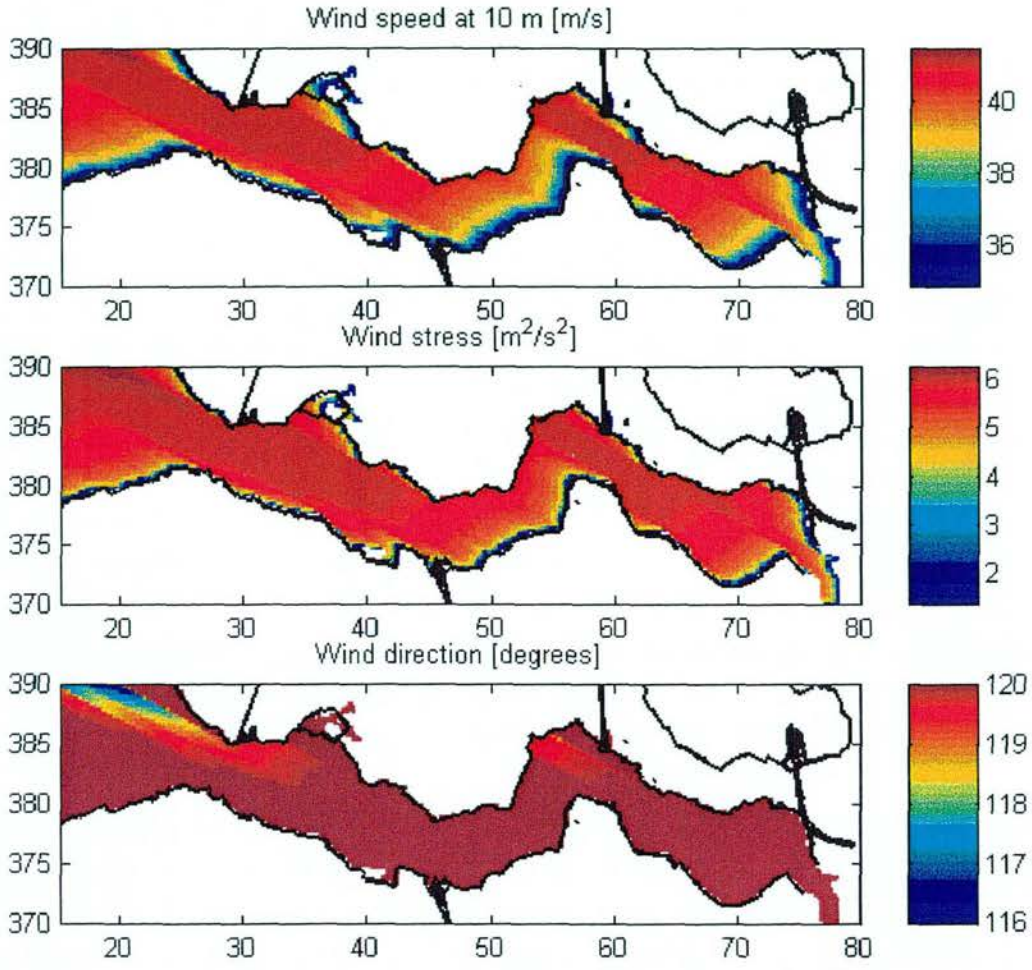

long-fetch-catastrophe-summer

Wind speed at 10 m above land 35 m/s from 120°
Temperature land: 20° C
Potential temperature air above land: 20° C
Temperature water 20° C
Roughness land: 10 cm, roughness water: 0.018 u_*^2/g

Spatial variation of surface wind speed, wind stress and wind direction in the Westerschelde for a land and water temperature of 20°			
Source term investigation SWAN	A162	Alkyon	Fig 3.6

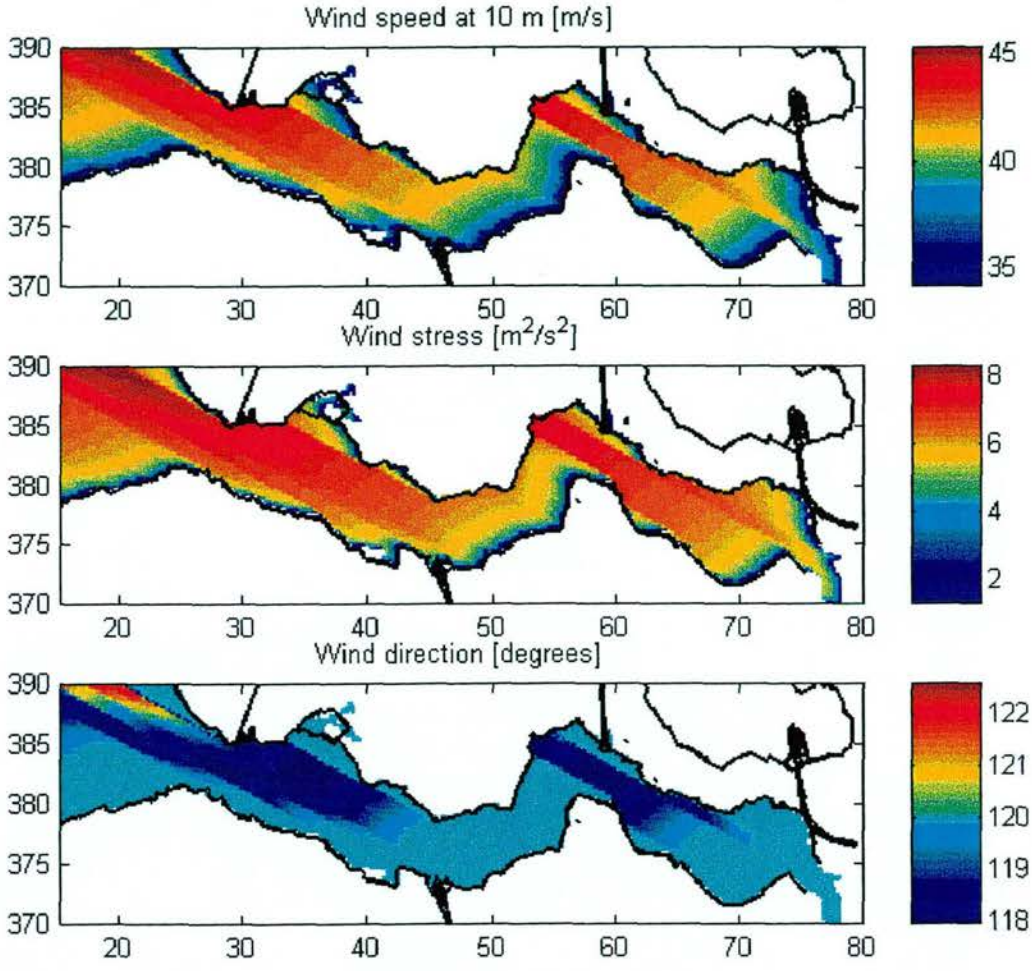

long-fetch-catastrophe-autumn

Wind speed at 10 m above land 35 m/s from 120°
Temperature land: 10° C
Potential temperature air above land: 10° C
Temperature water 20° C
Roughness land: 10 cm, roughness water: 0.018 u_*^2/g

Spatial variation of surface wind speed, wind stress and wind direction in the Westerschelde for a land temperature of 10° and a water temperature of 20°			
Source term investigation SWAN	A162	Alkyon	Fig 3.7

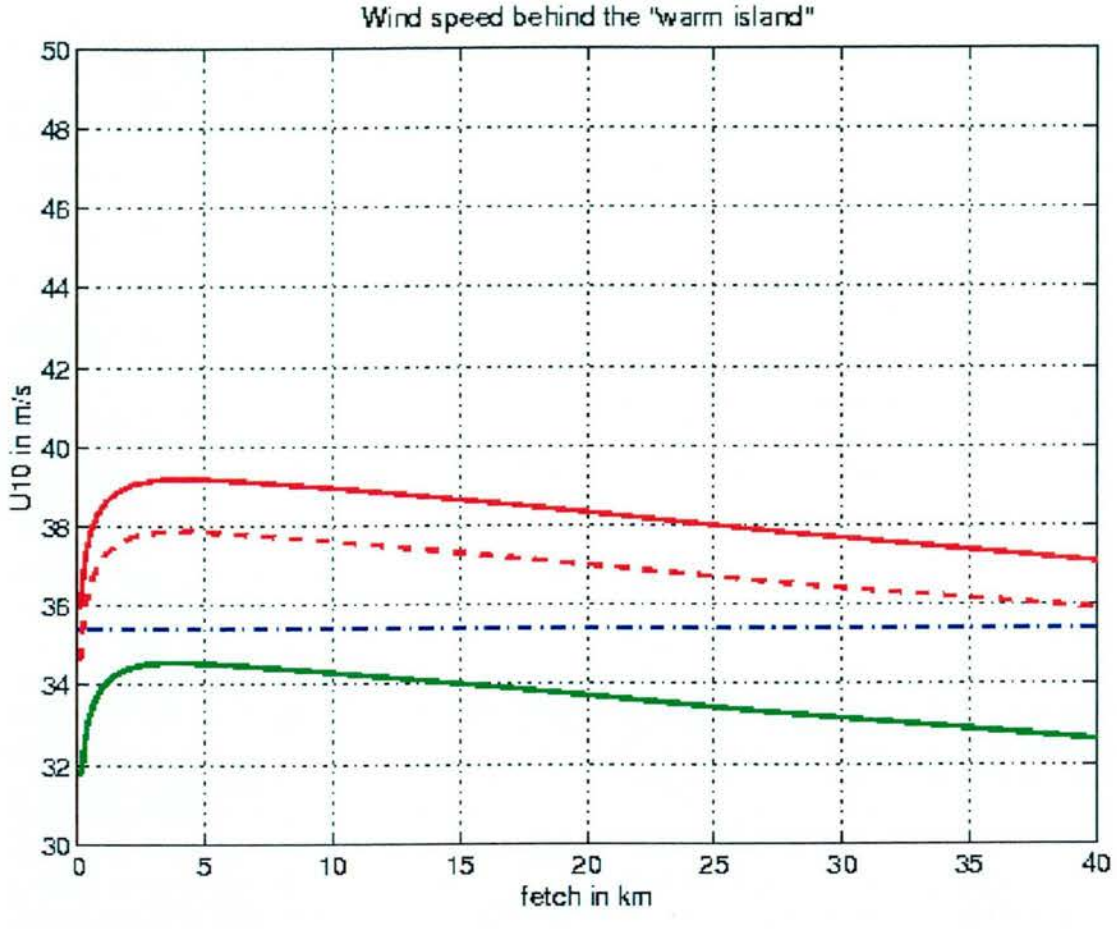

green line: island infinite width;red full line: island width 100 km;red dashed: island 25 km; blue: only water.

Wind speed at 10 m as a function of the distance behind an island for a relatively warmer island of variable widths			
Source term investigation SWAN	A162	Alkyon	Fig 3.8

fig3-9.m

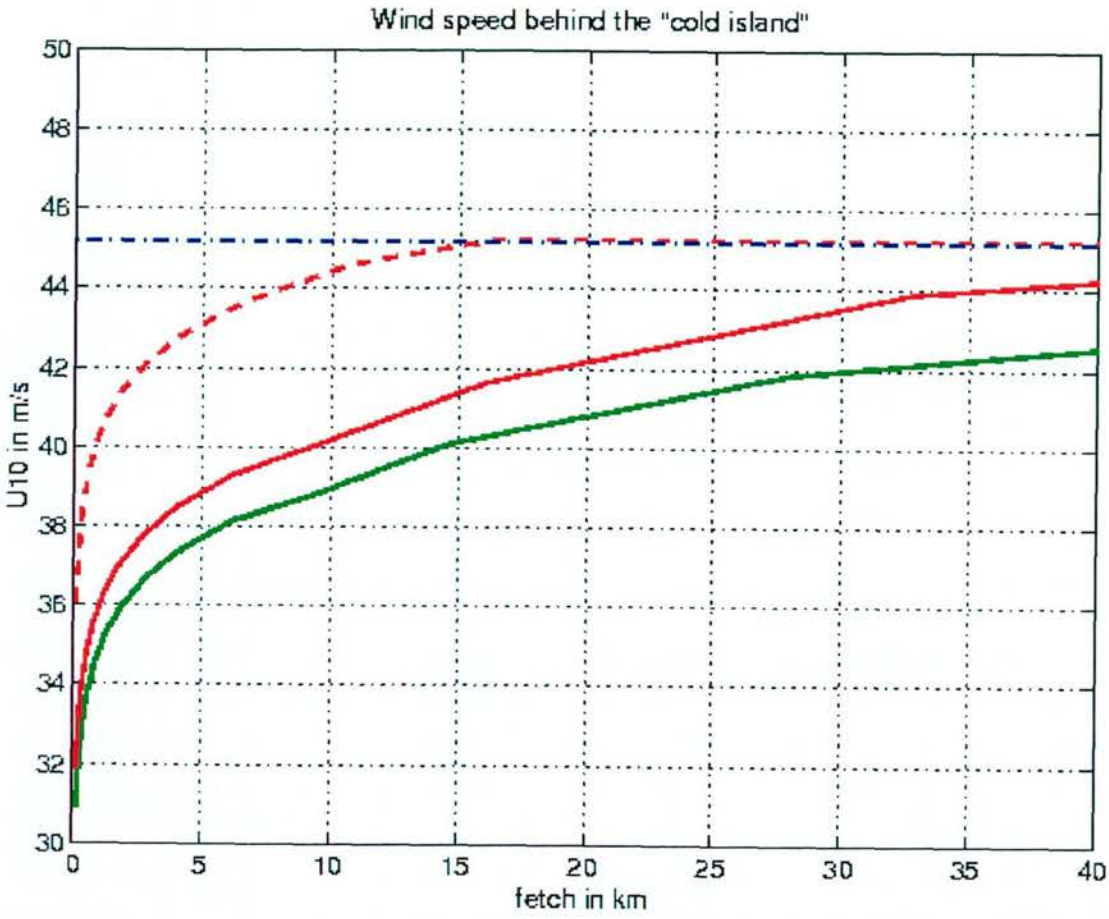

island is stable, this can decreases the wind speed behind it.Green line: island infinite width; red full line: island width 100 km; red dashed: island 25 km; blue: only water.

Wind speed at 10 m height as a function of fetch behind an island for a relatively cold island for various islands widths			
Source term investigation SWAN	A162	Alkyon	Fig 3.9

fig3-10.m

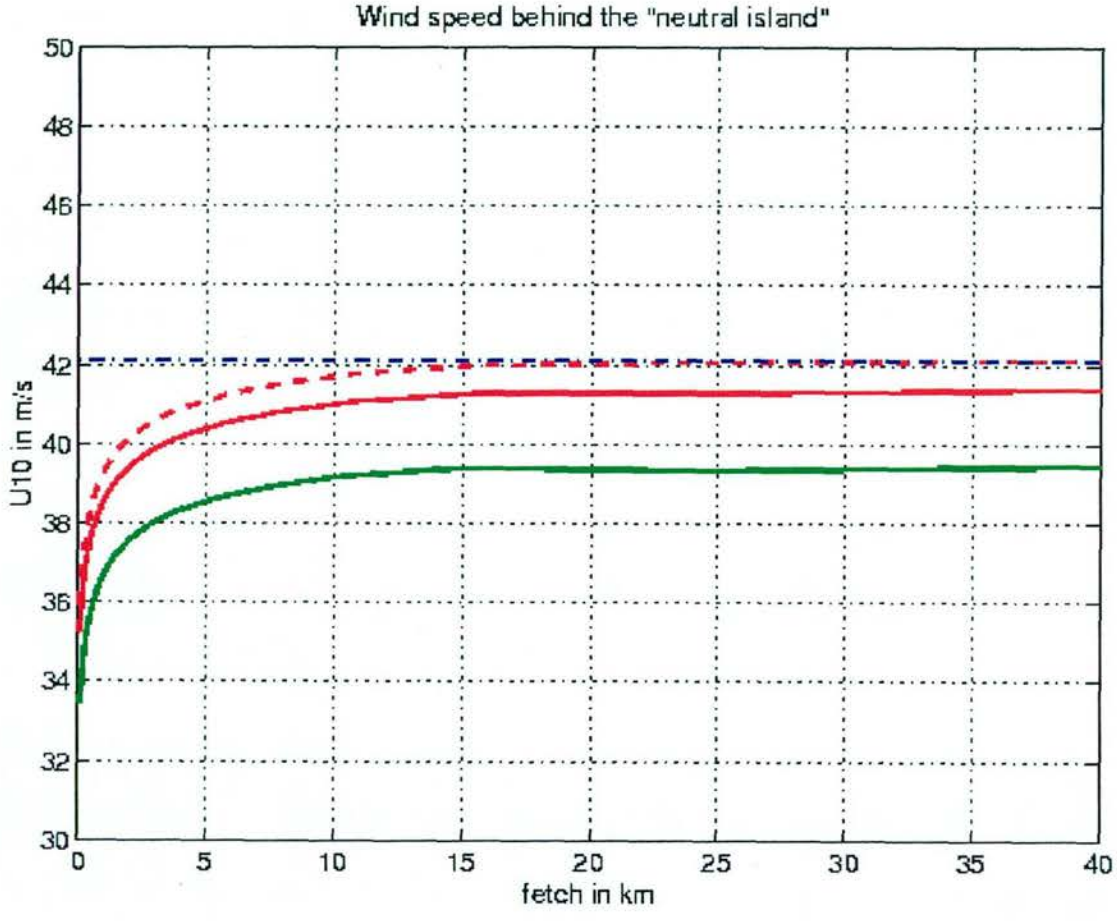

Green line: island infinite width; red full line: island width 100 km; red dashed: island 25 km; blue: only water.

Wind speed at 10 m height as a function of fetch behind an island for a neutral island for various island widths

fig3-11.m

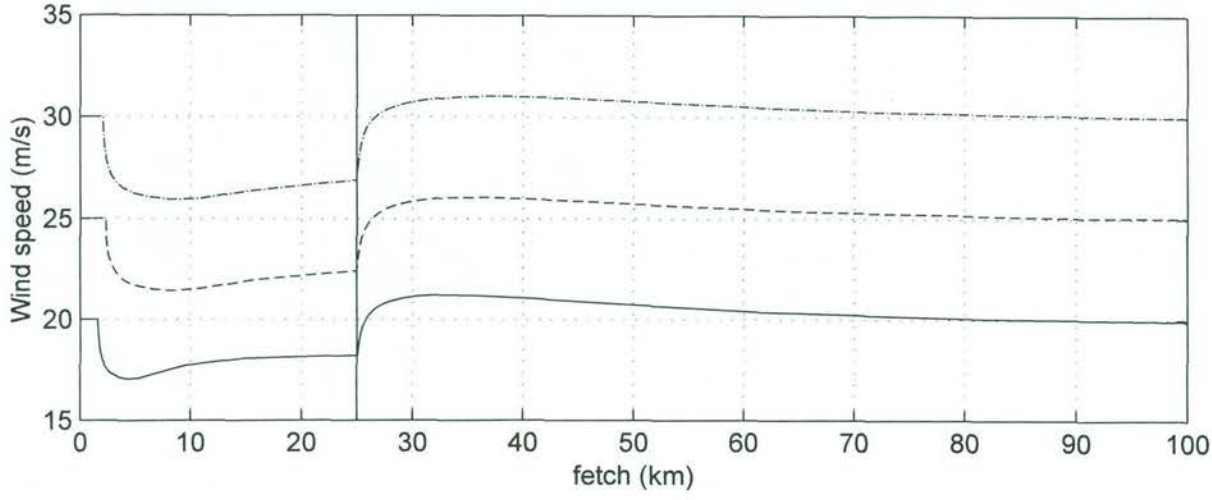

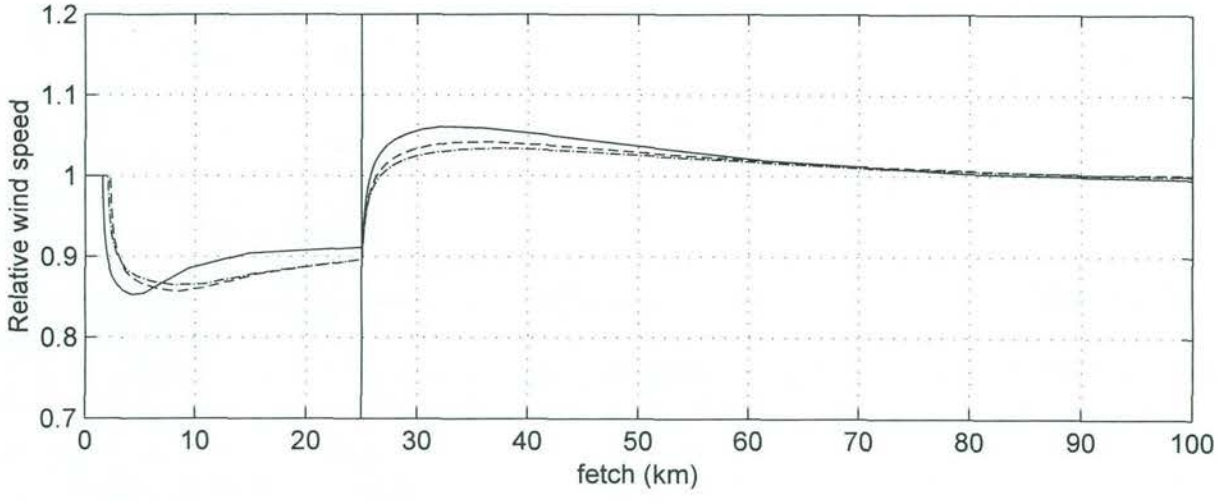

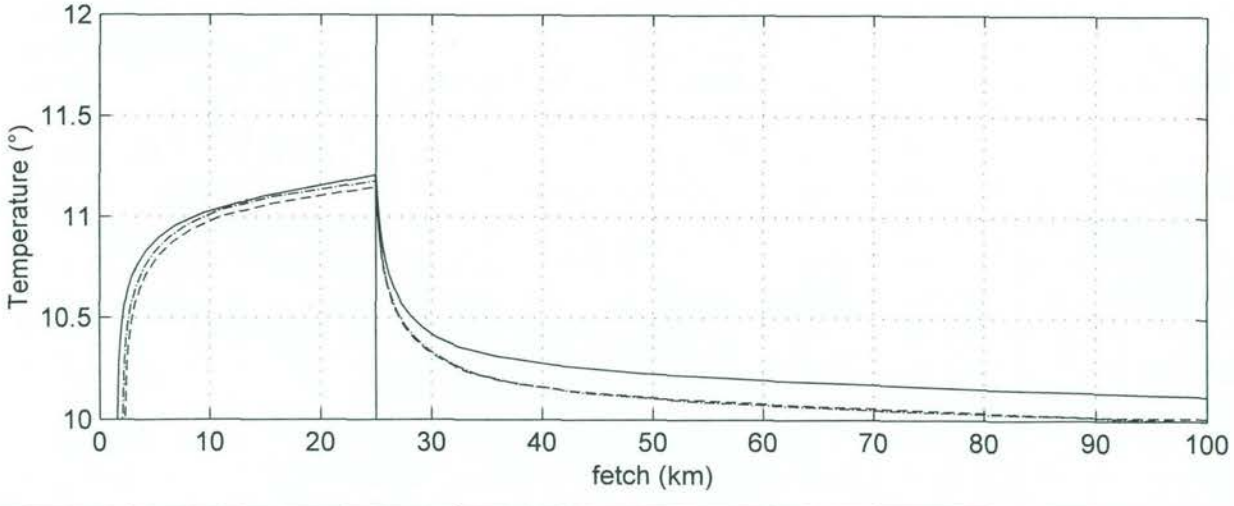

Variation of absolute and relative wind speed and temperature
for temperature differences of +5°C,
for wind speeds of 20 m/s (-), 25 m/s (- -) and 30 m/s (-.)

fig3-12.m

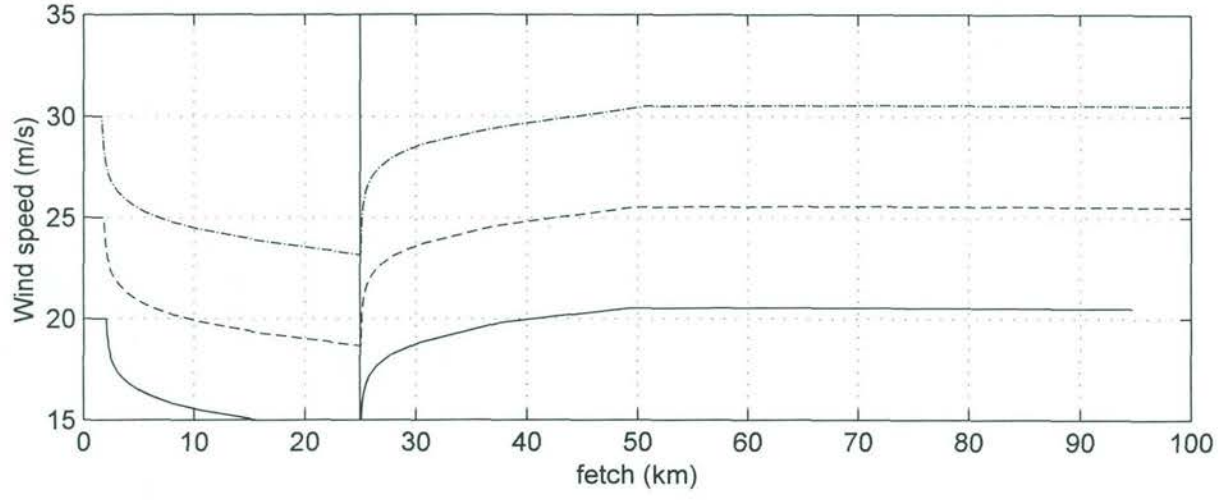

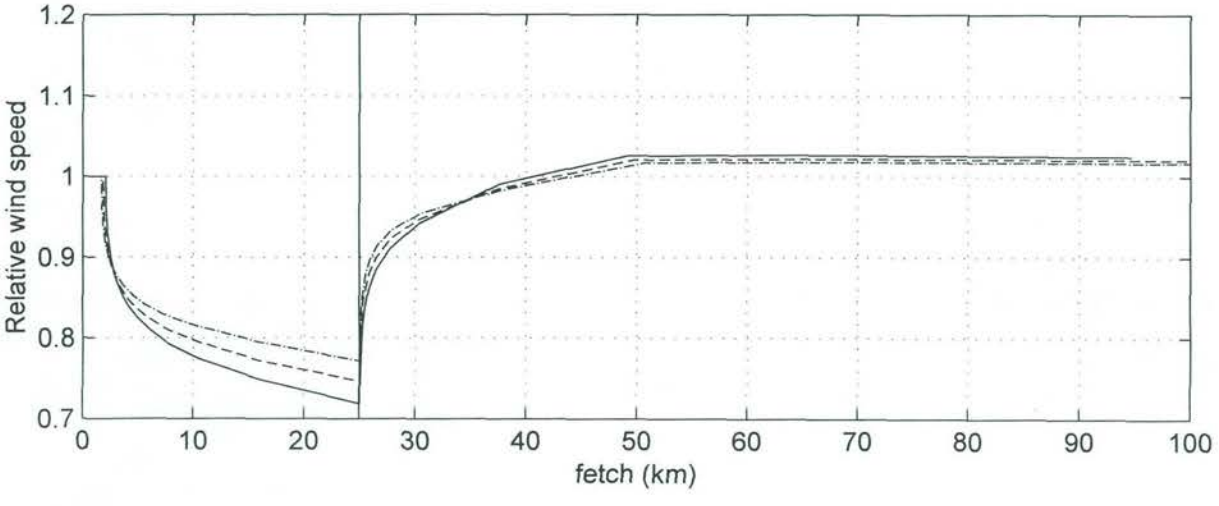

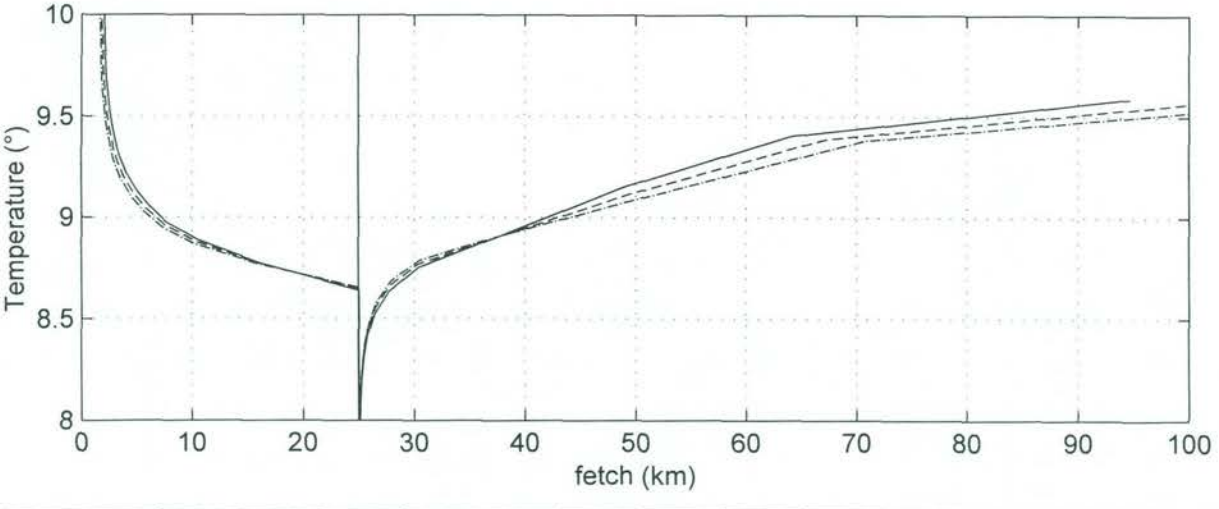

Variation of absolute and relative wind speed and temperature
for temperature differences of -5°C
for wind speeds of 20 m/s (-), 25 m/s (- -) and 30 m/s (-.)

Source term investigation SWAN | A162 | Alkyon | Fig 3.12

fig3-13.m

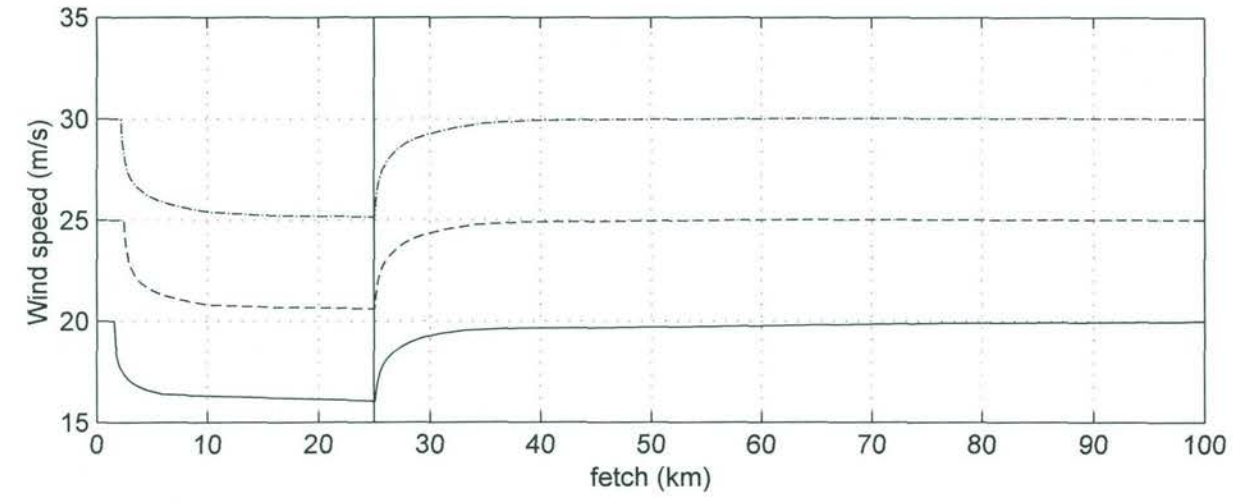

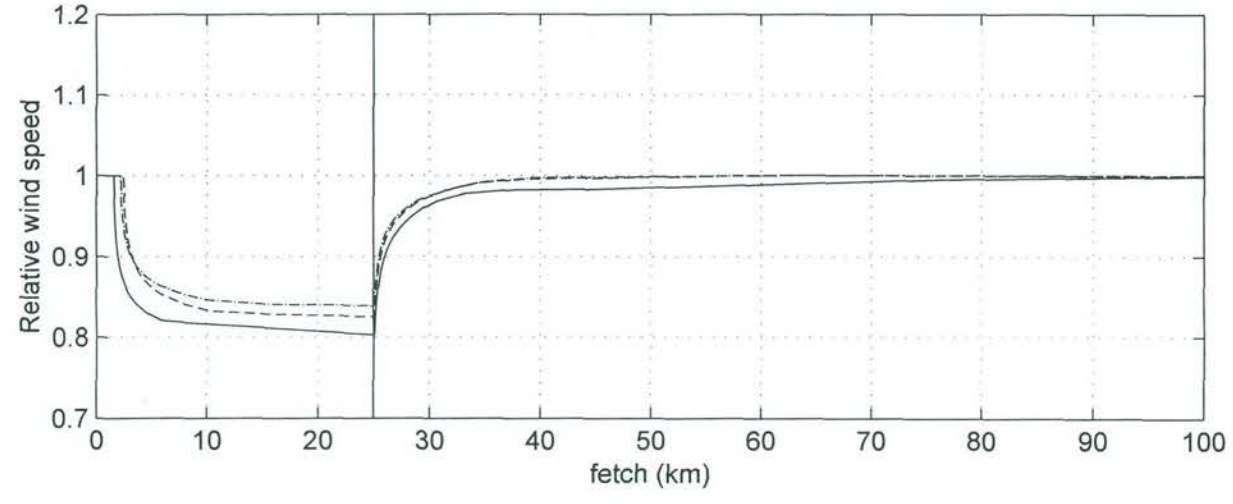

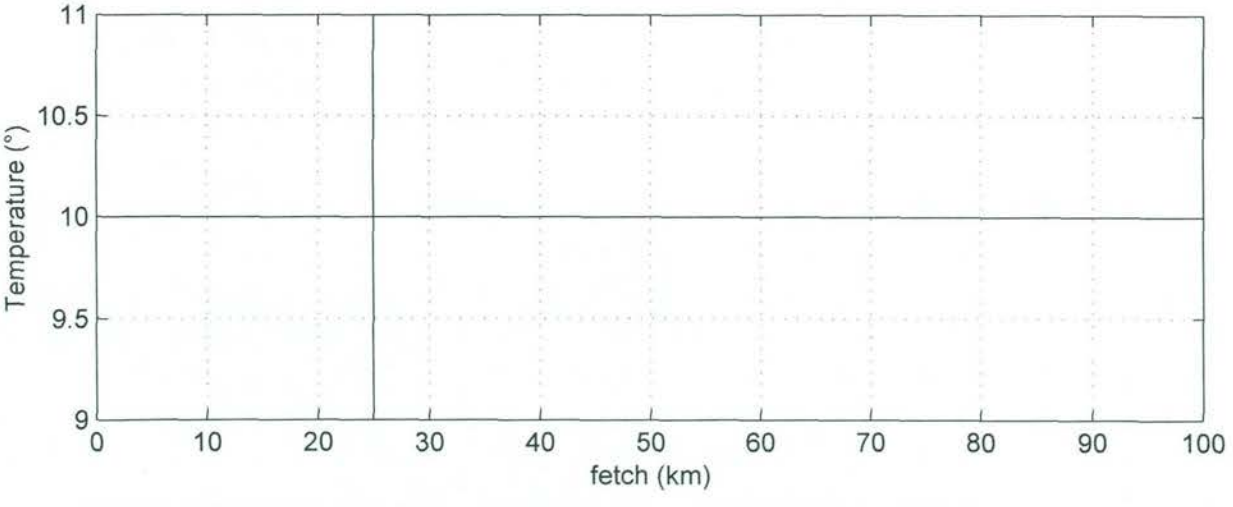

Variation of absolute and relative wind speed and temperature
for temperature differences of 0°C
for wind speeds of 20 m/s (-), 25 m/s (- -) and 30 m/s (-.)

fig3-14.m

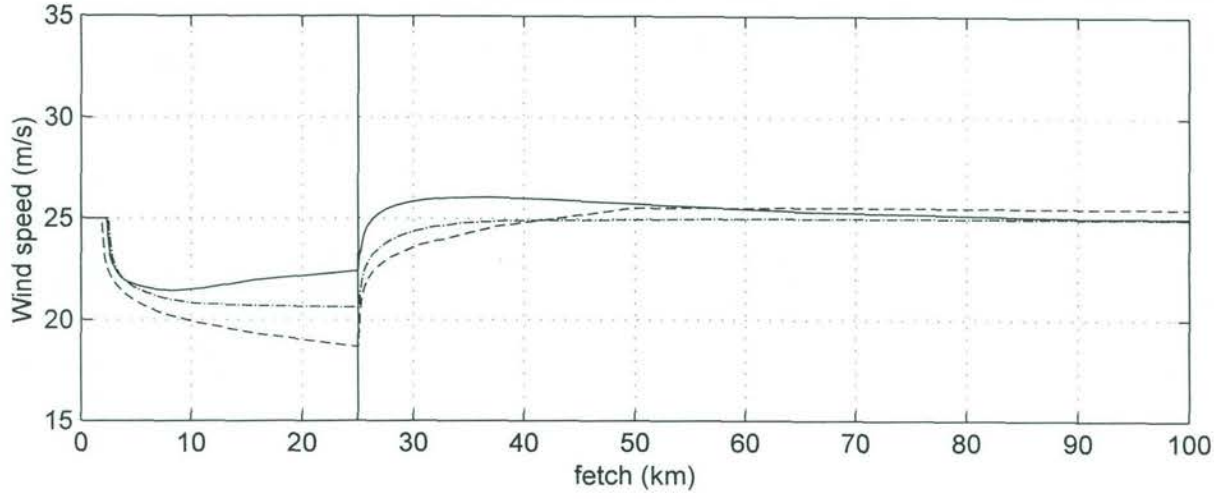

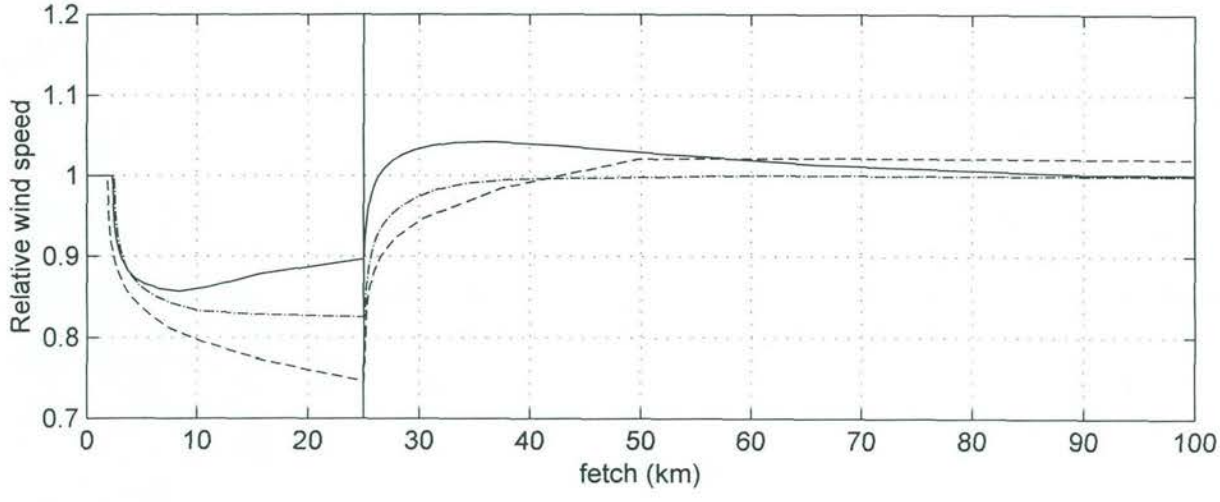

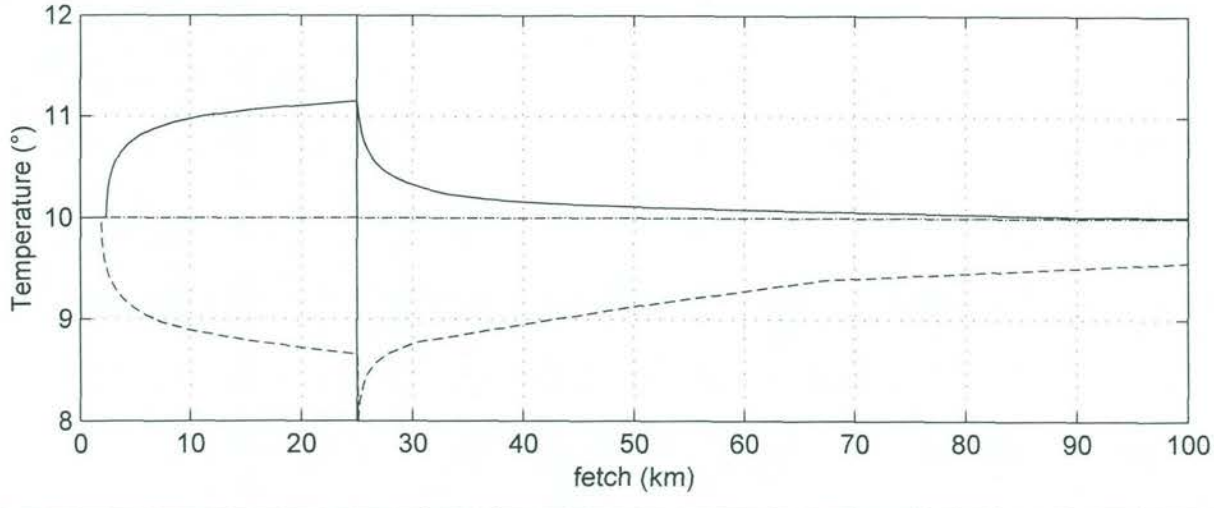

Variation of absolute and relative wind speed and temperature for temperature differences of +5°C (--), -5°C (- -) and 0°C (-.) for a wind speed of 25 m/s

Source term investigation SWAN | A162 | Alkyon | Fig 3.14

fig3-15.m

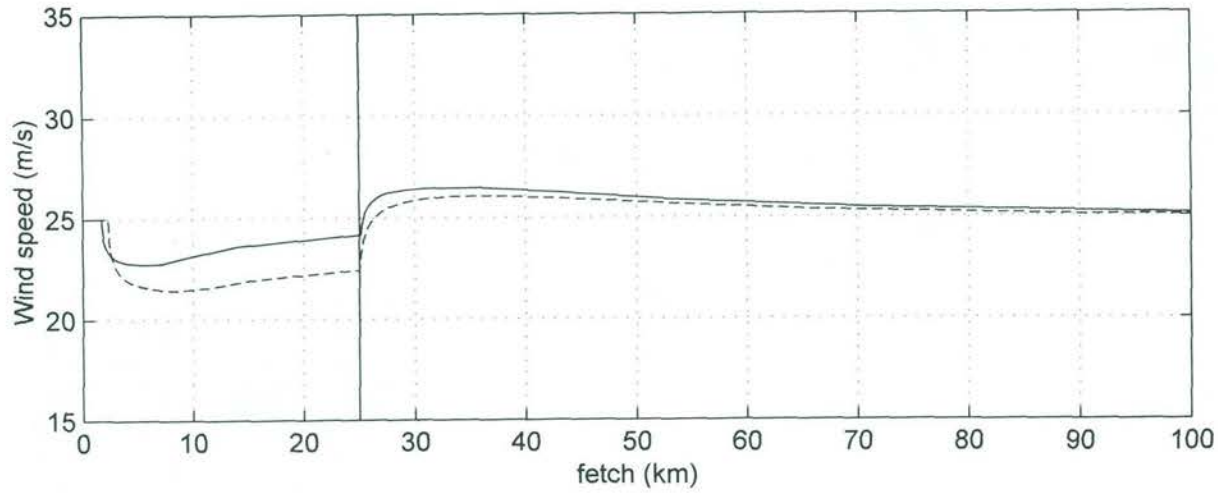

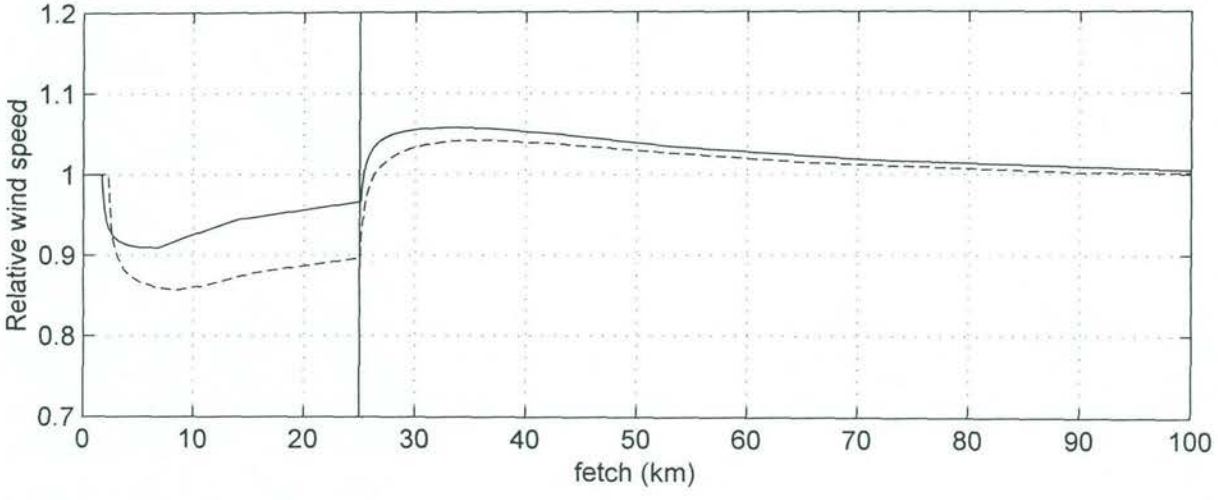

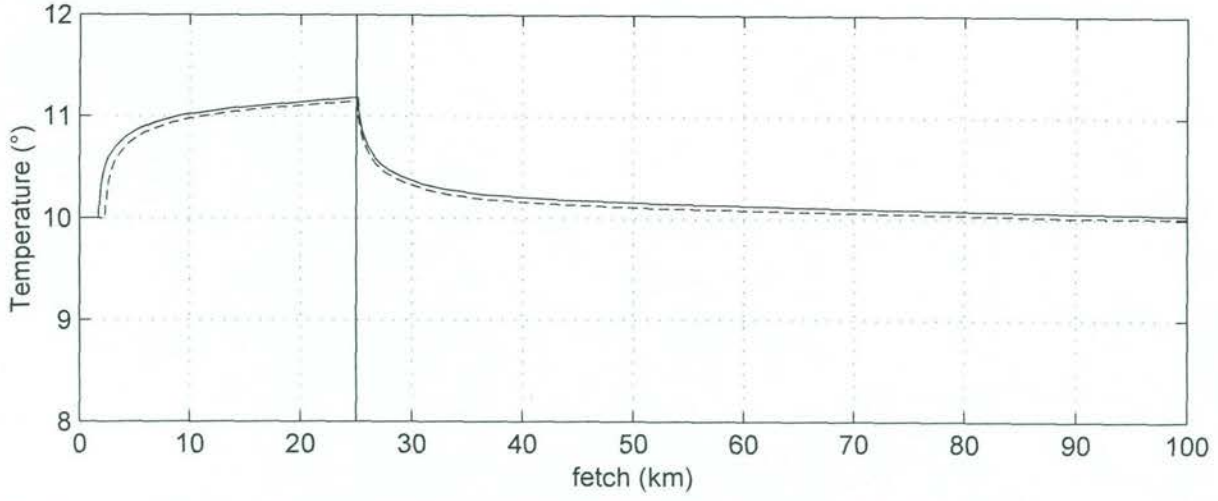

Variation of absolute and relative wind speed and temperature
temperature difference of +5°C and a wind speed of 25 m/s
surface roughnesses of 0.05 (m) (--) and 0.1 (m) (- -)

Source term investigation SWAN | A162 | Alkyon | Fig 3.15

fig3-16.m

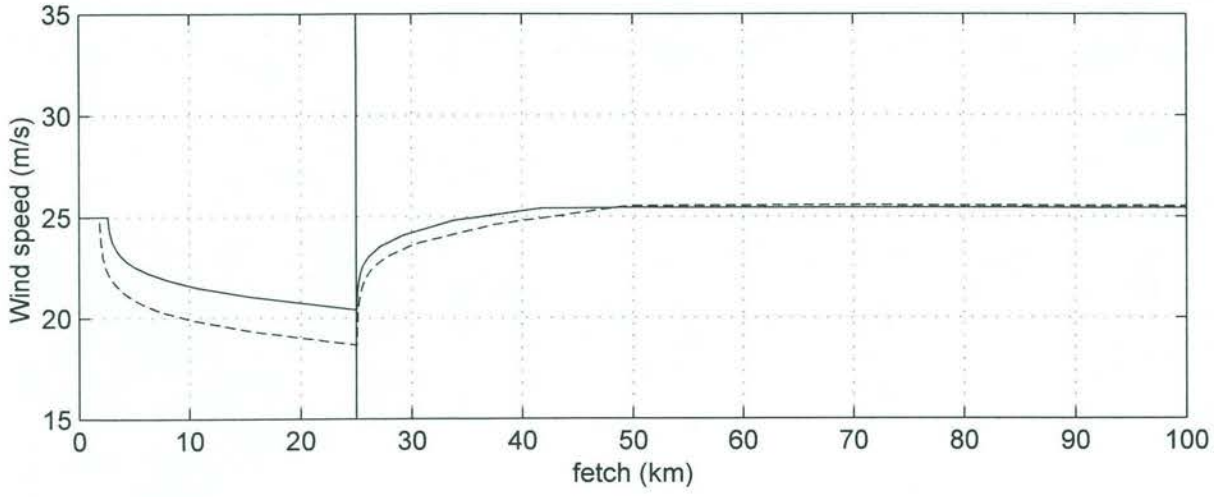

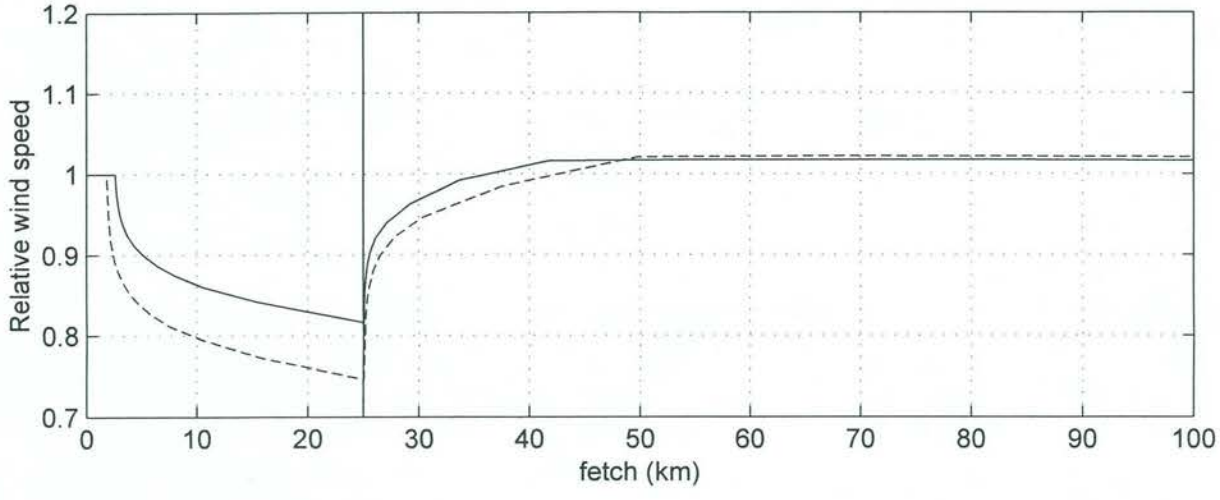

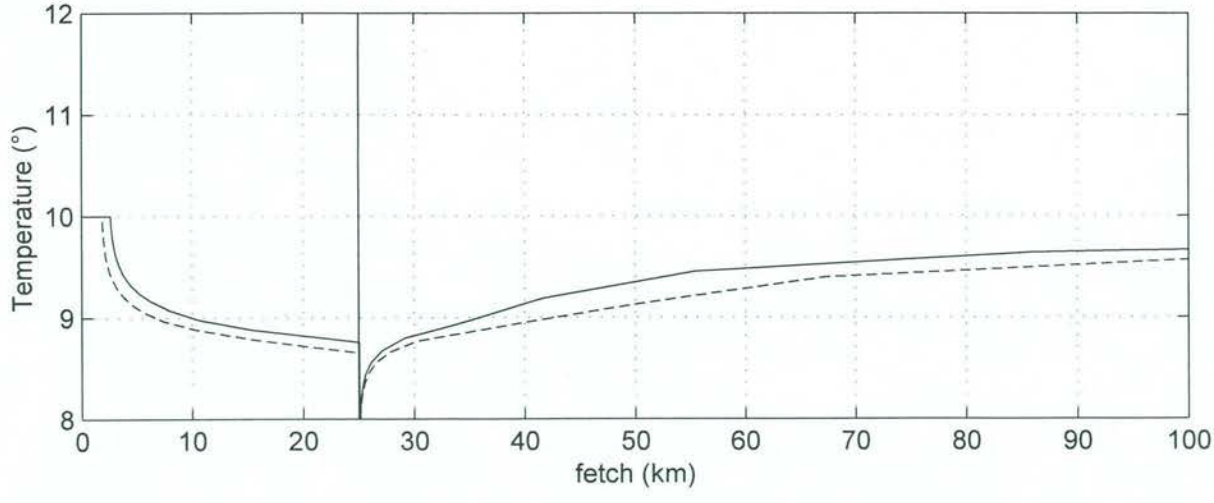

Variation of absolute and relative wind speed and temperature
temperature difference of -5°C and a wind speed of 25 m/s
surface roughnesses of 0.05 (m) (--) and 0.1 (m) (- -)

Source term investigation SWAN	A162	Alkyon	Fig 3.16

fig3-17.m

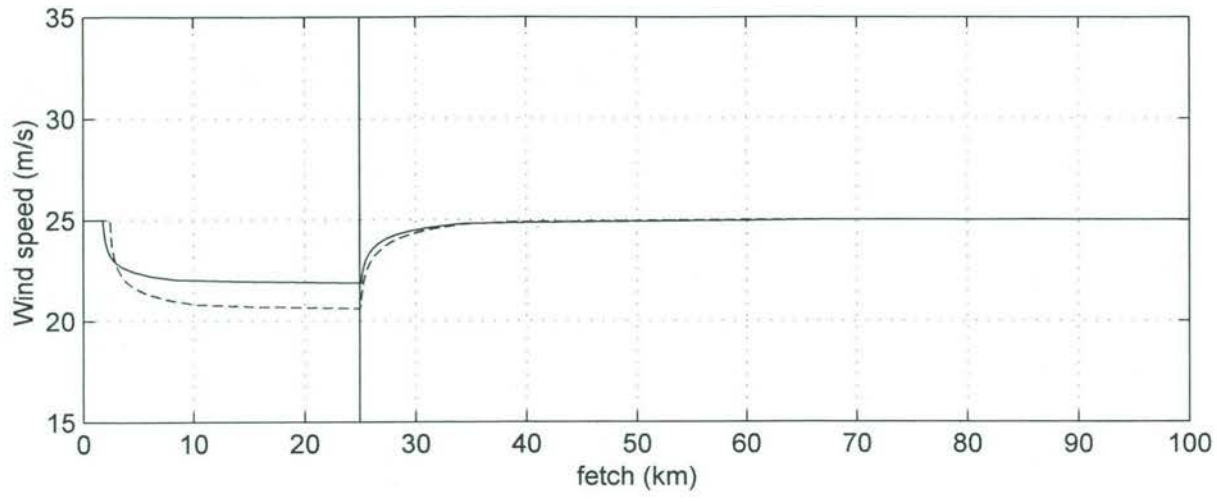

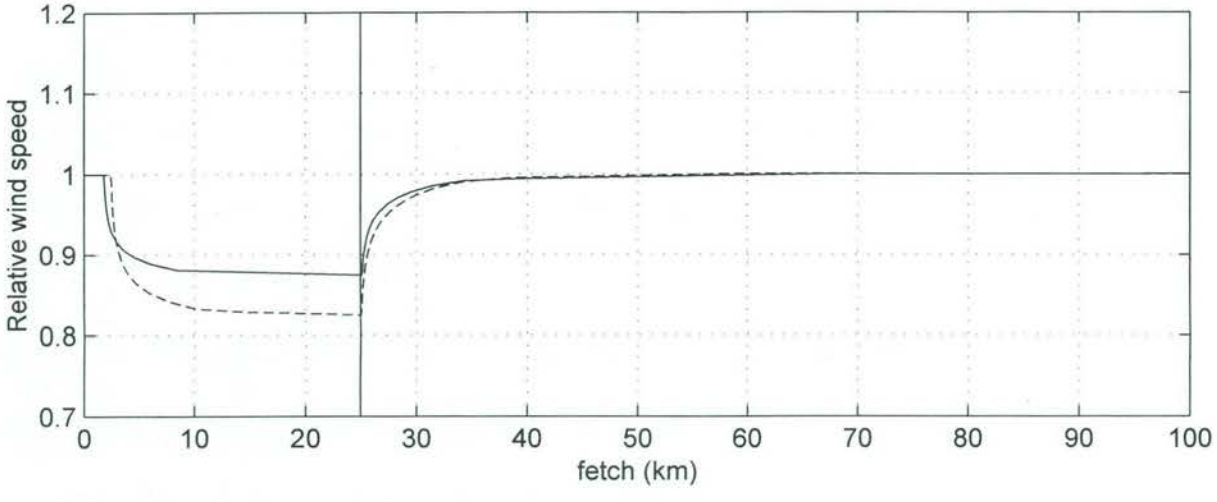

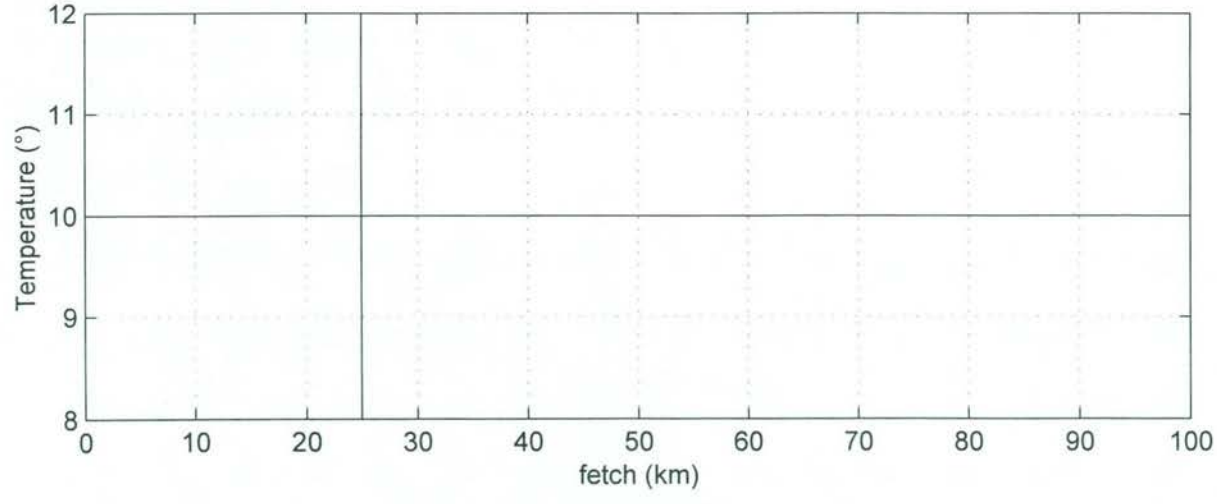

Variation of absolute and relative wind speed and temperature
temperature difference of 0°C and a wind speed of 25 m/s
surface roughnesses of 0.05 (m) (--) and 0.1 (m) (- -)

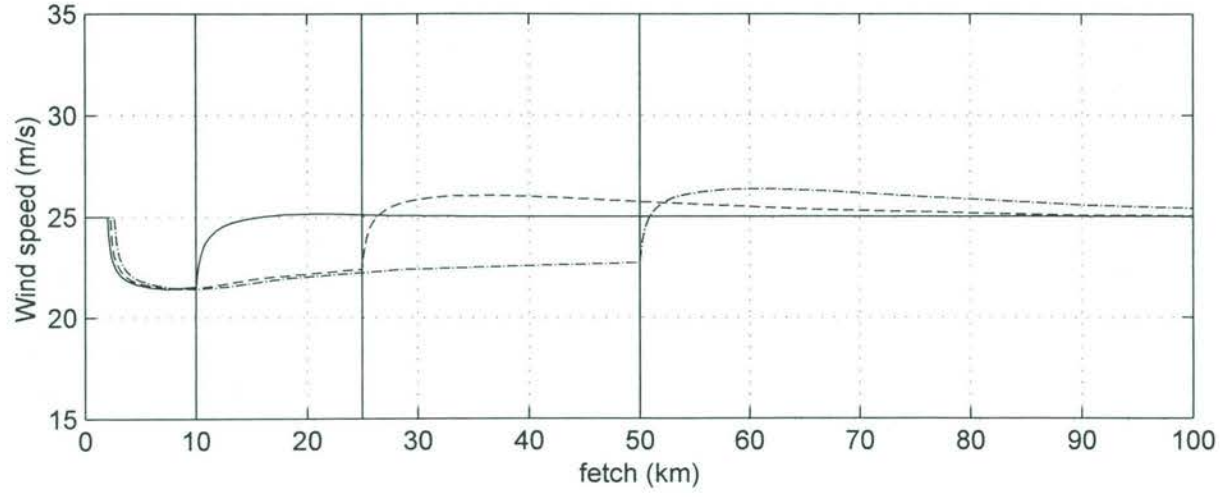

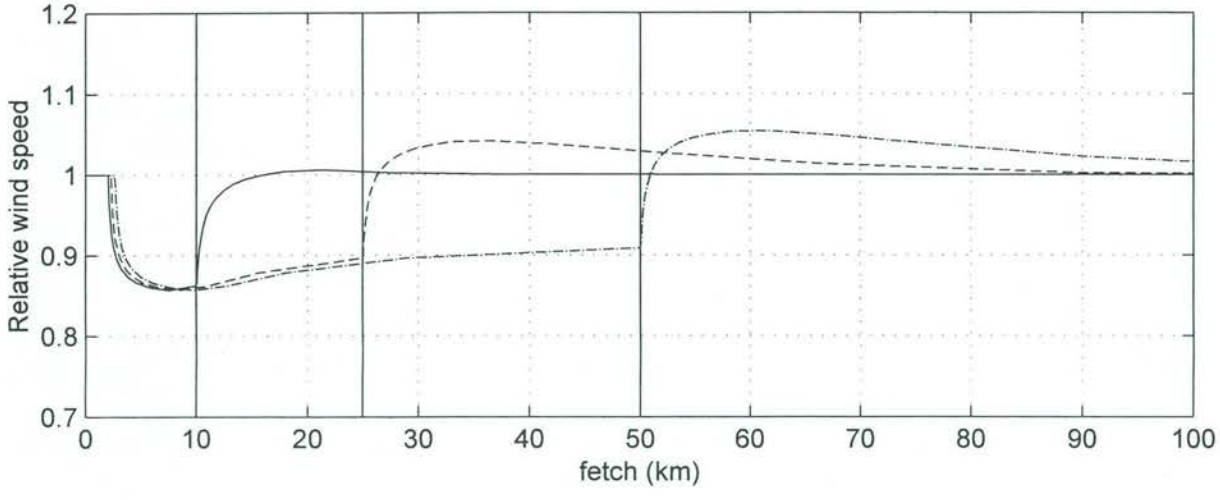

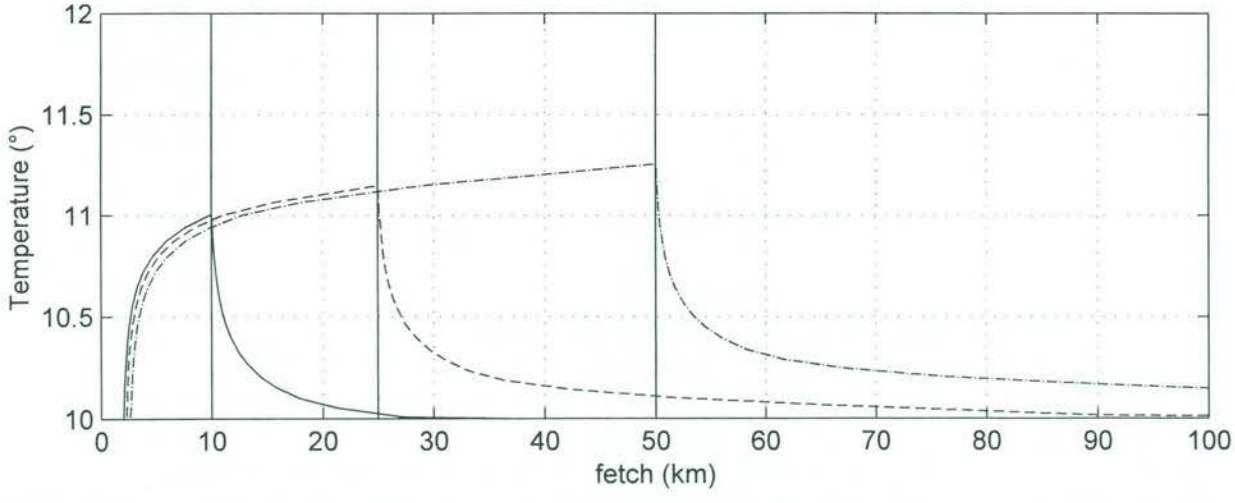

Variation of absolute and relative wind speed and temperature for temperature differences of +5°C, a wind speed of 25 m/s and an island width of 10 km (-), 25 km (- -) and 50 km (-.)

Source term investigation SWAN	A162	Alkyon	Fig 3.18

fig3-19.m

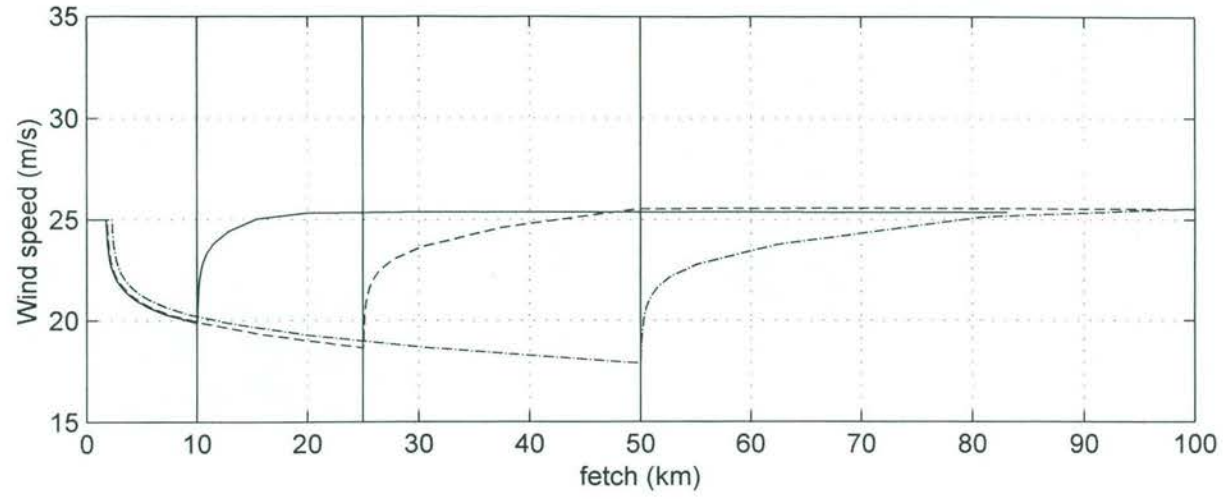

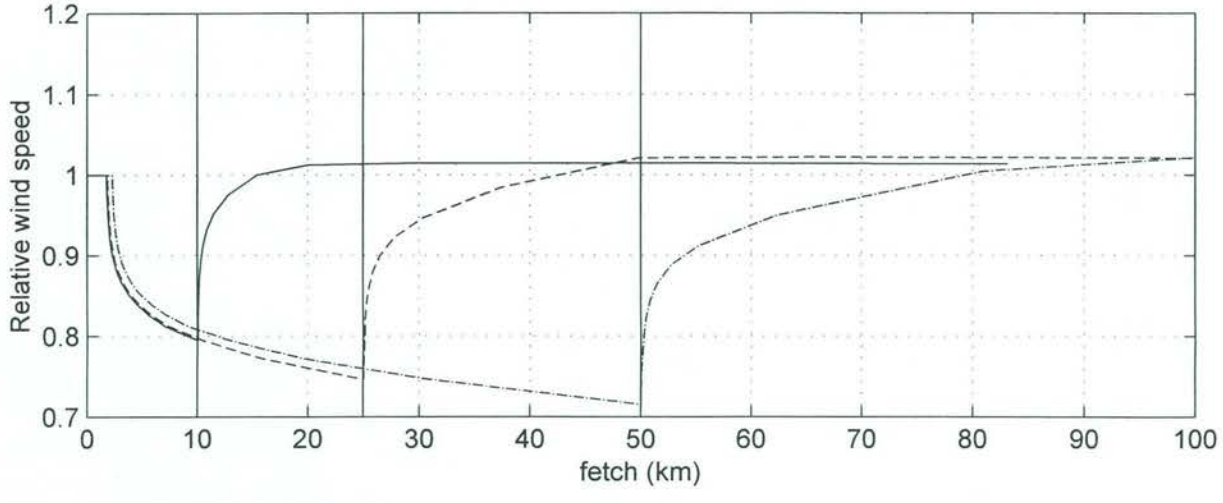

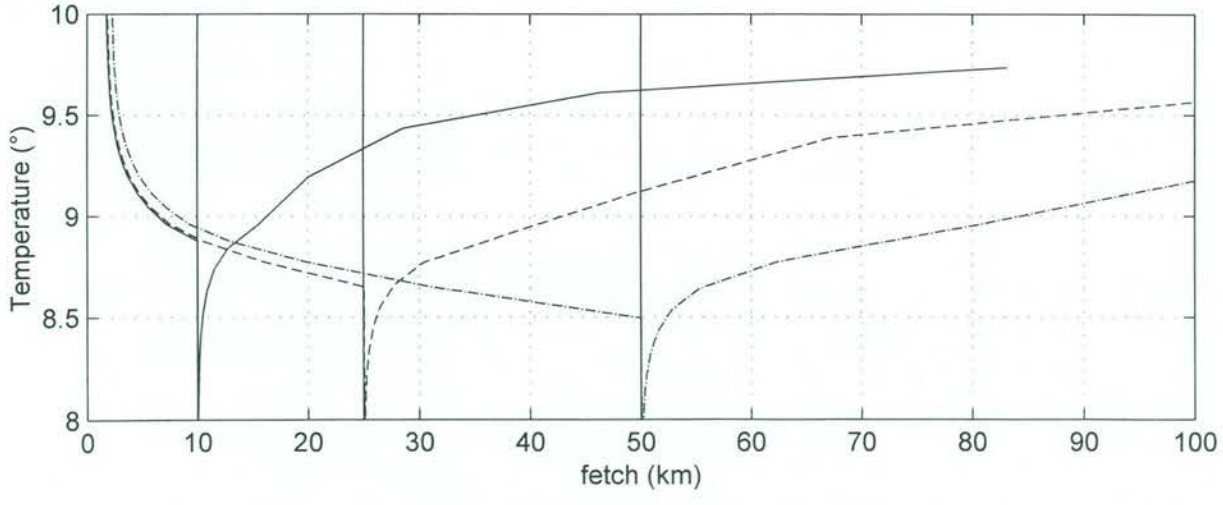

Variation of absolute and relative wind speed and temperature for temperature differences of -5°C, a wind speed of 25 m/s and an island width of 10 km (-), 25 km (- -) and 50 km (-.)

fig3-20.m

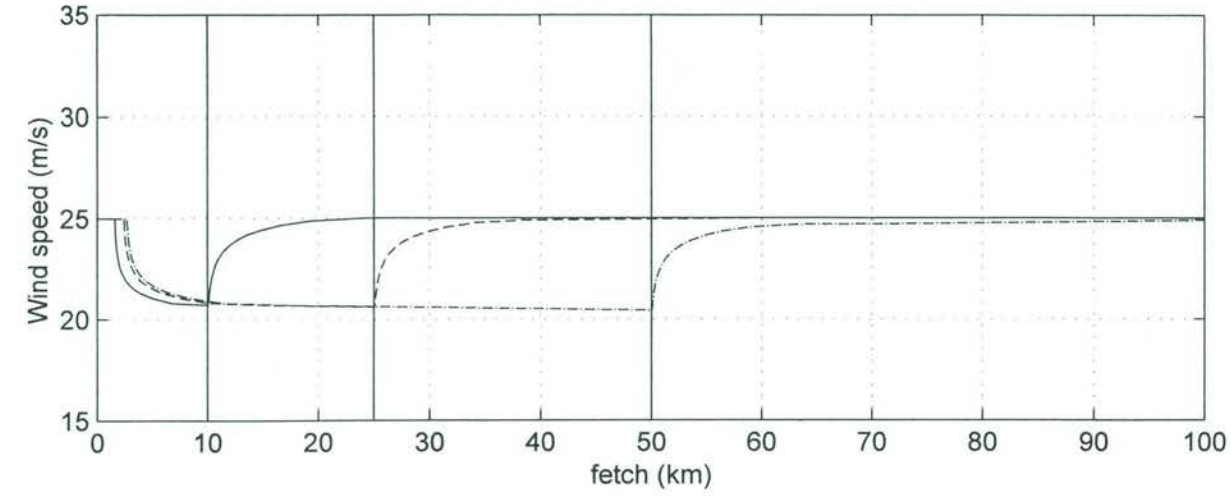

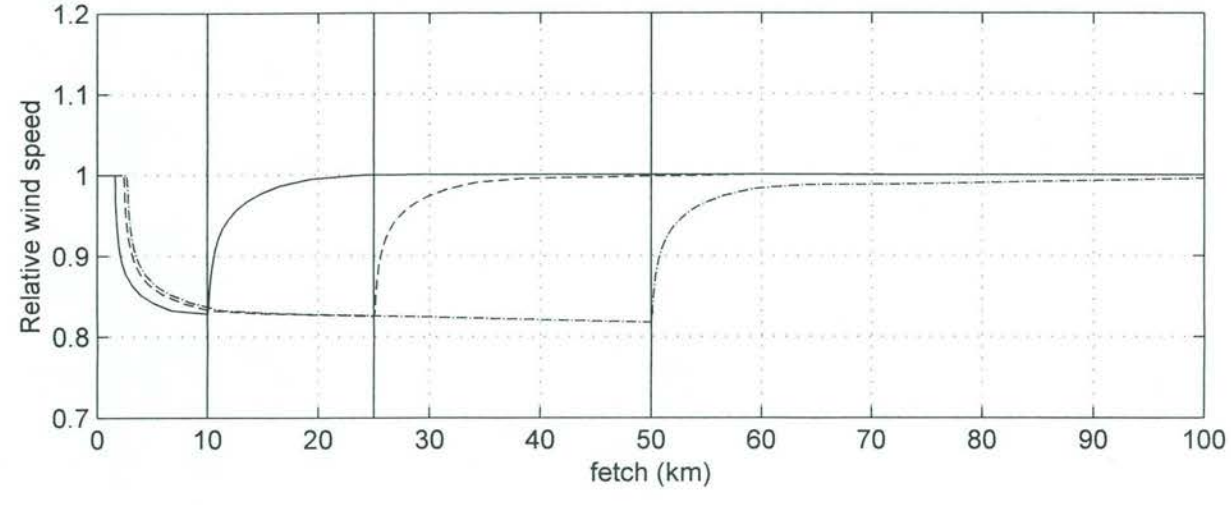

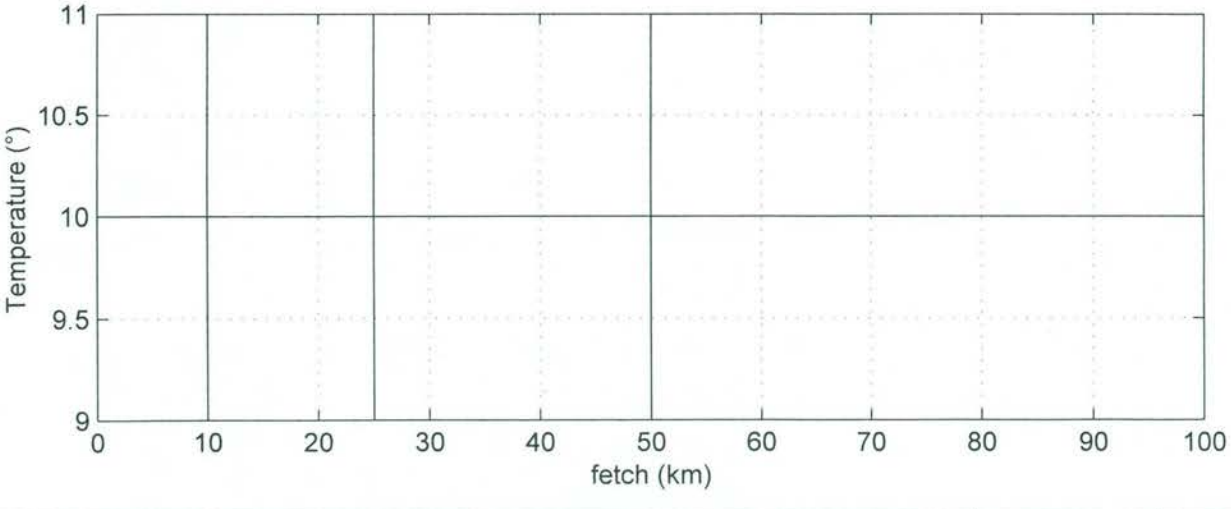

Variation of absolute and relative wind speed and temperature for temperature differences of 0°C, a wind speed of 25 m/s and an island width of 10 km (-), 25 km (- -) and 50 km (-.)

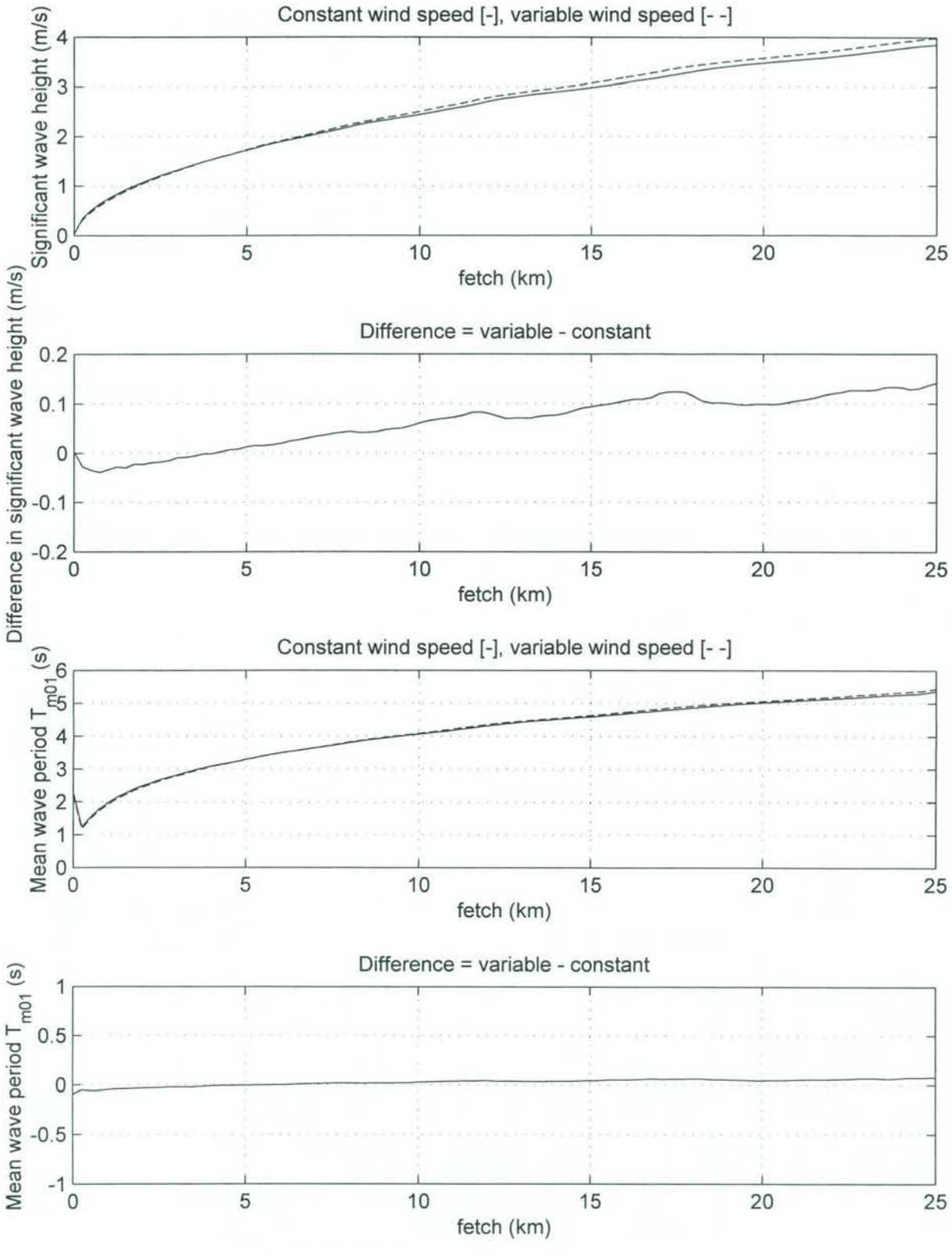

Comparison of significant wave height H_s and mean wave period T_{m01} for a constant wind speed of 25 m/s and for spatially varying wind field for the case of a warm island, temperature difference of +5°C

Source term investigation SWAN	A162	Alkyon Fig 3.21

fig3-22.m

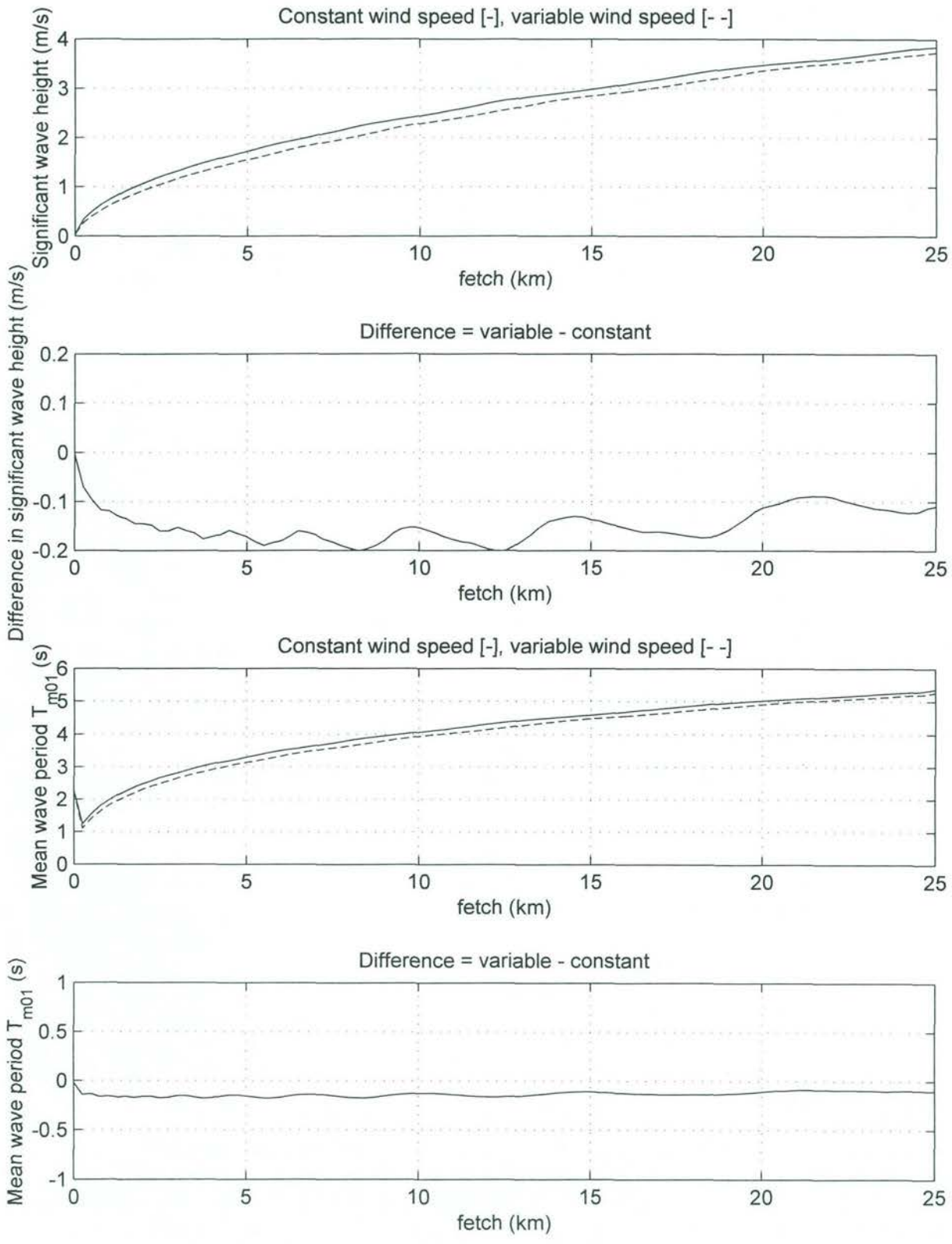

Comparison of significant wave height H_s and mean wave period T_{m01} for a constant wind speed of 25 m/s and for spatially varying wind field for the case of a warm island, temperature difference of -5°C

Source term investigation SWAN	A162	Alkyon	Fig 3.22

fig3-23.m

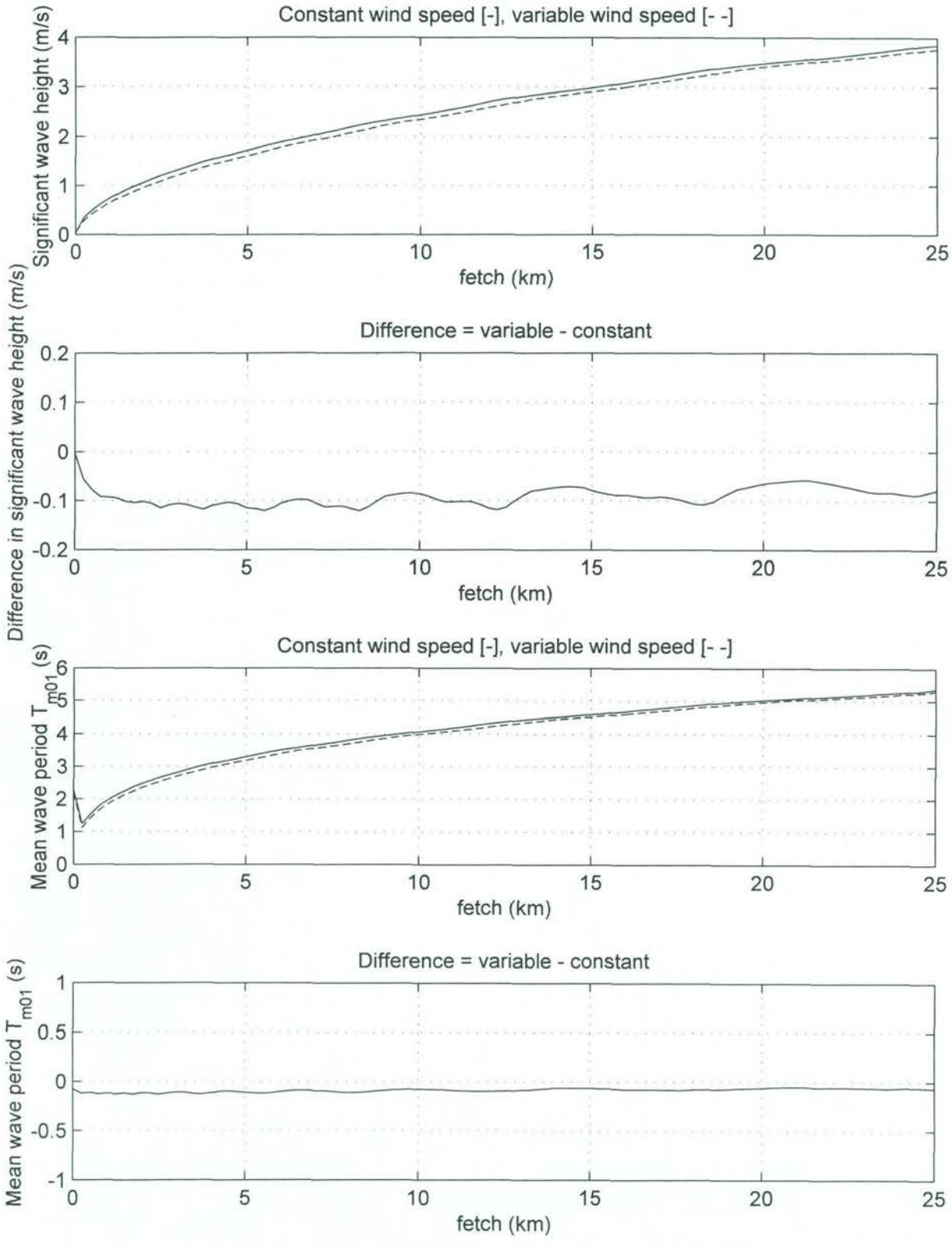

Comparison of significant wave height H_s and mean wave period T_{m01} for a constant wind speed of 25 m/s and for spatially varying wind field for the case of a warm island, temperature difference of 0°C

Source term investigation SWAN	A162	Alkyon	Fig 3.23

fig3-24.m

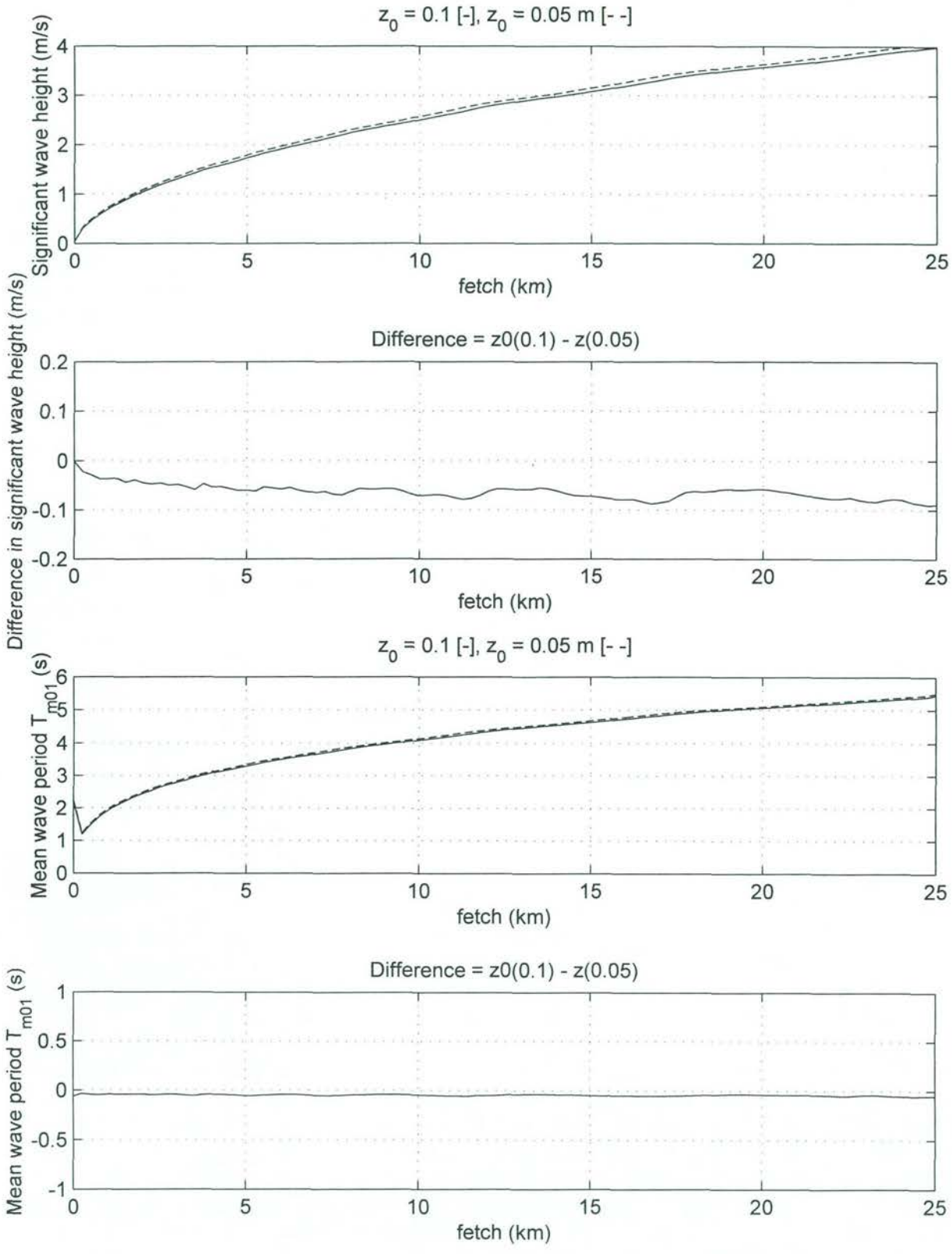

Comparison of significant wave height H_s and mean wave period T_{m01} spatially varying wind field and surface roughness of 0.05 m [-] and 0.1 m [-] for the case of a warm island, temperature difference of +5°C

Source term investigation SWAN	A162	Alkyon	Fig 3.24

fig3-25.m

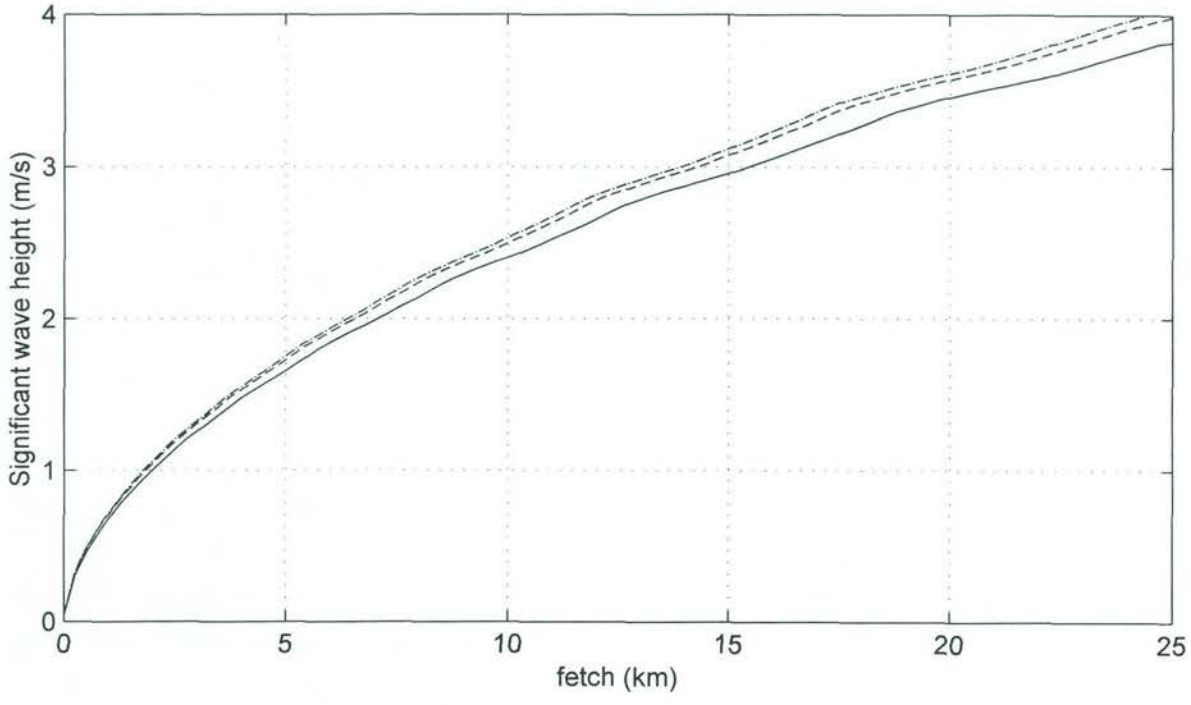

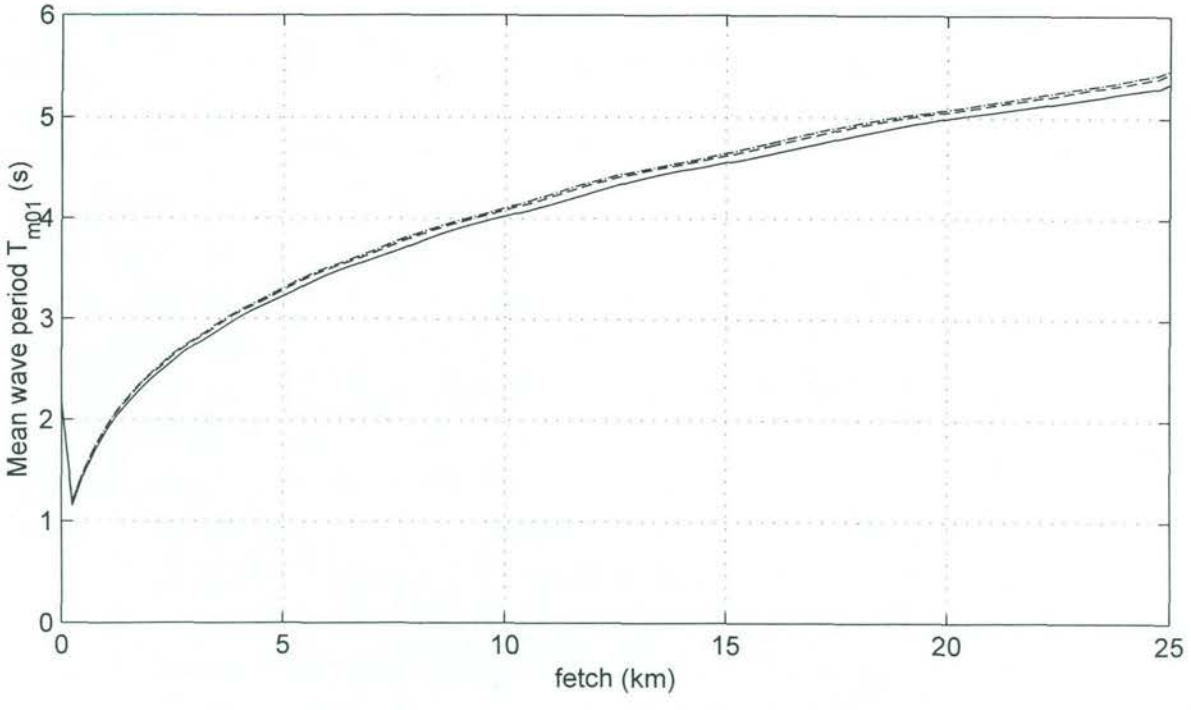

Comparison of significant wave height H_s and mean wave period T_{m01} spatially varying wind field and surface roughness of 0.1 and U_{10} = 25 m/s for island widths of 10 km [-], 25 km [- -] and 50 km [-.]

Source term investigation SWAN	A162	Alkyon	Fig 3.25

fig3-26.m

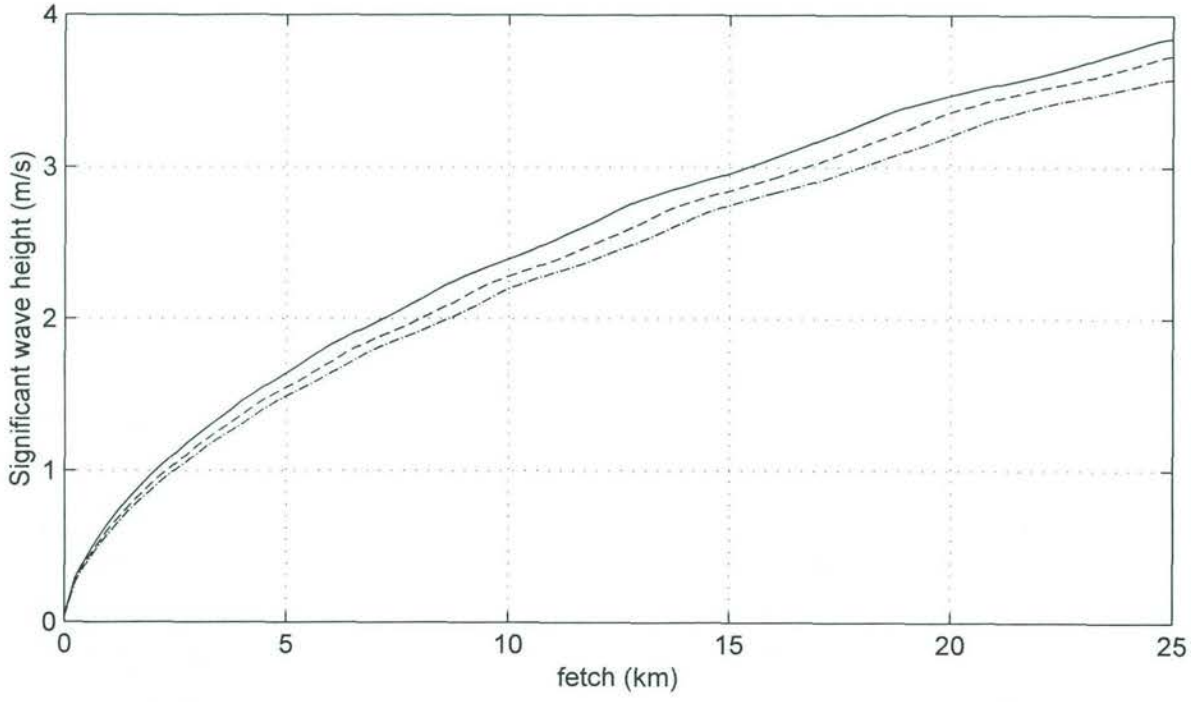

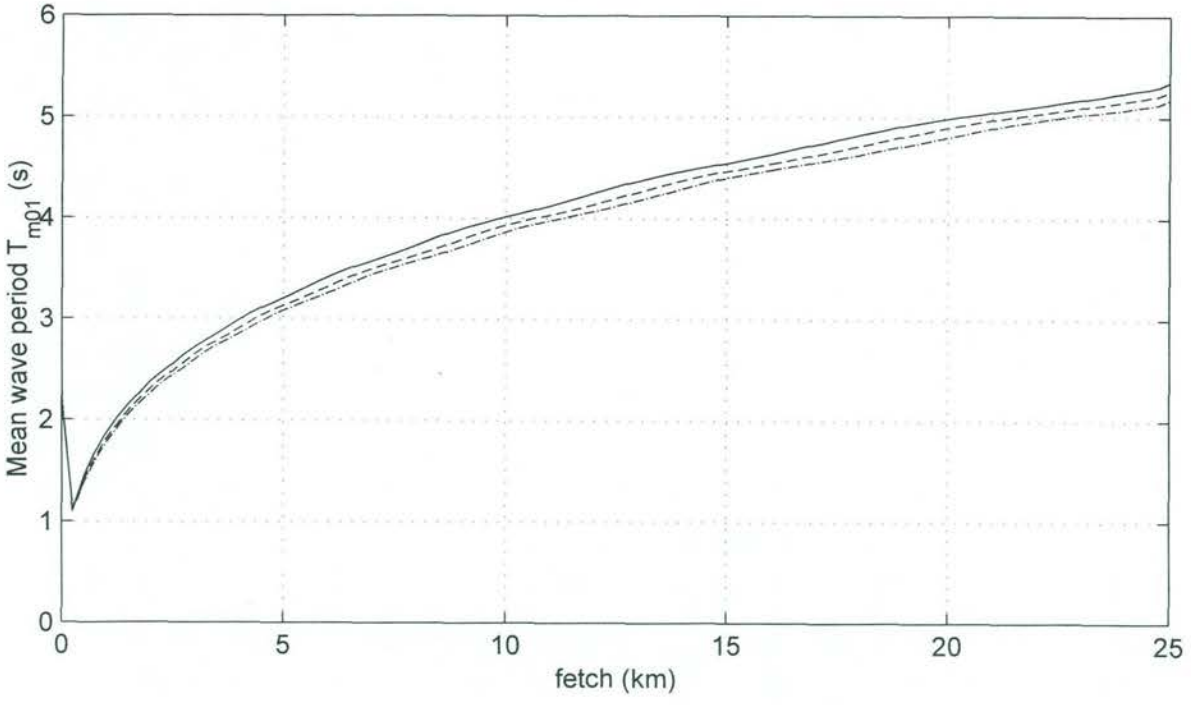

Comparison of significant wave height H_s and mean wave period T_{m01} spatially varying wind field and surface roughness of 0.1 and U_{10} = 25 m/s for island widths of 10 km [-], 25 km [- -] and 50 km [-.], cold island

fig3-27.m

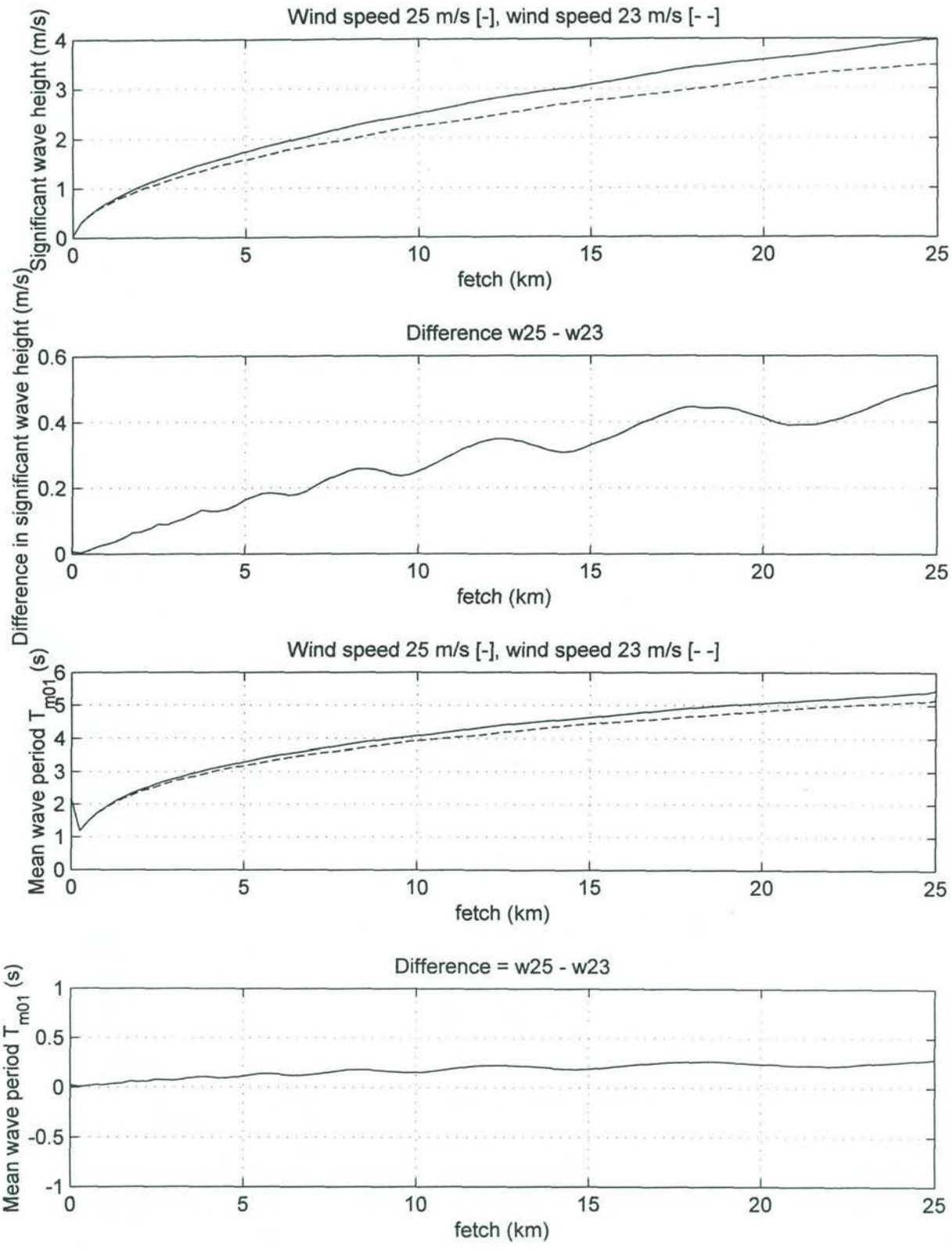

Comparison of significant wave height H_s and mean wave period T_{m01} spatially varying wind field and surface roughness of 0.1 island widths of 25 km and a constant wind speed of 23 m/s [-] and 25 m/s[- -]

fig4-1.m

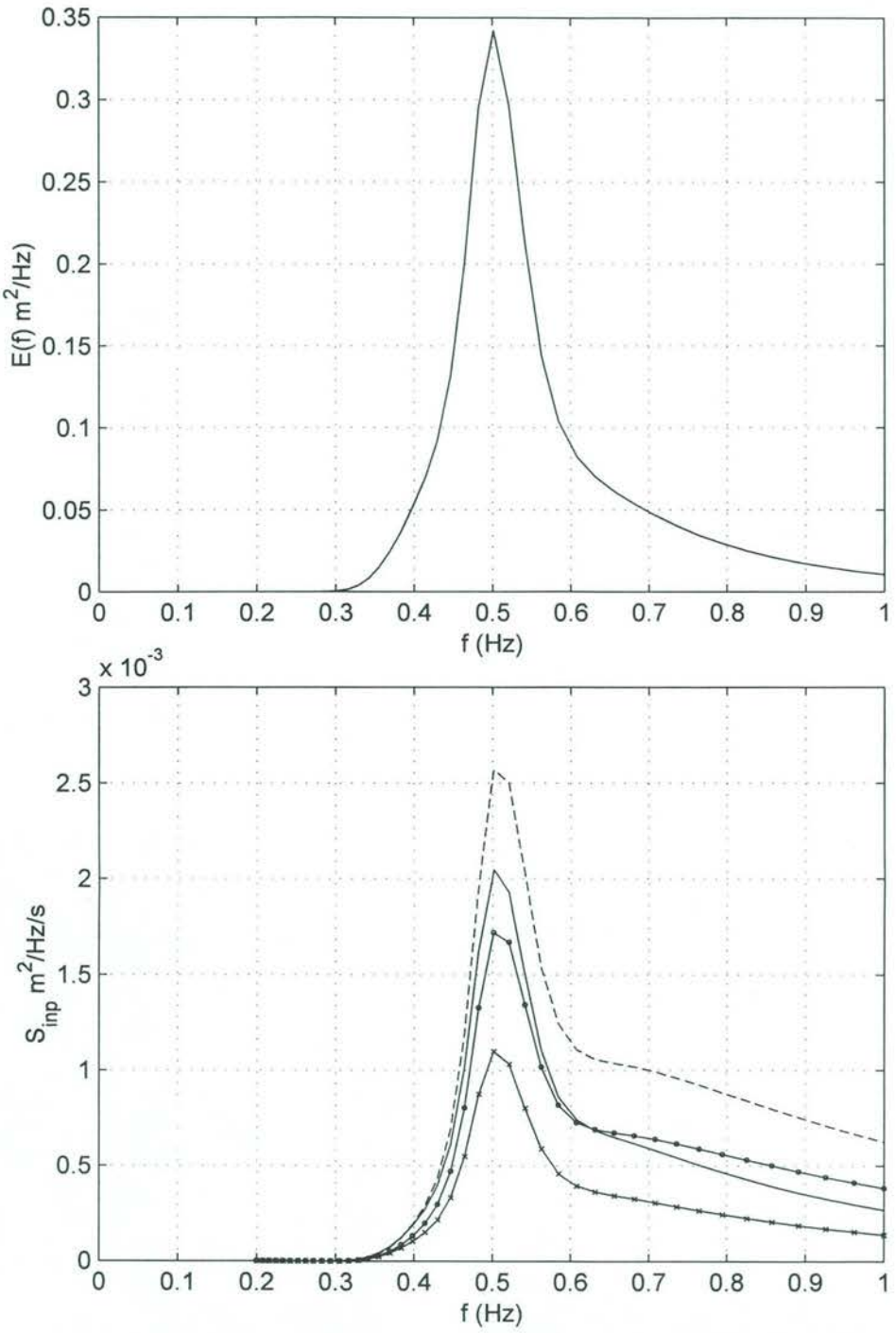

Komen et al., 1984
Janssen, 1991
Burger and Makin, 1993
Stewart, 1974

Comparison of various wind input source functions
for a JONSWAP spectrum with f_p = 0.5 Hz and a wind speed of 20 m/s

fig4-2.m

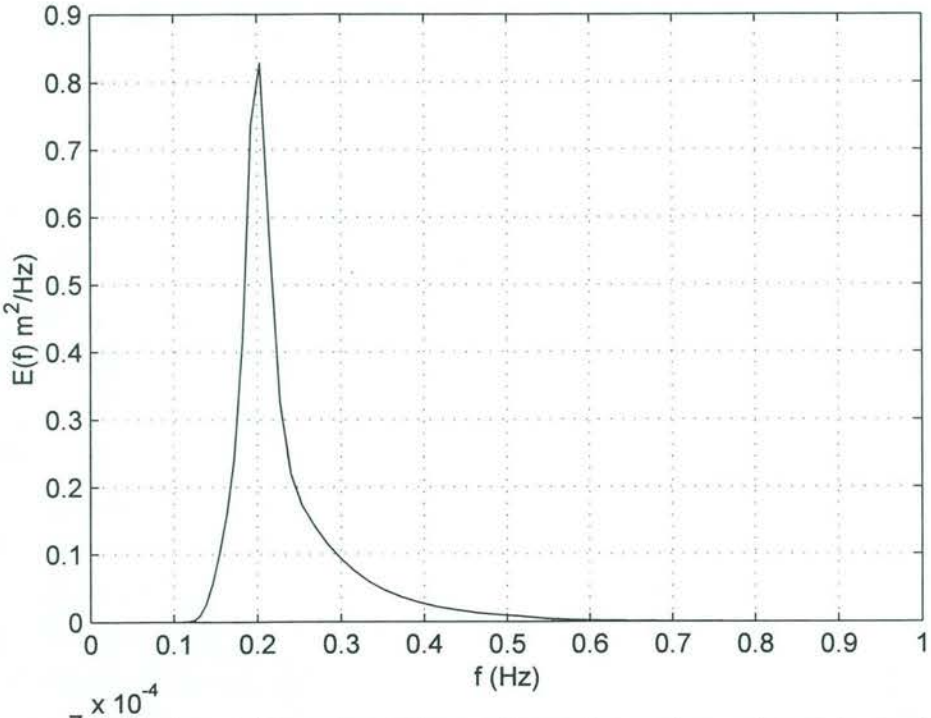

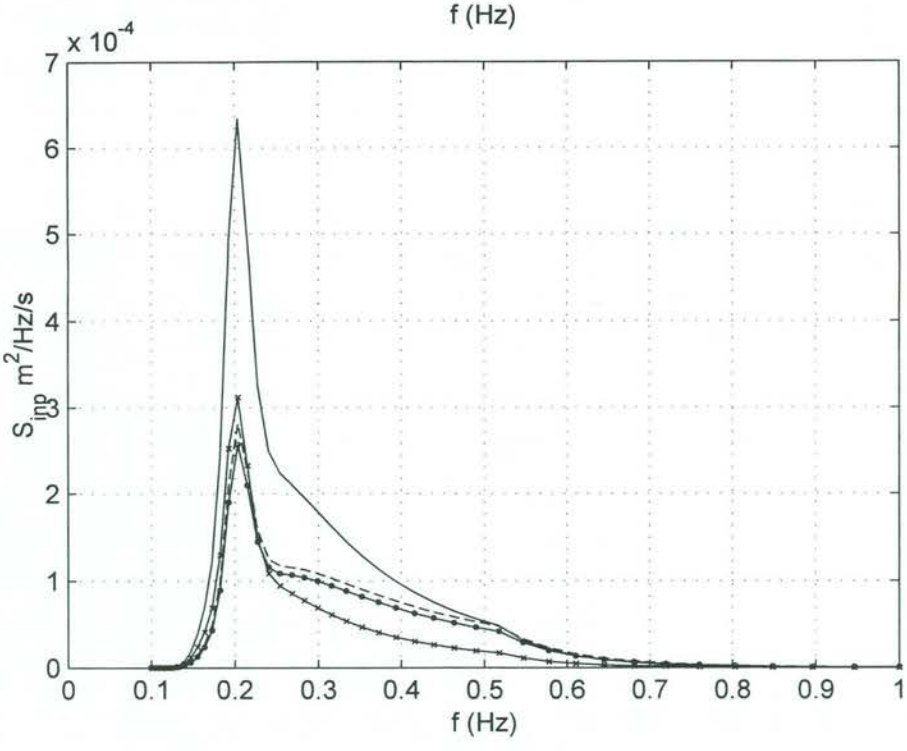

Komen et al., 1984
Janssen, 1991
Burger and Makin, 1993
Stewart, 1974

Comparison of various wind input source functions
for a JONSWAP spectrum with f_p = 0.2 Hz and a wind speed of 20 m/s

fig4-3.m

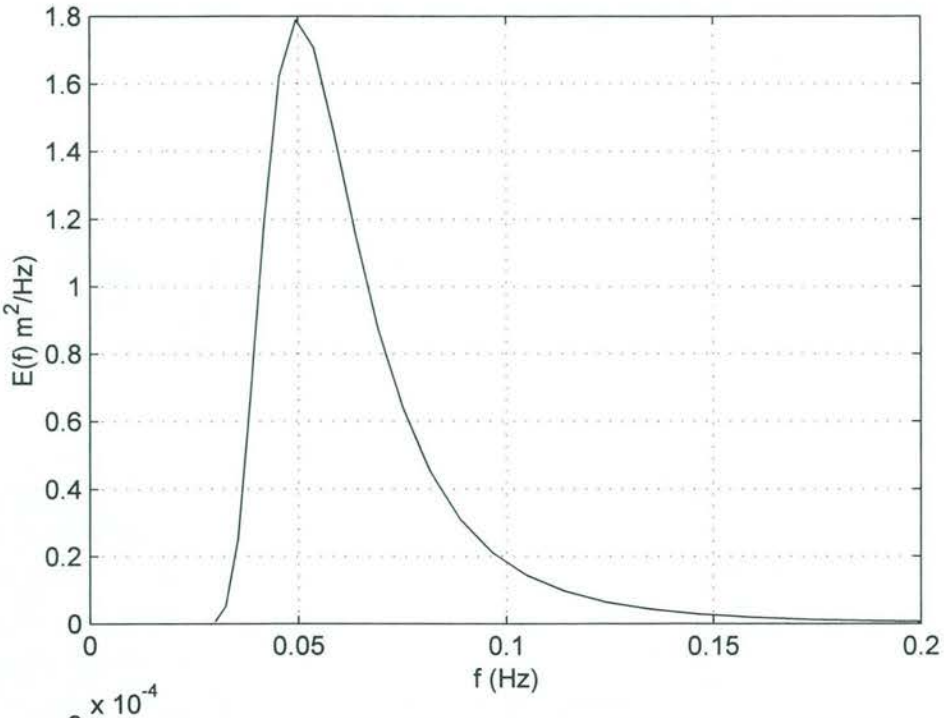

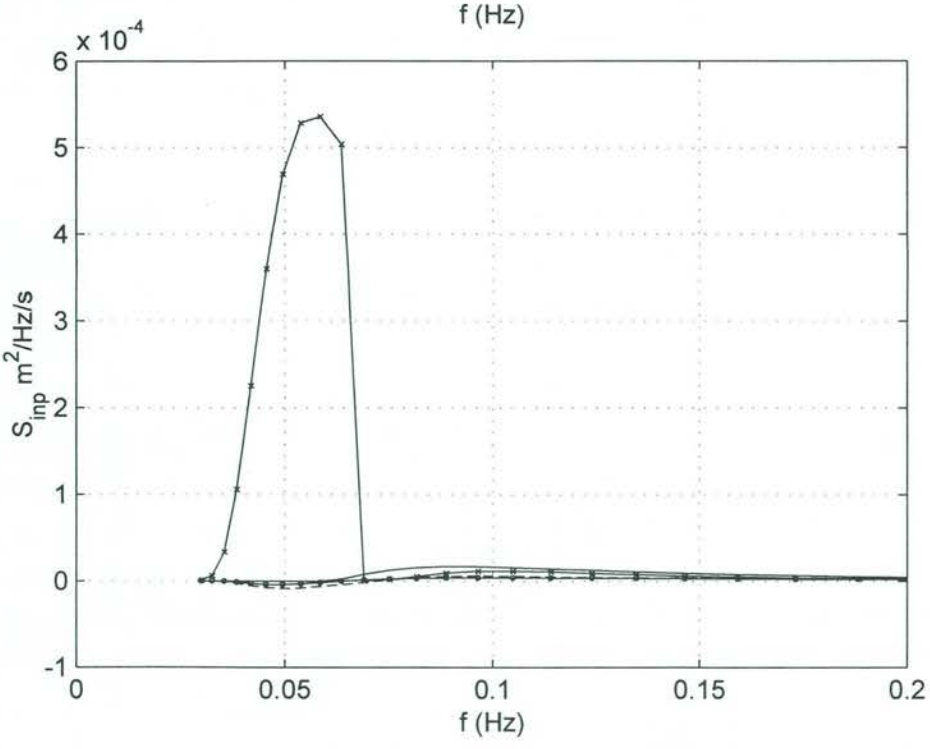

Komen et al., 1984
Janssen, 1991
Burger and Makin, 1993
Stewart, 1974

Comparison of various wind input source functions for a Pierson-Moskowitz spectrum with f_p = 0.05 Hz and a wind speed of 20 m/s

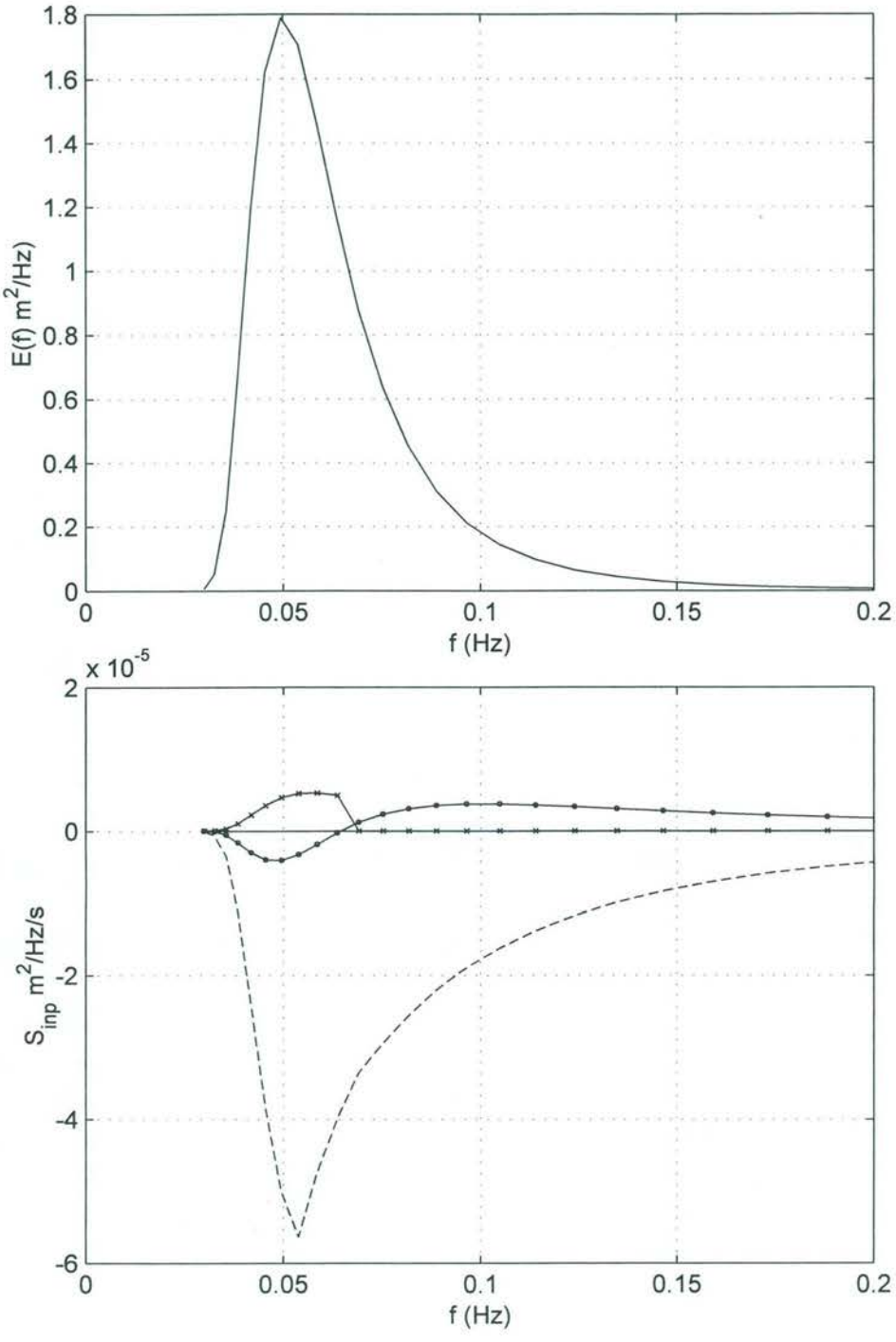

Comparison of various wind input source functions for a Pierson-Moskowitz spectrum with f_p = 0.05 Hz and an opposing wind speed of 20 m/s

Source term investigation SWAN	A162	Alkyon	Fig 4.4

fig4-5.m

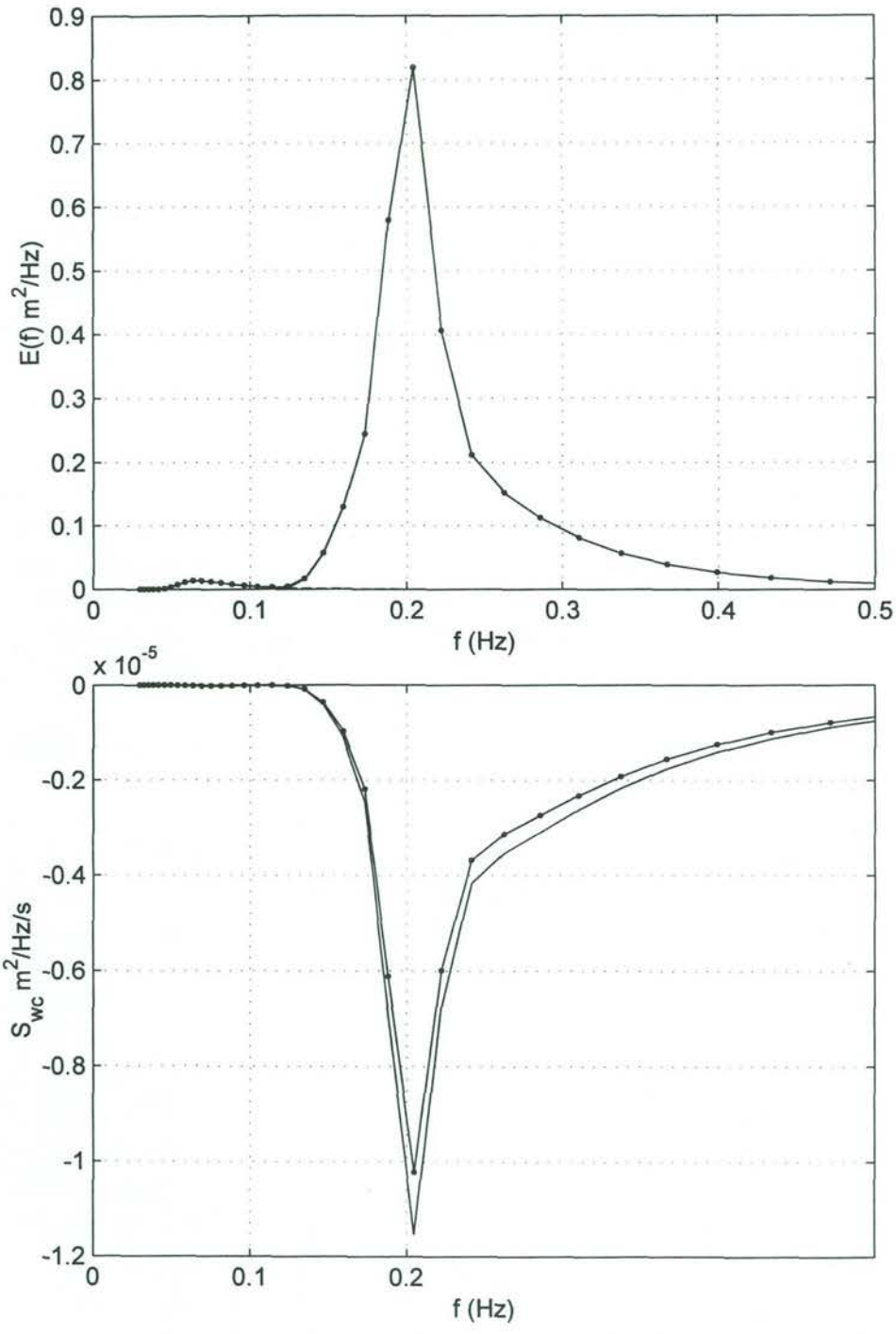

Sea

Swell

Sea + swell

White-capping dissipation for a wind sea spectrum, a swell spectrum and a combined sea-swell system
Sea: T_p=5 s, H_s=1 m, Swell: T_p=15 s, H_s=0.1 m

fig4-6.m

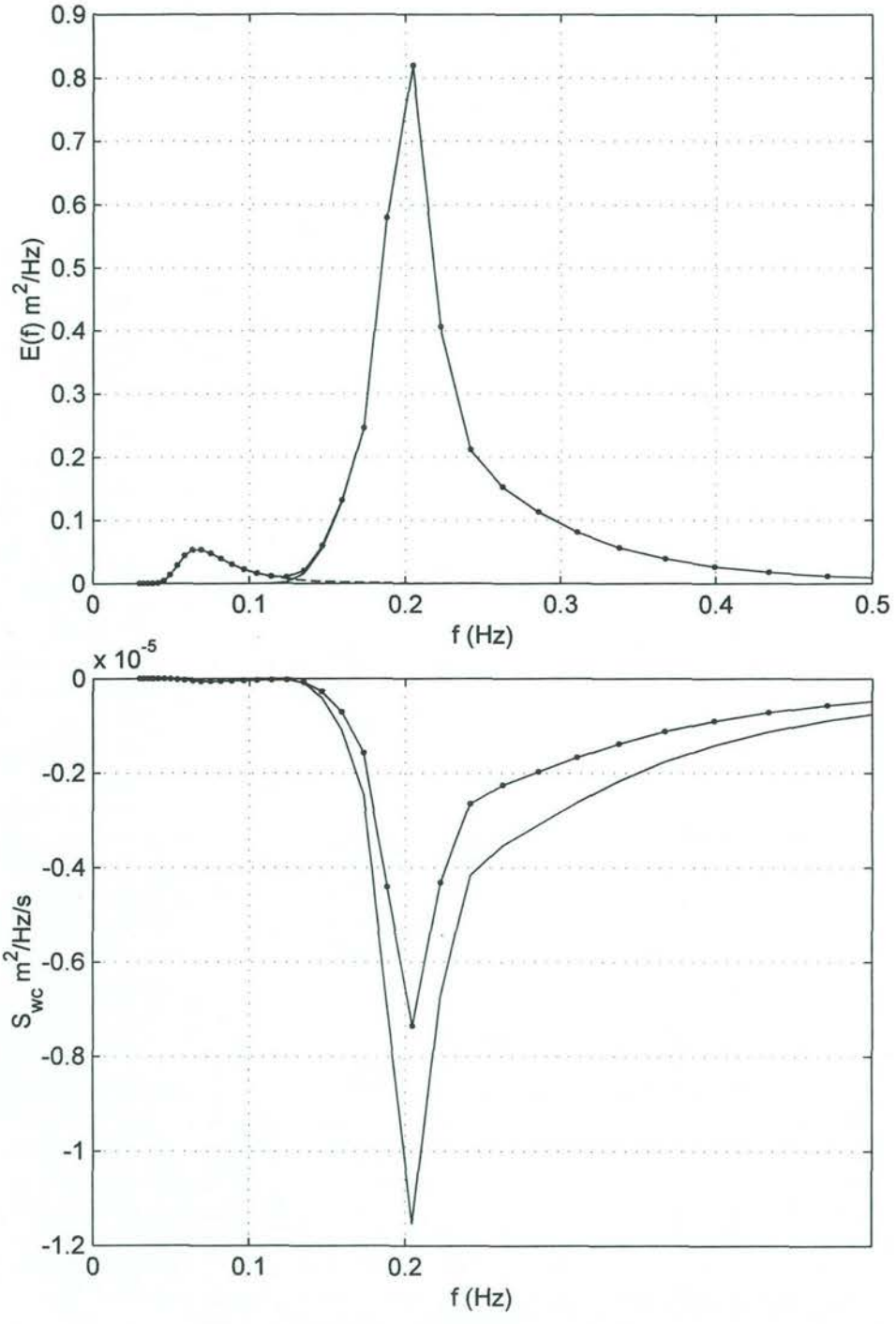

White-capping dissipation for a wind sea spectrum, a swell spectrum and a combined sea-swell system
Sea: T_p=5 s, H_s=1 m, Swell: T_p=15 s, H_s=0.2 m

fig4-7.m

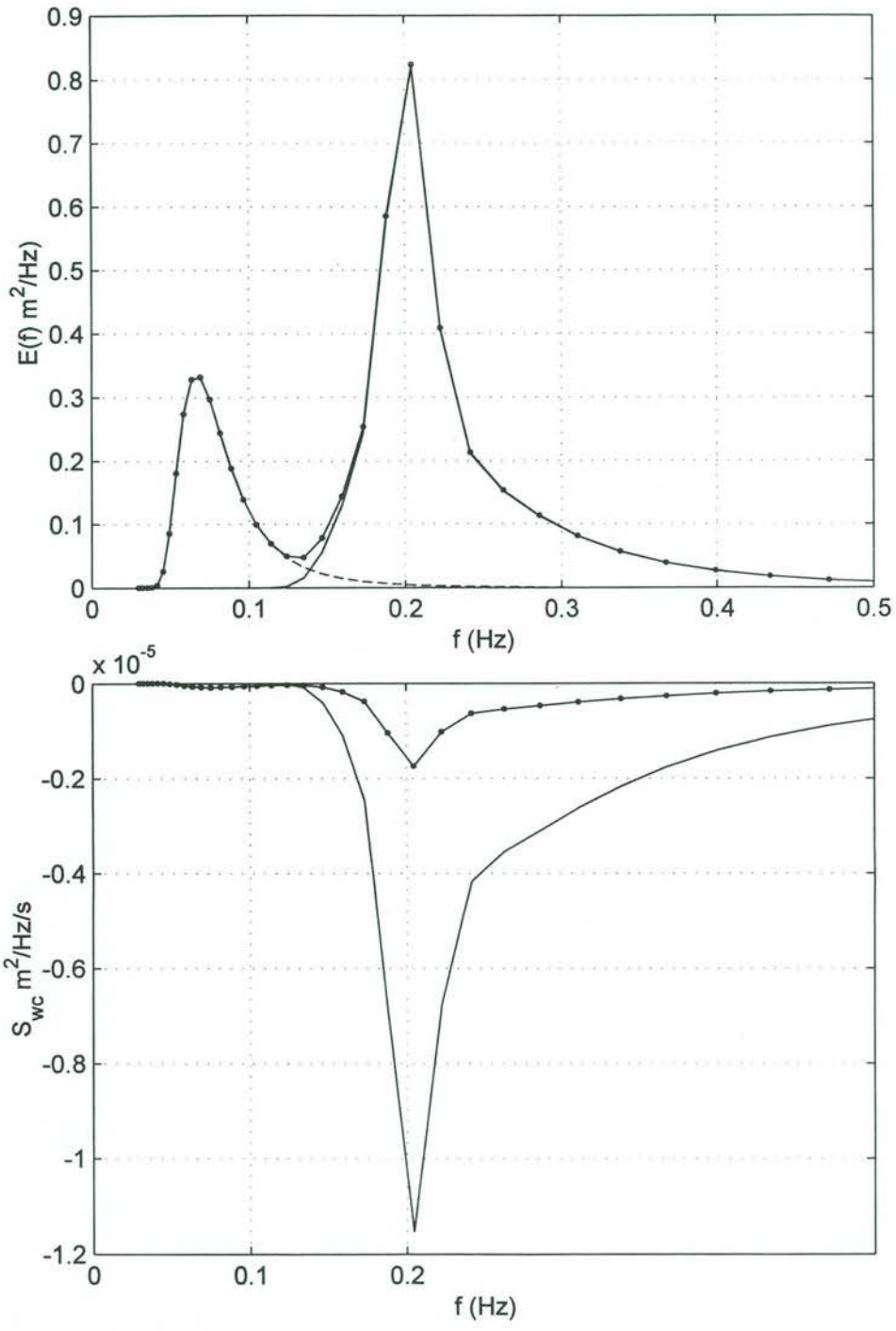

White-capping dissipation for a wind sea spectrum, a swell spectrum and a combined sea-swell system
Sea: T_p=5 s, H_s=1 m, Swell: T_p=15 s, H_s=0.5 m

Source term investigation SWAN	A162	Alkyon	Fig 4.7

fig4-9.m

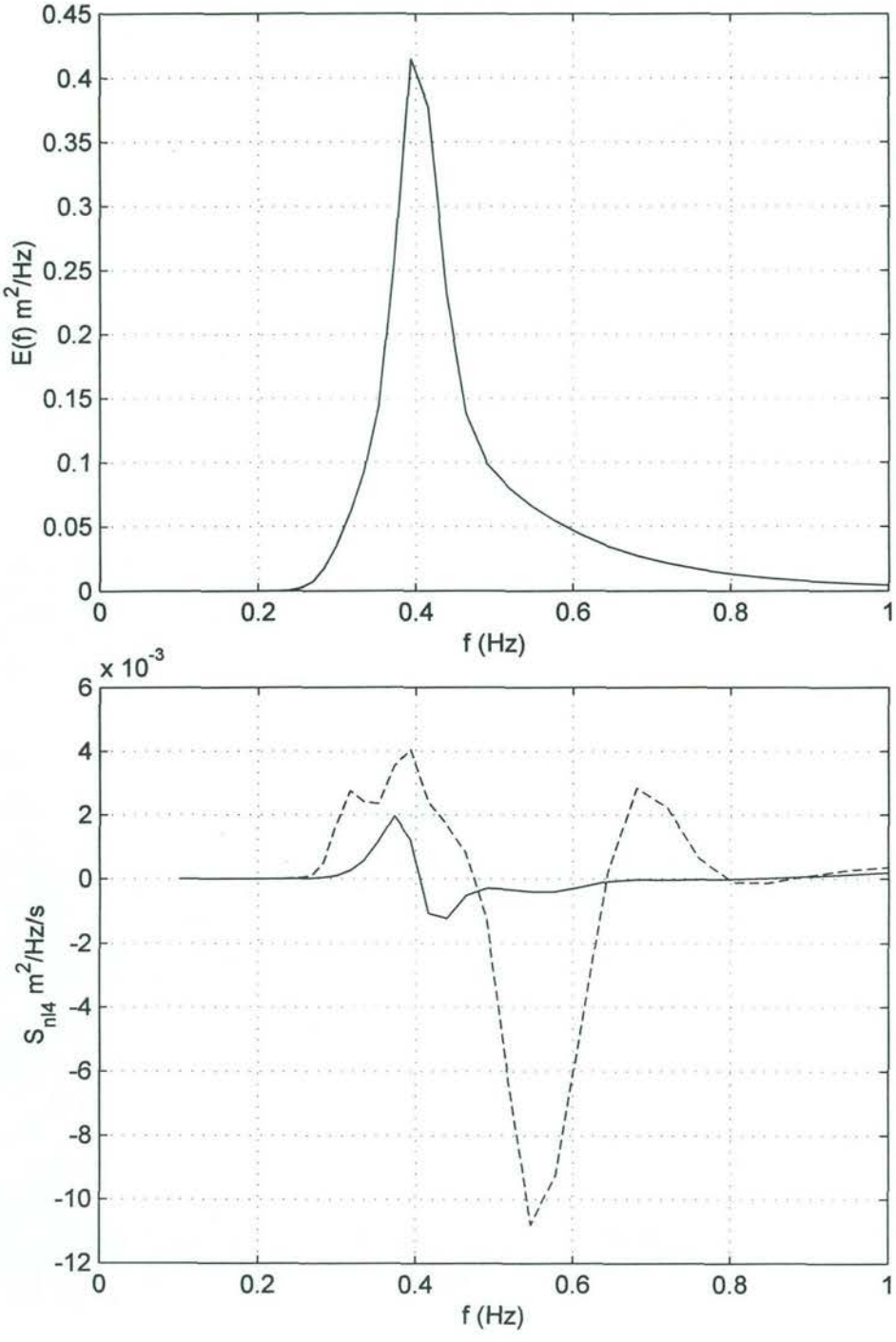

Comparison of non-linear interactions computed with the DIA and with the exact method of Tracy and Resio
JONSWAP spectrum T_p=2.5 s, H_s=1 m, Gamma = 3.3

fig4-10.m

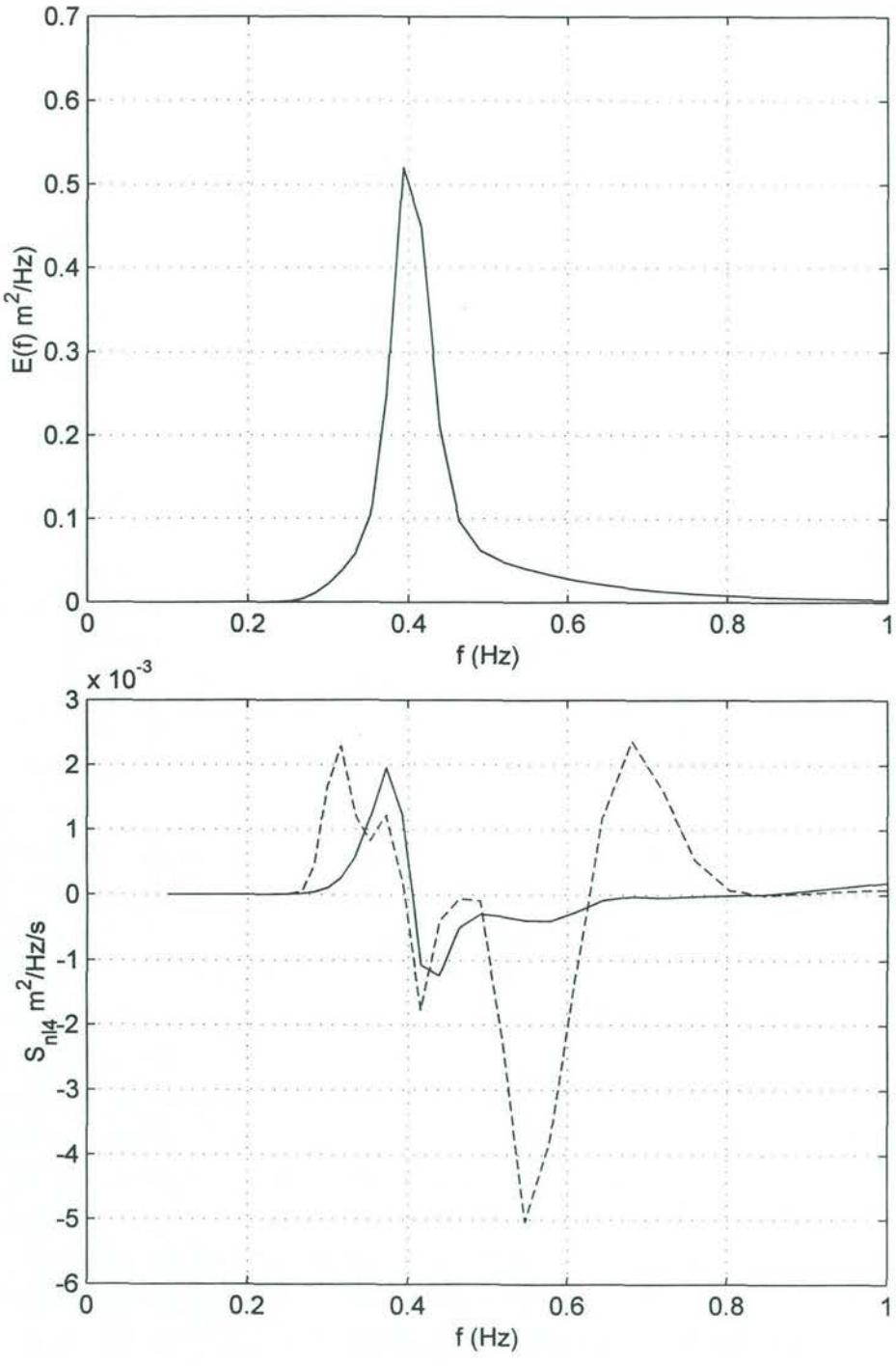

Comparison of non-linear interactions computed with the DIA and with the exact method of Tracy and Resio
JONSWAP spectrum T_p=2.5 s, H_s=1 m, Gamma = 7

Source term investigation SWAN	A162	Alkyon	Fig 4.10

fig4-11.m

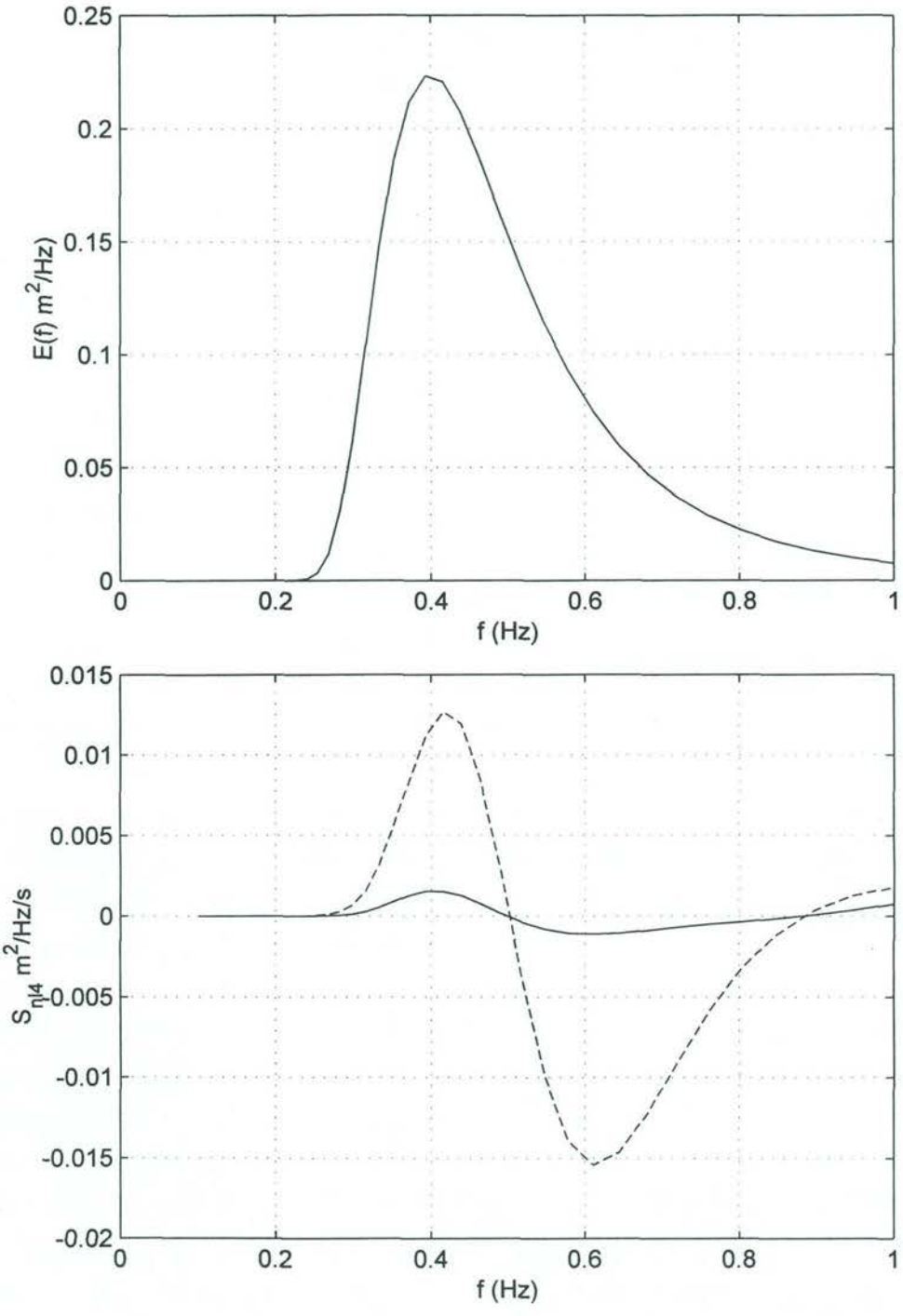

Comparison of non-linear interactions computed with the DIA and with the exact method of Tracy and Resio JONSWAP spectrum T_p=2.5 s, H_s=1 m, Gamma = 1			
Source term investigation SWAN	A162	Alkyon	Fig 4.11

fig4-12.m

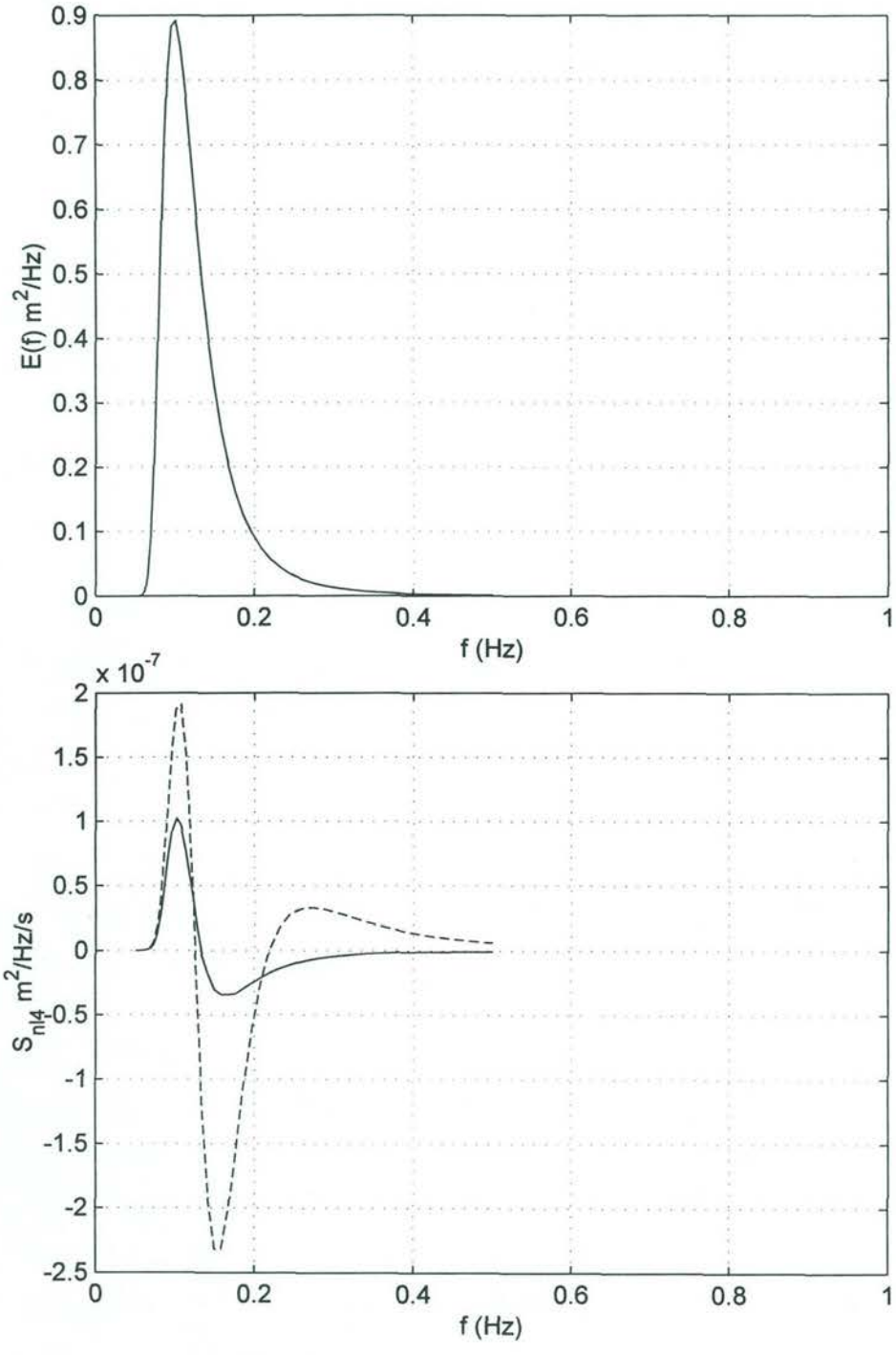

Comparison of non-linear interactions computed with the DIA
and with the exact method of Tracy and Resio
JONSWAP spectrum T_p=10 s, H_s=1 m, Gamma = 1

fig4-13.m

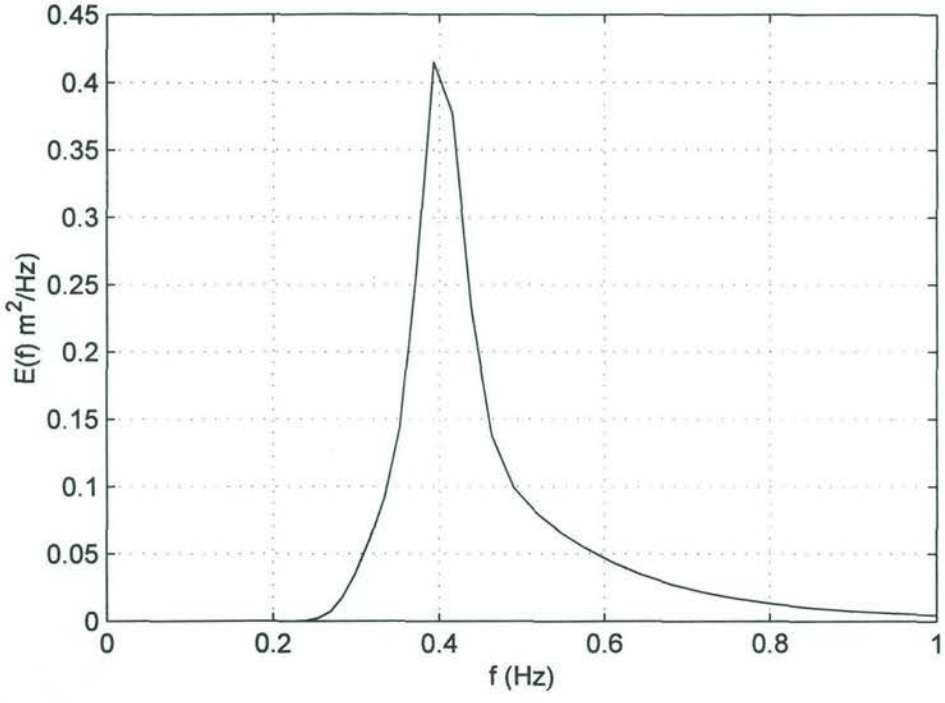

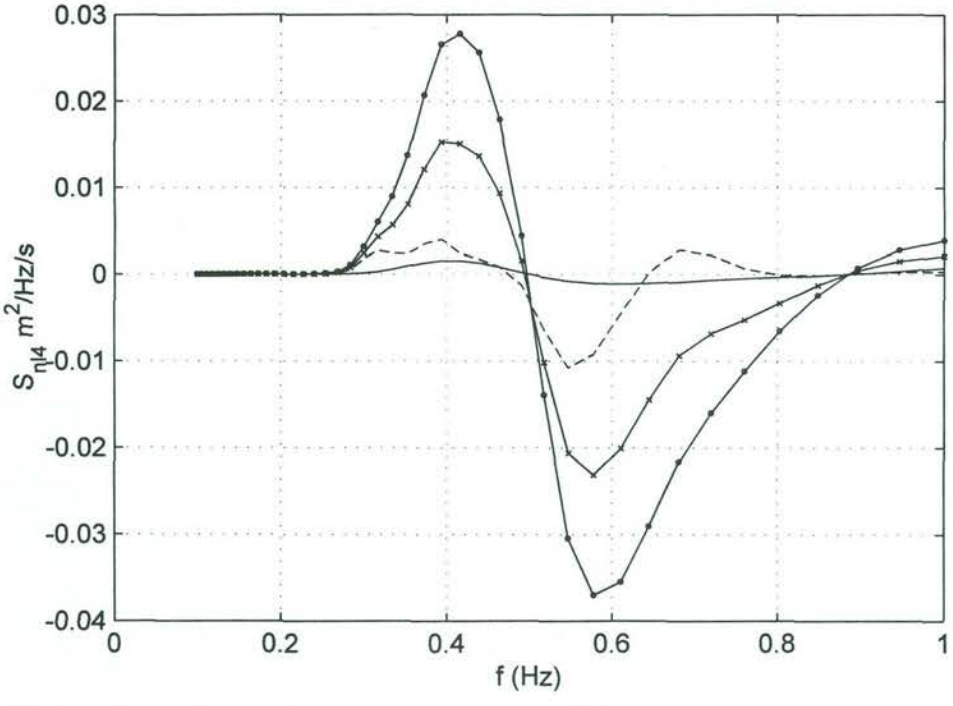

Exact

DIA /lambda = 0.20

DIA /lambda = 0.25

DIA /lambda = 0.30

Comparison of non-linear interactions
JONSWAP spectrum T_p=4 s, H_s=1 m, Gamma = 3.3
for /lambda = 0.2, 0.25 and 0.3

Source term investigation SWAN | A162 | Alkyon | Fig 4.13

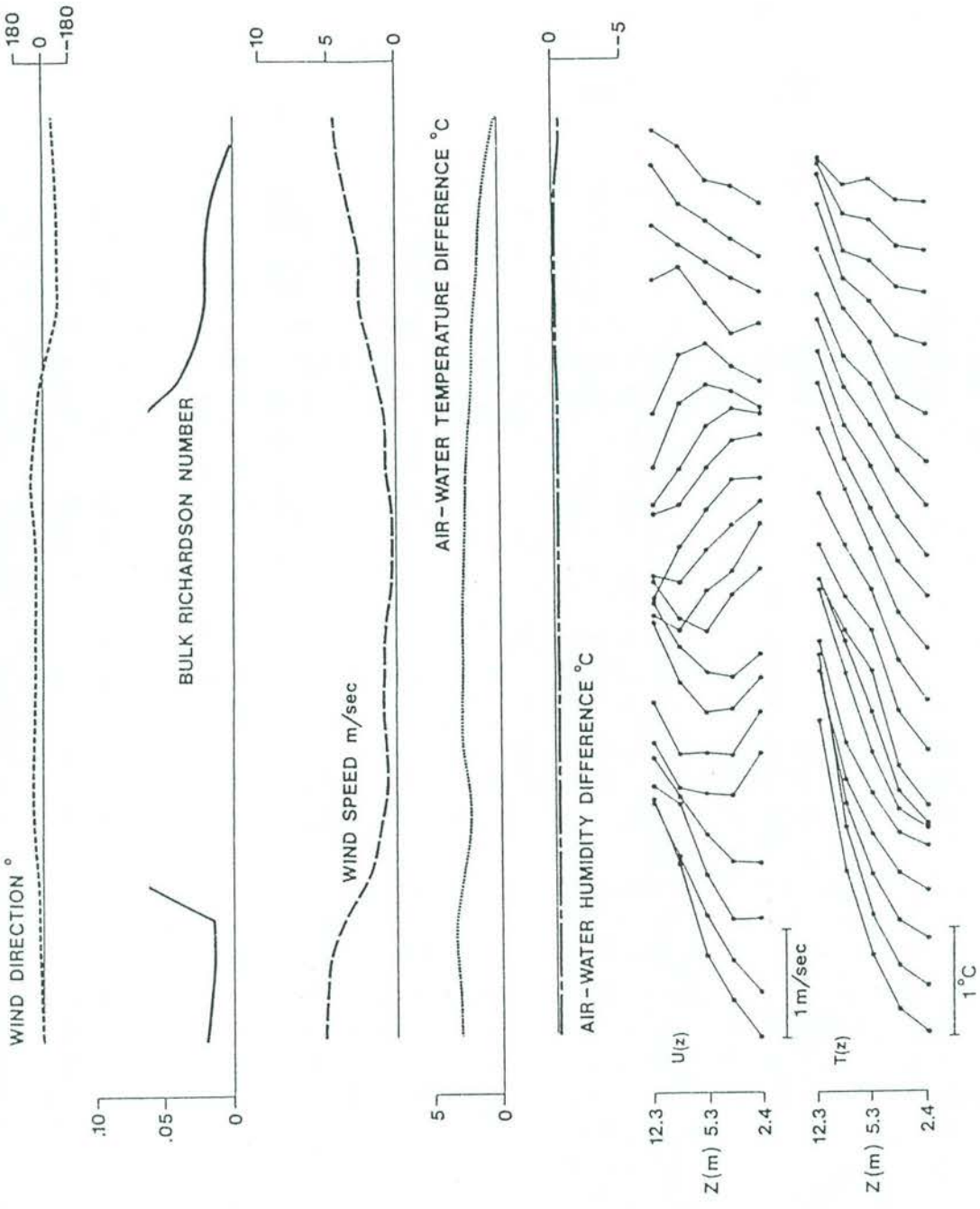

Wave induced wind speed after a change in wind direction
Reproduced from Donelan and Dobson (1997)

Source term investigation SWAN | A162 | Alkyon | Fig 5.1

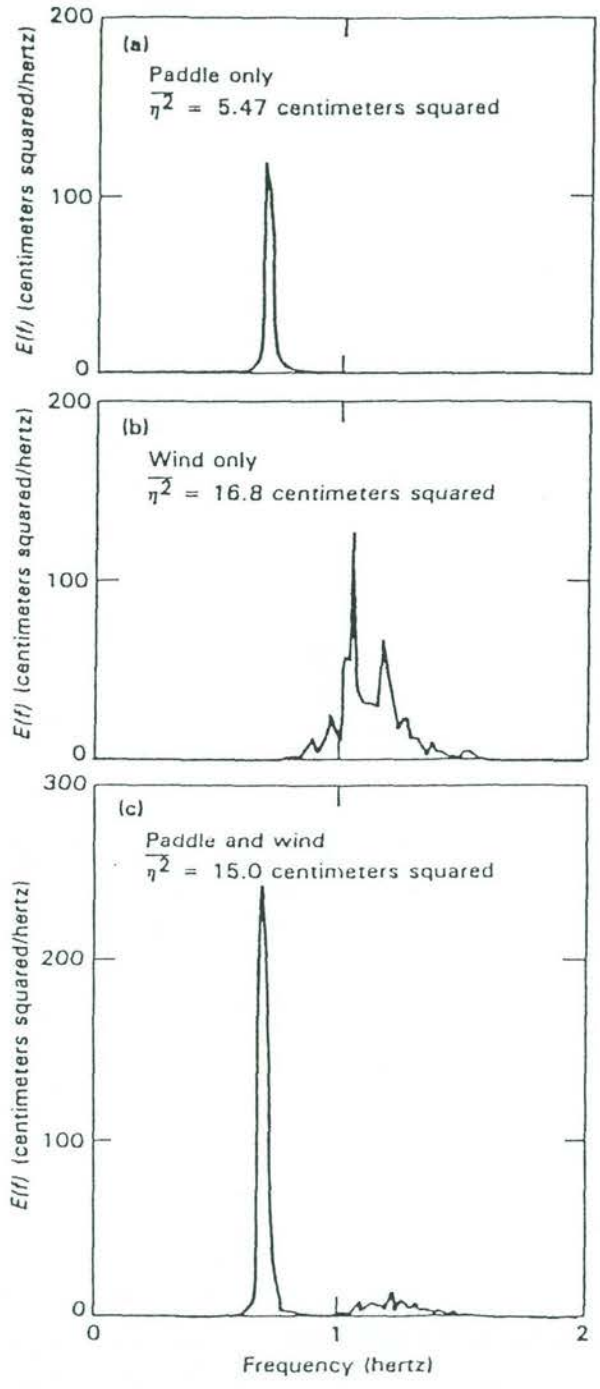

Fig 3. —Wave spectra at 50 meters fetch in a laboratory wind-wave tank. (a) The spectrum of a continuous train of 0.707-hertz paddle-generated waves of steepness $ak = 0.067$. (b) The spectrum of a pure wind sea with measured wind of 11 meters per second at 26 centimeters height. (c) The spectrum of waves with wind and paddle excited together as in (a) and (b).

Reproduced from Donelan 1987

fcase

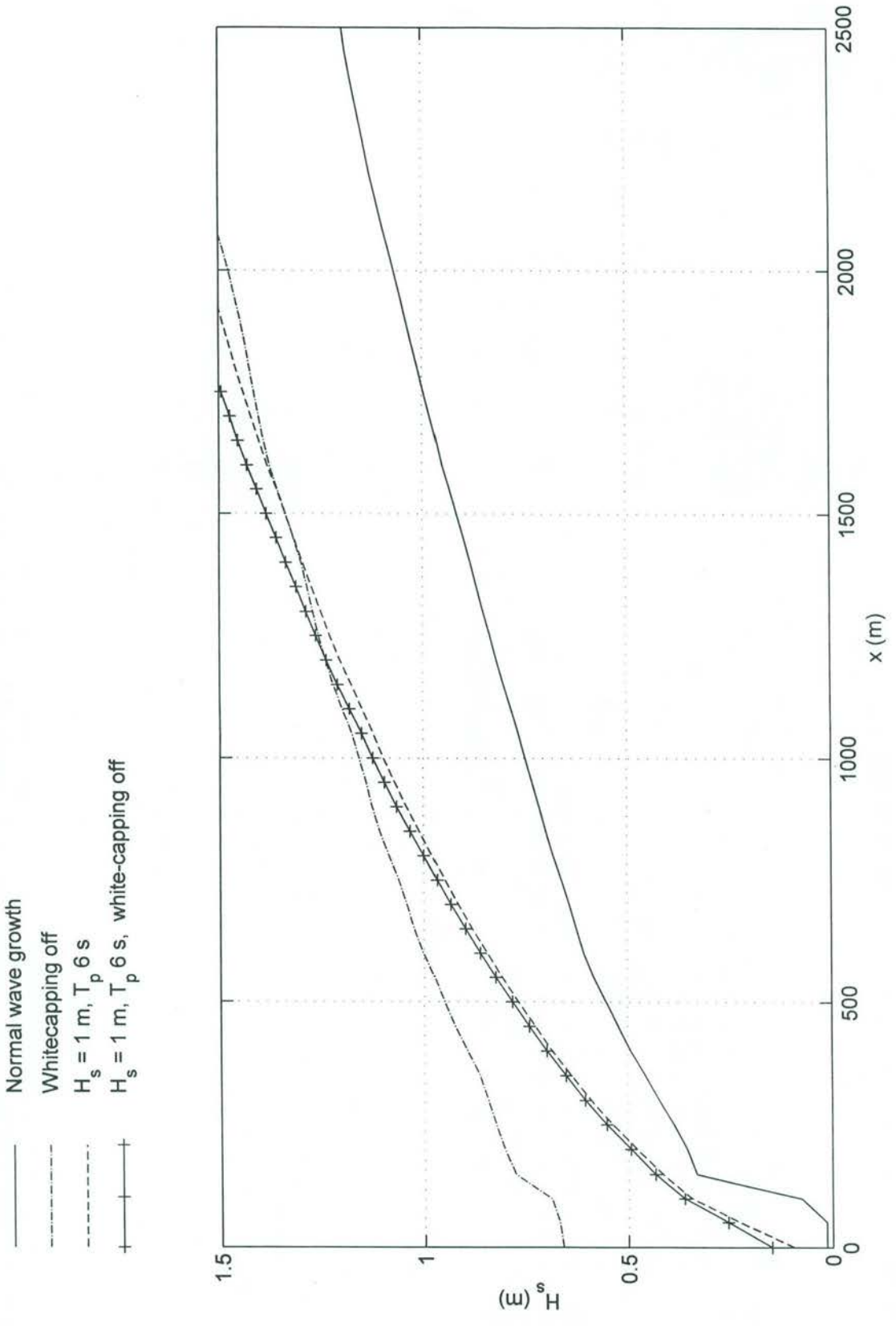

Variation of significant wave height along fetch showing the effect of the wave boundary condition and the effect of whitecapping

Source term investigation SWAN | A162 | Alkyon | Fig. 5.3

fcase

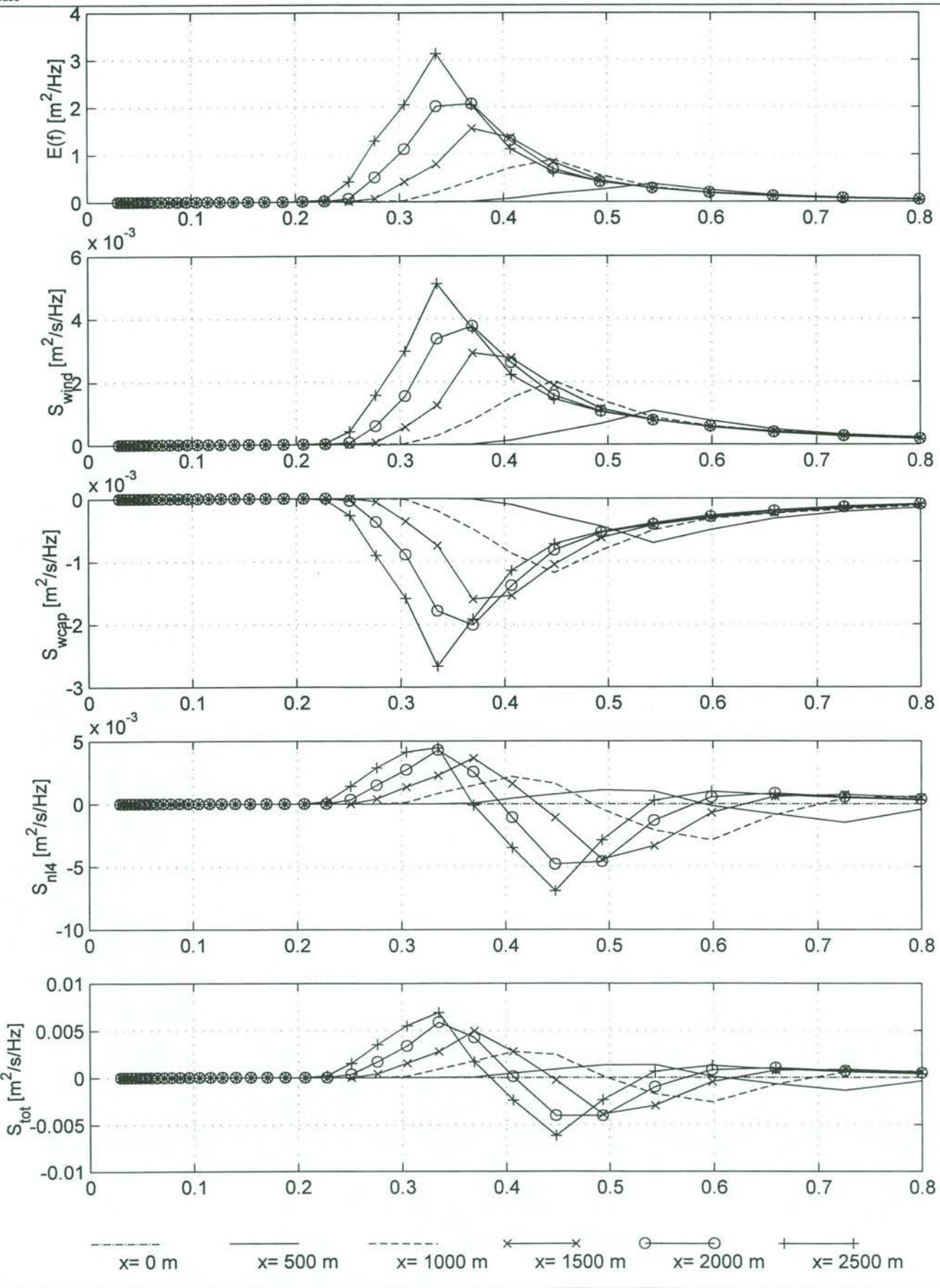

Development of spectrum and source terms
Wind speed 20 m/s, Fetch 2500 m
Whitecapping on, no wave boundary condition

Source term investigation SWAN | A162 | Alkyon | Fig. 5.4

fcase

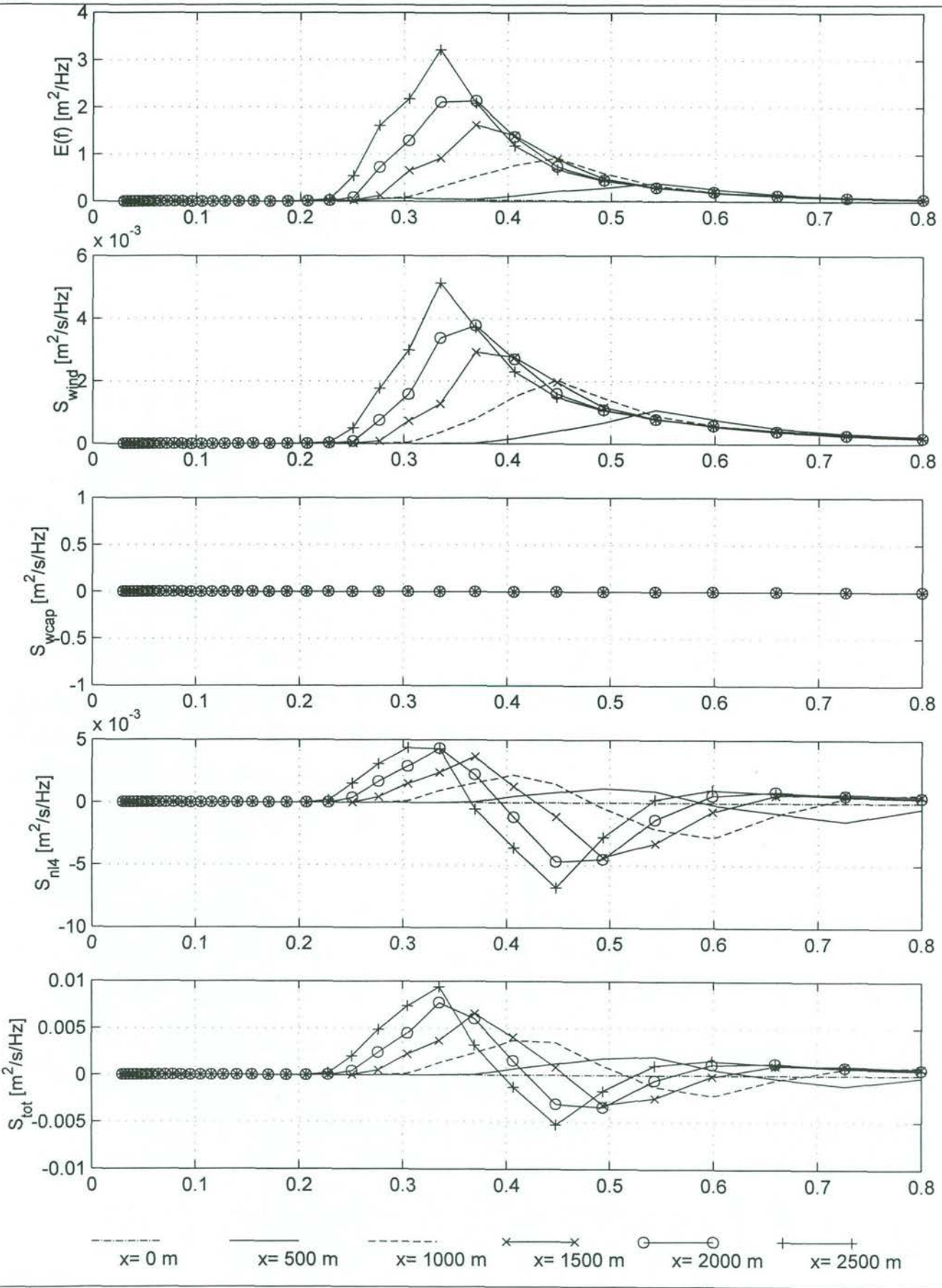

Development of spectrum and source terms
Wind speed 20 m/s, Fetch 2500 m
Whitecapping off, no wave boundary condition

Source term investigation SWAN | A162 | Alkyon | Fig. 5.5

fcase

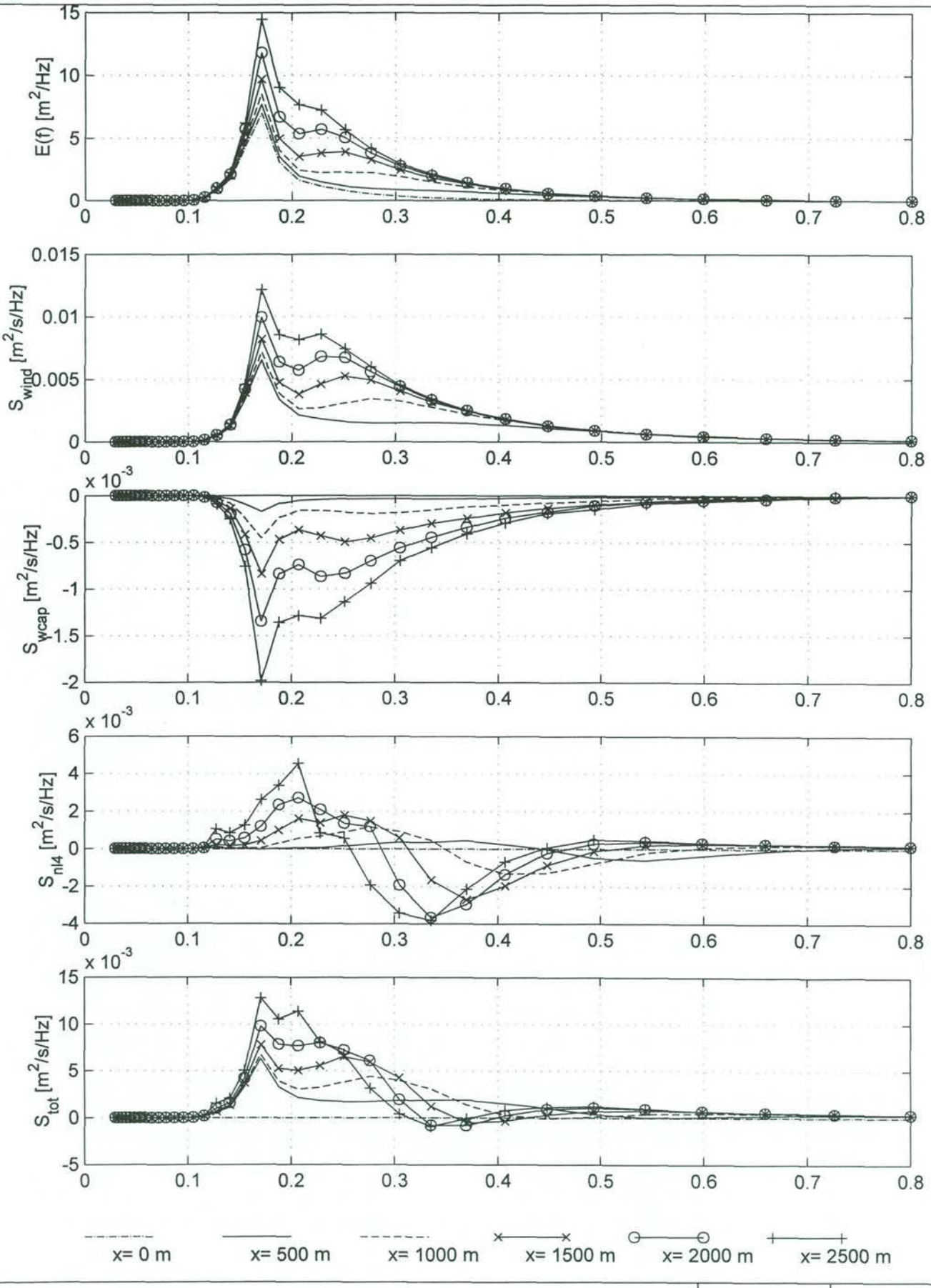

Development of spectrum and source terms
Wind speed 20 m/s, Fetch 2500 m
Whitecapping on, H_s = 1 m, T_p = 6 s

Source term investigation SWAN | A162 | Alkyon | Fig. 5.6

fcase

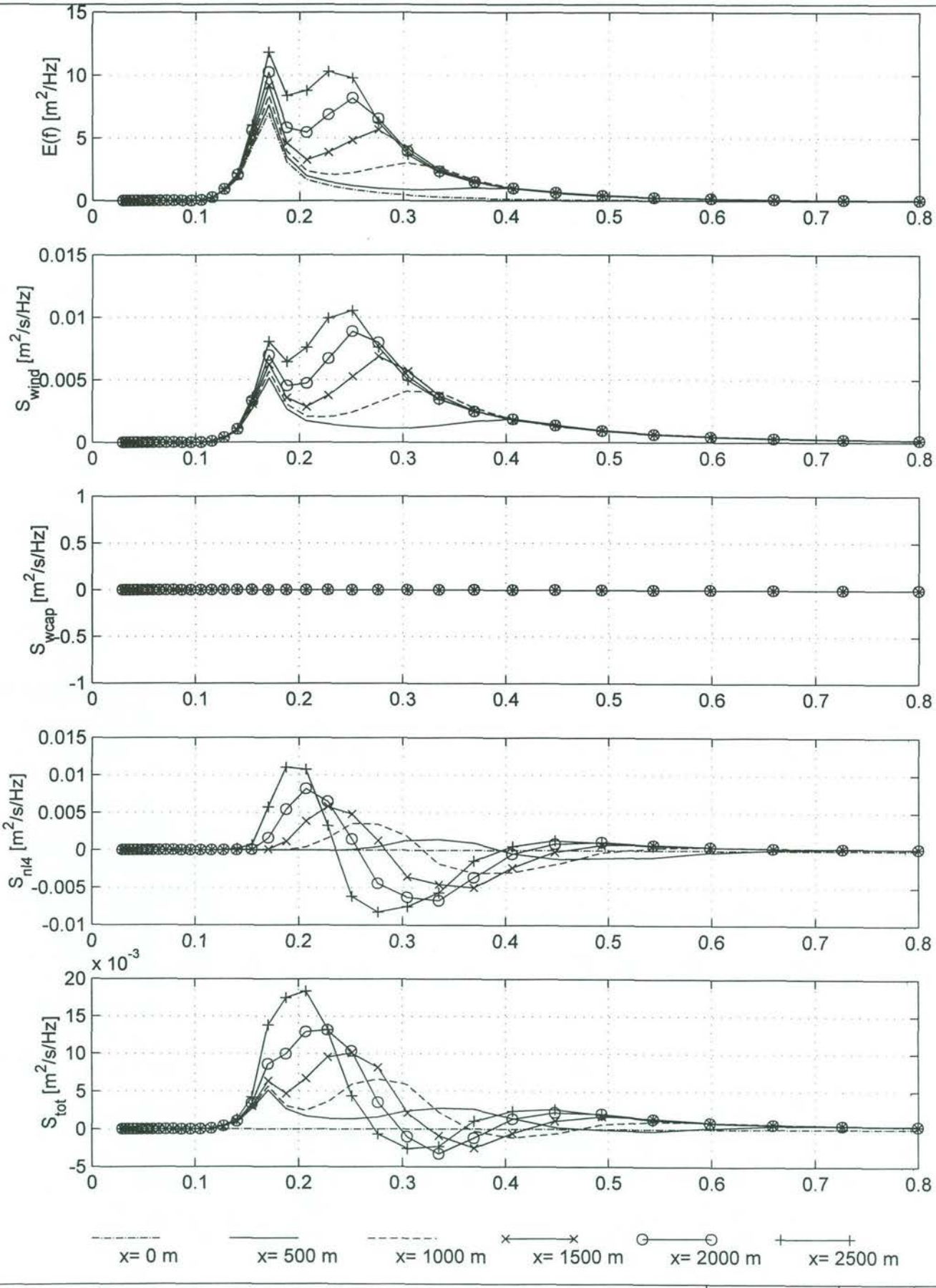

Development of spectrum and source terms
Wind speed 20 m/s, Fetch 2500 m
Whitecapping off, H_s = 1 m, T_p = 6 s

Source term investigation SWAN | A162 | Alkyon | Fig. 5.7

fig6-1.m

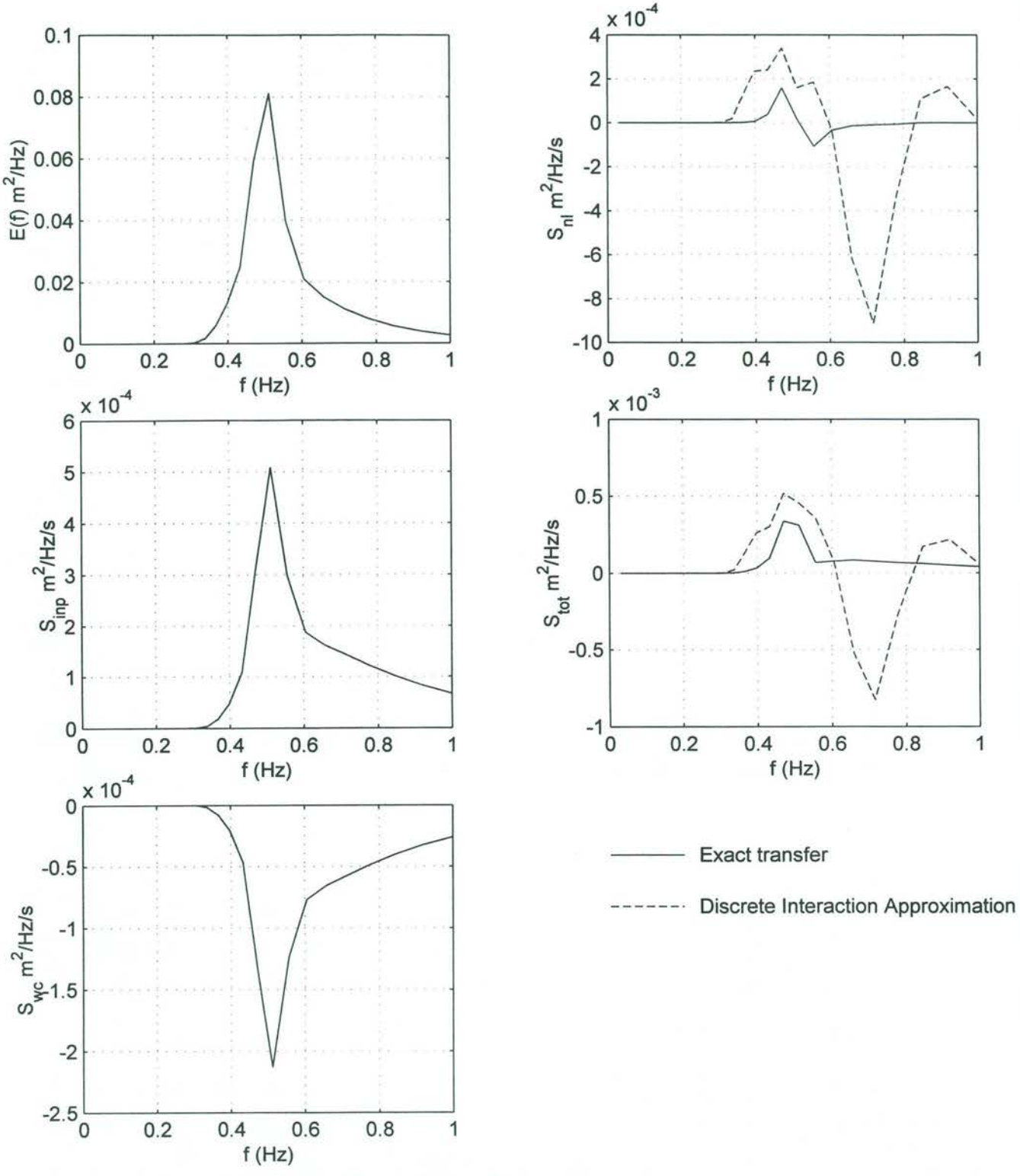

Source term balance for a JONSWAP spectrum
T_p = 2 s, H_s = 0.5 m, U_{10} = 20 m/s
Nonlinear interactions computed with DIA and Exact method

Source term investigation SWAN	A162	Alkyon	Fig 6.1

fig6-2.m

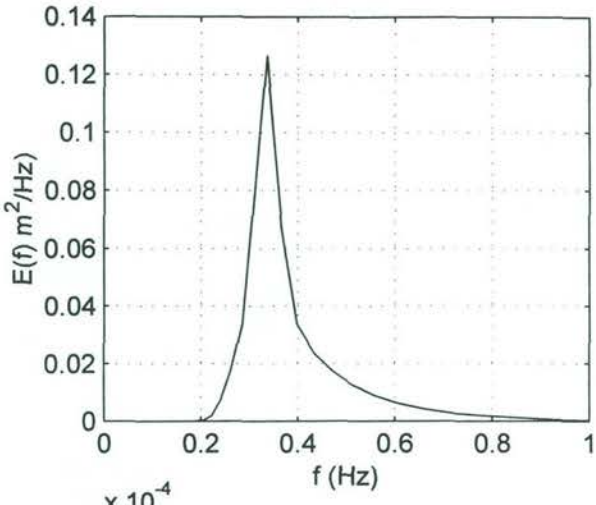

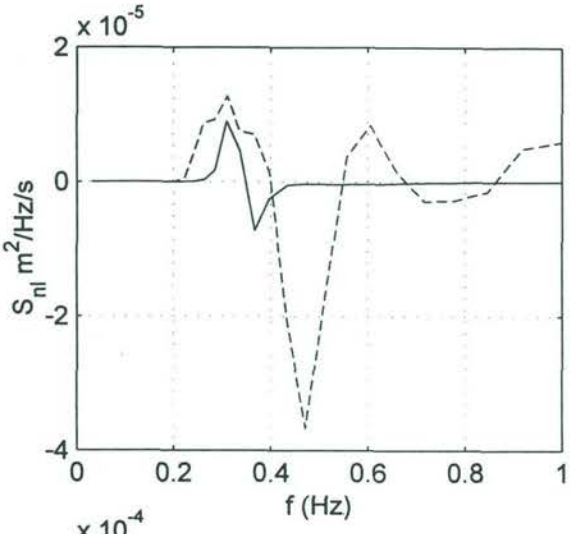

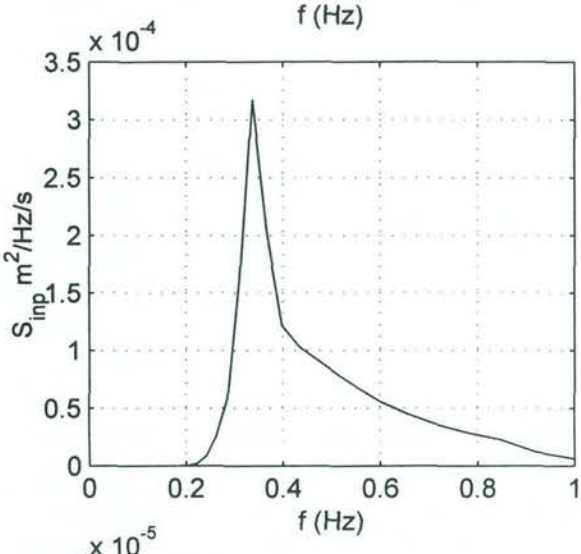

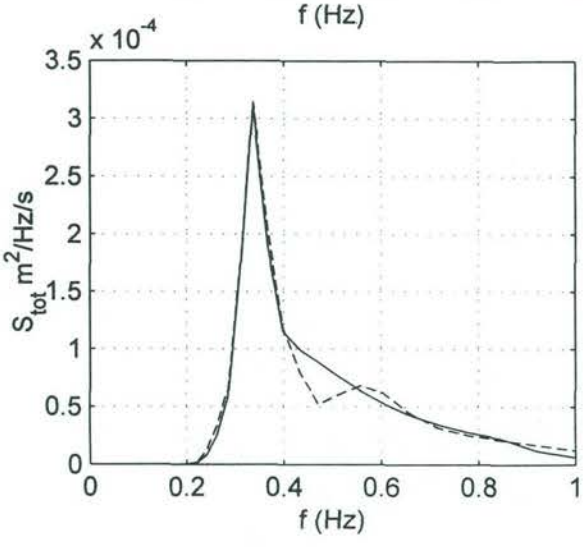

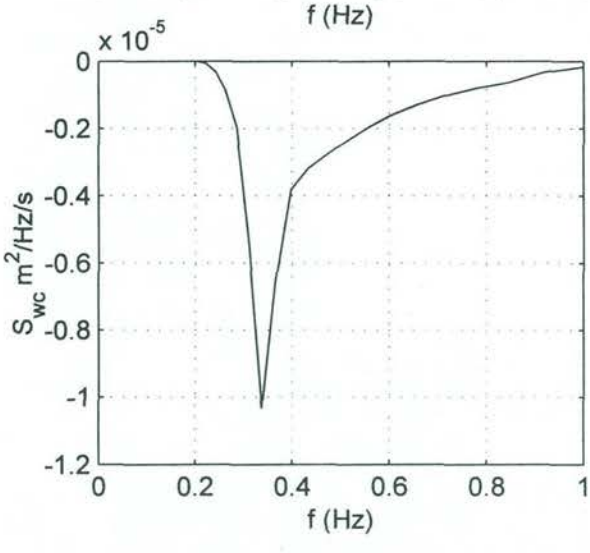

Exact transfer

Discrete Interaction Approximation

Source term balance for a JONSWAP spectrum
T_p = 3 s, H_s = 0.5 m, U_{10} = 20 m/s
Nonlinear interactions computed with DIA and Exact method

Source term investigation SWAN | A162 | Alkyon | Fig 6.2

fig6-3.m

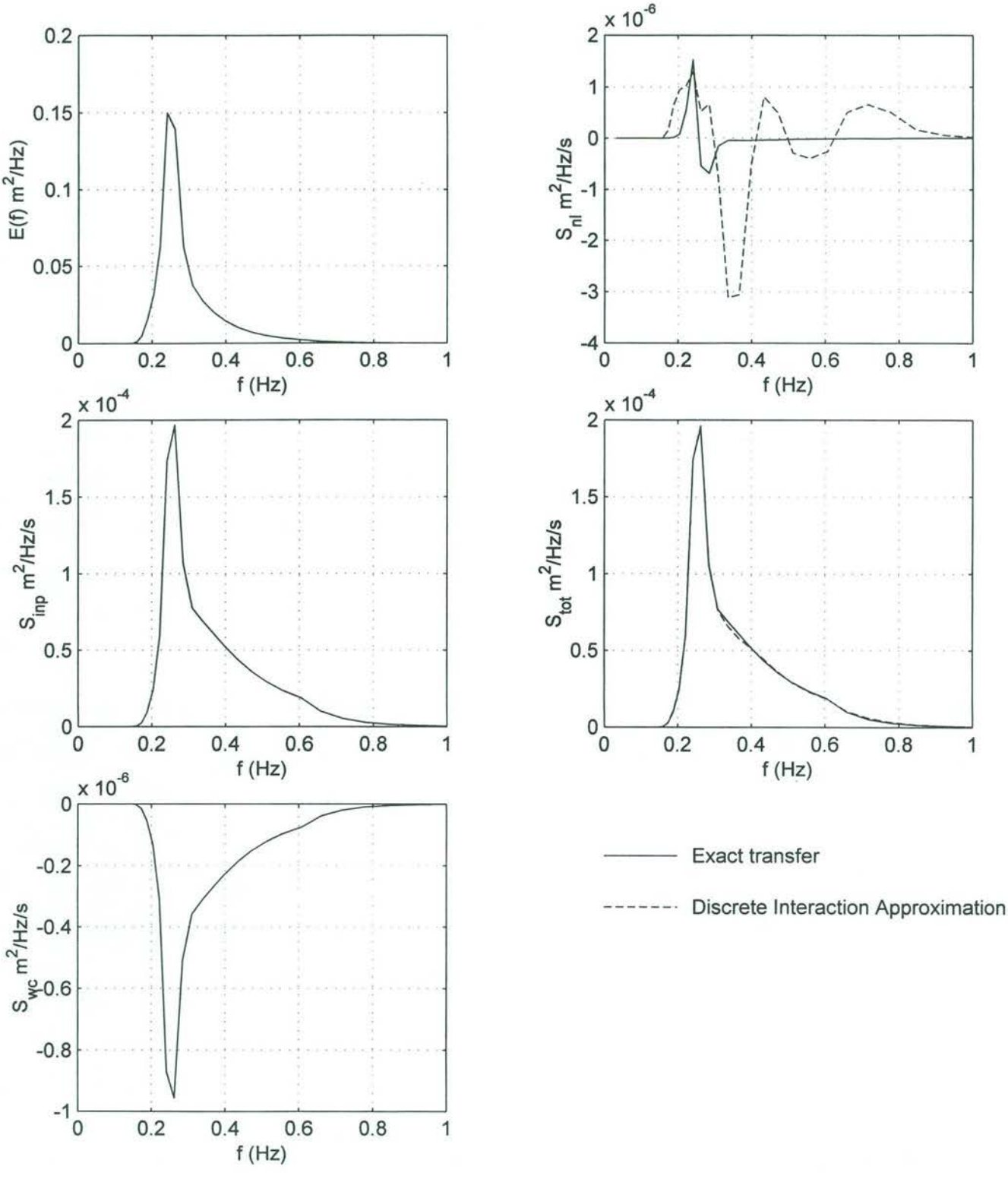

Source term balance for a JONSWAP spectrum
T_p = 4 s, H_s = 0.5 m, U_{10} = 20 m/s
Nonlinear interactions computed with DIA and Exact method

Source term investigation SWAN | A162 | Alkyon | Fig 6.3

fig6-4.m

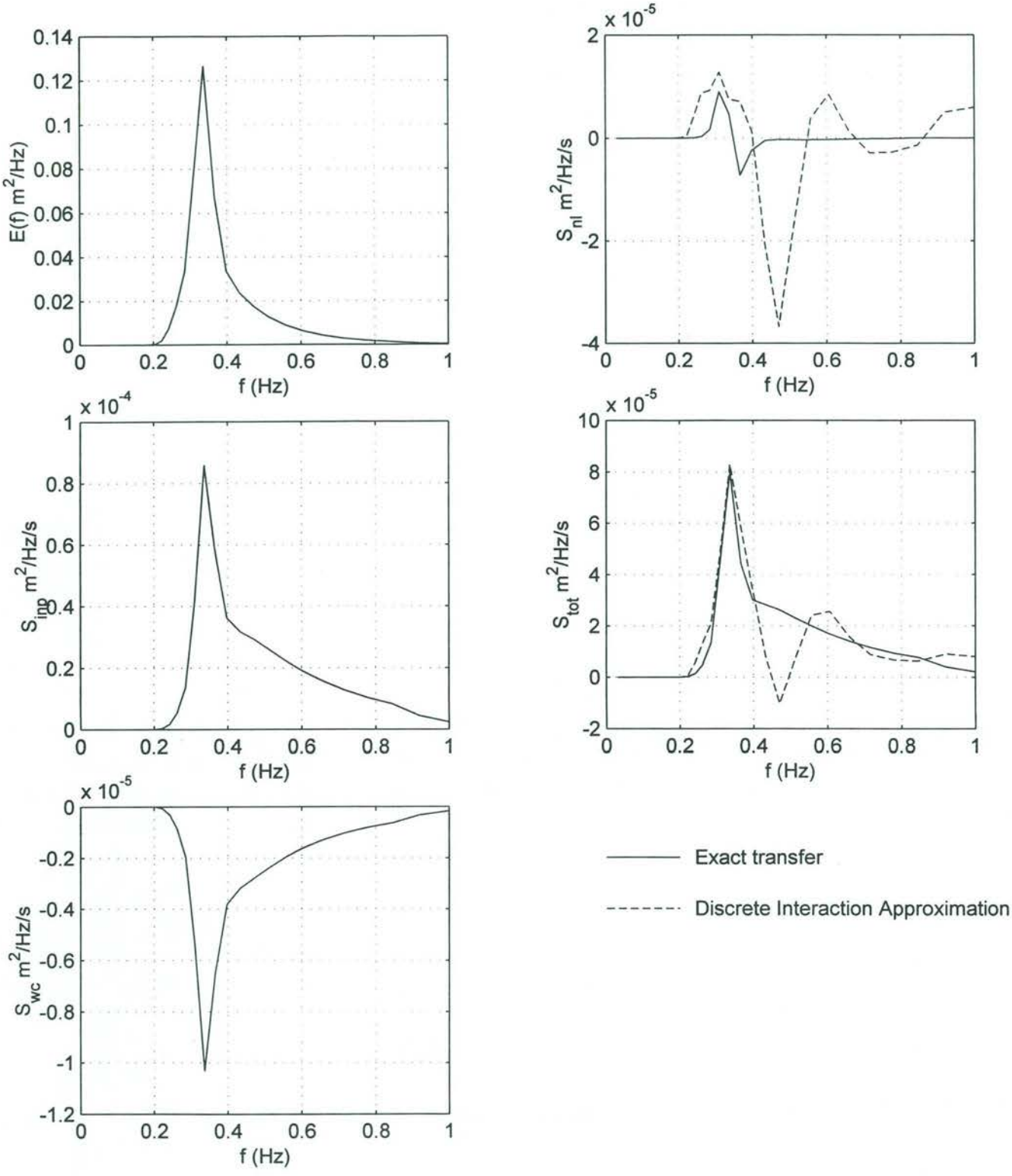

Source term balance for a JONSWAP spectrum
T_p = 3 s, H_s = 0.5 m, U_{10} = 10 m/s
Nonlinear interactions computed with DIA and Exact method

Source term investigation SWAN | A162 | Alkyon | Fig 6.4

fig6-5.m

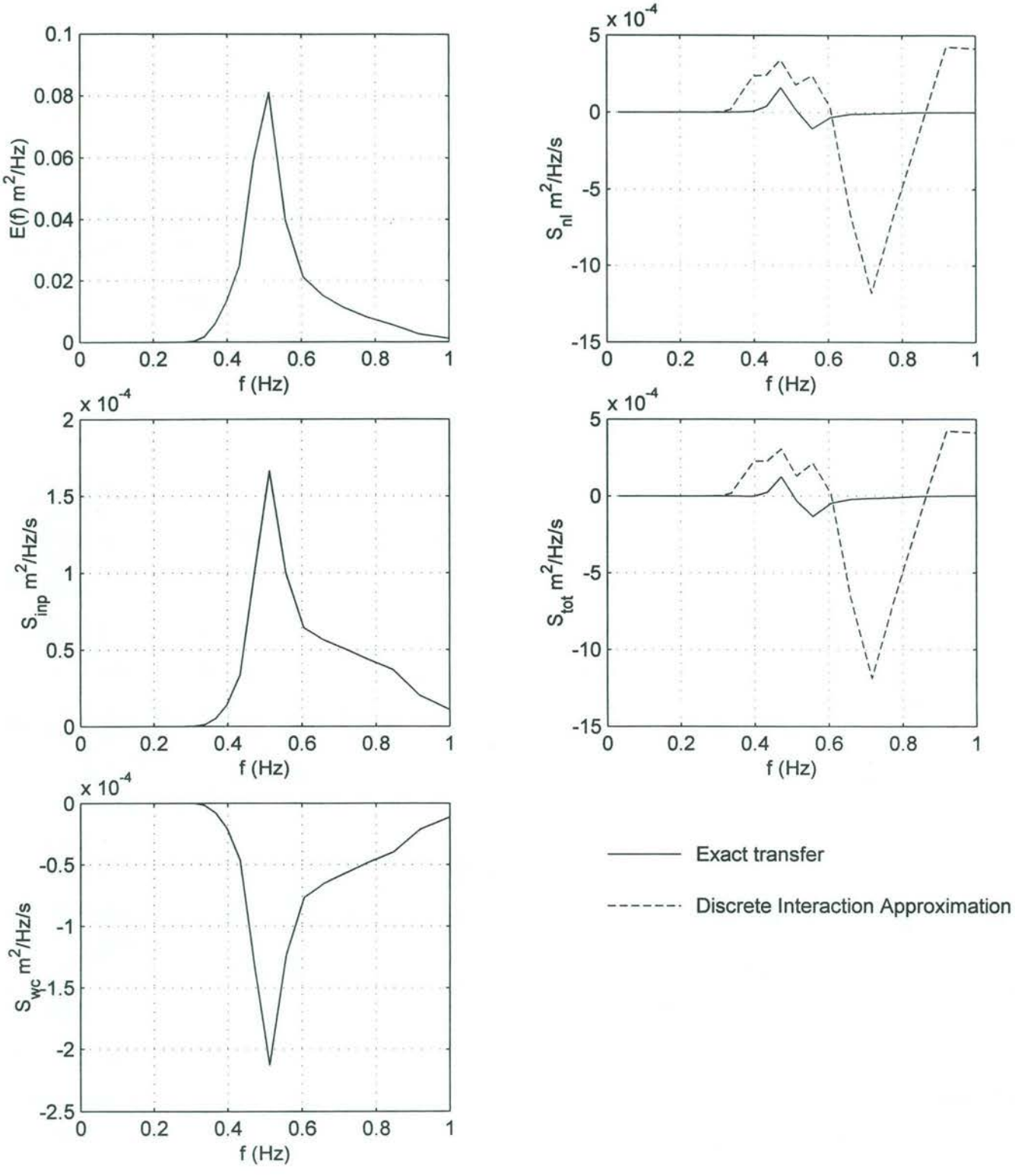

Source term balance for a JONSWAP spectrum
T_p = 2 s, H_s = 0.5 m, U_{10}= 10 m/s, $f_{cut\ off}$=0.8 Hz
Nonlinear interactions computed with DIA and Exact method

Source term investigation SWAN | A162 | Alkyon | Fig 6.5

fig6-6.m

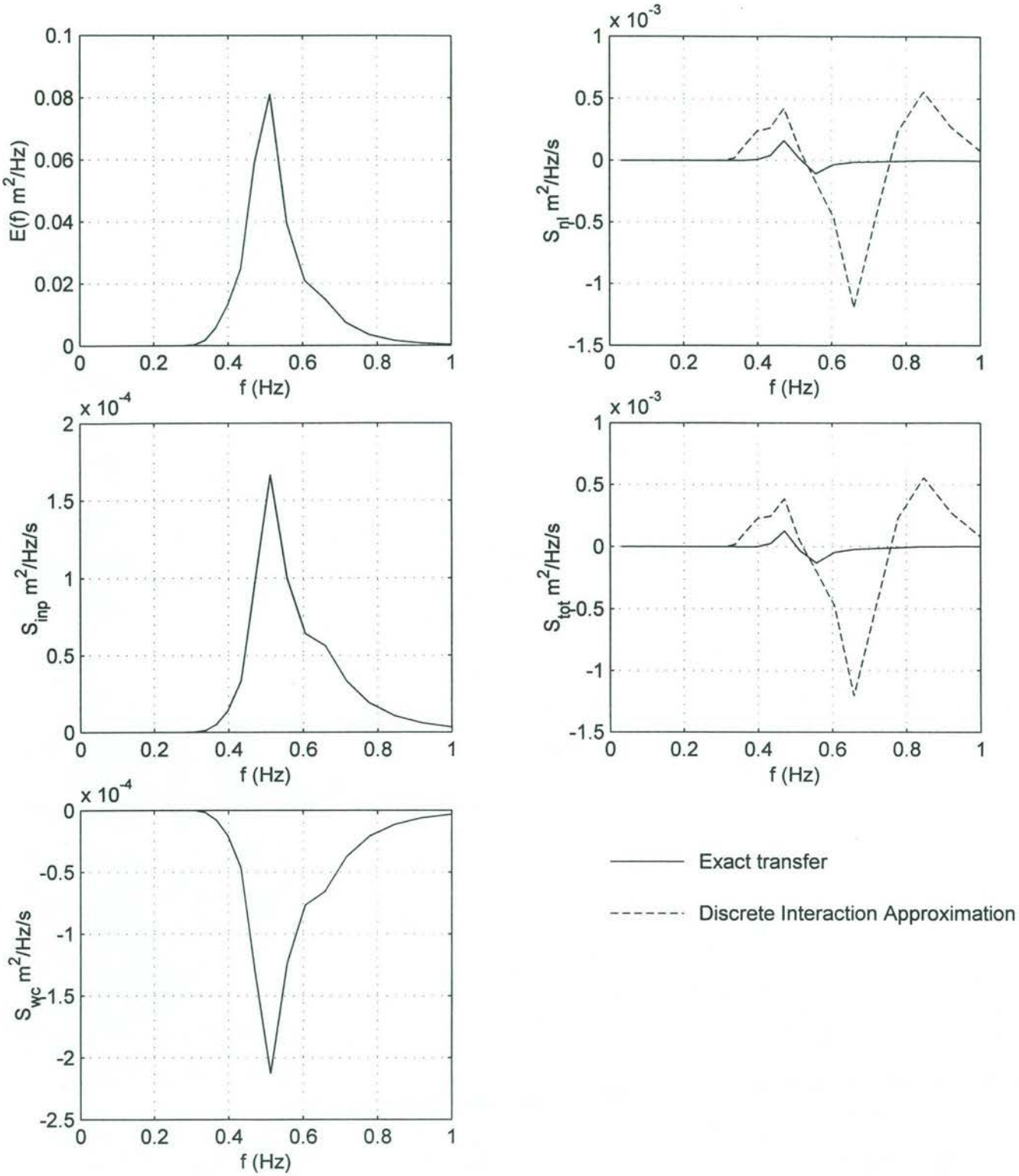

Source term balance for a JONSWAP spectrum
T_p = 2 s, H_s = 0.5 m, U_{10}= 10 m/s, $f_{cut\ off}$=0.6 Hz
Nonlinear interactions computed with DIA and Exact method

Source term investigation SWAN | A162 | Alkyon | Fig 6.6

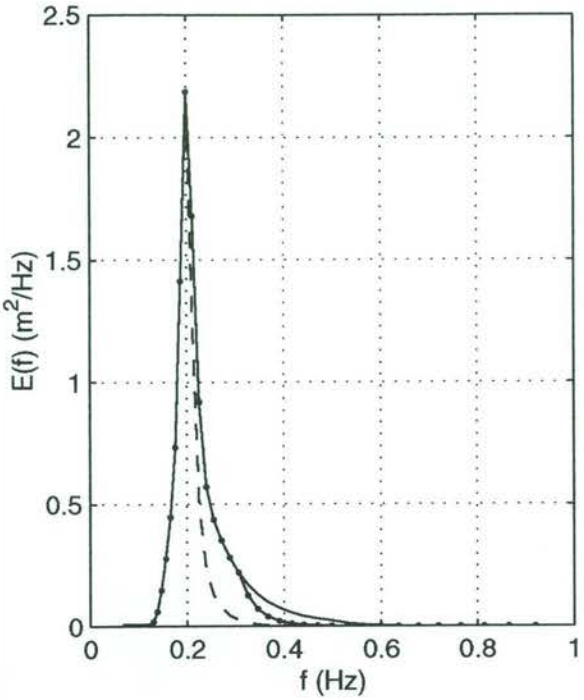

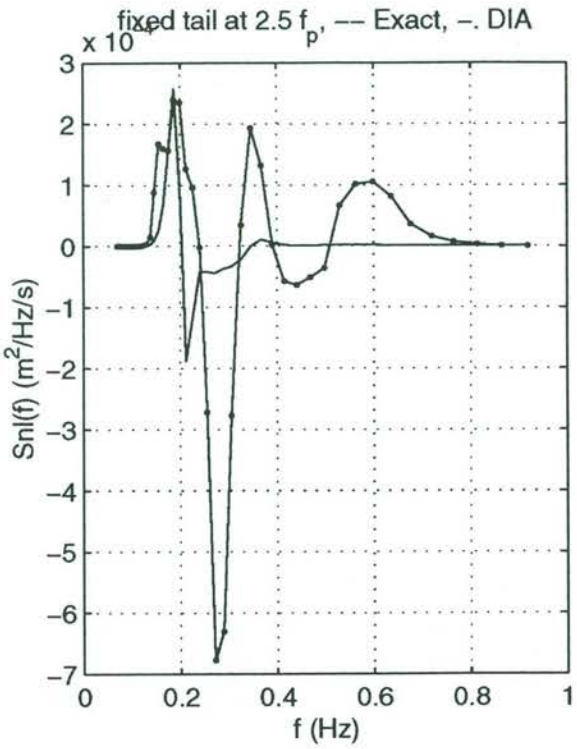

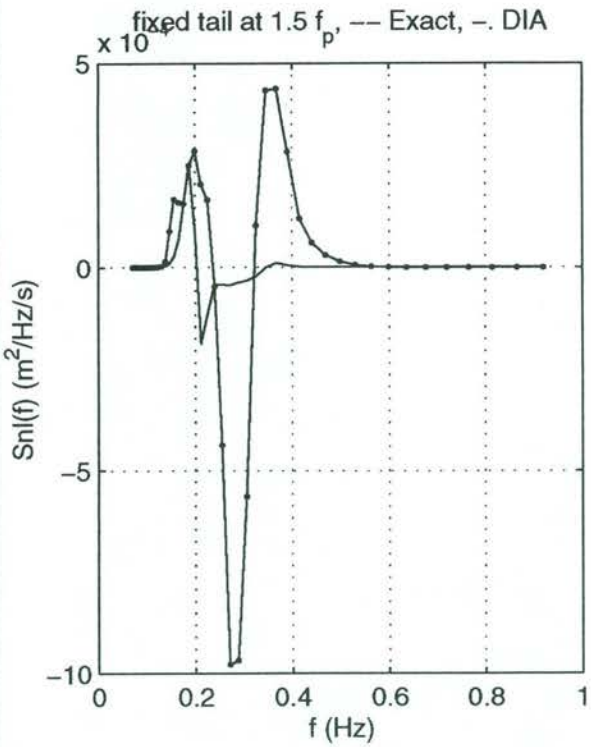

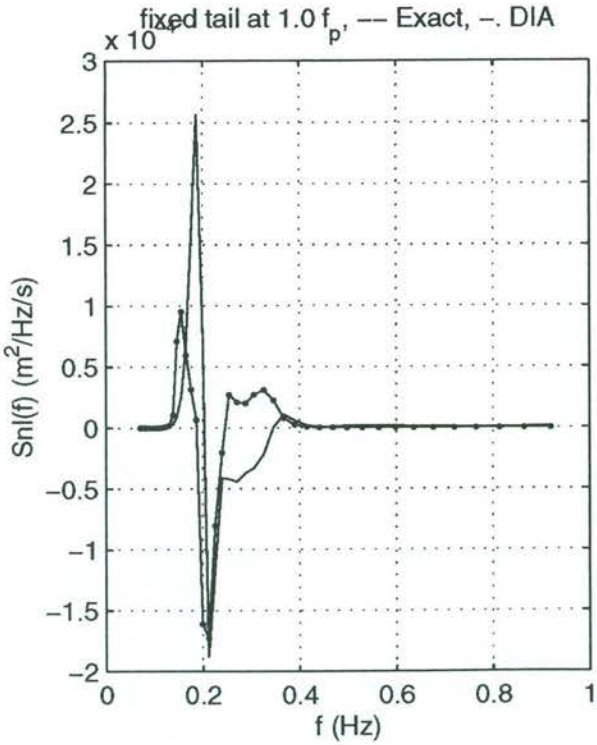

Effect of position of fixed tail on nonlinear interations
JONSWAP spectrum, f_p = 0.2 Hz, Gamma=3.3, tail: f^{-5}

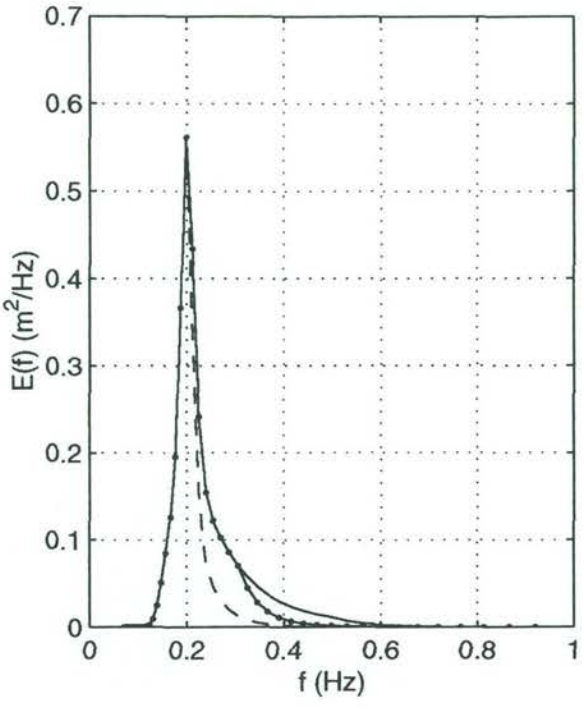

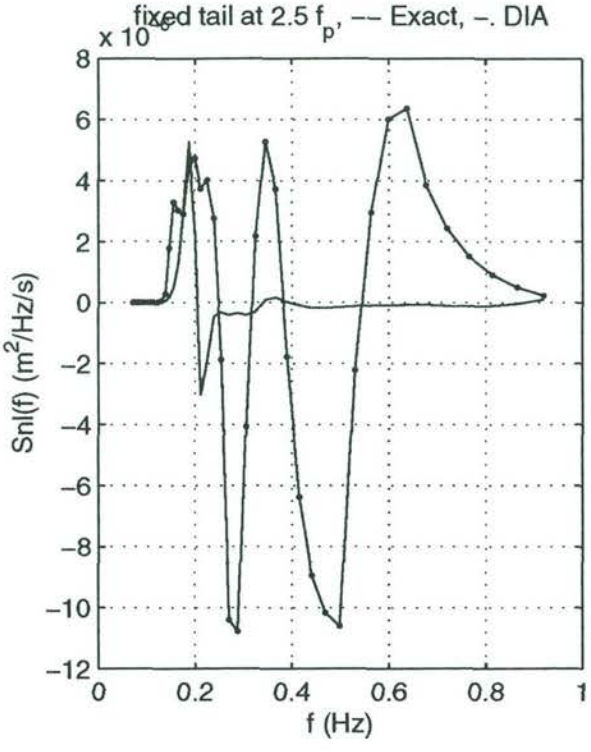

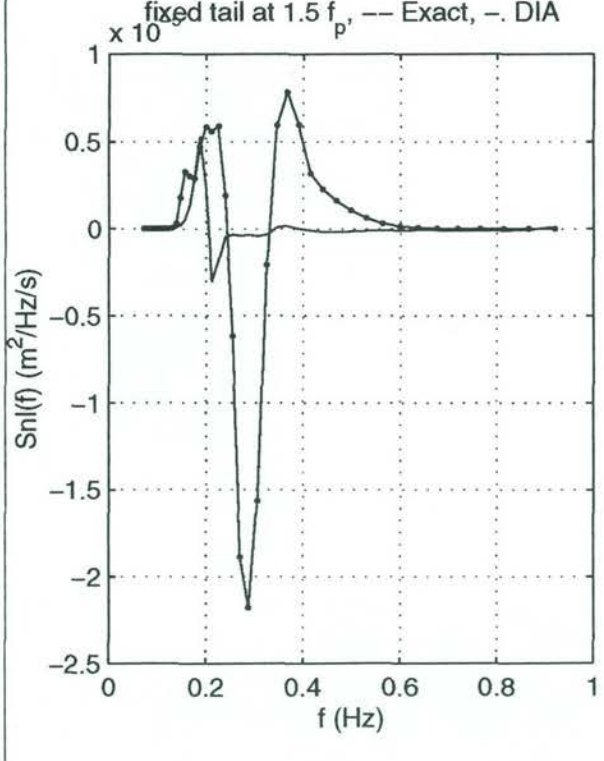

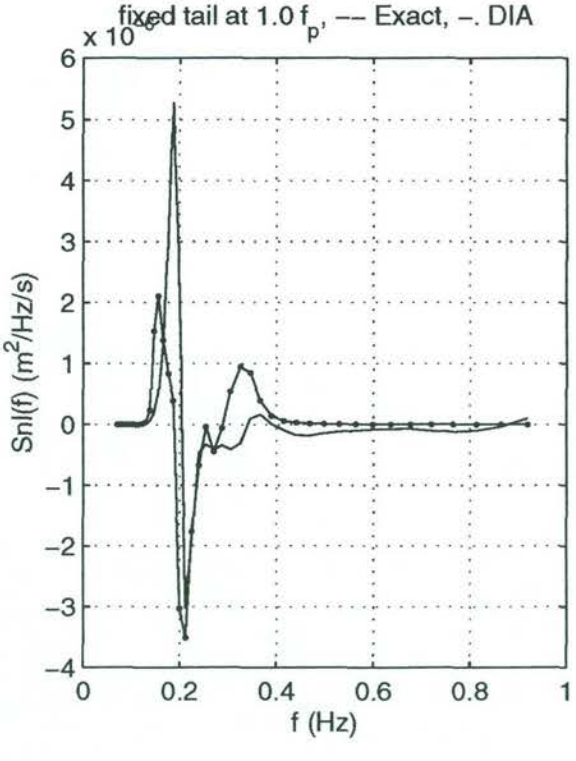

Effect of position of fixed tail on nonlinear interations
JONSWAP spectrum, f_p = 0.2 Hz, Gamma=3.3, tail: f^{-4}

fig7-1.m

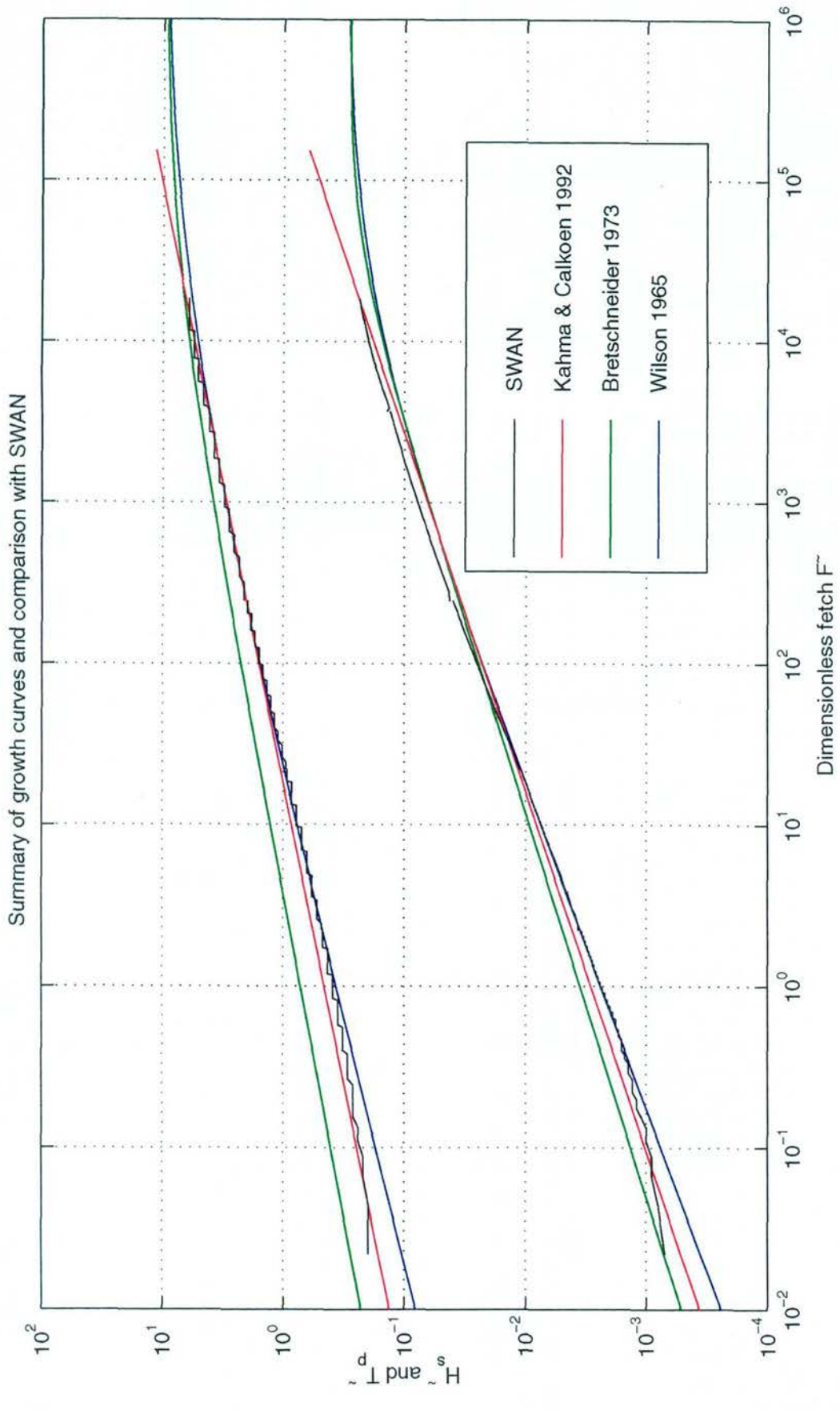

Summary of growth curves for fetch-limited wave growth
and comparison with SWAN computation (black line)
Strict convergence criterion

Source term investigation SWAN | A162 | Alkyon | Fig. 7.1

fig7-2.m

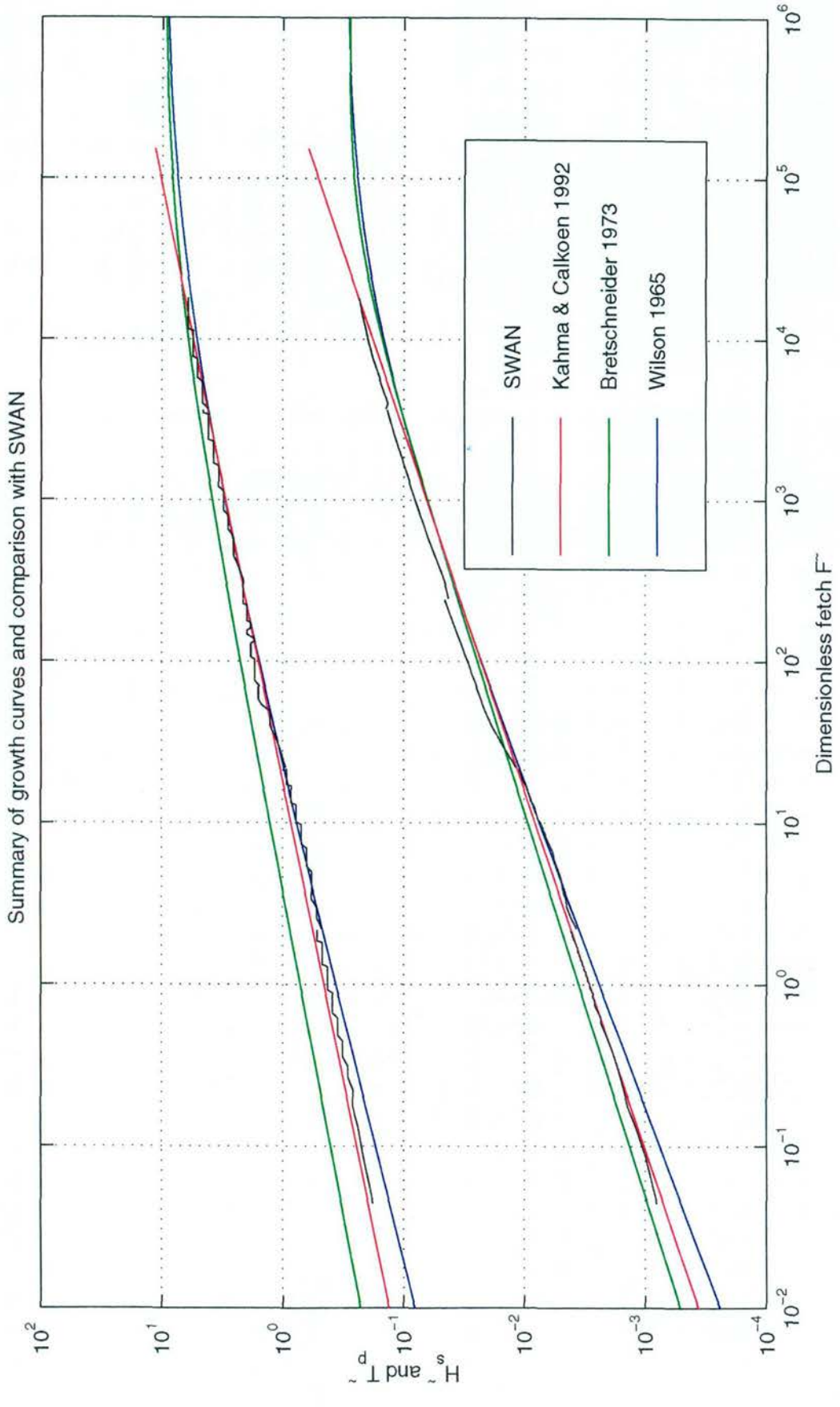

Summary of growth curves for fetch-limited wave growth
and comparison with SWAN computation (black line)
Operational convergence criterion

Source term investigation SWAN	A162	Alkyon	Fig. 7.2

fig7-3.m

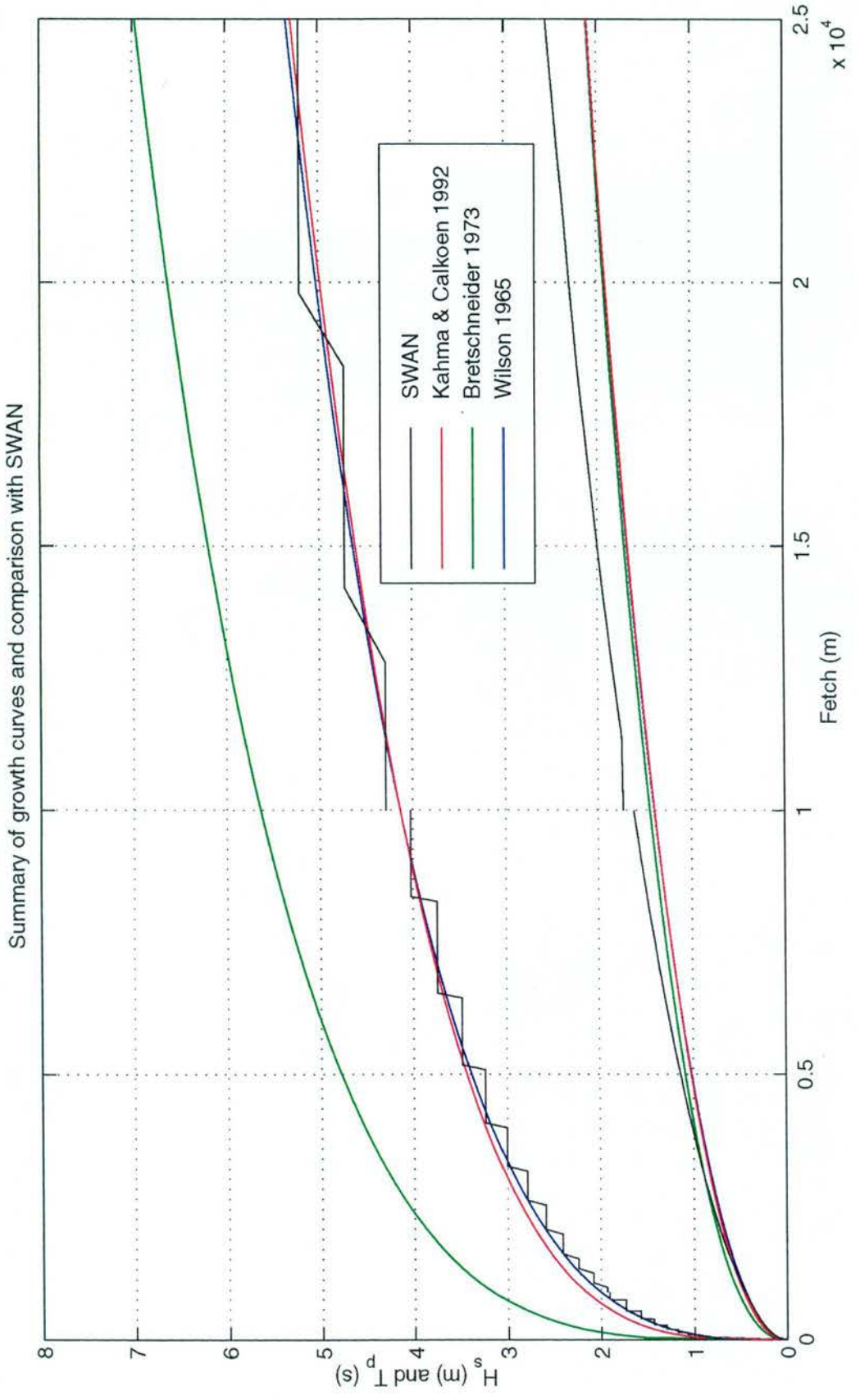

Summary of growth curves for fetch–limited wave growth
and comparison with SWAN computation for a fetch of 25 km
Strict convergence criterion

Source term investigation SWAN | A162 | Alkyon | Fig. 7.3

fig7-4.m

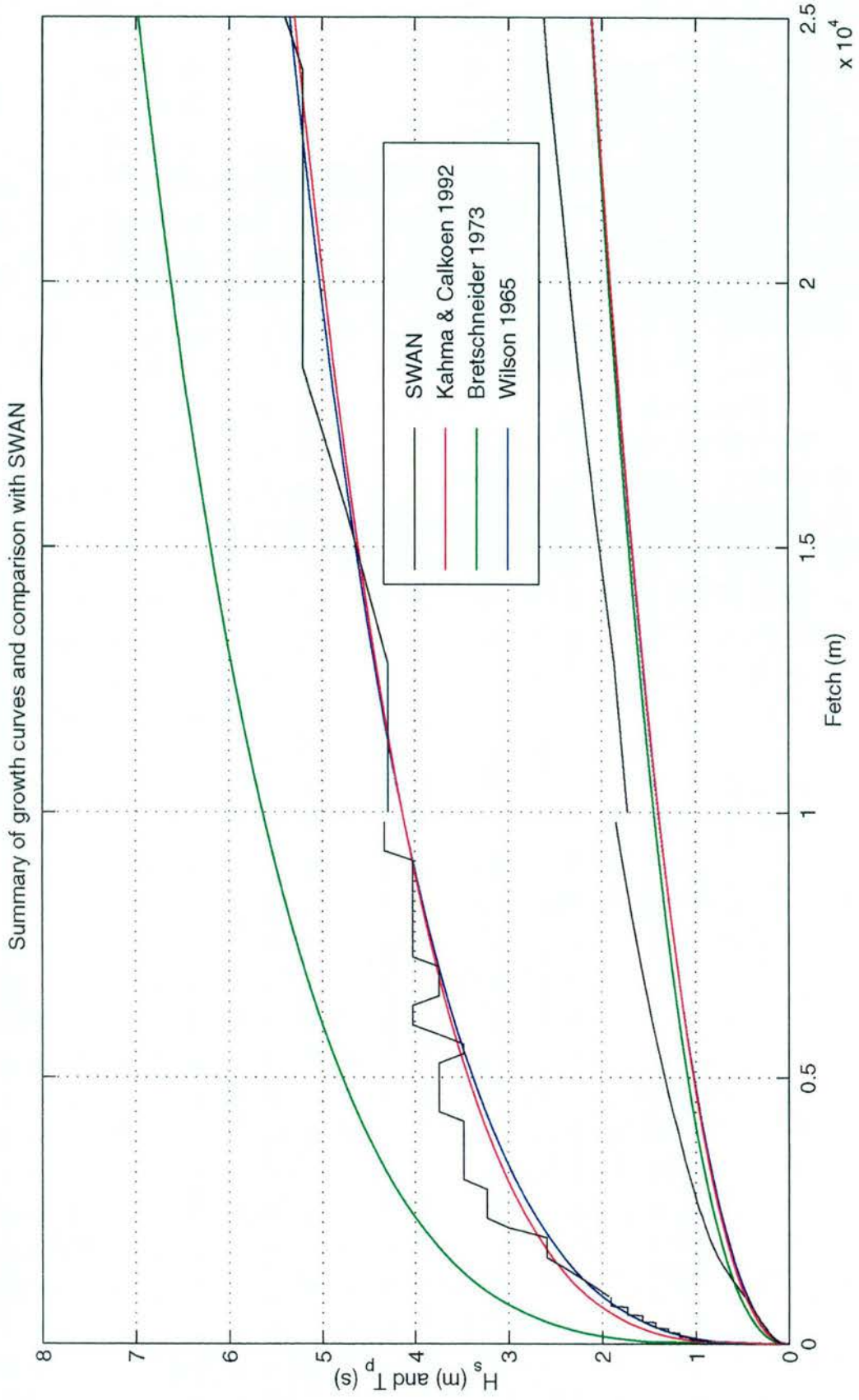

Summary of growth curves for fetch-limited wave growth
and comparison with SWAN computation for a fetch of 25 km
Operational convergence criterion

fig7-5.m

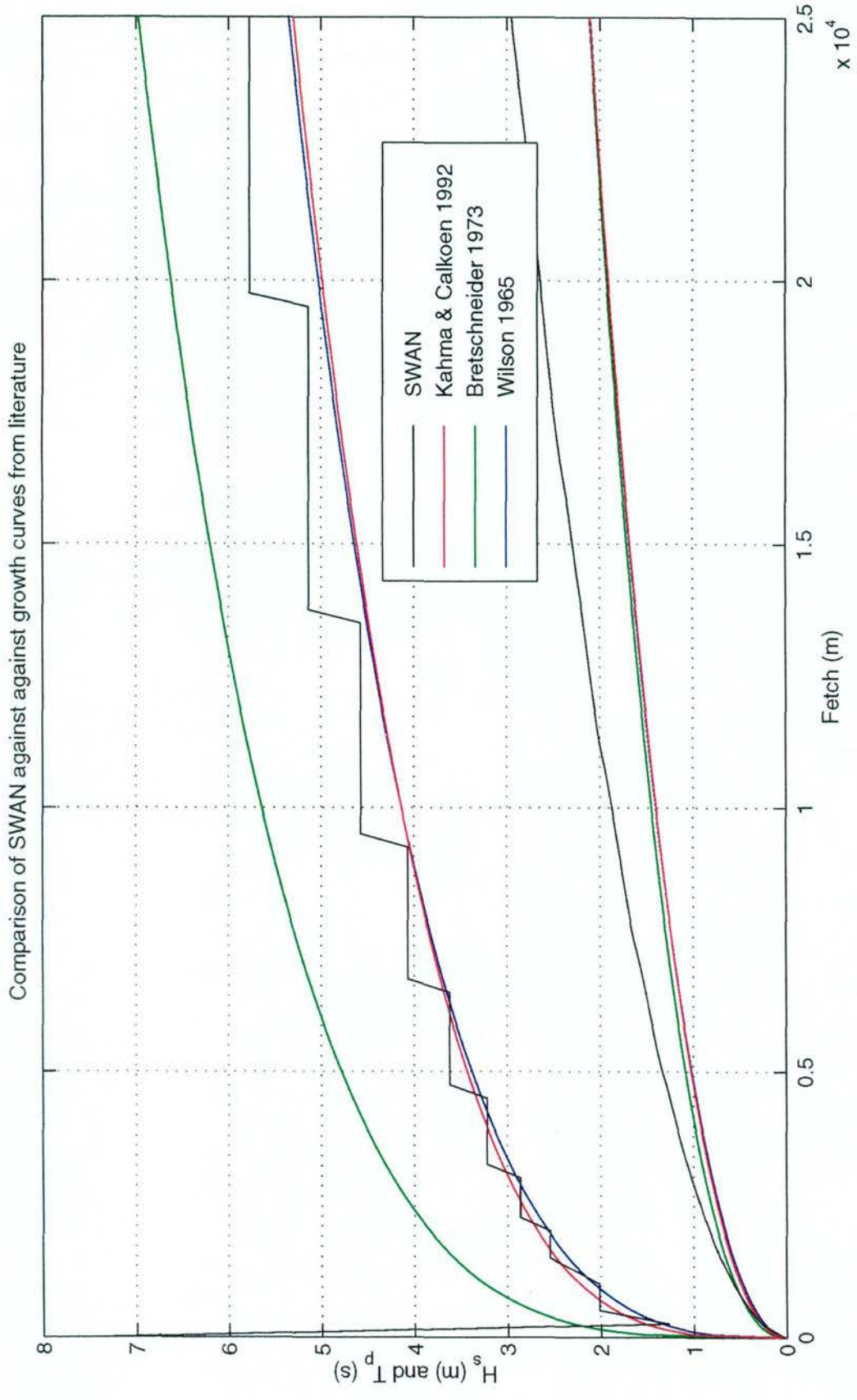

Growth curves for fetch-limited wave growth
and comparison with SWAN computation for a fetch of 25 km
Operational convergence criterion and a grid step of 50 m

Source term investigation SWAN | A162 | Alkyon | Fig. 7.5

fig7-6.m

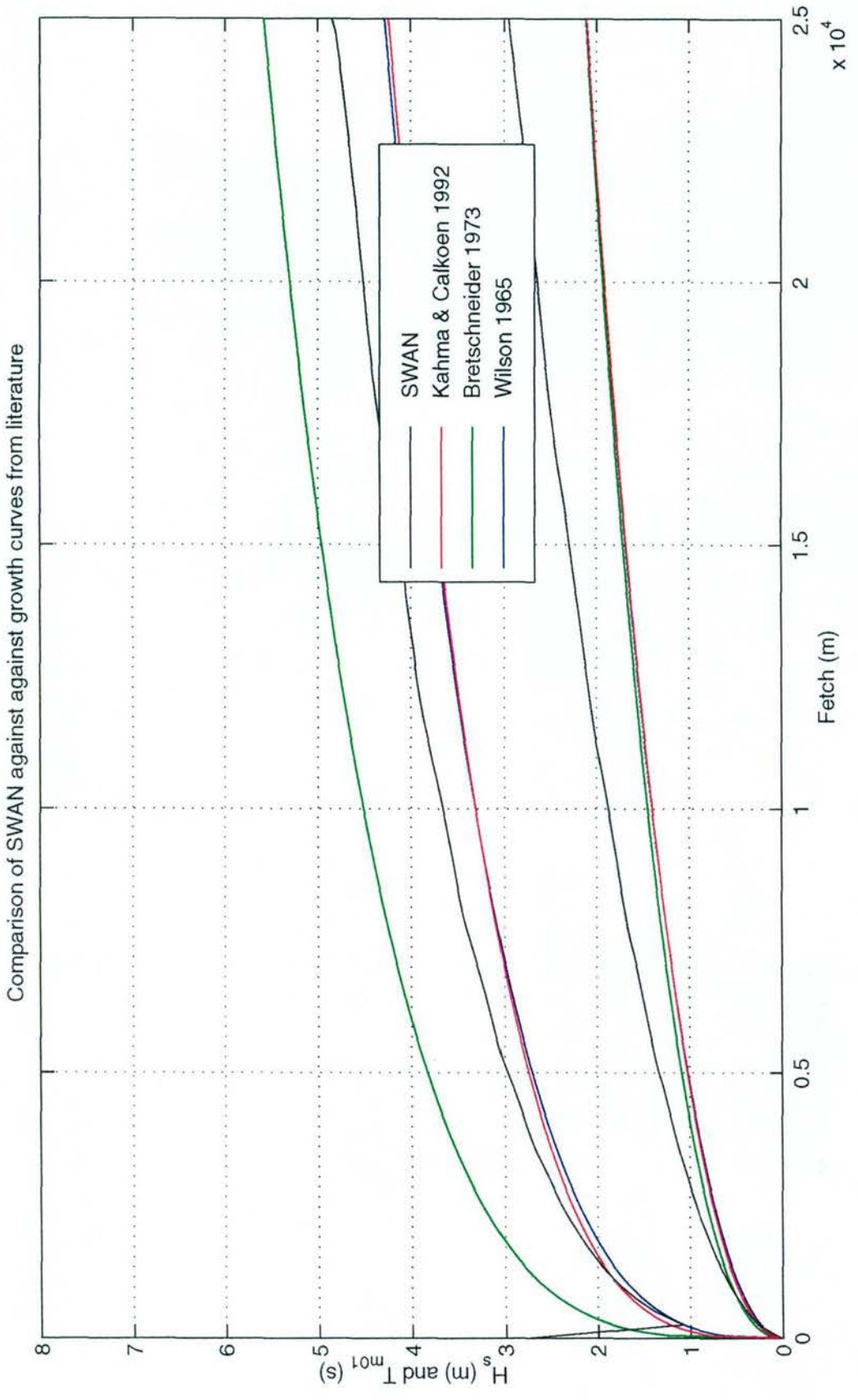

Growth curves for fetch-limited wave growth, H_s and T_{m01}
and comparison with SWAN computation for a fetch of 25 km
Operational convergence criterion and a grid step of 50 m

Source term investigation SWAN | A162 | Alkyon | Fig. 7.6

fig7-7.m

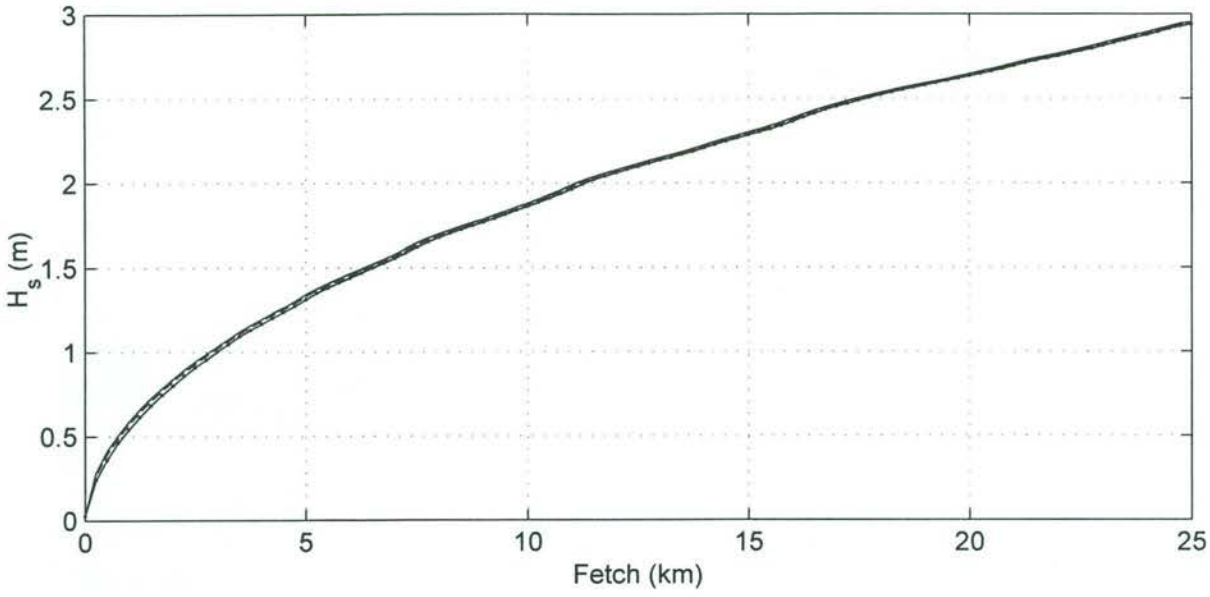

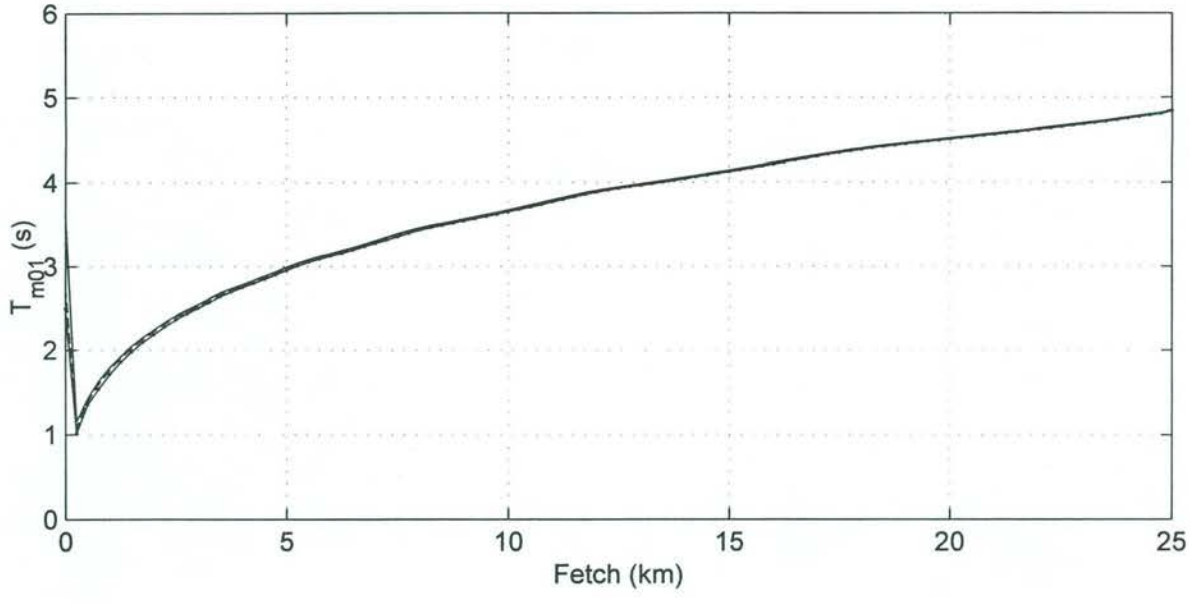

Step size 100 m

Step size 50 m

Step size 20 m

Sensitivity of SWAN with respect to step size
SWAN comparison for a fetch of 25 km and a wind speed of 20 m/s
Step size of 20 m, 50 m and 100 m

Source term investigation SWAN	A162	Alkyon	Fig. 7.7

fig7-8.m

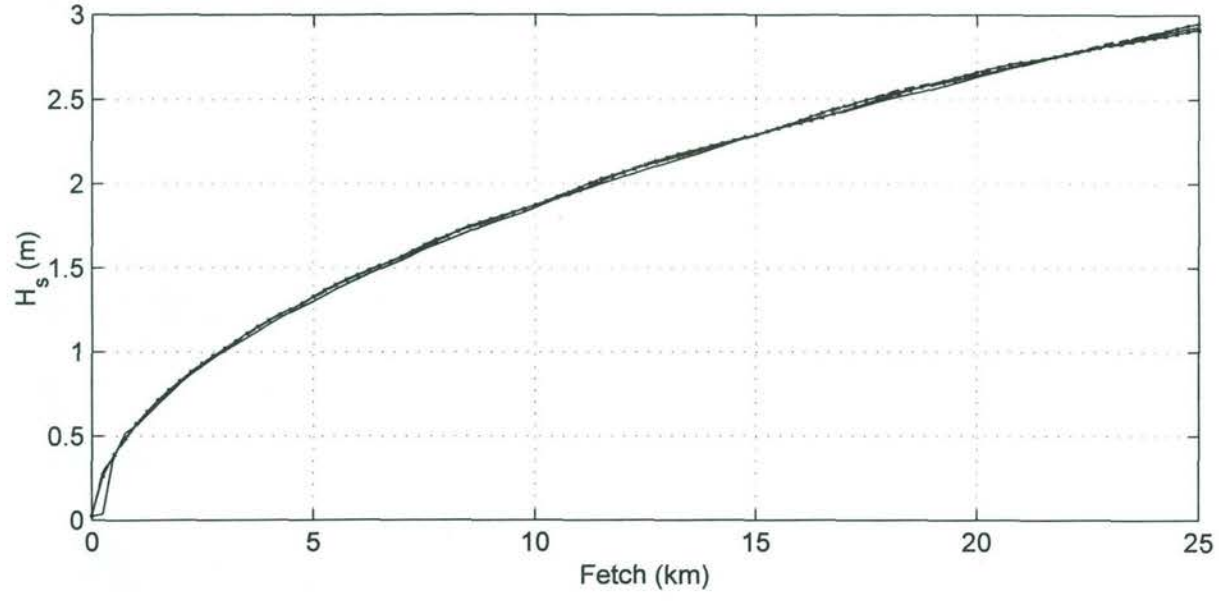

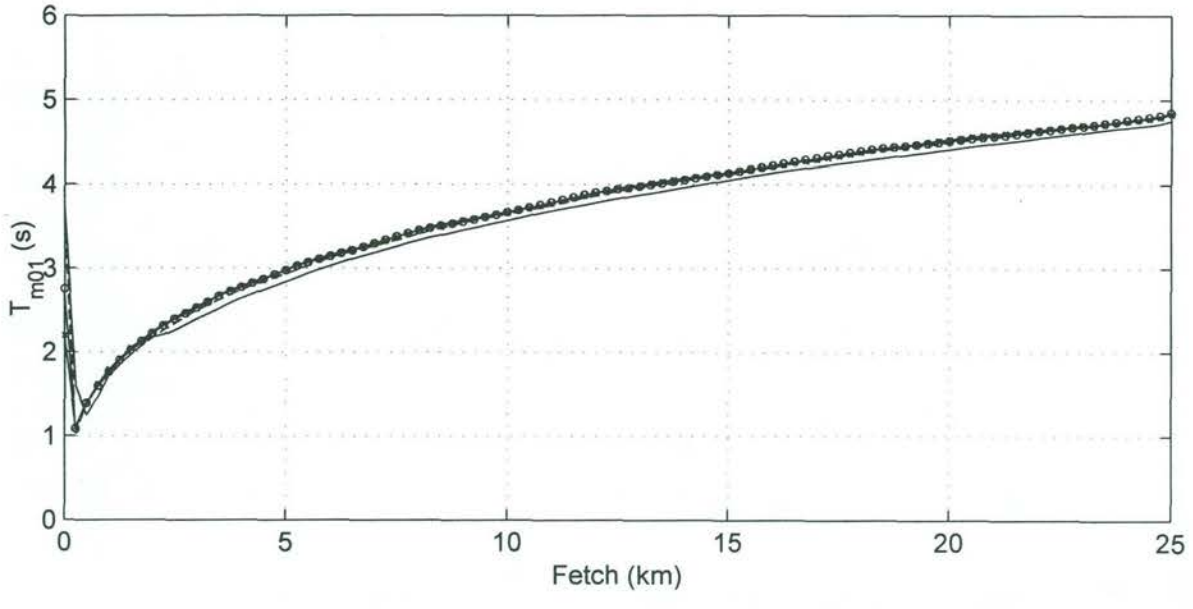

Cut-off frequency 1.2 Hz
Cut-off frequency 1.0 Hz
Cut-off frequency 0.8 Hz
Cut-off frequency 0.6 Hz

Sensitivity of SWAN with respect to cut-off frequency
SWAN comparison for a fetch of 25 km and a wind speed of 20 m/s
Cut-off frequencies: 0.6 0.8 1.0 and 1.2

fig7-9.m

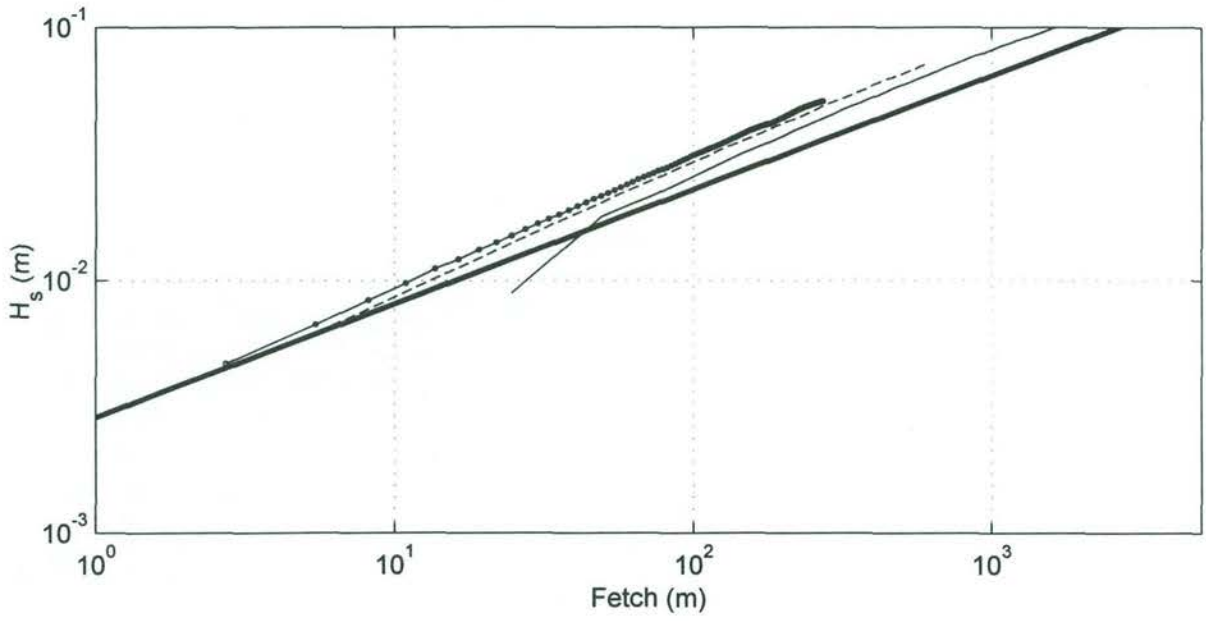

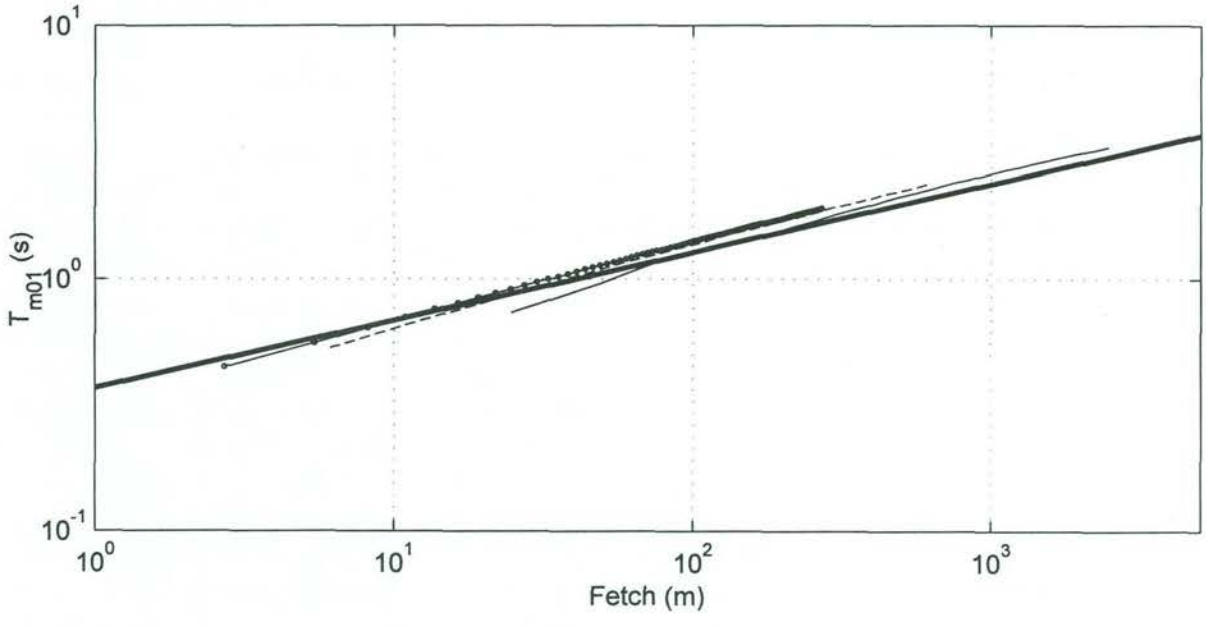

Kahma and Calkoen
Wind speed 30 m/s
Wind speed 20 m/s
Wind speed 10 m/s

Sensitivity of SWAN with respect to wind speed
Fetch of 25 km and wind speeds of 10, 20 and 30 m/s
Non-dimensionalisation with wind speed U_{10} (Kahma & Calkoen)

Source term investigation SWAN | A162 | Alkyon | Fig. 7.9

fig7-10.m

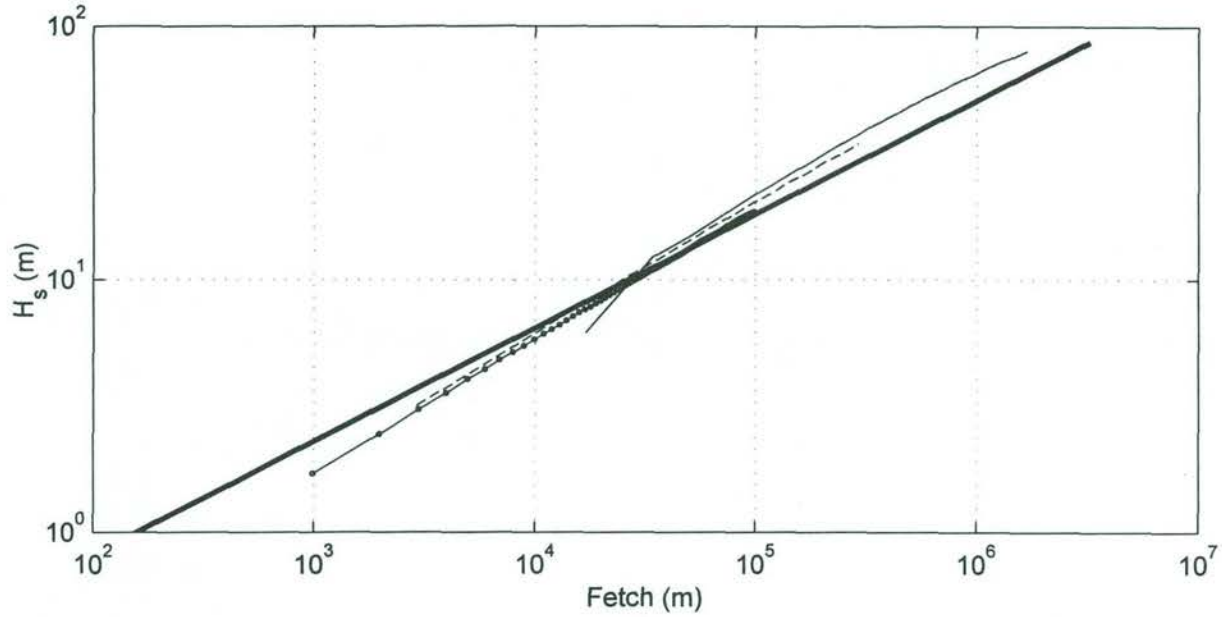

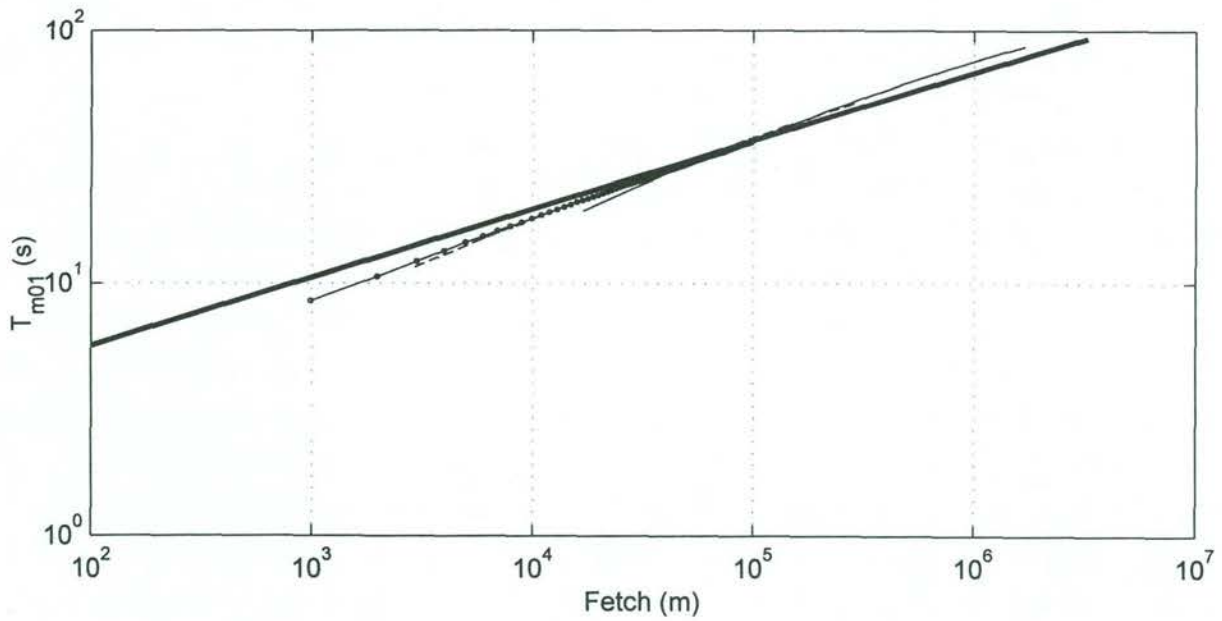

Kahma and Calkoen
Wind speed 30 m/s
Wind speed 20 m/s
Wind speed 10 m/s

Sensitivity of SWAN with respect to wind speed
Fetch of 25 km and wind speeds of 10, 20 and 30 m/s
Non-dimensionalisation with the friction velocity u_* (Kahma and Calkoen)

Source term investigation SWAN	A162	Alkyon	Fig. 7.10

fig7-11.m

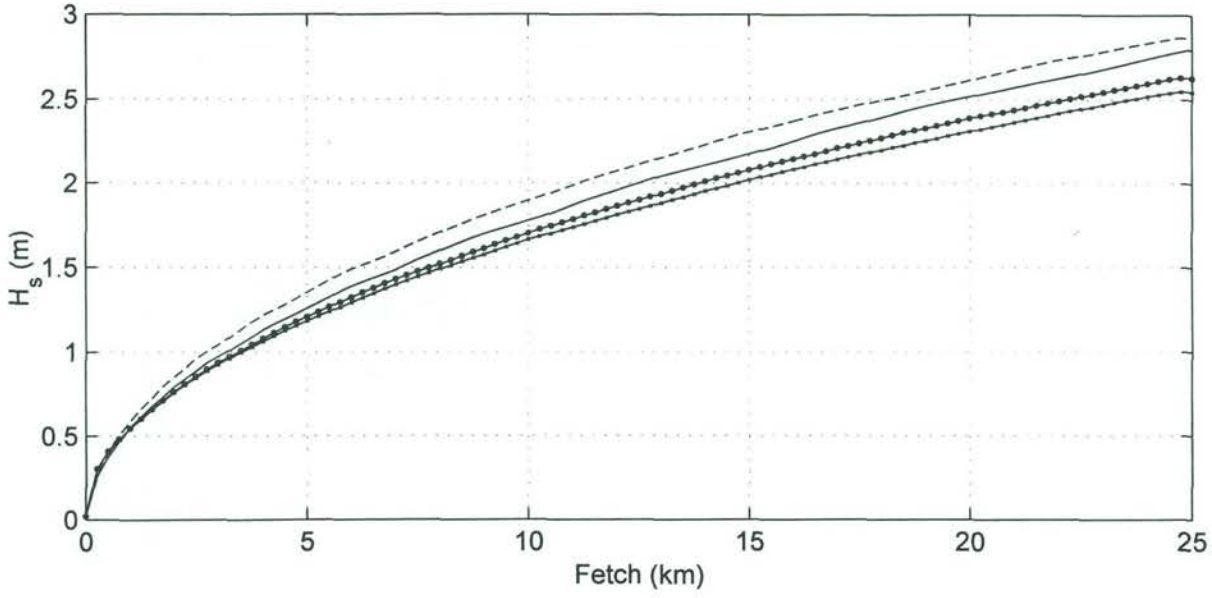

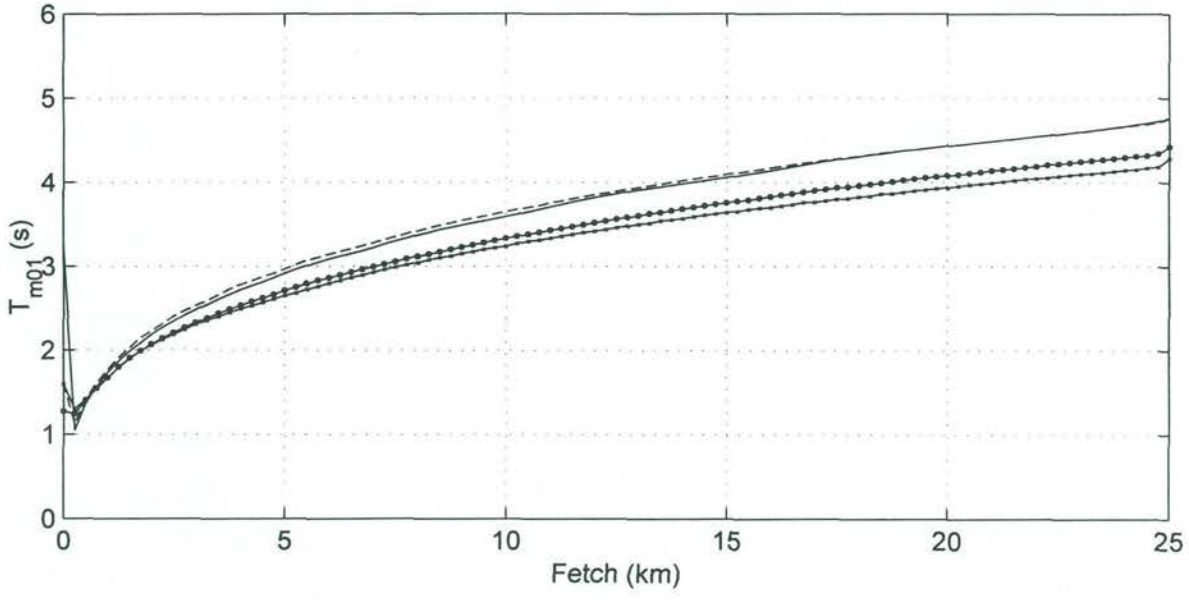

Number of iterations 60
Number of iterations 20
Number of iterations 10
Number of iterations 5

Sensitivity of SWAN with respect to number of iterations
SWAN comparison for a fetch of 25 km and a wind speed of 20 m/s
Number of iterations 5, 20, 40 and 60

Source term investigation SWAN | A162 | Alkyon | Fig. 7.11

FIGtom.m

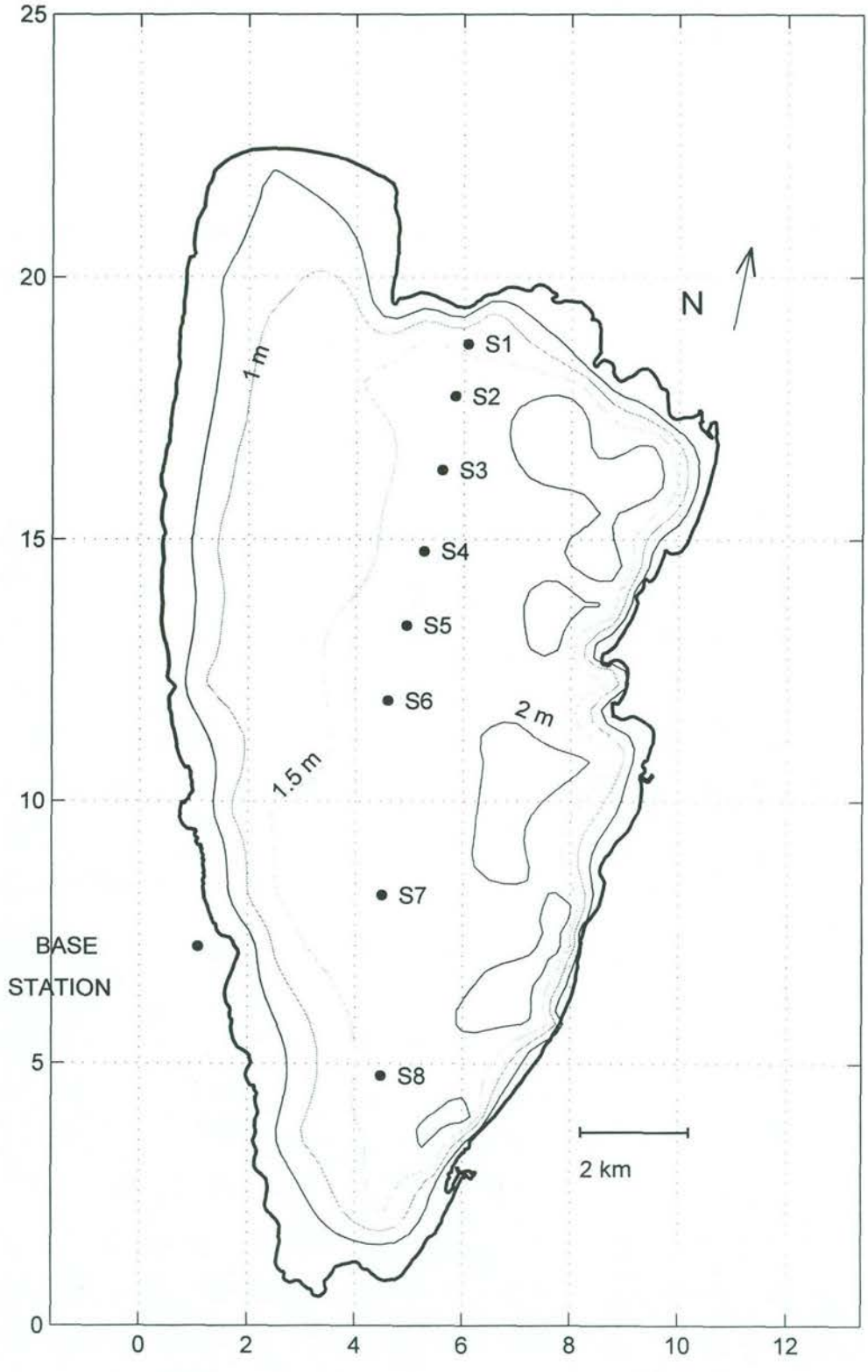

Bottom topography of Lake George
and locations measurements poles

Source term investigation SWAN | A162 | Alkyon | Fig. 8.1

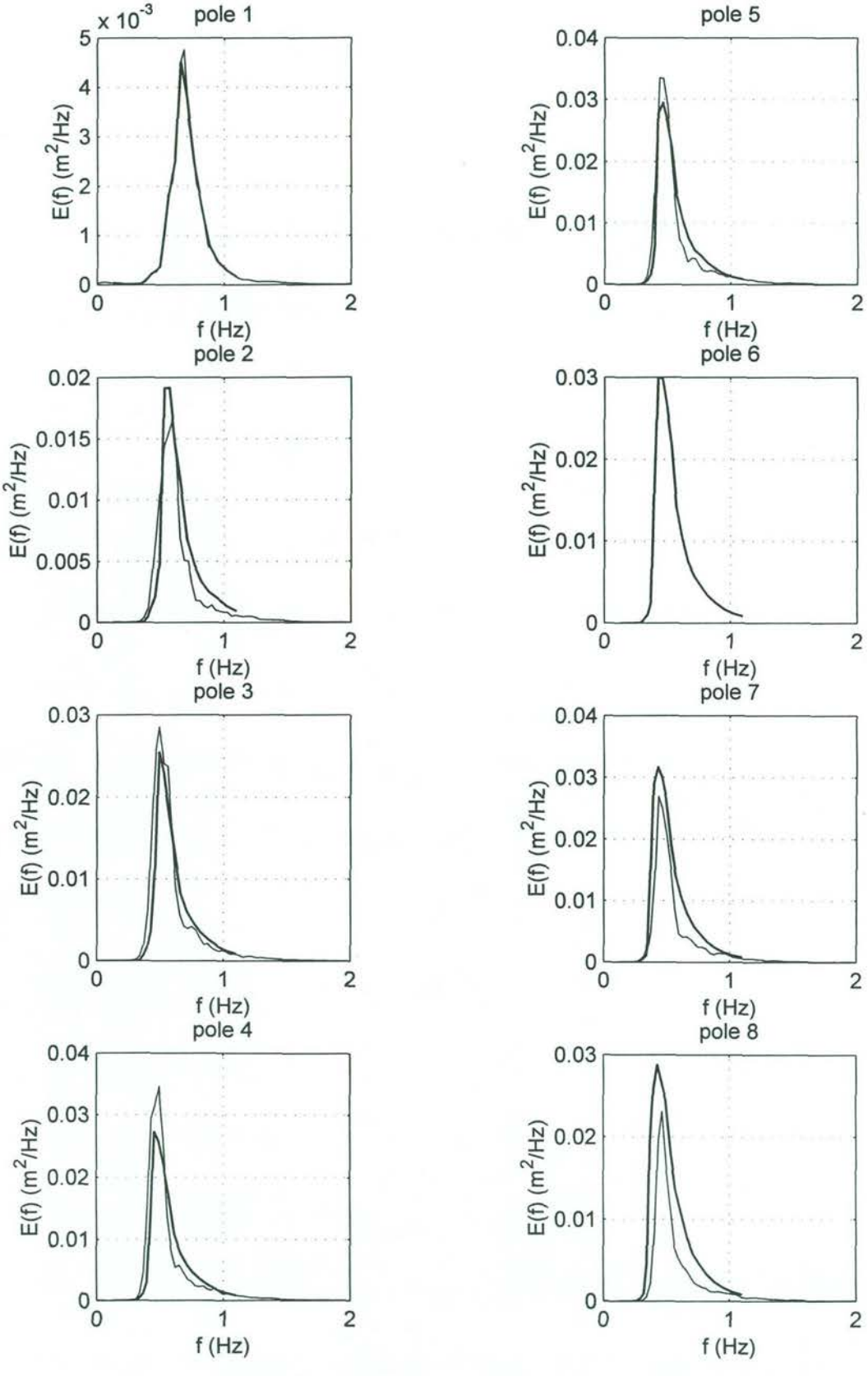

Comparison of observed (thin line) and computed (thick line) spectral development in Lake George Case 4: Date and hour 920512 12:00		Case 4	SWAN
		Lake George	
Source term investigation SWAN	A162	Alkyon	Fig. 8.2

ftab

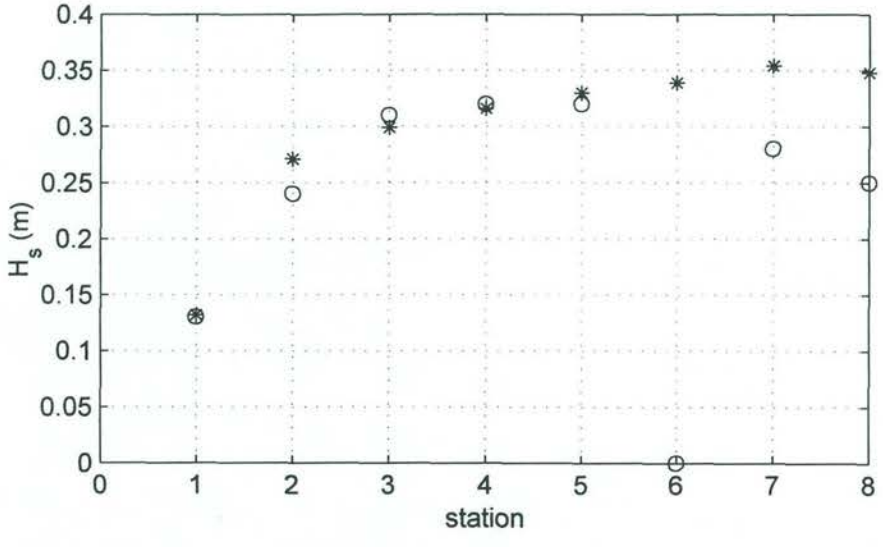

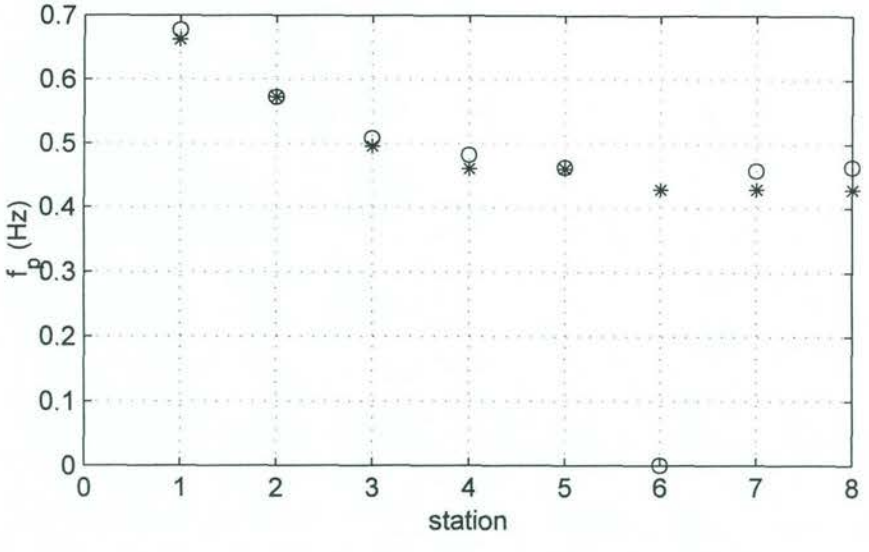

Comparison of significant wave height an peak period as observed (o) and computed (*) with SWAN Date and hour: 920512 12:00		Case 4	SWAN
		Lake George	
Source term investigation SWAN	A162	Alkyon	Fig. 8.3

figscat2

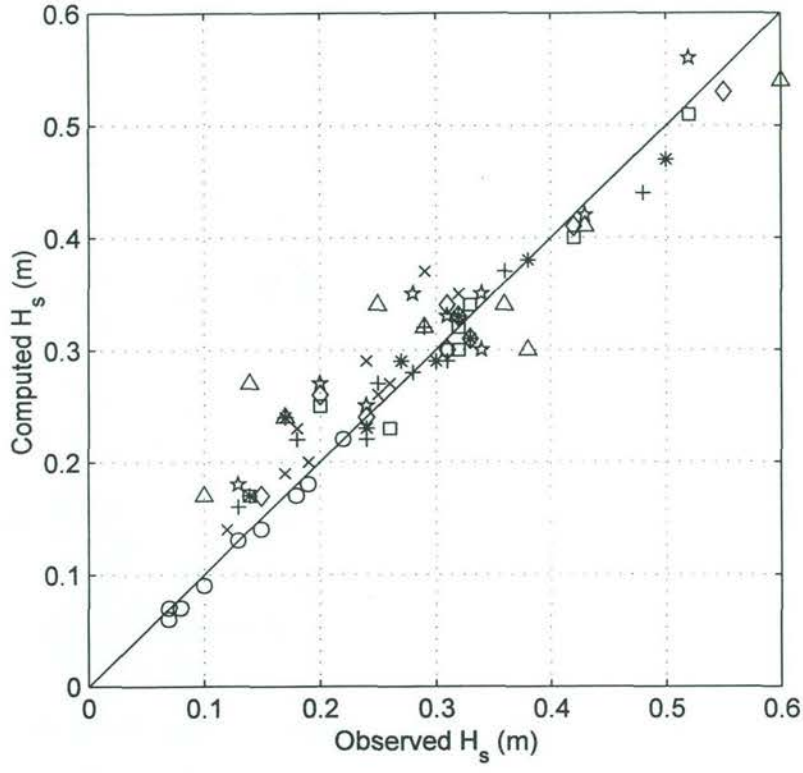

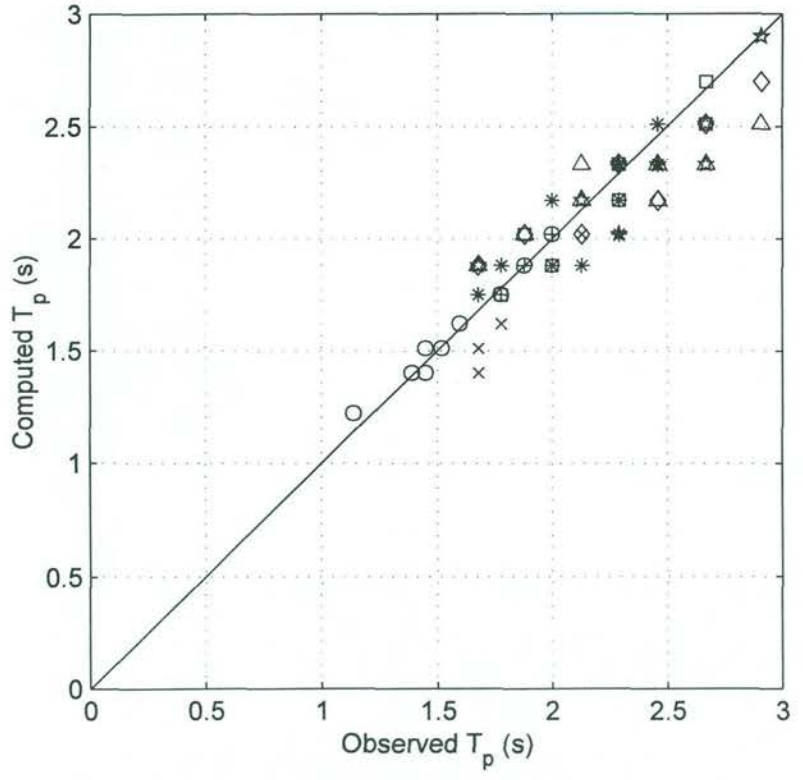

Comparison of observed and computed wave conditions in Lake George Comparison of significant wave height H_s and peak period T_p	SWAN	
	Lake George	
Source term investigation SWAN	A162	Alkyon Fig. 8.4

figscat2

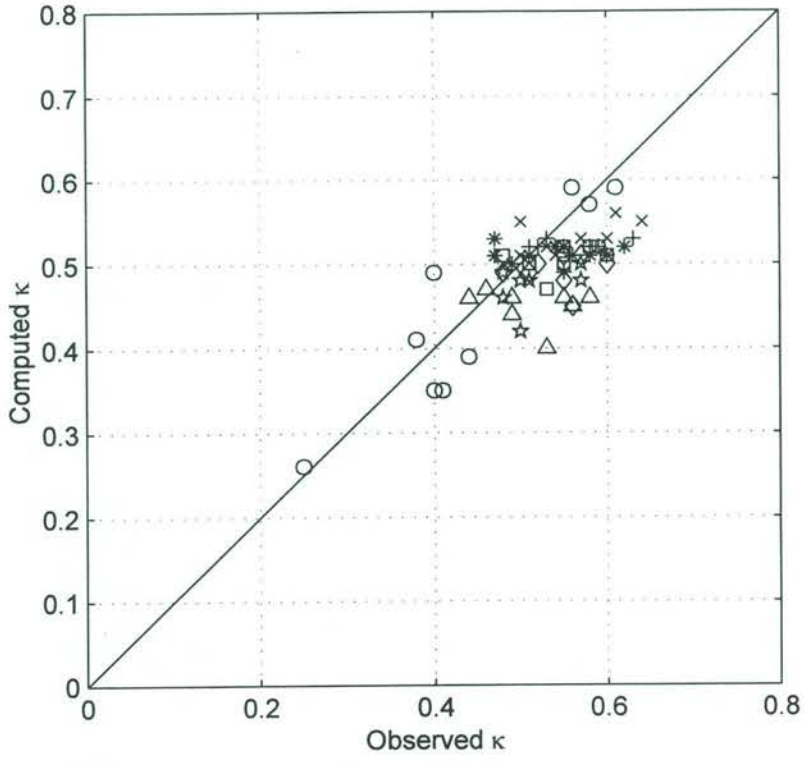

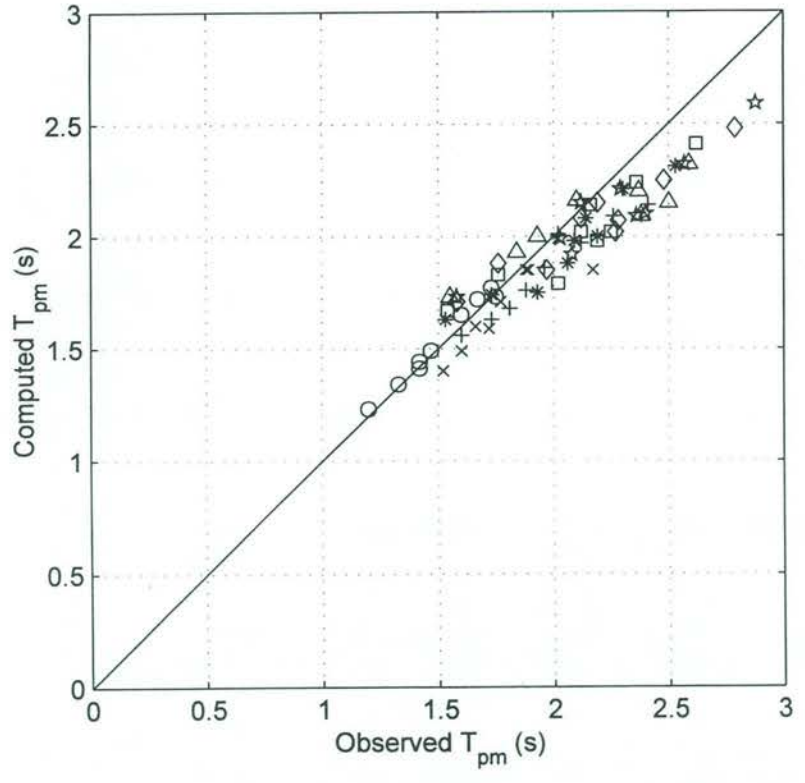

○ Station 1

× Station 2

\+ Station 3

✳ Station 4

□ Station 5

◇ Station 6

☆ Station 7

△ Station 8

Comparison of observed and computed wave conditions in Lake George Comparison of spectral narrowness κ and block peak period T_{pm}	SWAN	
	Lake George	
Source term investigation SWAN	A162	Alkyon Fig. 8.5

figscat2

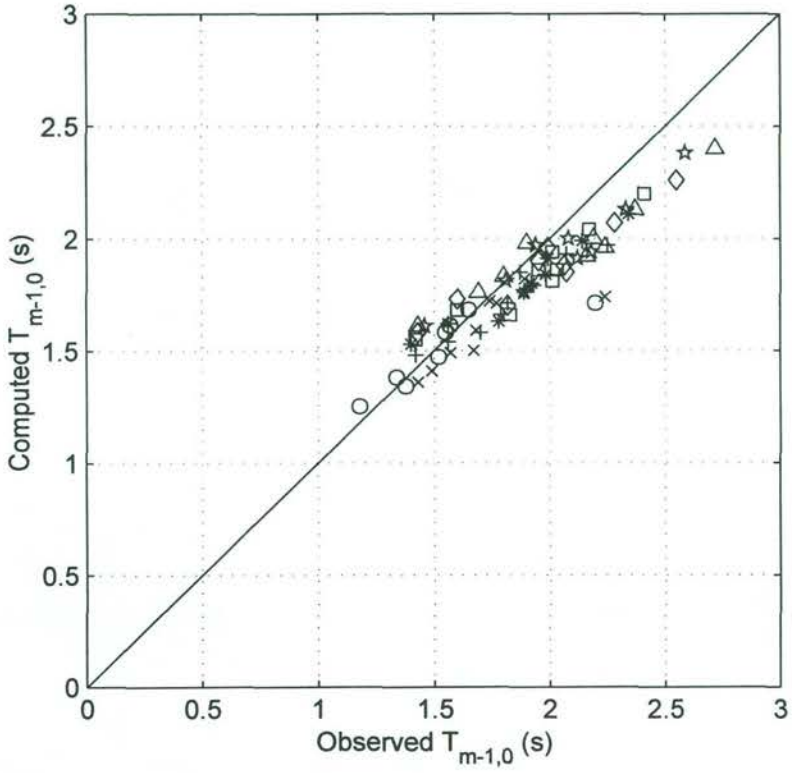

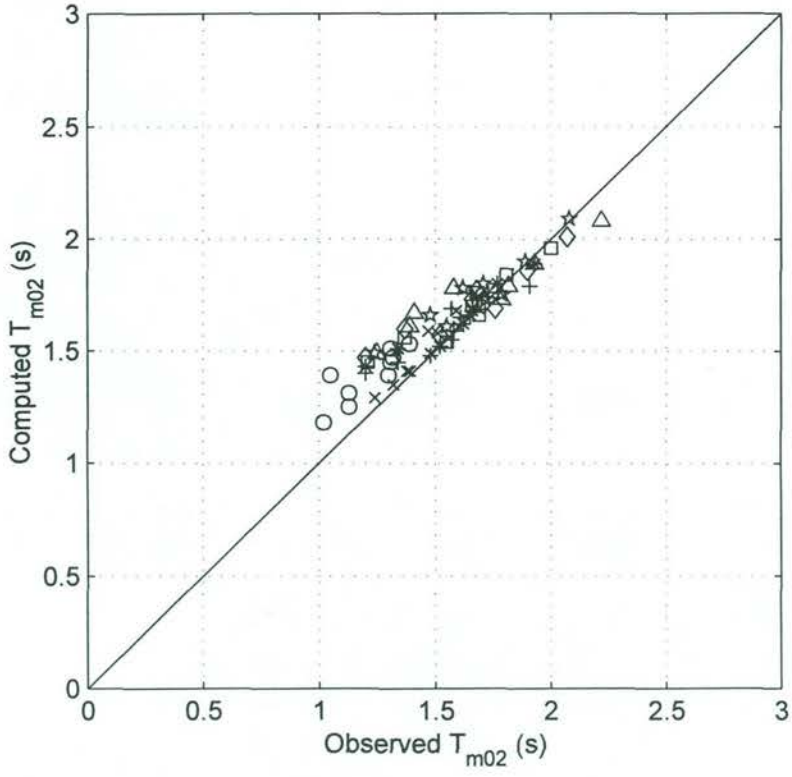

Comparison of observed and computed wave conditions in Lake George
Comparison of mean periods $T_{m-1,0}$ and T_{m02}

SWAN

Lake George

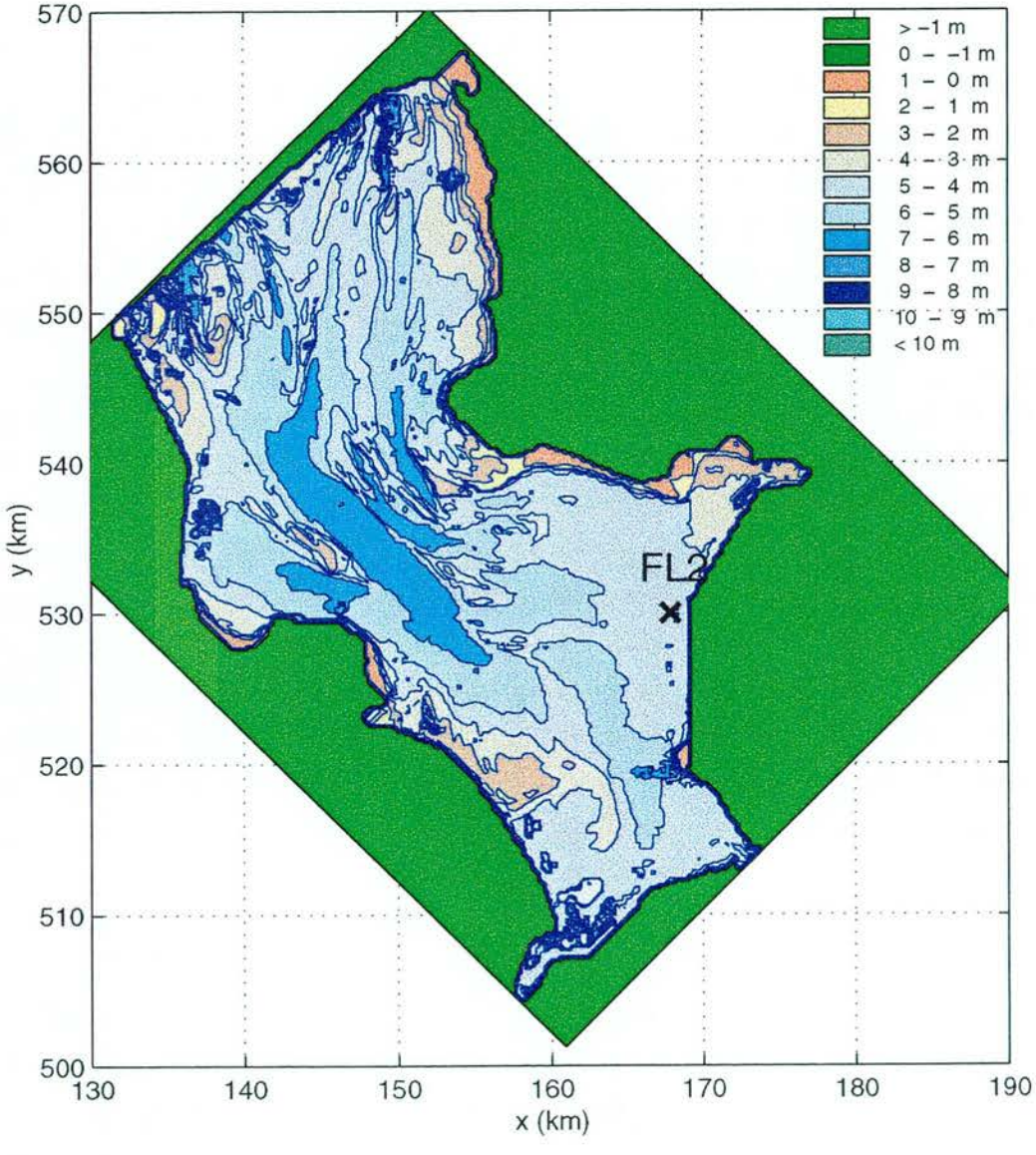

Bottom topography of IJsselmeer and location of measurement station FL2

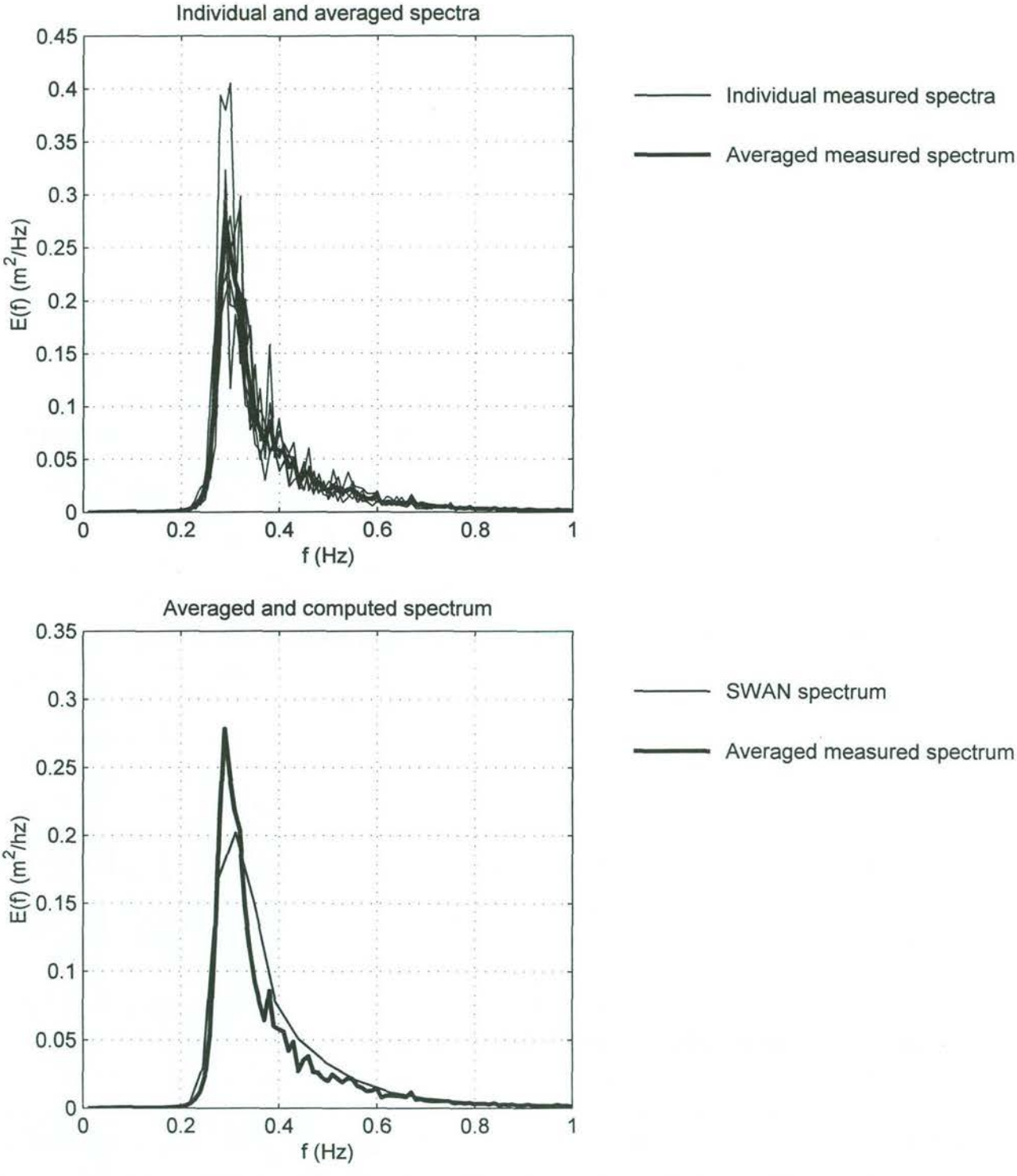

Comparison of (averaged) measured wave spectrum with computed SWAN spectrum for location FL2 in the IJsselmeer Date and times of measurements: '4-5/12/94.20-01'		SWAN	Y01
		IJsselmeer: FL2	
Source term investigation SWAN	A162	Alkyon	Fig. 8.8

yfigscat

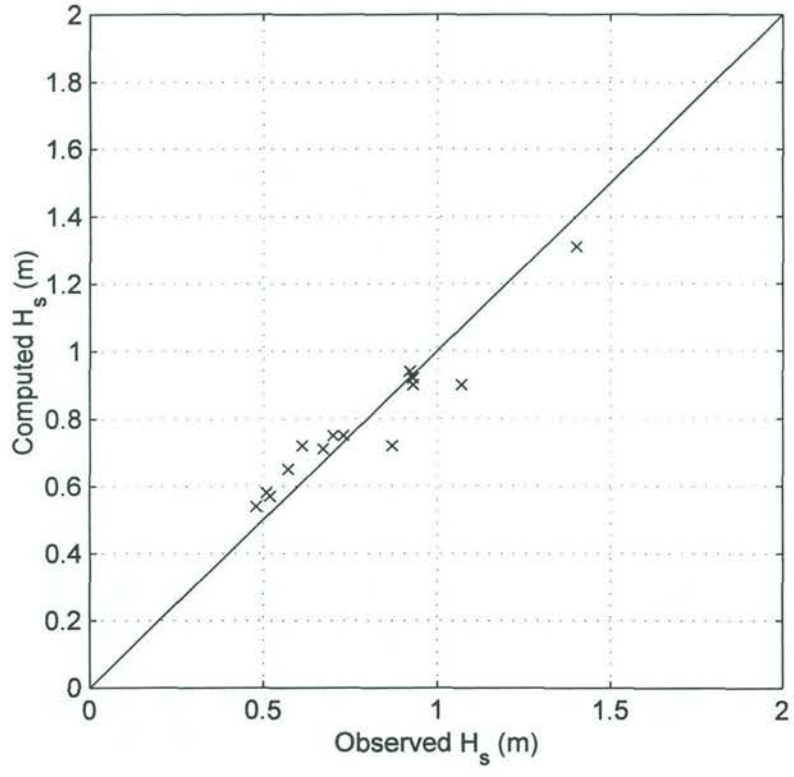

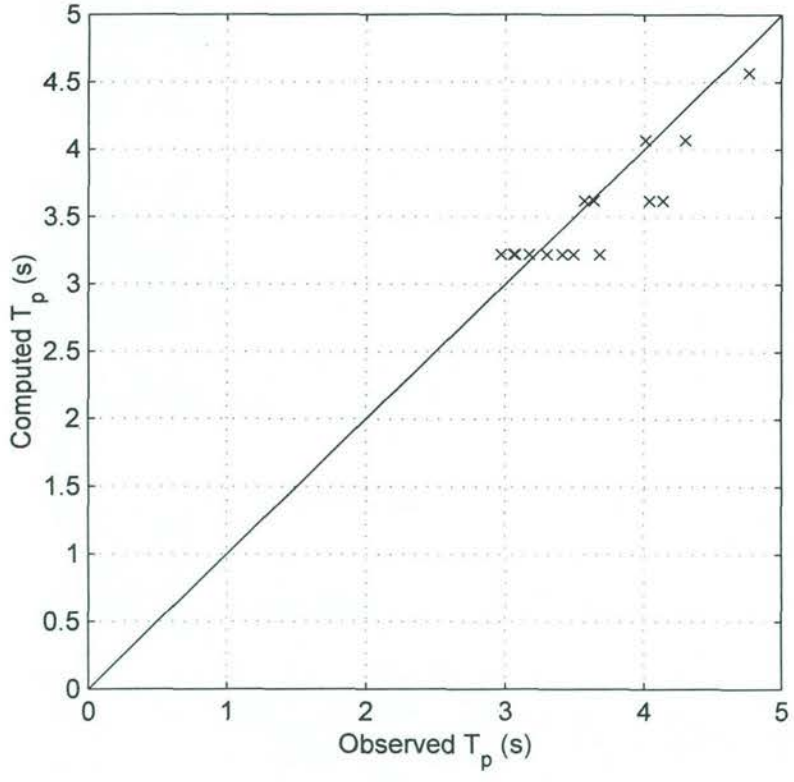

Comparison of observed and computed wave conditions in IJsselmeer Comparison of significant wave height H_s and peak period T_p		SWAN	
		IJsselmeer: FL2	
Source term investigation SWAN	A162	Alkyon	Fig. 8.9

yfigscat

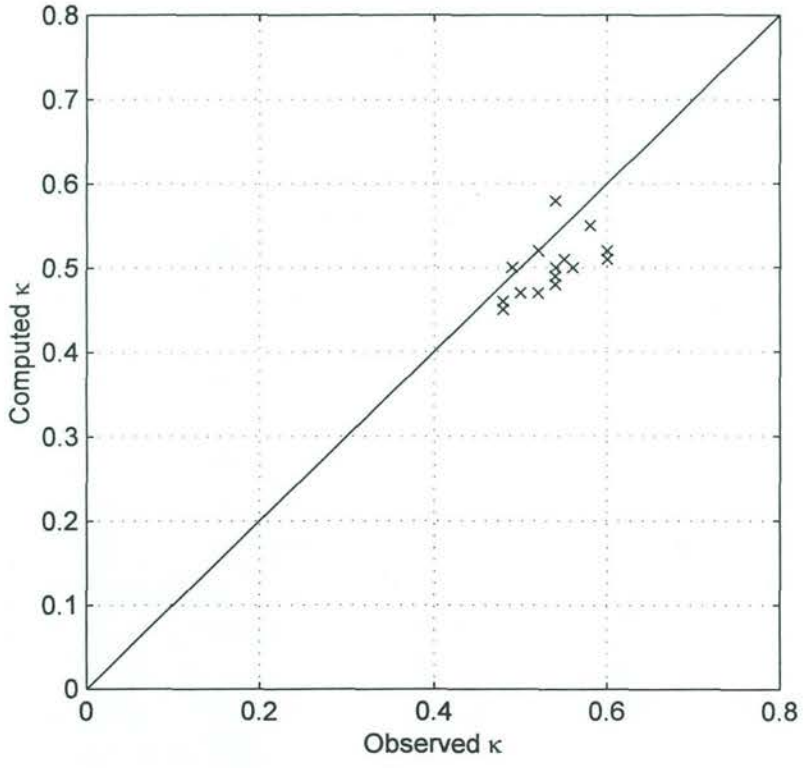

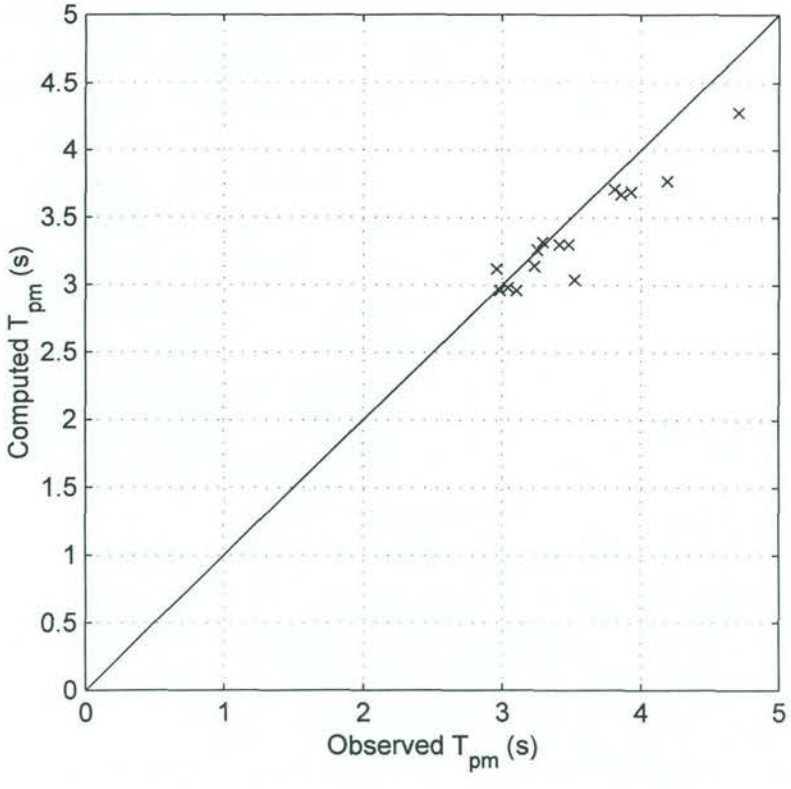

Comparison of observed and computed wave conditions in IJsselmeer Comparison of spectral narrowness κ and mean block peak period T_{pm}		SWAN	
		IJsselmeer: FL2	
Source term investigation SWAN	A162	Alkyon	Fig. 8.10

yfigscat

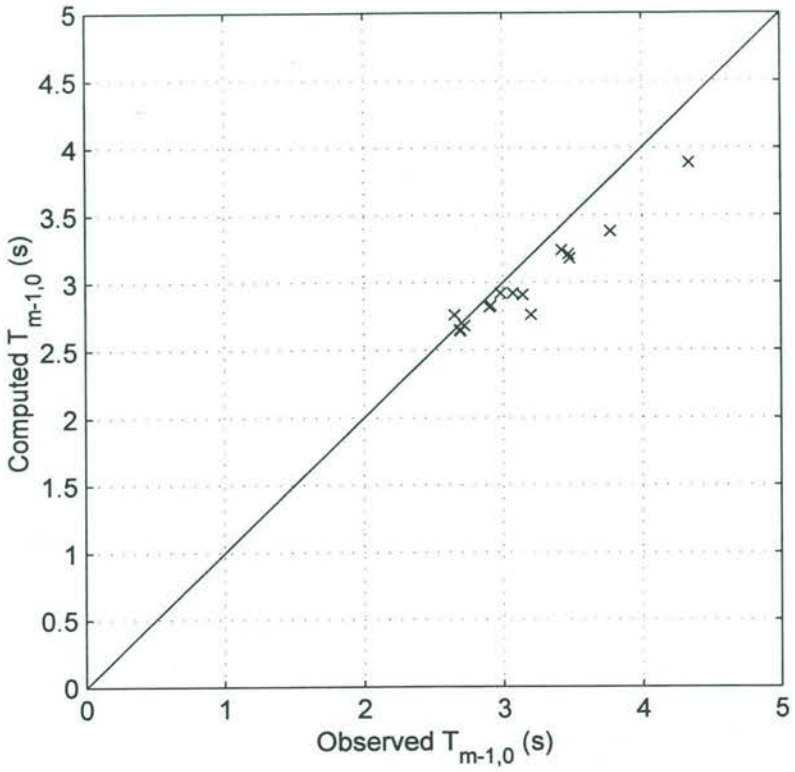

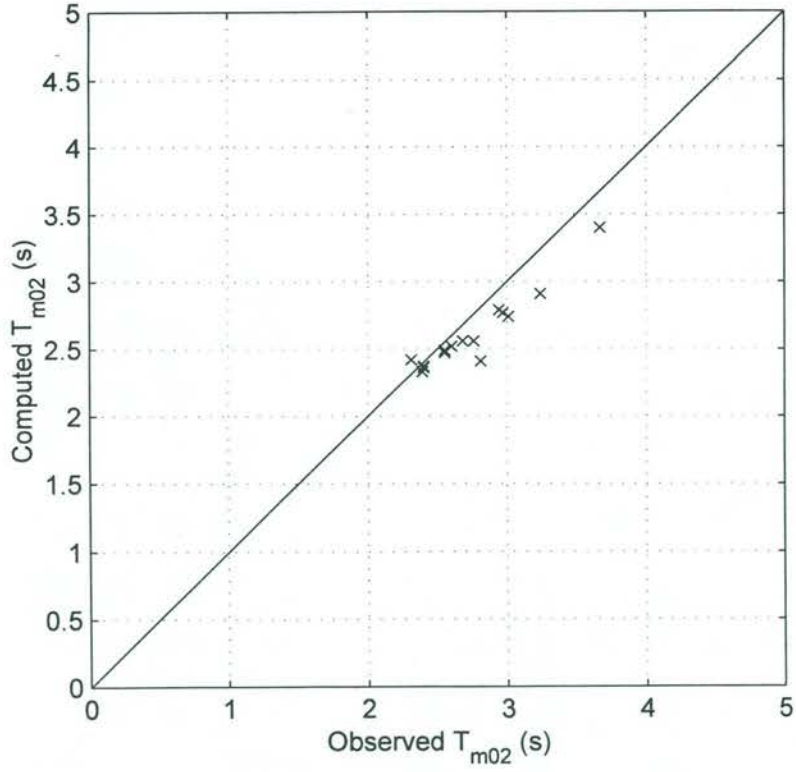

Comparison of observed and computed wave conditions in IJsselmeer Comparison of mean periods $T_{m-1,0}$ and T_{m02}	SWAN	
	IJsselmeer: FL2	
Source term investigation SWAN	A162 Alkyon	Fig. 8.11

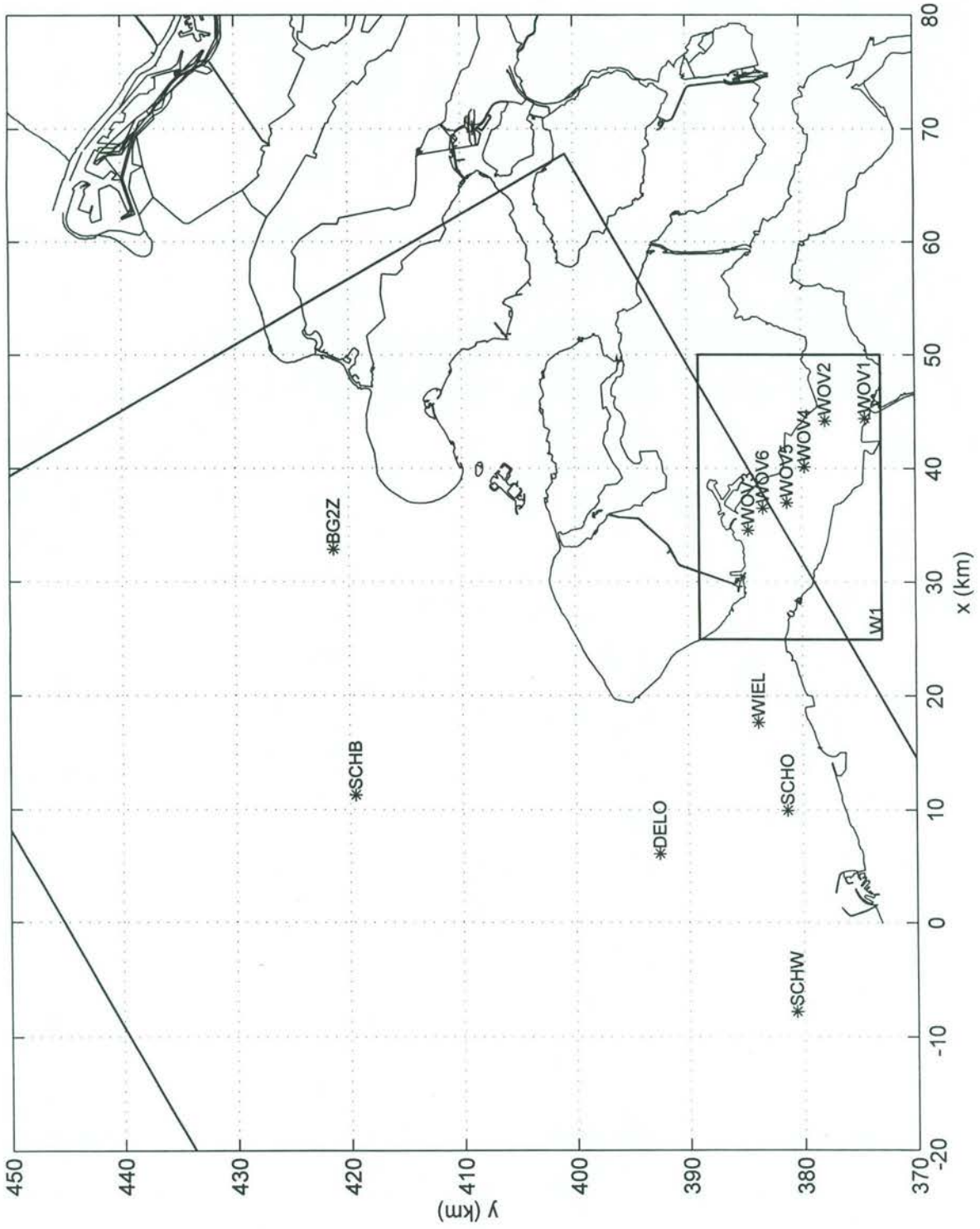

Overview of Westerschelde estuary and measurement locations and computational grids

SWAN

Source term investigation SWAN A162 Alkyon Fig. 8.12

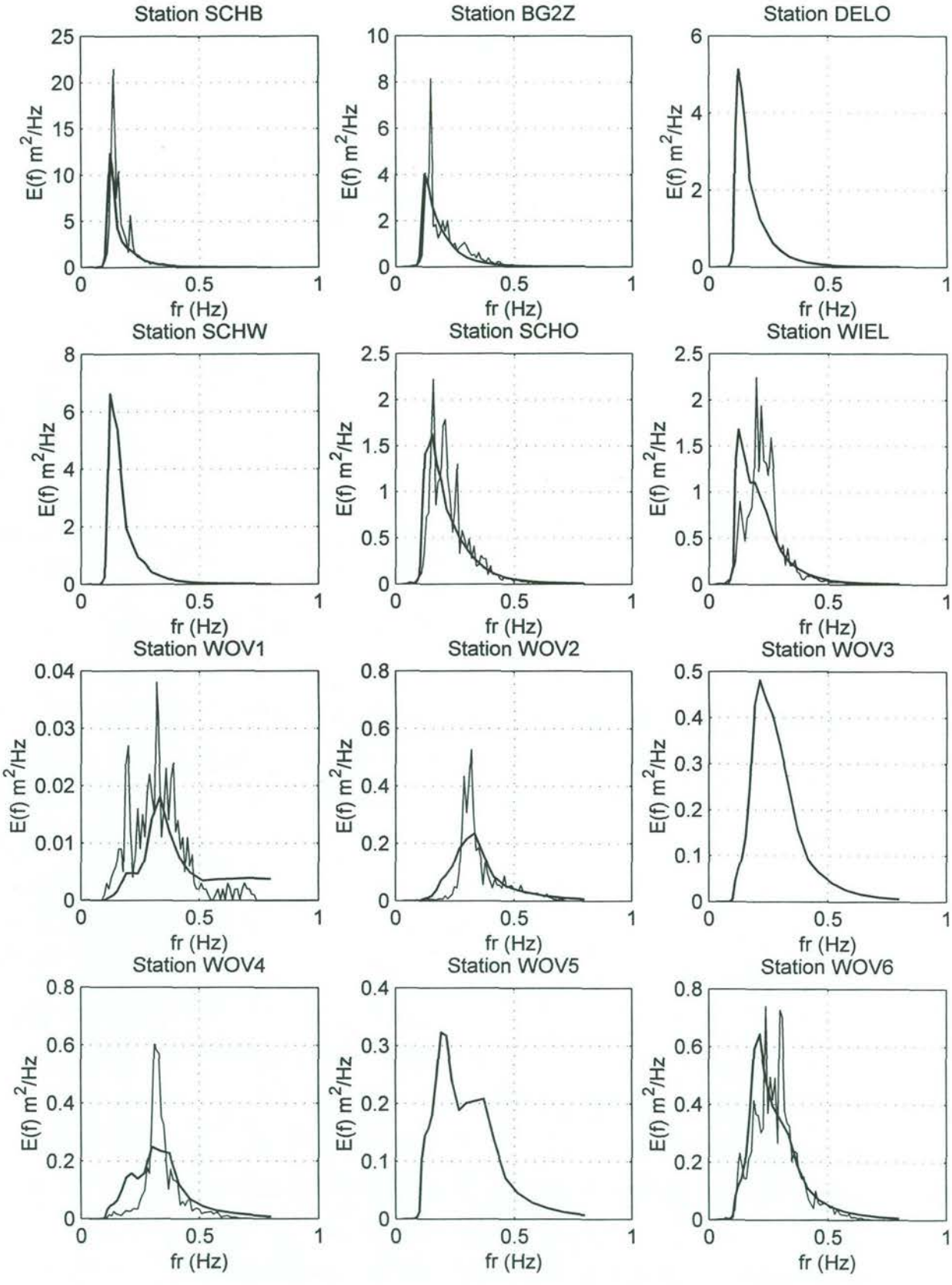

Observed and computed spectra in the Westerschelde estuary
for all stations and for storm 7 date and time: 911223 1530
Observed spectrum (thin line) Computed spectrum (thick line)

SWAN	Storm 7
Westerschelde	

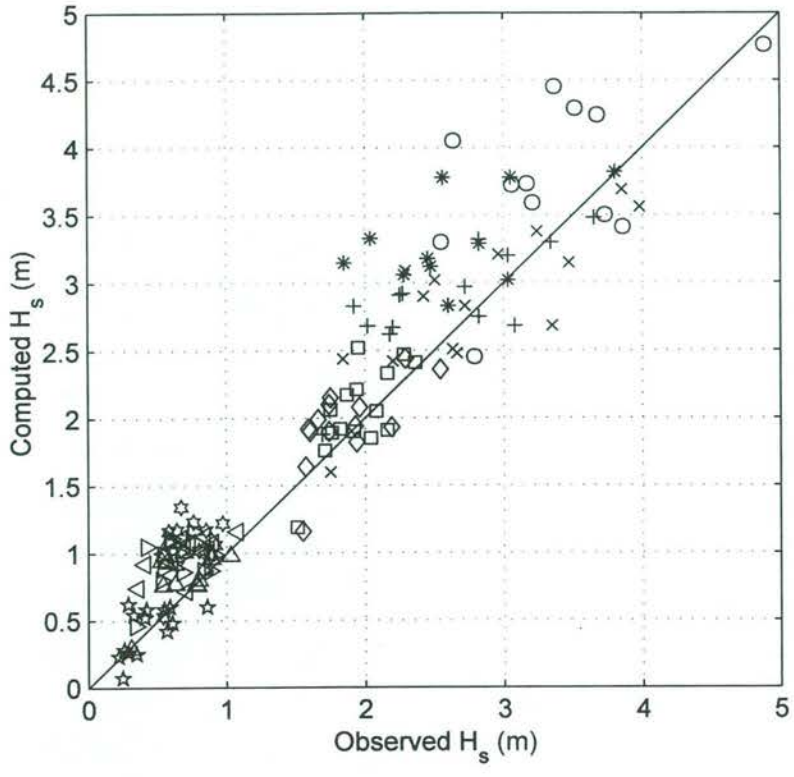

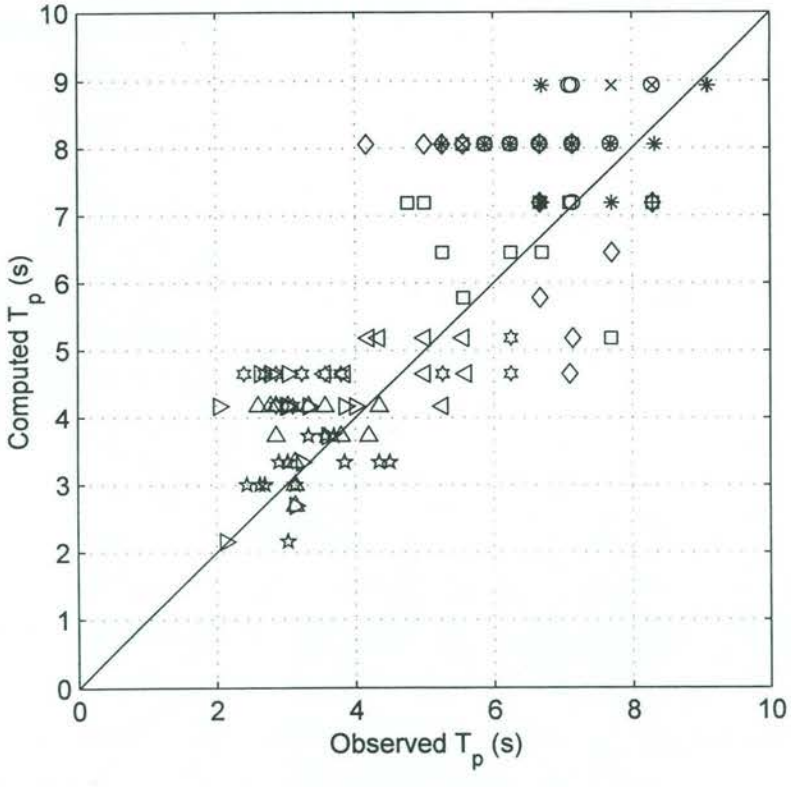

○ Station BG2Z
× Station DELO
+ Station SCHW
✳ Station SCHO
□ Station WIEL
◇ Station WOV1
☆ Station WOV2
△ Station WOV3
◁ Station WOV4
▷ Station WOV5
✡ Station WOV6

Comparison of observed and computed wave conditions in Westerschelde Comparison of significant wave height H_s and peak period T_p	SWAN	
	Westerschelde	
Source term investigation SWAN	A162	Alkyon Fig. 8.14

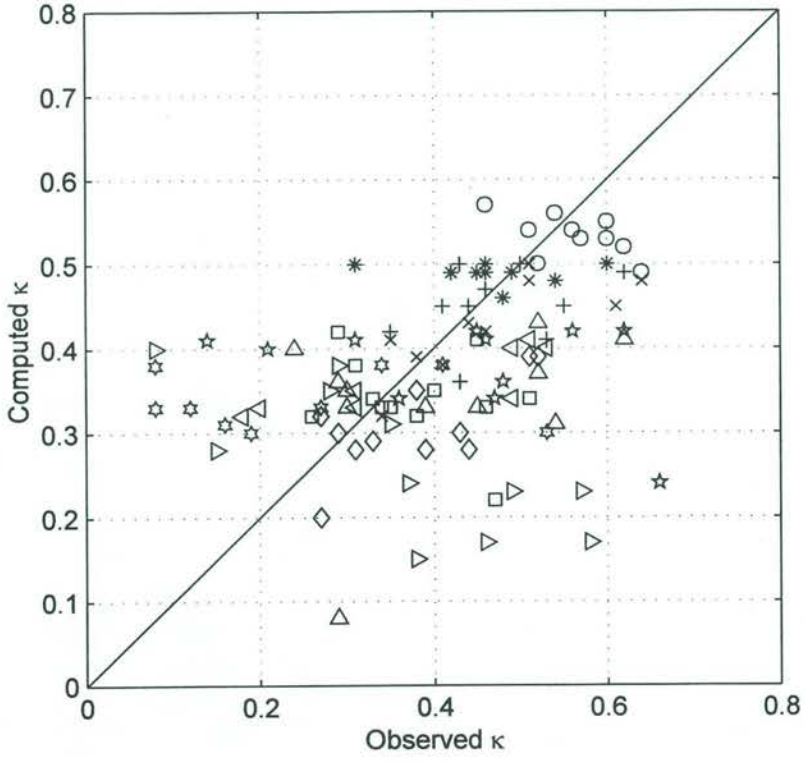

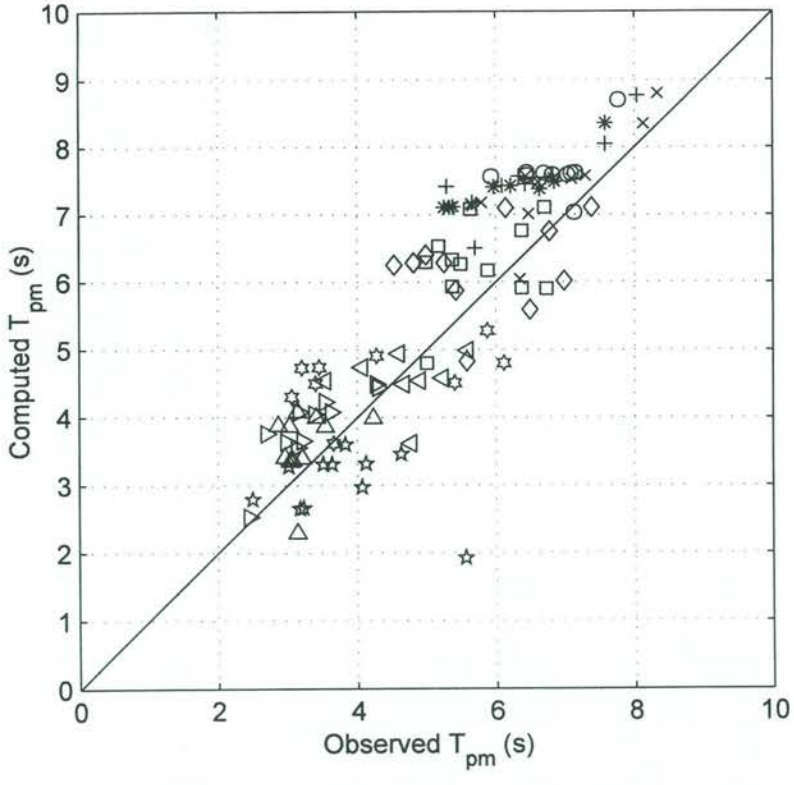

○ Station BG2Z
× Station DELO
+ Station SCHW
✱ Station SCHO
□ Station WIEL
◇ Station WOV1
☆ Station WOV2
△ Station WOV3
◁ Station WOV4
▷ Station WOV5
✡ Station WOV6

Comparison of observed and computed wave conditions in Westerschelde Comparison of spectral narrowness κ and mean peak period T_{pm}	SWAN	
	Westerschelde	
Source term investigation SWAN	A162	Alkyon Fig. 8.15

File figwscat.m /Date: 1999/07/07 /Time: 10:58:42

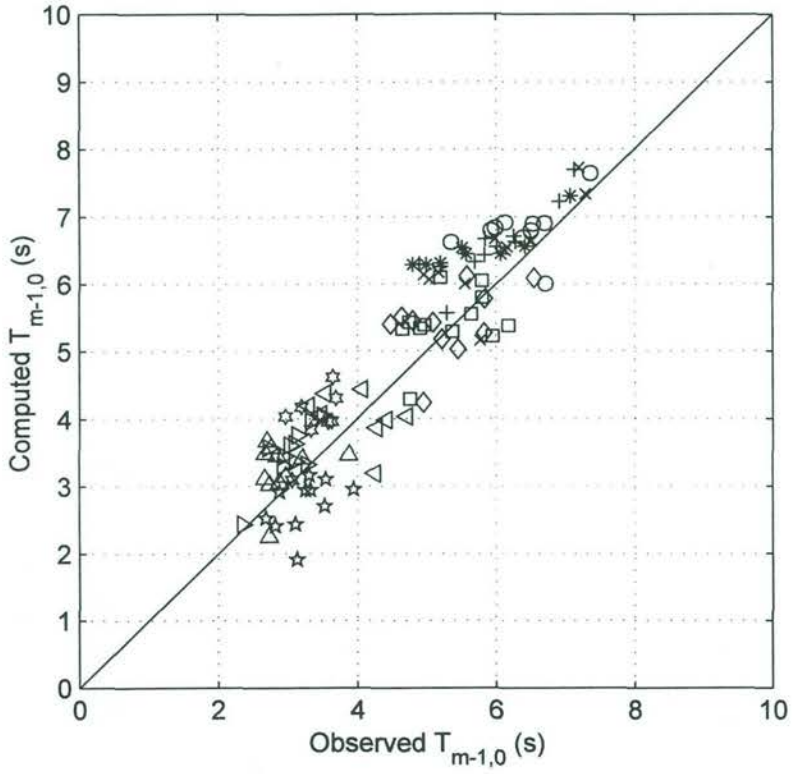

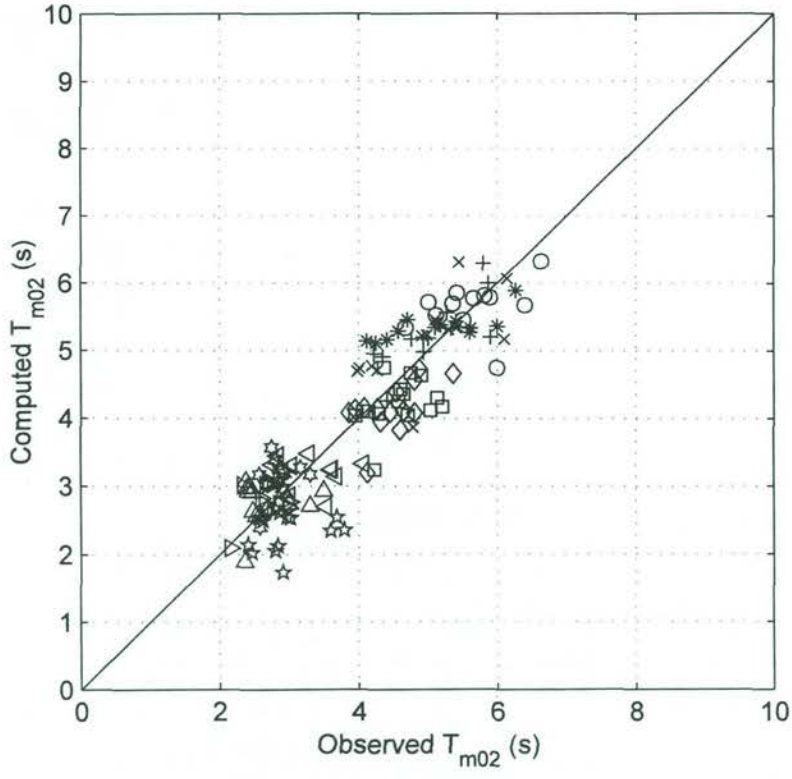

○ Station BG2Z
× Station DELO
+ Station SCHW
✳ Station SCHO
□ Station WIEL
◇ Station WOV1
☆ Station WOV2
△ Station WOV3
◁ Station WOV4
▷ Station WOV5
✡ Station WOV6

Comparison of observed and computed wave conditions in Westerschelde Comparison of mean periods $T_{m-1,0}$ and T_{m02}	SWAN	
	Westerschelde	
Source term investigation SWAN	A162	Alkyon Fig. 8.16

fig9x.m

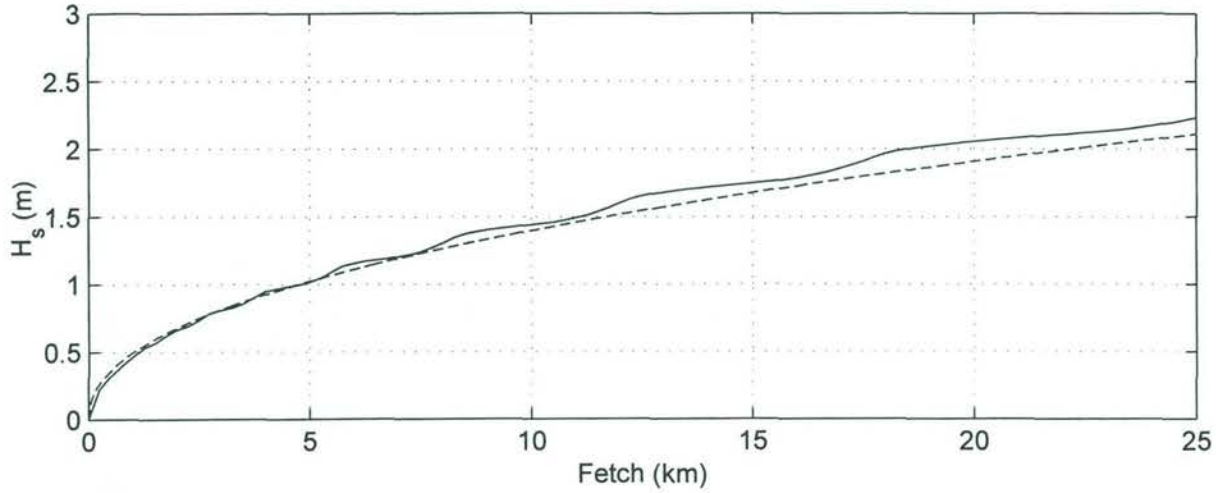

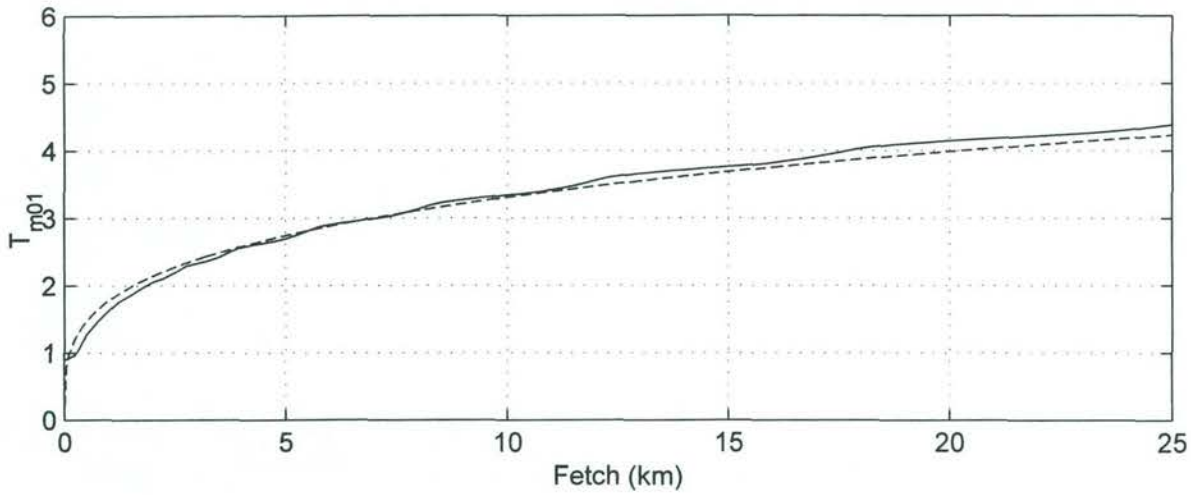

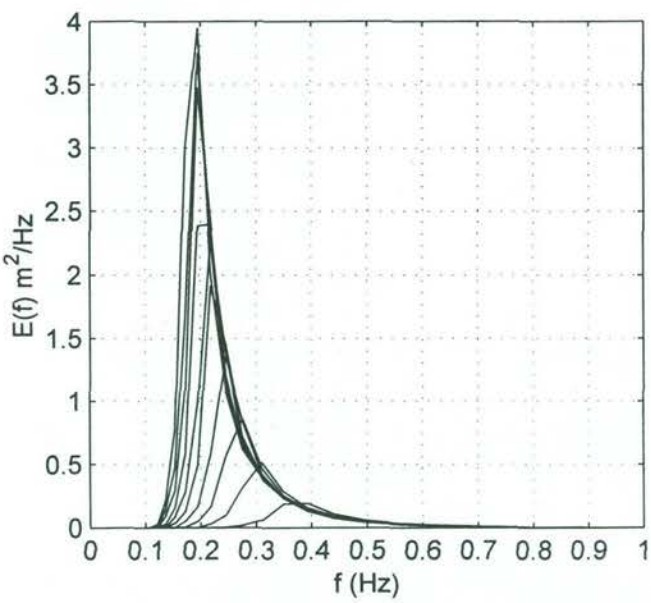

Growth curve of K&C

calibrated SWAN

Calibration of SWAN against growth curve of Kahma and Calkoen Comparison for a fetch of 25 km and a wind speed of 20 m/s		Case 1	
Source term investigation SWAN	A162	Alkyon	Fig. 9.1

fig9x.m

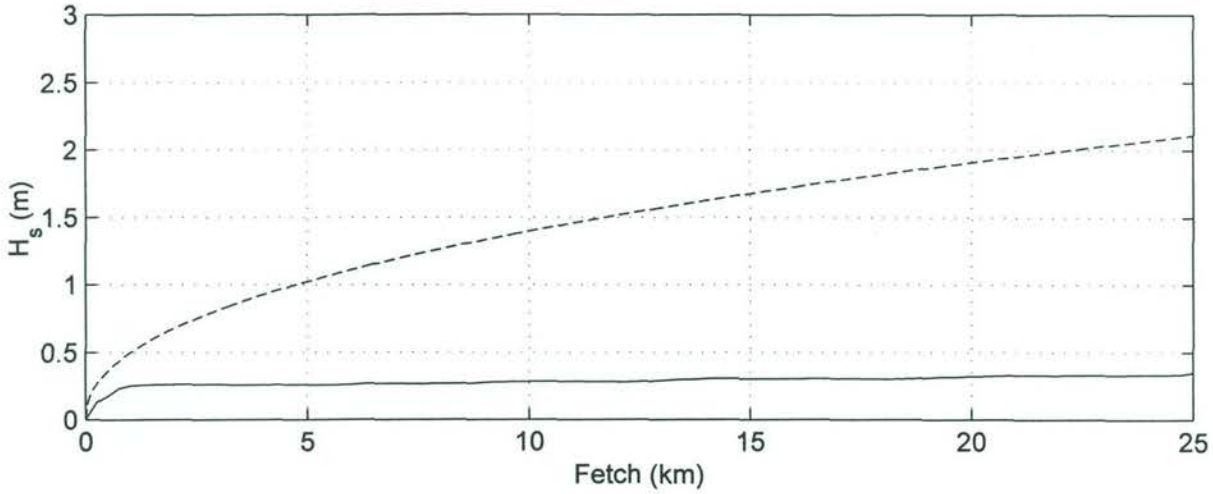

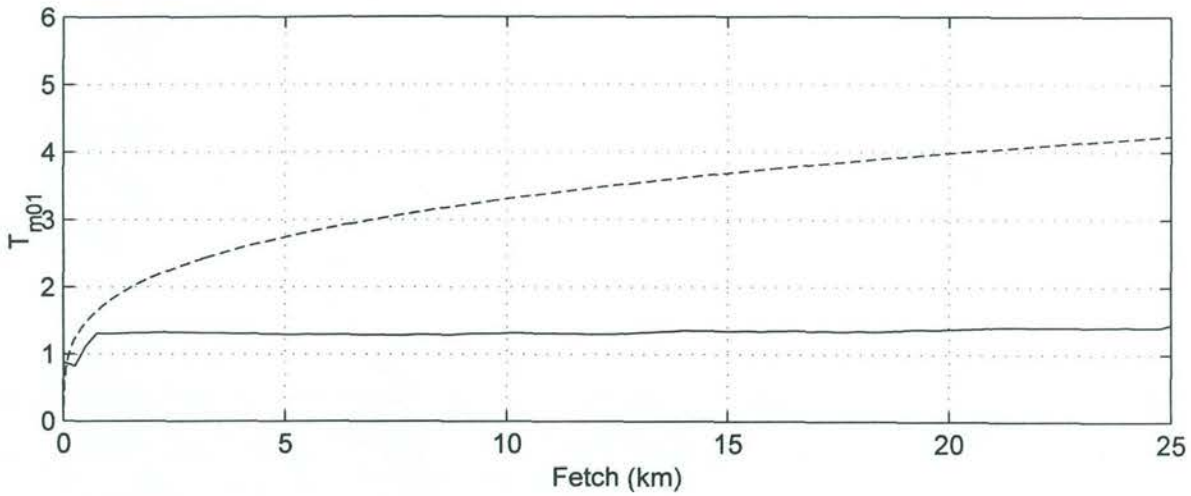

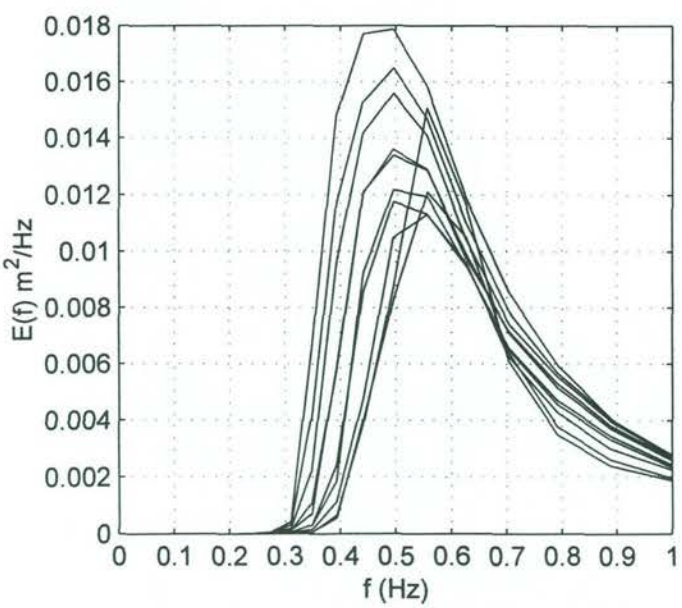

Growth curve of K&C

calibrated SWAN

Calibration of SWAN against growth curve of Kahma and Calkoen
Comparison for a fetch of 25 km and a wind speed of 20 m/s

Case 2

Source term investigation SWAN A162 Alkyon Fig. 9.2

fig9x.m

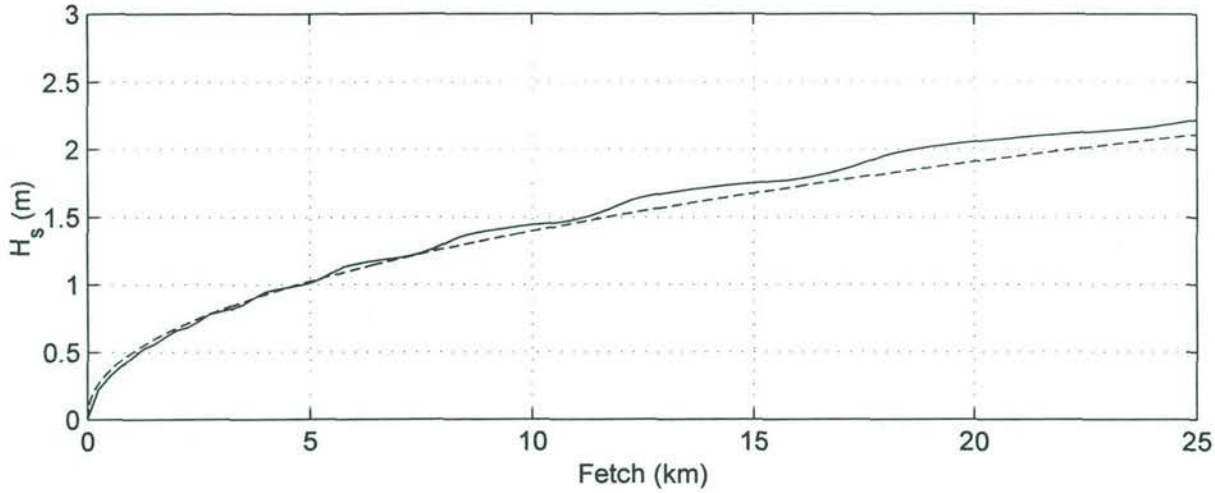

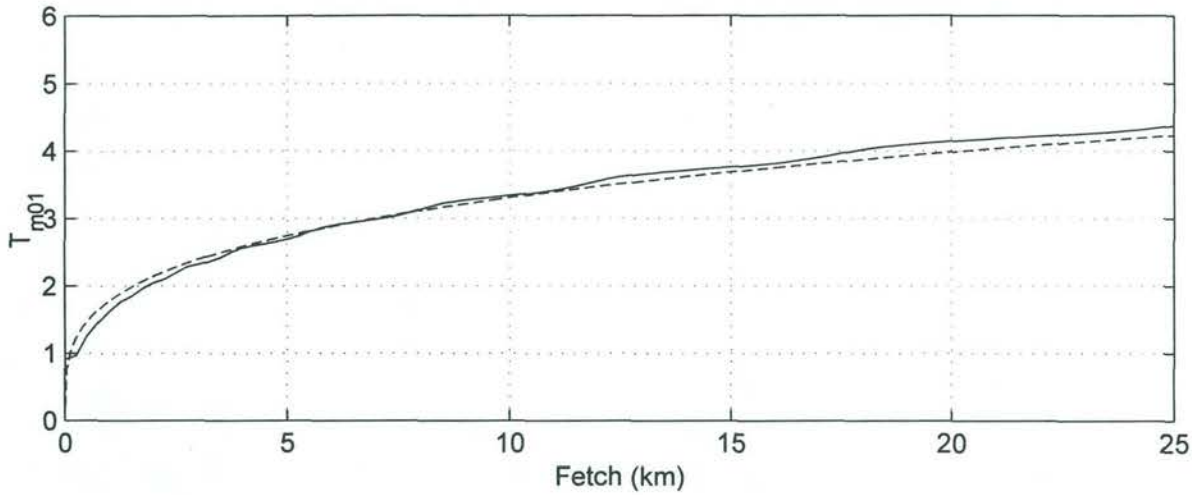

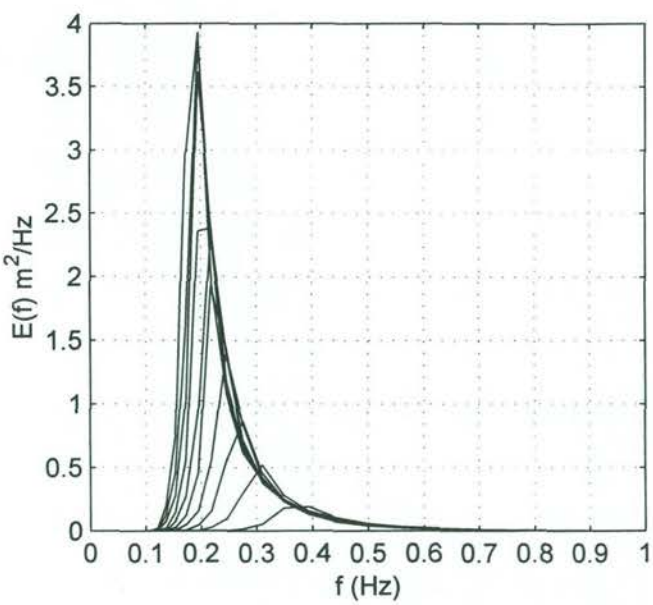

Growth curve of K&C
calibrated SWAN

Calibration of SWAN against growth curve of Kahma and Calkoen Comparison for a fetch of 25 km and a wind speed of 20 m/s	Case 3		
Source term investigation SWAN	A162	Alkyon	Fig. 9.3

fig9x.m

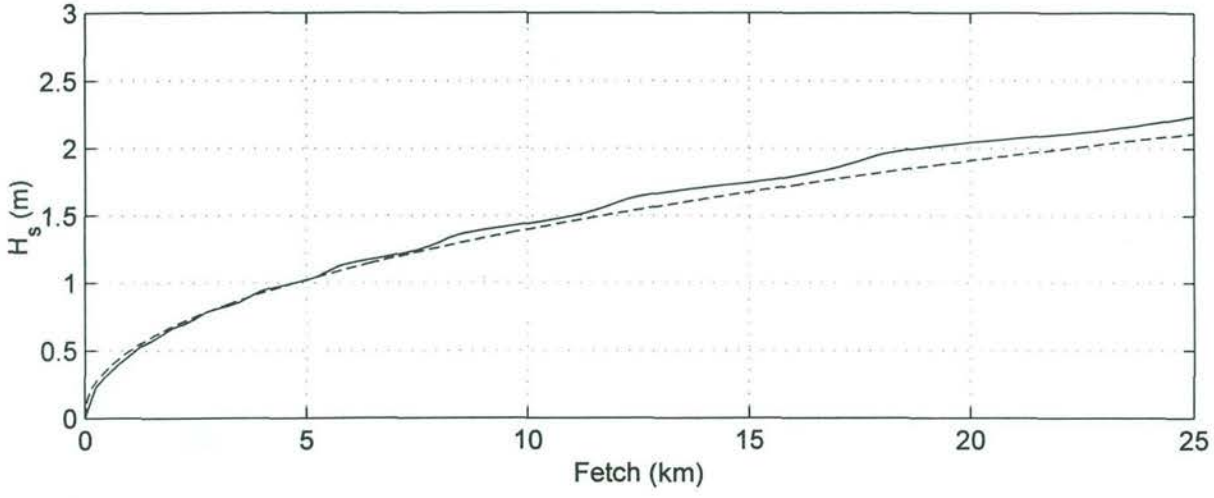

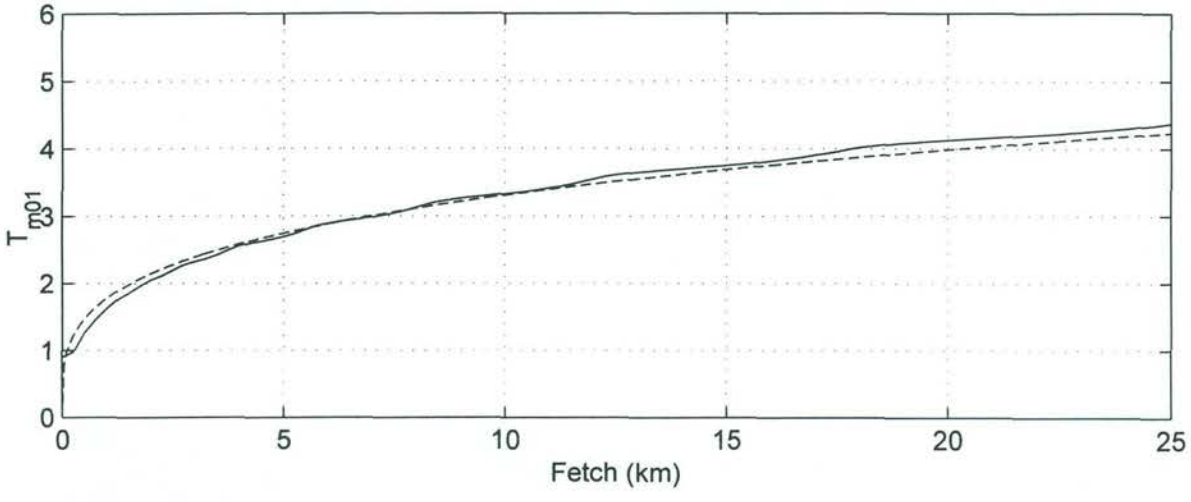

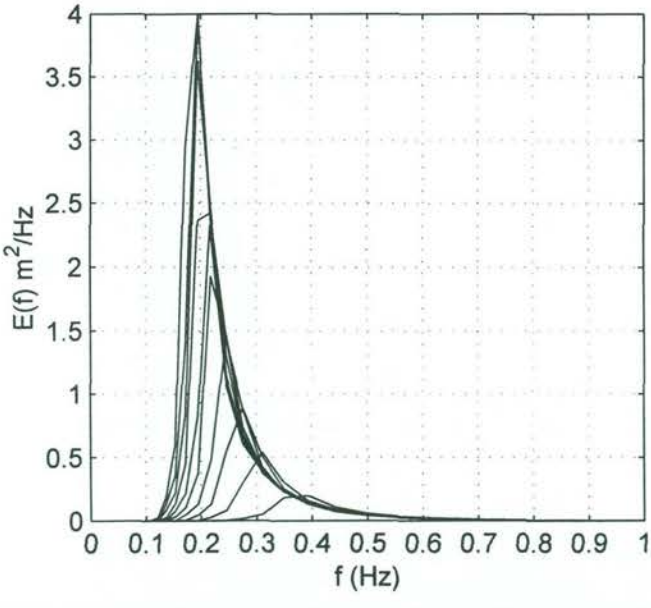

Growth curve of K&C
calibrated SWAN

Calibration of SWAN against growth curve of Kahma and Calkoen
Comparison for a fetch of 25 km and a wind speed of 20 m/s

Case 4

Source term investigation SWAN A162 Alkyon Fig. 9.4

Appendix A

Parametric deep water growth curves

1 Introduction

The concept of parametric growth curves is to express the time or fetch evolution of statistical properties of wind waves in terms of dimensionless variables which solely depend on wind speed. In principle a large number of variables may control the wave growth. But it has been suggested by Kitaigorodskii (1962) that in an idealised situation only wind speed is important. The first attempts to describe the evolution of wind waves were made by Sverdrup and Munk (1947) during the second world war.

A nice overview of deep water and finite depth growth curves has been given by Holthuijsen (1980). Many equations in this appendix have been found in this reference.

There is an ongoing debate whether or not the physical variables should be normalised with the wind speed U_{10} or with the friction velocity u_* (Holthuijsen, 1980, and Janssen et al., 1987). In this note expressions are given for both types.

Growth curves are expressed in terms of the following dimensionless quantities of time T, fetch F, significant wave height H_s, total wave variance E, and a wave period. For the wave period a number of quantities have been used, such as the peak period Tp, the mean wave period T_m (based on the first frequency moment of the energy density spectrum) and the significant wave period T_s (based on time domain mean period).

$$\tilde{T} = \frac{gT}{U_{10}} \qquad T_* = \frac{gT}{u_*}$$

$$\tilde{H} = \frac{gH_s}{U_{10}^2} \qquad H_* = \frac{gH_s}{u_*^2}$$

$$\tilde{F} = \frac{gF}{U_{10}^2} \qquad F_* = \frac{gF}{u_*^2}$$

$$\tilde{\varepsilon} = \frac{g^2 m_0}{U_{10}^4} \qquad \varepsilon_* = \frac{g^2 m_0}{u_*^4}$$

$$\tilde{\nu} = \frac{\omega_p U_{10}}{g} \qquad \nu_* = \frac{\omega_p u_*}{g}$$

in which $\omega_p = 2\pi f_p$. The relation between the wind speed at 10 m height U_{10} and the friction velocity u_* is given by:

$$u_*^2 = C_d U_{10}^2$$

in which C_d is the drag coefficient.. A relation between the drag coefficient and the wind speed U_{10} has been given by Wu (1982):

$$C_d(U_{10}) = \begin{cases} 1.2875 \times 10^{-3} & for \quad U_{10} < 7.5 m/s \\ (0.8 + 0.065\, s/m\, U_{10}) \times 10^{-3} & for \quad U_{10} \geq 7.5 m/s \end{cases}$$

2 Growth curves

Deep water growth curves have been published by Wilson (1955, 1965), Bretschneider (1973), Hasselmann et al. (1973) and Kahma and Calkoen (1992). These equations are summarised below.

Wilson (1955)

$$\tilde{H} = 0.26 \tanh(0.01 \tilde{F}^{1/2})$$

$$\tilde{T} = 1.4 \times 2\pi \tanh\left(0.0436 \tilde{F}^{1/3}\right)$$

Wilson (1965)

The growth curves of Wilson are given for the significant wave height Hs and the significant wave period Ts:

$$\tilde{H} = 0.30\left[1 - \left(1 + 0.004\sqrt{\tilde{F}}\right)^{-2}\right]$$

$$\tilde{T} = 1.37 \times 2\pi \left[1 - \left(1 + 0.008 \tilde{F}^{1/3}\right)^{-5}\right]$$

Bretschneider (1973)

$$\tilde{H} = 0.283 \tanh\left(0.0125 \tilde{F}^{0.42}\right)$$

$$\tilde{T} = 1.37 \times 2\pi \tanh(0.077 \tilde{F}^{0.25})$$

Hasselmann et al. (1973)

Based on the results of the JONSWAP experiment the following growth curves have been determined for the case of a stationary, homogeneous wind blowing perpendicularly offshore.

$$\tilde{\varepsilon} = 1.6 \times 10^{-7} \tilde{F}$$

$$\tilde{\nu} = 3.5 \tilde{F}^{-0.33}$$

In addition they also determined the growth curve for the Phillips' constant of a JONSWAP spectrum:

$$\alpha_p = 0.076 \tilde{F}^{-0.22}$$

Hasselmann et al. (1973) suggest a drag coefficient $C_d(U_{10})$ of 10^{-3} to convert the wind speed at 10 m height to the friction velocity u_*. From this it follows that the growth curves can also be written as:

$$\varepsilon_* = 1.6 \times 10^{-4} F_*$$

$$\nu_* = 1.082 F_*^{-0.33}$$

$$\alpha_p = 0.35 F_*^{-0.22}$$

Kahma and Calkoen (1992)

Based on a reanalysis of the JONSWAP data set they derived three sets of growth curves. One set for unstable stratification, one for a stable stratification and a composite set. In addition they provide growth curves both normalised with the wind speed U_{10} and the friction velocity u_*.

For a stable stratification the curves are based on 108 observations:

$$\tilde{\varepsilon} = 9.3 \times 10^{-7} \times \tilde{F}^{0.77}$$

$$\tilde{\nu} = 12 \times \tilde{F}^{-0.24}$$

$$\varepsilon_* = 2.1 \times 10^{-3} \times F_*^{0.79}$$

$$\nu_* = 2.3 \times F_*^{-0.25}$$

For unstable stratification the curves are based on 94 observations:

$$\widetilde{\varepsilon} = 5.4 \times 10^{-7} \times \widetilde{F}^{0.94}$$

$$\widetilde{\nu} = 14 \times \widetilde{F}^{-0.28}$$

$$\varepsilon_* = 4.7 \times 10^{-4} \times F_*^{0.95}$$

$$\nu_* = 3.6 \times F_*^{-0.28}$$

The composite dataset

$$\widetilde{\varepsilon} = 5.2 \times 10^{-7} \times \widetilde{F}^{0.9}$$

$$\widetilde{\nu} = 13.7 \times \widetilde{F}^{-0.27}$$

$$\varepsilon_* = 6.5 \times 10^{-4} \times F_*^{0.9}$$

$$\nu_* = 3.08 \times F_*^{-0.27}$$

3 Conversion to Hs, Tp and Tm

For practical purposes, e.g. the comparison with computational results, the growth curves are converted to expressions in terms of the significant wave height H_s, the peak period Tp and the mean (spectral) wave period T_m. As noted in Section 1, various measures for the wave period have been used in parametric growth curves. The following relations will be used to convert different measures of the wave period:

$$\frac{T_p}{T_m} = c_{pm} = 1.25$$

$$\frac{T_p}{T_s} = c_{ps} = 1.087$$

then it follows that:

$$\frac{T_s}{T_m} = c_{sm} = 1.15$$

Using the above relations the growth curves for Hs, Tp and Tm and made non-dimensional by the wind U_{10}. Below the expressions are given for Wilson (1965), Bretschneider (1973) and Kahma and Calkoen (1993, composite dataset).

Wilson (1965)

$$\tilde{H}_s = 0.30\left[1-\left(1+0.004\sqrt{\tilde{F}}\right)^{-2}\right]$$

$$\tilde{T}_p = c_{ps}\,1.37\times 2\pi\left[1-\left(1+0.008\tilde{F}^{1/3}\right)^{-5}\right]=10.76\left[1-\left(1+0.008\tilde{F}^{1/3}\right)^{-5}\right]$$

$$\tilde{T}_m = \frac{1.37\times 2\pi}{c_{sm}}\left[1-\left(1+0.008\tilde{F}^{1/3}\right)^{-5}\right]=7.49\left[1-\left(1+0.008\tilde{F}^{1/3}\right)^{-5}\right]$$

Bretschneider (1973)

$$\tilde{H}_s = 0.283\tanh\left(0.0125\tilde{F}^{0.42}\right)$$

$$\tilde{T}_p = c_{ps}\,1.37\times 2\pi\tanh(0.077\tilde{F}^{0.25}) = 9.36\tanh(0.077\tilde{F}^{0.25})$$

$$\tilde{T}_m = \frac{1.37\times 2\pi}{c_{sm}}\tanh(0.077\tilde{F}^{0.25}) = 7.49\tanh(0.077\tilde{F}^{0.25})$$

Kahma and Calkoen (1992)

For the composite dataset the following relations are found for a scaling with U_{10}:

$$\tilde{H}_s = 4\sqrt{\tilde{E}} = 2.88\times 10^{-3}\,\tilde{F}^{0.45}$$

$$\tilde{T}_p = \frac{2\pi}{\tilde{\nu}} = 0.459\tilde{F}^{0.27}$$

$$\tilde{T}_m = \frac{\tilde{T}_p}{c_{pm}} = 0.367\tilde{F}^{0.27}$$

for a scaling with u_*

$$H_s^* = 4\sqrt{\varepsilon_*} = 0.102\times 10^{-3}\,F_*^{0.45}$$

$$T_p^* = \frac{2\pi}{\nu_*} = 2.040F_*^{0.27}$$

$$T_m^* = \frac{T_p^*}{c_{pm}} = 1.632F_*^{0.27}$$